PROCEEDINGS OF

THE GHRSST XVIII SCIENCE TEAM MEETING

Qingdao, China
5th – 9th June 2017

ISSN 2049–2529
Issue Version 3.0

Edited by the GHRSST Project Office

Meeting hosted and sponsored by
The Ocean University of China (OUC)

Co-sponsored by
The National Ocean Satellite Application Center
K. C. Wong Education Foundation

GHRSST Project Office

Gary Corlett, Project Coordinator
gpc@ghrsst.org

Silvia Bragaglia-Pike, Project Administrator
gpa@ghrsst.org

www.ghrsst.org

The GHRSST Project Office is funded by the European Union.

Table of Contents

SECTION 1: AGENDA

MONDAY, 5th JUNE 2017		
Plenary Session I: Introduction ***Chair:*** *Anne O'Carroll* ***Rapporteur:*** *Gary Corlett*		
09:00-09:05	*Anne O'Carroll*	*Welcome to GHRSST!*
09:05-09:25	*Ge Chen*	*SST oceanography: A few examples*
09:25-09:45	*Anne O'Carroll*	*Introduction to GHRSST*
09:45-10:05	*Ken Casey*	*GHRSST Products and Services*
10:05-10:20	*Gary Corlett*	*Logistics*
11:40-12:00	*Feng Lu*	*Overview of remote sensing at CMA*
12:00-12:20	*Sujuan Wang*	*SST operations at CMA*
12:20-12:40	*Qian Feng*	*The application of satellite remote sensing techniques in NSOAS*
12:40-13:00	*Liying Wan*	*Global high-resolution forecasting system and its validation in NMEFC*
Plenary Session II: Applications ***Chair:*** *Helen Beggs* ***Rapporteur:*** *Stéphane Saux Picart*		
14:00-14:20	*Gentemann, Chelle*	*Satellite sea surface temperatures along the west coast of the United States during the 2014-2016 Northeast Pacific marine heat wave*
14:20-14:40	*Li, Xu*	*Analyze SST within the NCEP GFS*
14:40-15:00	*Santoleri, Rosa*	*Improving the altimeter derived geostrophic currents using sea surface temperature images: Feasibility study and application on real datasets*
15:00-15:30	*Open discussion led by session chair*	

Posters Session (See full list of Posters in Section 3)

TUESDAY 6th JUNE 2017		
Plenary Session III: Product developments ***Chairs:*** *Andy Harris* ***Rapporteur:*** *Igor Tomazic*		
09:30-09:50	*Mittaz, Jonathan*	*AVHRR Level 1 errors and uncertainties: The FIDUCEO approach*
09:50-10:10	*Koner, Prabhat*	*Quasi-deterministic cloud detection for infrared sea surface temperature retrieval from satellite imager measurements*
10:10-10:30	*Wang, Sujuan*	*FY-3C VIRR operational sea surface temperature product*
10:30-10:50	*Chen, Chuqun*	*Sea surface temperature in South China Sea retrieved from Chinese satellite FY-3B VIRR data*
10:50-11:10	*Embury, Owen*	*SST retrieval methods in the ESA Climate Change Initiative*
11:40-12:00	*Ignatov, Alex*	*ACSPO SSST products and monitoring for GOES-16 and Himawari-8*
12:00-12:20	*Petrenko, Boris*	*Diurnal cycles in the NOAA ACSPO "depth" and "skin" SSTs from the new generation ABI/AHI geostationary sensors*
12:20-12:40	*Gangwar, Rishi Kumar/ Thapliyal, Pradeep*	*Radiative transfer model based bias correction in INSAT-3D/3DR thermal observations to improve sea surface temperature retrieval*
12:40-13:00	*Piollé, Jean-François*	*Copernicus Sentinel-3 match-up databases - Felyx in support to satellite Cal/Val*
14:00-15:30	*Open discussion led by session chair*	

Posters Session (See full list of Posters in Section 3)

WEDNESDAY 7th JUNE 2017		
Plenary Session IV: Surface fluxes ***Chair:*** *Chelle Gentemann* ***Rapporteur:*** *Salvatore Marullo*		
08:30-08:50	*Zhang, Haifeng/ Beggs, Helen*	*Evaluation of sea surface temperature diurnal variation models against MTSAT-1R data in the tropical warm pool*
08:50-09:10	*Wong, Elizabeth/ Minnett, Peter*	*The response of the ocean thermal skin layer with air-sea surface heat fluxes*
09:10-09:30	*Liu, Timothy*	*Sea surface temperature influence on ocean carbon cycle*
09:30-10:00	*Open discussion led by session chair*	
Plenary Session V: Sampling ***Chair:*** *Peter Cornillon* ***Rapporteur:*** *Prasanjit Dash*		
10:30-10:50	*Wu, Fan*	*Evaluation of the precision in Level 2 VIIRS and AVHRR sea surface temperature fields*
10:50-11:10	*Ding, Yanni*	*ACSPO L3U SST products*
11:10-11:30	*Mao, Chongyuan*	*Feature resolution in OSTIA L4 analyses*
11:30-12:00	*Open discussion led by session chair*	

12:00-17:00	Afternoon Team Building.

18:00-21:00	GHRSST Dinner at the Cape Golden Ocean Restaurant.

THURSDAY 8th JUNE 2017		
Plenary Session VI: Climate ***Chairs:*** *Jon Mittaz* ***Rapporteur:*** *Owen Embury*		
09:30-09:50	*Baker-Yeboah, Sheekela*	*Pathfinder version 5.3 AVHRR Level-2 processed global sea surface temperature*
09:50-10:20	*Minnett, Peter*	*Long-term global time series of MODIS and VIIRS SSTs*
10:20-11:00	*Merchant, Christopher*	*Progress towards V2.0 SST CCI climate data record*
11:30-11:50	*Saux Picart, Stéphane*	*OSI SAF sea surface temperature reprocessing of MSG/SEVIRI archive*
11:50-12:20	*Høyer, Jacob*	*Generating an SST climate data record from passive microwave observations*
12:20-12:40	*Marullo, Salvatore*	*Long-term changes in the Northwestern Atlantic and Mediterranean SSST from 1982 To 2016: A contribution of the operational oceanography to the determination of the present-day climate*
12:40-13:00	*Open discussion led by session chair*	
14:00-15:30	*R/GTS Update (Groups)*	
16:00-17:00	*R/GTS Update (Plenary)*	
17:00-18:00	*Planning for next year (Groups)*	

18:00-21:00	Advisory Council
Meeting of the GHRSST Advisory Council For further information, please contact: Chelle Gentemann	

FRIDAY 9th JUNE 2017		
Plenary Session VIII: In situ ***Chair:*** *Alexander Ignatov* ***Rapporteur:*** *Werenfrid Wimmer*		
09:00-09:20	*Guan, Lei*	*Shipboard measurements of sea surface skin temperature in the Northwest Pacific*
09:20-09:40	*Beggs, Helen*	*IMOS ship SST for satellite SST validation*
09:40-10:00	*Liu, Chunying*	*The improvement of ICOADS 3.0 and its application to DOISST*
10:00-10:30	*Open discussion led by session chair*	
Closing Session ***Chair:*** *Anne O'Carroll* ***Rapporteur:*** *Gary Corlett*		
11:00-11:20	*Piollé, Jean-François*	*The Medspiration project*
11:20-11:40	*Donlon, Craig*	*ESA support to the GHRSST Project Office*
11:40-12:15	*Task Team assignments for next year*	
12:15-12:45	*Review of action items*	
12:45-13:00	*Wrap-up/closing remarks*	
Close of GHRSST XVIII		

SECTION 2: PLENARY SESSION SUMMARY REPORTS

PLENARY SESSION II: APPLICATIONS

SESSION II REPORT

Chair: Helen Beggs[(1)] – Rapporteur: Saux Picart Stéphane[(2)]

(1) Bureau of Meteorology, Melbourne, Australia, Email: Helen.Beggs@bom.gov.au
(2) Météo-France, France, Email: stephane.sauxpicart@meteo.fr

1 INTRODUCTION

This is a brief summary of the presentations and discussions during the SST Applications Session held in the afternoon of Monday 5th June 2017 at the 18th GHRSST Science Team Meeting, Qingdao, China.

2 CHELLE GENTEMANN: SATELLITE SSTS ALONG THE WEST COAST OF THE U.S. DURING THE 2014-2016 NORTH-EAST PACIFIC MARINE HEAT WAVE

- Used JPL MUR 1 km L4 SST analysis to study 2014-2016 North-East Pacific Marine Heat Wave
- Produced climatology from the average monthly SST from 10 years of MUR and calculated anomalies on a monthly basis from MUR SSTs.
- Also used HadiSST climatology from 1910 – 2010.
- Massive event 0.5 K higher than climatology with a peak of 6.2 K
- Correlated the SST anomalies with wind speeds
- May 2015: weaker upwelling than usual.
- July 2015: higher SST than usual.
- Upwelling index is insufficient to describe the reality. Upwelling warm water is not the same as upwelling cold water. There was some exception (short) when upwelled water was very cold, but never for very long.
- This study demonstrated the usefulness of MUR GHRSST-L4 to monitor coastal upwelling anomalies in a region with generally clear skies, and therefore high availability of high-resolution infrared SST data.

Questions:

Q: How did you define the anomaly?

Chelle: Monthly anomaly over 12 years.

Cause of the anomaly: Stationary atmospheric high pressure ridge. See paper by Bond (2015). Winds were second lowest on record.

Q: Why not model coastal upwelling?

Chelle: I calculated upwelling forcing from the wind. There were small anomalies in upwelling, but the change in the ecosystem was correlated to the temperature of the upwelled water not with the upwelling itself.

Somebody: Heat wave was more a new cycle after the 1998 type.

Helen Beggs: How confident are you that MUR captured the upwelling? Is there a comparison with SST L3 products? MUR is a good improvement to standard optimal interpolation, but it does appear to smooth out features in some coastal regions, such as the Great Barrier Reef.

Andy Harris: There is generally very good coverage of infra red satellite data off the coast of California, which explains why MUR is good in this study (although less good in other parts of the world). Also, tides play a role on the comparison with drifting buoys.

3 XU LI: ANALYSE SST WITHIN THE NCEP GFS

- Ensemble Kalman Filter (EnKF) method used for direct assimilation of SST every 6 hours into the NCEP GFS Numerical Weather Prediction (NWP) Model.
- Used COARE Fairall model
- SST has been improved and is generated 6-hourly with the NCEP GFS
- Weather prediction impact: Positive in the tropics, neutral to positive for NH and SH
- The study demonstrated a novel application of GHRSST-L2P data to potentially improve NWP forecasts

Questions:

Andy: Do you see any impact on the wind field?

Xu Li: Not looked into the details.

Q: Why use foundation temperature?

Xu Li: It is more practical because error covariance construction easier (?).

Other: Easier to compare. Don't have a model to get skin-temperature.

If you had very fine vertical resolution?

Craig Donlon: Foundation SST is designed to assist assimilation teams. Diurnal variability is very difficult to model and requires a lot of data. In the future you will be able to use SST as a diagnostic temperature.

Peter Cornillon: It depends what you are interested in.

Much discussion around what constitutes a "foundation SST" and how best to estimate.

4 ROSA SANTOLERI: IMPROVING THE ALTIMETER DERIVED GEOSTROPHIC CURRENTS USING SST IMAGES: FEASIBILITY STUDY AND APPLICATION ON REAL DATASETS.

- Implemented a method to combine SST and altimetry data to improve the altimeter derived surface currents
- Method required the current velocity field to obey the SST evolution equation and inverse it for the velocity vector.
- Applied the method on successive SST images using the low resolution, geostrophic altimeter velocities as background velocities.
- Over a year, new method showed significant improvement to current estimation on global comparison to drifting buoy velocities, when using high-resolution SST fields.
- This approach of linking dynamic fields can potentially be used to interpret ocean colour data.

Questions:

Craig Donlon: This kind of approach is very important to GHRSST - linking dynamic fields. It can be used to interpret ocean colour data.

Somebody: What is H in the heat equation? In a model h is integrated over the 10 m. In SST h is very small. You have to consider some depth, because of the heat transport.

SATELLITE SEA-SURFACE TEMPERATURES ALONG THE WEST COAST OF THE UNITED STATES DURING THE 2014-2016 NORTHEAST PACIFIC MARINE HEAT WAVE

Chelle L. Gentemann[(1)], Melanie R. Fewings[(2)], and Marisol García-Reyes[(3)]

(1) Earth and Space Research, Seattle, Washington, USA. cgentemann@esr.org
(2) Dept. of Marine Sciences, Univ. of Connecticut, Groton, Connecticut, USA. melanie.fewings@uconn.edu
(3) Farallon Institute, Petaluma, California, USA. marisolgr@faralloninstitute.org

1 ABSTRACT

From January 2014 to August 2016, sea-surface temperatures (SSTs) along the Washington, Oregon, and California coasts were significantly warmer than usual, reaching a maximum SST anomaly of 6.2°C off southern California. This marine heat wave occurred alongside the Gulf of Alaska marine heat wave, and resulted in major disturbances in the California Current ecosystem and massive economic impacts. Here, we use satellite and blended reanalysis products to report the magnitude, extent, duration, and evolution of SSTs and wind stress anomalies along the west coast of the continental United States during this event. Nearshore SST anomalies along the entire coast were persistent during the marine heat wave, and only abated seasonally, during spring upwelling-favorable wind stress. The coastal marine heat wave weakened in July 2016 and disappeared by September 2016.

2 INTRODUCTION

The presentation was based on Gentemann et al. (2017).

3 REFERENCES

Gentemann, C. L., M. R. Fewings, and M. García-Reyes (2017), Satellite sea surface temperatures along the West Coast of the United States during the 2014–2016 northeast Pacific marine heat wave, *Geophys. Res. Lett.*, 44(1), 312-319, doi:10.1002/2016GL071039.

ANALYZE SST WITHIN THE NCEP GFS

Xu Li[(1)], John Derber[(2)], Shrinivas Moorthi[(2)]

(1) IMSG at EMC/NCEP/NOAA, USA, Email: xu.li@noaa.gov
(2) EMC/NCEP/NOAA, USA, Email: John.Derber@noaa.gov
(2) EMC/NCEP/NOAA, USA, Email: Moorthi.Shrinivas@noaa.gov

ABSTRACT

In the current NCEP GFS, the oceanic component is represented by a single thermal variable, the Sea Surface Temperature (SST), which is prescribed with a combination of the SST analysis at the initial time and monthly SST climatology.

The term NSST (Near-Surface Sea Temperature) is introduced to describe the oceanic vertical temperature structure near the surface due to the diurnal warming and sub-layer cooling physics processes.

The NSST project aims to improve SST within the NCEP GFS by analyzing the SST together with the atmospheric analysis variables with the advanced GSI assimilation techniques and resolving the SST diurnal variability in the forecasting mode.

The foundation temperature (T_f) is selected as the analysis variable, the high frequency variability is simulated by the NSST Model, including a diurnal warming model and a sub-layer cooling parameterization scheme.

The observations used are the satellite radiances available in NCEP GFS atmospheric data assimilation system (GSI) plus AVHRR GAC radiances and in situ sea water temperature.

All the data are assimilated directly by relating the foundation temperature to the observations with a radiative transfer model (CRTM) and NSST Model.

The evaluation of the T_f analysis has shown improvement over NCEP RTG SST analysis in terms of O-B against buoys observations. The same improvement can be seen for the satellite radiance data assimilation. As to the weather prediction, there is a positive impact in tropics.

The comparison with other SST analysis products is underway.

PLENARY SESSION III: PRODUCTS DEVELOPMENTS

SESSION III REPORT

Chair: Andy Harris[(1)] – Rapporteur: Igor Tomazic[(2)]

Mittaz, Jonathan: AVHRR Level 1 errors and uncertainties: The FIDUCEO approach

Acknowledged whole team. Explained what is Fiduceo – Horizon 2020 project applying metrology techniques to satellite L1 (FCDR)/Level (CDR) datasets. Defined metrology and traceability – stressing that Metrology GUM is very important document. It is not only to trace all uncertainties, but also by removing systematic errors data are improved. At Level 1 it starts with traceability tree through calibration equation. Every term is break down into many underlying fundamental processes and looking for different sources of error (SRF, PRT representation, ...). Description of the +O term in cal. Eq – forcing investigation of assumptions to characterise known of unknowns. Through AVHRR examples – is it ok to have quadratic assumption for non-linearity effect, etc.

The effect of +O term is small for L1 but should be much bigger for L2. Described the AVHRR effect - how Fiduceo defines different uncertainty components (random, systematic, correlated). Around 12 effect tables for AVHRR – examples are detector noise, effect of solar contamination and thermal environment bias. Detector noise, random but temporary variable. Solar contamination of ICT – 4 prds, usually it is averaged but simple averaging is not representative. Thermal env. Bias – with orbit drifts the thermal env changes introducing a time variable term correlated with instrument temperature. For NOAA 19 there is change of the environment, for MetopA is OK – same orbit all the time. NOAA 09 and 12 – more complex since the orbit drifted. Project is also addressing harmonisation across different sensors. For FCDF this is crucial to reduce any errors. There will be three sets of FCDR file formats: easy (lat/lon/angles/quality/BT + random and non-random unc for all channels at pix level), full (all effects table information, unc + all covariances and error corr. Information) and ensamble (N deviations from Easy FCDR BTs). Beta Easy FCDR available before the end of year for beta testing. It is not only about uncertainty but also about improved radiances!!! Fiduceo workshop in April/May 2018.

Koner, Prabhat: Quasi-deterministic cloud detection for infrared sea surface temperature retrieval from satellite imager measurements

Presented two papers from RSE as a reference to the presentation. Described all the satellite data and its download sources, forward model, in situ and model data. They proposed quantitative test for cloud algorithm. Previous validations are based on visually estimated cloud amounts (Kotarb et al., 2009). New quantitative test is called experimental filter (EXF), and is using in situ SST data and radiative transfer model to define the metrics (below 1 is cloud free). It was tested with existing cloud detections (GOES-13 and MODIS-A). Many outliers and cloud leakages using the standard cloud. Validation done using SST4 with coefficients calculated based on matchups Nov2013. Presented history of cloud detections using spectral differences. Presented normalised spectral differences in cloud and mask error algorithm – spectral difference between MODIS 13.4 and 11 could be explored more. Presented RT double difference tests – using 3.9 and 4 µm - unique in cloud literature. First applied to GOES-13 and improved for MODIS. Showed spatial coherence test: 5x5 grid box (max-cpix<0.6K) – but more then 0.3 K/km fronts are screened out. Additional cloud detection using pdsst scheme: Ttls developed for 3- parameter retrieval. Showed

GOES-13 time series (2010-2014) using different cloud schemes (Bayesian and cloud and error mask) over 50 months and with 5 milions of matchups. Data coverage increased for CME mask and average MTLS RMSE reduced for 22%. For MODIS-A time series comparsion between CEM and operational cloud mask show improvement from 0.51 to 0.34 K. CEM is independent of locations, season and sensor. Not yet fully optimised and can be improved. Currently works only on matchups, but ready for operational use.

Wang, Sujuan: FY-3C VIRR operational sea surface temperature product

Presented operational SST product derived from VIRR (visible infrared radiometer) aboard FY-3C satellite. Overview of the full SST scheme: matchup, regression, retrieval, validation and discussion. For matchups, iQUAM is used by extracting 3x3 pixel box centred on VIRR measurement. Operational MDB is built with 20 days delay. For regression, matchup window is 1.1 km in space and 1 hour in time, only high-accuracy drifters are used. Separate regression for daytime and nighttime – solar zenith angle (Sza<85 daytime, otherwise nighttime). Least-square reg. used + outliers removed using median±2STD. Validation statistics on monthly basis. NLSST(D) is the best algorithm from 3 day time sst algorithms (MCSST, QDSST, NLSST). Accuracy of NOAA19 is better compared to FY-3C/VIRR. Based on MDB analysis, above 119 SZA, TC_N is the best, but when used in sst retrieval the performance of TC_N is worse compared to MC_N. Contamination of 3.7µm and in twilight. Quality control – SST quality control: uniformity test, ref_sst test, zenith and glint test. SST quality flag is stored in packed 8-bit word. Validation of FY-3C/VIRR SST against in situ data and global gridded L4 SST. Coeffs derived from Oct-Dec2015 and validated using Nov2016-Jan2017. Comparison of VIRR and MODIS SST with in situ data – warm bias after October 2014. Cal_coeffs were updated, the SST_coeffs updated two months later. During that time SST bias increased. Between Feb2015-Jan2016 second version of SST coeffs is used. There is warm bias in the night time. BB temperature increased in the same period, without changing the calib coefficients. Form Jan2016 new set of SST coefficient is used. Cloud contamination still exist. There is a striping effect. There is a sensor performance degradation, and the performance of 3.7 um band of VIRR is worse than N19 AVHRR. Summary, FY-3C against in situ: daytime bias is 0.17 k with std 0.52 K, and nighttime std is 0.54 K. Agains OISST, the daytime bias is -0.1 K with 0.8 K std and nighttime bias is 0.01 K with 0.78 K std.

Chen, Chuqun: Sea surface temperature in South China Sea retrieved from Chinese satellite FY-3B VIRR data

Description of the SST, FY-3 satellite, VIRR instrument and South China Sea (marginal sea, area 3.500.000 km2, 2-23N, 103-118E). Presented a cloud detection (He, Q.J. 2011), matchup method using ship observation data (2 years, 20607 matchups). NLSST algorithm (Walton et al., 1998) was selected. Half of the samples in daytime and nighttime are selected for testing and the other half for coefficient generation. The least absolute deviation method is applied to analyse errors between the ship and satellite SST. For SCS, daily and then monthly and seasonal mean is generated for 2015. Compared against Modis-retrieved SST, and similar pattern was observed. The highest monthly SST mean occurs in June, instead of July, mainly due to the stronger Monsoon and vertical mixing in July. Acknowledged project from National Natural Science Foundation of China and Chinese Academy of Sciences.

Embury, Owen: SST retrieval methods in the ESA Climate Change Initiative

CCI - programme to produce satellite based CDR, targeting 13 ECVs including SST. For SST-CCI CDR - retrieval should be independent of in situ SST measurements, quantified accuracy and sensitivity, uncertainty estimates, harmonised for stability. Reference sensors are ATSR 1,2 and AATSR, meteorological sensors AVHRR/2s and AVHRR/3s with GAC L1, OSTIA SST daily analyses. Primary retrieval is skin-SST. Differences against in situ drifters as function of wind speed and time difference. Performed skin-to-depth adjustment using Fairall Kantha-Clayson model (UKMO code) to correct for time/depth differences and different satellite overpass time. ATSR SST retrieval – update from ACR project, linear regression based on RT simulation, coefficients banded by TCWV, nadir and forward path and year. Interpolate between bands as required. Accurate RT simulations: Line-by line: LBLRTM using 2100 profiles from ERA-40 (Chevallier 2002). Calculated aerosol scattering using RTTOV and DISORT. Retrieval coeffs. Independent of in situ SST and using aerosol-robust formulation for ATSR1 (not needed for others). Described AATSR 12 micron anomaly (~0.2 K colder than expected). During ARC, could not use 12 as reference. Used dual-view 3.7 and 11 as reference. Small error in non-linearity adjustment, 40 nm shift in SRF. In SST-CCT Phase II uses D3 – including 12 um channel retrieval as reference. D3 biases are small, D2 biases ~0.1 K. D3 expected to be the best retrieval due to the higher information content from more channels. Use D3 as reference and correct D2 to match D3. Comparison against in situ (drifters, moored, radiometers). ATSR MDB is 10 times smaller compared to AATSR MDB. ATSR SST uncertainties: due to correlated effects and random BT noise. Atmospheric correction smoothing - reducing noise without reducing features. Atmospheric correction parameter is function of atmospheric state and is replaced by NxN average to give noise-reduced SST. This introduce correlated uncertainties and L3 is calculated from unsmoothed SST. After smoothing, fronts more clear. Described AVHRR SST retrieval based on OE (forward model and tangent linear matrix) and defined uncertainties. AVHRR BT improvements include new solar contamination, per-pixel nedt calculated from space view counts. Cold biases in SST retrievaldue to strat. aerosol from Mount Pinatubo and El Chichon. Avhrr is not capabale of atsr style aerosol robust retrieval. Avhrr smoothed OE is extend smoothed of Merchant et al, 2013. Include average BTs in observation vector, only central pixels for retrieval is used, but surrounding clear-sky pixels are used for smoothing. Surrounding SST pixel is independent of centre pixel. Uncertainties: random, locally correlated, systematic, depth adjustment and L3 sampling.

Ignatov, Alex: ACSPO SSST products and monitoring for GOES-16 and Himawari-8

Acknowledged all colleagues for different system components. GOES-R from Nov 2016 in constellation with Himawari-8. Long-term validation. GOES-R was renamed to GOES-16. Still in experimental phase, not yet operational. Nov 2017 -> moved to GOES-East position. 2018: launch of GOES-S. Himawari-8: Oct 2014. Apr 2015: pre-op ACSPO 2P SST generated. Jul2015: operational. H9 launched in Nov 2016, now in testing/storage mode. Geos-R and H-8/9 form a new gen geo SST constellation. Same imagers ABI and AHI. Heritage NOAA SST products: G13, G15, MSG3, H7. Current new-gen configuration: G16 and H8. Future new constellation: G17, G16, MTG, H8. Indian Ocean – 2025 – new geo station satellite. Abi/AHI much better, at least 2x better compared to GOES/H7. More bands for SST, 8.6, 10.4, 11.2 and 12.4 + 3.9 to preserve continuities. Spatial 2 km, compared to 4 km, temporal resolution 15 or 10 min. ACSPO ABI/AHI algorithm. Depths SST: obtained by piece-wise regression vs. in situ SSTs. Presented clear-sky mask tests, and current SST algorithm. ABI SST vs VIIRS: presented the problem with clear sky masking – overflagging and comparison with VIIRS. For new ABI there is noise over fronts and some striping. Similar to AHI, there is overflagging. G16/ABI and H8/AHI SST vs. in situ. Specification is +-0.2 K – mean SST sat – drifter. For SD specification is 0.6 K. Currently they are all within specification. Opening data by the end of summer.

Performed comparison with sub-skin SST without SSES bias correction and with depth SST with SSES bias correction. There will be reprocessing of G16 and H8 SST. Diurnal cycle in ABI/AHI SSTs. Showed monthly mean between satellite SST and CMC as average difference over full disk space and one month, both for H8 and G16. Calculated both for subskin and depth SST. Diurnal cycle (amplitude) is ~0.5 K. But, depth SST is 0.2 K smaller compared to skin SST. Depth SST is slightly left. Based on one month (2017-05). Similar processing for different products: G15, G13, H07 and MSG.

Petrenko, Boris: Diurnal cycles in the NOAA ACSPO "depth" and "skin" SSTs from the new generation ABI/AHI geostationary sensors with ACSPO

ABI/AHI with ACSPO allows monitoring of diurnal cycle (DC) in SST. Quantitative estimation of DC shapes requires further SST optimisation. Big differences in SSTskin vs. SSTdepth. Two ABI/AHI SST products GR and PWR SST approximation of SSTskin and SSTdepth. The focus is how to improve ACSPO AHI/ABI product for DC monitoring. Presented current ACSPO SST algorithm – single set of coefficients for day/night to minimise discontinuities. Shown current differences between GR and PWR SST algorithms. Both algorithms use coefficients fitted to in situ measurements. There is residual DC magnitude wrt in situ (~0.15 K). To improve DC in SST depth – include SSTskin/SSTdepth bias. To parametrise this bias include wind speed and local solar time. New SST algorithm to include this variables: modified PWRdepth SST. Small improvements of PWRdepth SST SD wrt PWR SST SD wrt in situ SST. More consistent dependencies for day time and nighttime wind speed analysis. Comparison against local solar time (with CMC) shows DC magnitude closer to in situ SST and shifts the times of DC min/max closer to in situ SST. Improved skin SST (PWRskin SST) uses segmented SST domain, and coefficients are trained with "mean sensitivity=1". Statistics with PWRskin SST wrt GR against in situ for wind above 6 m/s shows SDs are smaller, mean sensitivity closer to 1 and SDs of sensitivities are smaller. Shown statistics for PWRskin as function of latitude – SST biases more uniform and SD is smaller. DC magnitude in PWRskin SST is significantly reduced – more uniform biases. Shown examples of GR, PWRskin and PWRdepth SST for AHI. DC magnitude and SD wrt CMC is reduced from GR→PWRdepth→ PWRskin. Max/min of DC in PWRdepth SST is later then in PWRskin and GR. PWRskin reduces diurnal signal when compared with GR SST. PWRskin SST reduces cloud leakages and SD, reduces cold SST anomaly over the Atlantic Ocean. Summary: two PWR algorithms developed, skin and depth to reproduce the diurnal cycle. PWRdepth account for dependencies on wind and LST, and improves reproduction of DC in in situ SST. PWRskin minimises regional biases and variations in sensitivity and improves the reproduction of DC in SSTskin. Future - find new source of ground truth for SSTskin and SSTskin validation, more testing.

Gangwar, Rishi Kumar/ Thapliyal, Pradeep: Radiative transfer model based bias correction in INSAT-3D/3DR thermal observations to improve sea surface temperature retrieval

Shown ISRO current satellites for EO. CNES-ISRO: Ocenasaat-2 ; MT(madras, saphir, scarab, rosa), saral (altika, argos). Scatsat-1; Oceansat-3 (OCM, SSTM, SCAT) (2018). GEO: INSAT-3d imager and sounder. Insat-3D/3DR/3DS imager and sounder. Launch 3D 2013; 3DR 2016. 3DS imager: 6 channel radiometer, 1 km for VIR/NIR, and 4 km for TIR. Shown all products: sst, cloudmask, fog, … Presented future Indian geo satellite (GISAT). Launch 2019. MX-LWIR, multispectral-long wave infrared. TIR channels, every 10 minnutes interval, 30-minutes triplet every 6 hour, 1.5 km. INSAT-3D SST operational algorithm: based on simulated dataset (MODTRAN RT model). SRF and NEDT. Coefficient generated for seven satellite zenith angles. Day-time and night time equation algorithm. New algorithm: based on PFAAST RT model + ECMWF training set. Single

SST equation – not using 3.9. Using zenith angle inside the algorithm. Cloud detection; average BT of clear pixels in neigh 3x3 pixel to reduce the noise. Quality control of derived SST using SSTclim. Bias correction in observation with respect to RT simulations. Correction is based on satellite zenith angle. Shown differences (and improvement) before and after BT correction for each channel wrt satellite zenith angle. Comparison against daytime MODIS are shown for INSAT-3D and 3DR. Differences is very small. Performed validation with in situ SST (15 min, and 4 km distance). Using bulk sst from iquam. Comparison between INSAT-3D/3DR with MODIS for day and nighttime and for operational algorithm and new modified algorithm. Bias and std are smaller in all cases. Conclusion: there are zenith angle dependant biases based on MODIS-SST analyses. Implemented RT model bias correction procedure using ECMWF and INSAT-3D/3DR matchup data. Modified algorithm shows improvement over the operational algorithm. Zenith angle dependency in observed TIR-1/2 BT require further investigation.

Piollé, Jean-François: Copernicus Sentinel-3 match-up databases - Felyx in support to satellite Cal/Val

Acknowledged everyone. Gave background on importance of performing intercomparisons. Description of felyx system. Extraction of data from static and dynamic sites, indexing metrics, and assembling in situ data. Main outputs are miniprods and metrics, assembled multi-sensor matchup files, display of metrics. Implementation is in pyhon, open source + open source frameworks for big data and distributed processing (ElasticSearch, RabbitMQ, Celery, …). Shown data access to Sentinel-3 SLSTR marine products over ODA and CODA. Presented in situ sources: CMESM (moored and drifting buoys and Argo data) and in situ radiometer network. Shown felyx MDB workflow: 2 h (12 h for Argo), 5 km, 21x21 box, +- 6 h in situ data history. In situ data: Coriolis (CMEMS), ISAR radiometer. S3 data: L1 IR channels, L2 (SST) – all fields + Metop-B/AVHRR, MSG/SEVIRI, OLCI. Shown content of MDB and presented full traceability of information in matchup using jupyter notebooks. Shown overview of all available MDBs with planned improvements and changes. Future improvements include ingestion of more radiometers, HR drifters, adding SLSTR visible channels, SST depth adjustments. Presented matchup monitoring, matchup analysis by G.Corlett and OSI SAF SLSTR MDB FA (A. MArsoun). Shown intercomparison of MDBs. Presented open source analytics using jupyter and kibana and integration in processing environment using ansible and airflow. Conclusion: felyx is open source framework for data intercomparison, collection of mappers for different products/formats. Metrics still further exploited. Major asset in S3 cal/val activity. Possible way forward for build consistent matchup dataset in GHRSST; sharing MDB; application for climate data record assessment. Possible group/task team on shared open source tools. Thanked ESA, EUMETSAT and IFREMER for supporting felyx development. Provided contact information for felyx, links to source code and virtual machine for testing felyx. New release in July with new deployment procedures and invited everyone for contribution and shared development.

AVHRR LEVEL 1 ERRORS AND UNCERTAINTIES: THE FIDUCEO APPROACH

Jonathan Mittaz[(1)], Christopher Merchant[(2)], Marine Desmons[(3)], Emma Woolliams[(4)]

(1) University of Reading, Reading, UK, Email: j.mittaz@reading.ac..uk
(2) University of Reading, Reading, UK, Email: c.merchant@reading.ac..uk
(3) University of Reading, Reading, UK, Email: m.desmons@reading.ac..uk
(4) National Physical Laboratory, Teddington, UK, Email: emma.woolliams@npl.co.uk

ABSTRACT

As part of the Fidelity and uncertainty in climate data records from Earth Observations (FIDUCEO) project (www.fiduceo.eu) we are creating a new improved Fundamental Climate Data Record (FCDR) for the AVHRR which will be used to generate SST CDRs. Unlike the current available AVHRR Level 1 data (such as that available from the NOAA archives), the FIDUCEO Level 1 will contain complex uncertainty information at the pixel level and higher which are based on metrological techniques. As such, the creation of this data involves a very detailed study of sources of error and uncertainty in the AVHRR, some of which can directly impact SST retrievals. In this presentation we will discuss the FIDUCEO approach to Level 1 data production and will show the different sorts of uncertainty that will be provided together with their error covariance structures. We will also discuss the FIDUCEO approach to sensor-to-sensor Harmonisation and will then show specific examples of remaining problems (such as variable noise sources) and other sources of IR calibration error (with proposed corrective solutions) that can impact SST generation. Finally we will report of the status of the FIDUCEO Level 1 data together with a description of the associated formats which range from an Easy format, an Ensemble format and a Full (all uncertainty components) format.

QUASI-DETERMINISTIC CLOUD DETECTION FOR INFRARED SEA SURFACE TEMPERATURE RETRIEVAL FROM SATELLITE IMAGER MEASUREMENTS

Prabhat Kumar Koner

ESSIC, University of Maryland, USA, Email: pkoner@umd.edu

ABSTRACT

Cloud detection is the part of the any product development from satellite infrared (IR) measurement. The product quality and error statics from IR satellite measurements are highly dependent on the cloud detection methodology. An innovative and novel cloud detection methodology, combining with spectral differences and radiative transfer calculation especially using powerful double difference method, will be presented. The quality of the new cloud detection has been compared with other prevalent cloud detection methods using error statics of the sea surface temperature (SST) retrieval and it is found that a significant increment of data coverage along with error reduction of retrieved SST. Both polar and geo-stationary orbital instruments, e.g. MODIS, VIIRS and GOES-13, are considered in this study.

FY-3C VIRR OPERATIONAL SEA SURFACE TEMPERATURE PRODUCT

Sujuan Wang [(1)], Peng Cui[(2)] , Peng Zhang[(3)],Feng Lu[(4)] ,Maonong Ran [(5)]

(1) National Satellite Meteorological Center, CMA ,Beijing, China, Email: wangsj@cma.gov.cn
(2) National Satellite Meteorological Center, CMA, Beijing, China, Email: cuipeng@cma.gov.cn
(3) National Satellite Meteorological Center, CMA, Beijing, China, Email: zhangp@cma.gov.cn
(4) National Satellite Meteorological Center, CMA, Beijing, China, Email: lufeng@cma.gov.cn
(5) Beijing HuaYun Shinetek Satellite Application Engineering Technology Company Limited, Beijing, China, Email: ranmn@cma.gov.cn

ABSTRACT

As the first operational polar-orbiting satellite of the second batch of FY-3, FY-3C was launched on 23 September 2013. The visible infrared radiometer (VIRR) is a 10-channel radiometer for multi-purpose imagery with 1.1km resolution at nadir. FY-3C Satellite data is processed by data preprocessing system (DPPS) and products generation system (PGS) of FY-3C ground segment. FY-3C/VIRR L1B data from DPPS and cloud mask product from PGS are used to estimate FY3C/VIRR SST.

FY3C/VIRR granule SST is derived from the split-window MCSST algorithm and stored in 5-minute granule (2048×1800 pixels). Based on the granule SST product, the 5km longitude/latitude grid daily, 10-day and monthly SST products are also derived, stored by daytime and nighttime separately.

The validation of the FY-3C/VIRR granule SST is done by using the operational MDB, and by comparison with daily Reynolds SST. It was shown that from 1 November 2016 to 31 January 2017, comparison with drifter (FY-3C minus in situ), the bias of daytime is 0.17K with a standard deviation of 0.52K, and the bias of nighttime is 0.07K with standard deviation of 0.54K. Comparison with daily Reynolds SST (FY-3C minus Reynold), the bias of daytime is -0.08K with a standard deviation of 0.76K, and the bias of nighttime is -0.05K with standard deviation of 0.78K.

MONTHLY SST RETRIEVED FROM FY-3B DATA IN SOUTH CHINA SEA

Chuqun Chen [(1)(2)*], Quanjun He[(3)], Shilin Tang [(1)(2)***], Haibin Ye[(1)]**

State key Lab of Tropical Oceanography, South China Sea Institute of Oceanology, Chinese Academy of Sciences, 164 West Xingang Road, Guangzhou, China, 510301.
University of Chinese Academy of Sciences, 19A Yuquan Road, Beijing, China, 100049.
The Guangdong Ecological meteorological Center, 312 Dongguanzhuang Road, Guangzhou, China, 510080.
*Emails: *cqchen@scsio.ac.cn, **hequanjunsx@163.com ; ***sltang@scsio.ac.cn*

ABSTRACT

In the surface layer of the ocean, Sea Surface Temperature (SST) is the most important parameter, which is widely applied for studying water masses, air-sea interaction, marine ecosystem and environment, and other subjects. In the last several decades, a great many satellites with thermal infrared sensors have been launched and huge thermal infrared remote sensing data were collected for detection of SST. With the continuous improvement on accuracy, the satellite remote sensing technique has become the dominant approach for SST detection.

In this presentation, the thermal infrared data collected by FY-3B were employed for retrieval of SST in the South China Sea. FY-3B is one of the second generation of Chinese meteorological satellite on polar orbit, it has VIRR (Visible Infrared Radiometer) sensor with 10 bands, of which, band 4 covers 10.3~11.3um and band 5 covers 11.5~12.5um, similar to NOAA/AVHRR.

The ship/bouy-measured in-situ SST dataset in 2011 and 2012 were collected and totally 20607 (of which 11419 in daytime and 9188 in nighttime) of the ship-measured SSTs were selected on consideration of the quality, the measurement time and the measurement location matching with cloudy-free Fy-3B data. Based on the well matched in-situ SST and FY-3B VIRR data, a non-linear SST (NLSST) algorithm was developed and applied for retrieval of SST in the South China Sea. The monthly mean SST distribution image maps of South China Sea were integrated. The monthly mean SST image maps show that the maximum monthly mean SST occurs in June, although in July and August there is a stronger solar heating. It possibly due to the monsoon-induced mixing, which results in lower SST.

1. INTRODUCTION

Sea Surface Temperature (SST) is the most important parameter, which is widely applied for studying water masses, air-sea interaction, marine ecosystem and environment, and other subjects. Scientists started to measure SST by remote sensing in 1960s[1]. However, thermal radiation received by satellite sensors surfers the effect of atmosphere (especially for absorbing of the water vapor in atmosphere) between earth and satellite[2]. Because the differential absorption properties of water vapor in the two channels enabled one to determine the water vapor absorption correction, scientists proposed to estimate the sea surface temperatures from two infrared window measurements with different absorption[3, 4].

At present, the satellite remote sensing has been the most important method to explore the global sea surface temperature (SST). Lots of sensors onboard the satellites have the ability to measure the SST, such as NOAA/AVHRR [5, 6], EOS/MODIS[7], NPP/VIIRS[8], GOES[9], MSG[10] and Himawari [11]. FengYun-3 (FY-3)[12] is the second generation polar-orbiting meteorological satellite series of China, and FY-3B is the second satellite launched in 2010. The visible infrared radiometer (VIRR)[13] is a main instrument aboard the FY-3B. VIRR has 10 bands, and the spectral ranges of the thermal infrared bands 4 and 5 are

10.3~11.3μm and 11.5~12.5μm, respectively, similar to NOAA/AVHRR. So the FY-3B/VIRR data can be used to retrieve the surface temperature of land and ocean.

In this presentation, the simultaneously ship/buoy observation SST data and satellite data were collected from 2011 to 2012, and the matchup dataset was generated to realize the SST algorithm. Also, this SST algorithm was applied to retrieve the SST products in South China Sea (SCS).

2. SST ALGORITHM

2.1. Selection of SST algorithm

Many algorithms have been developed to retrieve the SST for satellite remote sensing data [8, 14, 15]. The multiple-channel SST (MCSST) [5] and non-linear SST (NLSST)[16] algorithms are the most widely optional algorithms, they correct the atmospheric effect using the difference of brightness temperature of split window channels. The formula of these two algorithms is similar, but the NLSST used a first-guessed SST value to adjust the difference of brightness temperature between 11 and 12μm bands. The studies [16-18] showed that the NLSST had better accuracy than MCSST, so the NLSST was selected to retrieve the SST for VIRR data. The formula of NLSST is shown as following:

$$SST= k0+k1*T11+k2*Tsfc*(T11-T12)+k3*(T11-T12)*(\sec(\theta)-1.0), \quad (1)$$

where the T11 and T12 is the brightness temperature of 11 and 12μm bands. θ is the sensor zenith in angular. k0, k1, k2 and k3 are coefficients regressed by matchup dataset. Tsfc is the first guessed SST value. In this paper, the daily optimum interpolation SST (OISST)[19] is used as Tsfc and can be downloaded from the website of national centers for environmental information of NOAA.

2.2. Realization of SST algorithm

Firstly, the cloud detection[20, 21] is executed and the cloud and land data is removed from all VIRR data. Secondly, the anomaly values are eliminated from ship/buoy observation SST data. Then the matchup dataset is generated according to the rule of closest time and location. In final, there are 20607 samples in matchup dataset, of which 11419 samples in daytime and 9188 samples in nighttime. Half of the samples in daytime and nighttime are respectively chosen by random function, and used to acquire the coefficients of NLSST algorithm by building the multivariable linear regression model (see table 1).

Table 1 Regression coefficients of NLSST algorithm

	k_0	k_1	k_2	k_3
Daytime	13.8235	0.9452	0.0098	0.7259
Nighttime	5.0800	0.9776	0.0078	0.6933

2.3. Evaluation of SST algorithm

The another half of samples, i.e. 5710 samples in daytime and 4094 samples in nighttime, are independent from the samples used in realization of NLSST algorithm, so they can be used to test the accuracy of NLSST algorithm. The least absolute deviation method is applied to analyze the errors between the ship observation SST and retrieved SST. The error statics are shown in table 2.

Table 2 Error statics of retrieval results

	Bias(K)	Standard deviation (K)	Absolute deviation (K)	Correlation coefficient
Daytime	0.006	0.688	0.503	0.990
Nighttime	0.018	0.659	0.471	0.989

From the statistics, we can see the accuracy of developed algorithm is quite good and is consistent with that of other SST algorithms[18, 22, 23]. In addition, the plot between ship/buoy observation SST and satellite-retrieved SST and distribution of absolute errors are show in figure 1. The correlation is very high and distribution of error is reasonable.

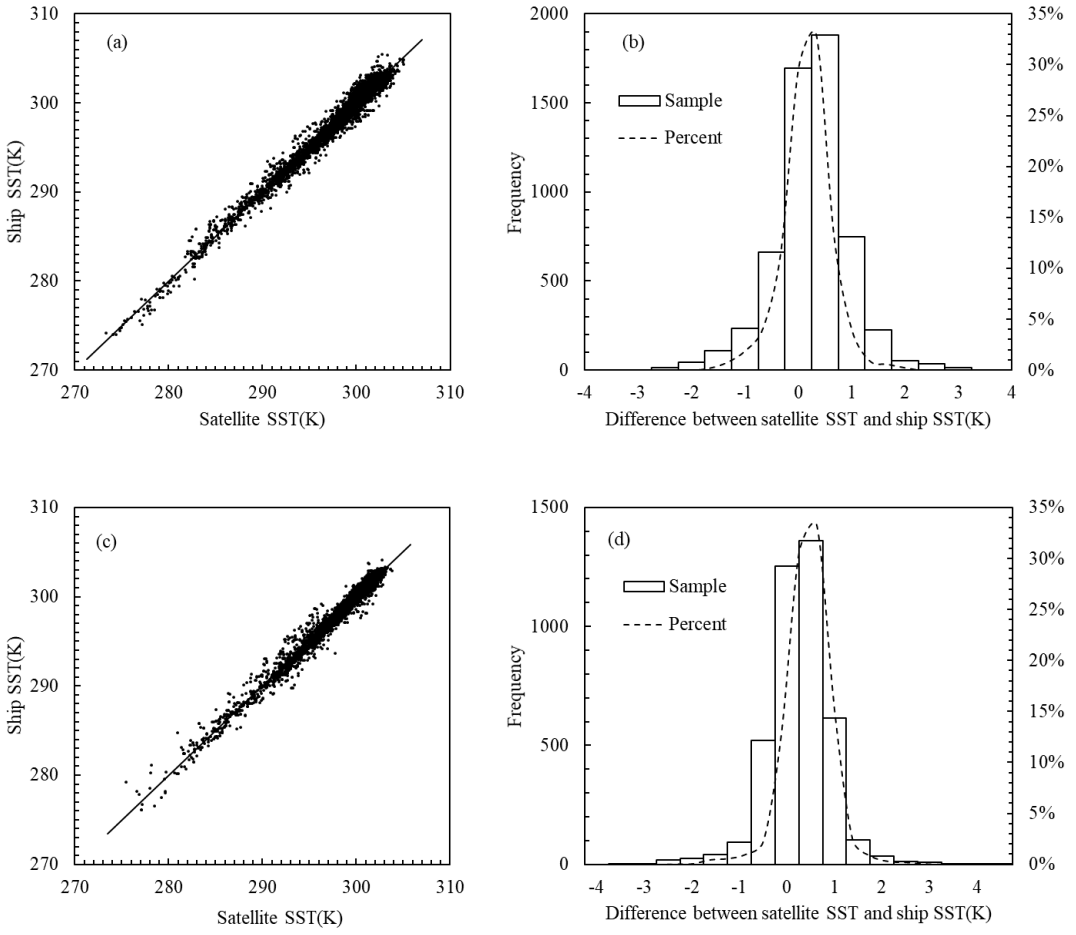

Figure 1 The correlation plot and error distribution between satellite SST and ship SST at daytime(a,b), nighttime(c,d)

3. THE SST IN THE SOUTH CHINA SEA

The developed NLSST algorithm is used to retrieve the SST products in SCS, and then the mean monthly SST is calculated. The mean monthly SST image maps over SCS in summer, 2015, are shown in Figure 2. According to the distribution of mean monthly SST (see figure 2), the maximum value of mean monthly SST in SCS occurs in June, instead of in July or August when there is greater solar radiation intensity. This is mainly related to the stronger surface-layer-mixing by the stronger monsoon over SCS in July or August, the cooler water from the subsurface layer decreases the SST of surface layer.

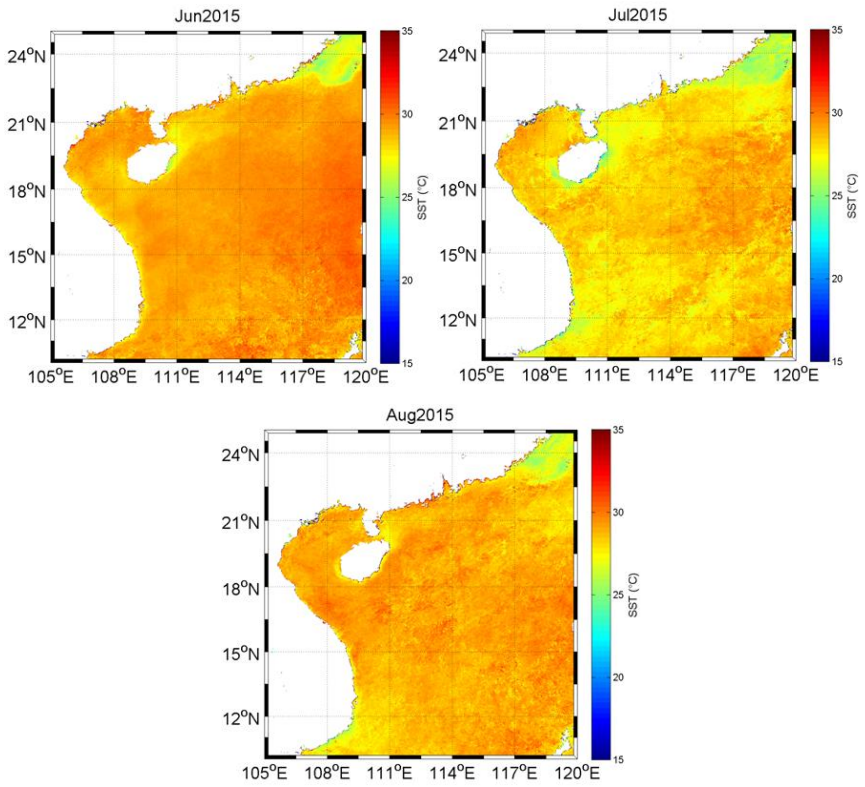

Figure 2 The mean monthly SST over South China Sea in Summer (June, July and August) of 2015

4. SUMMARY AND DISCUSSION

Based on the simultaneously FY-3B/VIRR data and ship/buoy observation SST data, the SST retrieval algorithm was developed. According to the evaluation of SST algorithm, all of the errors are less than 0.7K in daytime and nighttime. So this algorithm is capable of retrieving SST products from FY-3B/VIRR data.

The mean monthly SST products over SCS is retrieved. It can show the distribution of thermal fields and the characteristics of temperature variance in SCS. It is different from the mean monthly air-temperature, the maximum value of mean monthly SST in SCS occurs in June, instead of in July or August. As the stronger mixing in July and August reduces the surface SST value.

As the daily SST varies from the first day to the last day of a month. Generally, not all the 30 days' SST data are available due to clouds. So, the mean monthly SST depends on the date in which the SST is available. It should be better if consideration of dates of available SST in calculation of mean monthly SST.

5. ACKNOWLEDGEMENTS

The authors are very grateful to Guangzhou Meteorological Satellite Ground Station and NSMC/CMA for providing the FY-3B/VIRR data. Many thanks to NCEI/NOAA for providing OISST data. This research is jointly supported by The scientific research key project from Guangzhou city (No. 201707020031), pre-research project (No.201503) from Innovation Academy for Marine Information Technology, Chinese Academy of Sciences, and the National Natural Science Foundation of China (No. 41276182).

6. REFERENCES

1. Saunders, P.M., Aerial measurement of sea surface temperature in the infrared. Journal of Geophysical Research, 1967. 72(16): p. 4109-4117.
2. Anding, D. and R. Kauth, Estimation of sea surface temperature from space. Remote Sensing of Environment, 1970. 1: p. 217-220.
3. Prabhakara, C., G. Dalu, and Y.G. Kunde, Estimation of sea surface temperature from remote sensing in the 11- to 13-µm window region. Journal of Geophysical Research, 1974. 79(33): p. 5039-5044.
4. McMillin, L.M., Estimation of sea surface temperatures from two infrared window measurements with different absorption. Journal of Geophysical Research, 1975. 80(36): p. 5113-5117.
5. McClain, E.P., W.G. Pichel, and C.C. Walton, Comparative performance of AVHRR-based multichannel sea surface temperatures. Journal of Geophysical Research, 1985. 90(C6): p. 11587-11601.
6. Walton, C.C., Nonlinear multichannel algorithms for estimating sea surface temperature with AVHRR satellite data. Journal of Applied Meteorology, 1988. 27(2): p. 115-124.
7. Minnett, P.J., et al. Sea-surface temperature measured by the moderate resolution imaging spectroradiometer (MODIS). in Proceedings of the IGARSS 2002. 2002.
8. Petrenko, B., et al., Evaluation and selection of SST regression algorithms for JPSS VIIRS. Journal of Geophysical Research: Atmospheres, 2014. 119(8): p. 4580-4599.
9. Petrenko, B., et al., Development and evaluation of SST algorithms for GOES-R ABI using MSG SEVIRI as a proxy. Remote Sensing of Environment, 2011. 115(12): p. 3647-3658.
10. Le Borgne, P., H. Roquet, and C.J. Merchant, Estimation of sea surface temperature from the spinning enhanced visible and infrared imager, improved using numerical weather prediction. Remote Sensing of Environment, 2011. 115(1): p. 55-65.
11. Kurihara, Y., H. Murakami, and M. Kachi, Sea surface temperature from the new Japanese geostationary meteorological Himawari-8 satellite. Geophysical Research Letters, 2016. 43: p. 2015GL067159.
12. Dong, C., et al., An overview of a new Chinese weather satellite FY-3A. Bulletin of the American Meteorological Society, 2009. 90(10): p. 1531-1544.
13. He, Q., et al., FY-3A/VIRR SST retrieval using nonlinear algorithm. Meteorological Monthly, 2013. 39(1): p. 74-79.
14. Casey, K.S., et al., The past present, and future of the AVHRR pathfinder SST program, in Oceanography from Space, V. Barale, J.F.R. Gower, and L. Alberotanza, Editors. 2010, Springer Netherlands. p. 273-287.
15. Koner, P. and A. Harris, Sea surface temperature retrieval from MODIS radiances using truncated total least squares with multiple channels and parameters. Remote Sensing, 2016. 8(9): p. 725.
16. Walton, C.C., et al., The development and operational application of nonlinear algorithms for the measurement of sea surface temperatures with the NOAA polar-orbiting environmental satellites. Journal of Geophysical Reseach, 1998. 103(C12): p. 27999-28012.

17. Li, X., et al., Deriving the operational nonlinear multichannel sea surface temperature algorithm coefficients for NOAA-15 AVHRR/3. International Journal of Remote Sensing, 2001. 22(4): p. 699-704.
18. Hosoda, K. and H. Qin, Algorithm for estimating sea surface temperatures based on Aqua/MODIS global ocean data. 1. Development and validation of the algorithm. Journal of Oceanography, 2011. 67(1): p. 135-145.
19. Reynolds, R.W., et al., Daily high-resolution-blended analyses for sea surface temperature. Journal of Climate, 2007. 20(22): p. 5473-5496.
20. He, Q.-J., A daytime cloud detection algorithm for FY-3A/VIRR data. International Journal of Remote Sensing, 2011. 32(21): p. 6811-6822.
21. He, Q., Night-time cloud detection for FY-3A/VIRR using multispectral thresholds. International Journal of Remote Sensing, 2013. 34(8): p. 2876-2887.
22. Tu, Q., D. Pan, and Z. Hao, Validation of S-NPP VIIRS sea surface temperature retrieved from NAVO. Remote Sensing, 2015. 7(12): p. 17234-17245.
23. Huynh, H.-N.T., et al., Reconstruction and analysis of long-term satellite-derived sea surface temperature for the South China Sea. Journal of Oceanography, 2016: p. 1-20.

SST RETRIEVAL METHODS IN THE ESA CLIMATE CHANGE INITIATIVE

Owen Embury [(1)], Chris Merchant[(2)]

(1) Department of Meteorology, University of Reading, UK, Email: o.embury@reading.ac.uk
(2) Department of Meteorology, University of Reading, UK, Email: c.j.merchant@reading.ac.uk

ABSTRACT

The ESA Sea Surface Temperature Climate Change Initiative (SST-CCI) aims to produce a ~35 year record of satellite-only SST. The core products are level-2 and level-3 from the Along Track Scanning Radiometer (ATSR) and Advanced Very High Resolution Radiometer (AVHRR), and a level-4 SST analysis based on the Met Office OSTIA system.

In this presentation we describe the SST retrieval algorithms used in SST-CCI. For the ATSR instruments we use a dual-view retrieval based on methods developed for the ATSR Reprocessing for Climate project. For the AVHRR instruments we use Optimal Estimation referenced to the ATSR SST for consistency. In addition to the SST we also provide estimates of the uncertainty due to uncorrelated errors, synoptically correlated errors, and sampling errors. In order to reduce the effects of instrument noise in L2P products we use a multiple-pixel retrieval.

ACSPO SST PRODUCTS AND MONITORING FOR GOES-16 AND HIMAWARI-8

Alexander Ignatov[1], Irina Gladkova[1,2,3], Yury Kihai[1,2], Maxim Kramar[1,2], Andrew Fitzgerald[3], Boris Petrenko[1,2], Xinjia Zhou[1,4], Kai He[1,2], Yanni Ding[1,4]

(1) NOAA STAR, USA; Alex.Ignatov@noaa.gov
(2) GST, Inc, Greenbelt, MD, USA
(3) CCNY, New York, NY, USA
(4) CSU CIRA, Fort Collins, CO 80521, USA

ABSTRACT

New generation US geostationary satellite, GOES-R with the Advanced Baseline Imager (ABI) onboard, was launched on Nov. 19 2016 and renamed GOES-16 following the successful completion of initial onboard checks. A twin sensor, Advanced Himawari Imager (AHI), has been flown onboard Himawari-8 since Oct. 2014. ABI/AHI offer improved spectral coverage (5 bands at 3.7, 8.5, 10.4, 11.2, 12.3 μm), spatial resolution (2km), revisit time (10/15min), and radiometric/navigation/co-registration.

The focus of this presentation is on a new cloud masking procedure that exploits the wealth of high temporal resolution; and the new hourly ACSPO SST product and its evaluation using the redesigned and upgraded NOAA monitoring systems to include geo-related capability.

The cloud masking procedure, specifically designed for geostationary instruments, uses a combination of various time-space windows and is capable of differentiating the slower changing oceanic features from faster evolving atmospheric patterns. It leads to improved coverage, which is critically important especially in dynamic areas where traditional single-view cloud masking algorithms have consistent misclassifications.

The new hourly SST product targets users that need a diurnally resolved product but cannot afford the huge data volumes. ACSPO hourly ABI/AHI SST product will contain a representative hourly SST value in each pixel, following a continuous curve through the “upper envelope” of the original time-resolution clear-sky SST values. The resulting hourly product has larger spatial coverage and reduced spatial/temporal noise as compared to the current geostationary SST products.

Global evaluation using the SST Quality Monitor (SQUAM; www.star.nesdis.noaa.gov/sod/sst/squam/), including validation against the in situ Quality Monitor (iQuam; www.star.nesdis.noaa.gov/sod/sst/iquam/) data, and the regional evaluations in dynamic regions and coastal zones using the ACSPO Regional Monitor for SST (ARMS; www.star.nesdis.noaa.gov/sod/sst/arms/), suggest superior performance of the new generation NOAA geostationary SST products.

DIURNAL CYCLES IN THE NOAA ACSPO "DEPTH" AND "SKIN" SST FROM THE NEW GENERATION ABI/AHI GEOSTATIONARY SENSORS

Boris Petrenko[(1)], Alexander Ignatov[(2)], Maxim Kramar[(3)], Yury Kihai[(4)], Xinjia Zhou[(5)], Kai He[(6)]

(1) NOAA STAR and GST, Inc., USA, Email: boris.petrenko@noaa.gov
(2)NOAA STAR, USA, Email: alex.ignatov@noaa.gov
(3) NOAA STAR and GST, Inc., USA, Email: maxim.kramar@noaa.gov
(4) NOAA STAR and GST, Inc., USA, Email: yury.kihai@noaa.gov
(5) NOAA STAR and CSU CIRA, USA, Email: xinjia.zhou@noaa.gov
(6) NOAA STAR and CSU CIRA, USA, Email: kai.he@noaa.gov

1. INTRODUCTION

Processing data of the advanced radiometers flown onboard the new generation geostationary satellites, GOES-16 ABI and Himawari-8 AHI with the NOAA Advanced Clear-Sky Processor for Oceans (ACSPO) has shown the capability of monitoring the diurnal cycle (DC) in sea surface temperature (SST) (Kramar et al., 2016) but also revealed the need in further optimization of SST retrieval algorithms for quantitative estimation of DC magnitudes and shapes. Particularly, substantial difference between DCs in "skin" and "depth" sea layers calls for more specific targeting the retrievals at SSTskin or SSTdepth. Minimization of variability in biases and optimization of sensitivity appears to be a prerequisite for reliable estimation of diurnal SSTskin variations. These issues were addressed with the development of new algorithms for SSTskin and SSTdepth retrieval and their implementation within the experimental version of ACSPO. The paper describes these algorithms and presents results of initial validation with AHI data..

2. SST ALGORITHMS IN THE CURRENT ACSPO

Currently, the ACSPO system generates two SST products from AHI/ABI data with the regression equation using four radiometric bands:

$$T_S = a_0 + a_1 T_{11} + a_2(T_{11}-T_8) + a_3(T_{11}-T_{10}) + a_4(T_{11}-T_{12}) + [a_5 + a_6 T_{11} + a_7(T_{11}-T_8) + a_8(T_{11}-T_{10}) + a_9(T_{11}-T_{12})]S_\vartheta + [a_{10}(T_{11}-T_8) + a_{11}(T_{11}-T_{10}) + a_{12}(T_{11}-T_{12})]T_S^0 \quad (1)$$

Here, T_{11}, T_{13}, T_{14} and T_{15} are brightness temperatures observed in AHI (ABI) bands 11, 13, 14 and 15 (centered at 8.6, 10.4, 11.2 and 12.3 μm), $S_\vartheta = 1/cos(\vartheta) - 1$, ϑ is satellite view zenith angle, T_S^0 is analysis L4 SST (in ^oC) by the Canadian Meteorological Center (CMC) and $a_0, a_1, \ldots, a_{12}$ are regression coefficients, derived from matchups with *in situ* SST measured by drifting and moored buoys. Using a single equation for day and night minimizes DC discontinuities. The difference between the two ACSPO SSTs is in the definitions of regression coefficients.

The **Global Regression (GR) SST** is represented with the "sea_surface_temperature" layer in the output ACSPO GDS2 files. It is produced with a single set of coefficients trained by fitting *in situ* SST under the constraint that mean sensitivity to SSTskin is 0.95 within the global dataset of matchups (MDS) (Petrenko et al., 2016a). We use herein the definition of sensitivity by Merchant et al. (2009). The GR SST fits *in situ* SST with SD≈0.4 K and sensitivity to SSTskin ≈0.7 to 1.1. Relatively high sensitivity allows considering the GR SST an estimate of SSTskin. However, the accuracy of estimating the DC magnitude in SSTskin is questionable because of significant variability in biases and sensitivity, typical for global regression algorithms.

The second ACSPO product, **Piecewise Regression (PWR) SST**, is obtained from ACSPO GDS2 files as the difference between "sea_surface_temperature" and "SSES_bias" layers. The PWR SST uses specific sets of coefficients for multiple segments of the SST domain, defined in the space of regressors (Petrenko et al., 2016b). The PWR SST coefficients are found by unconstrained fitting *in situ* SST within each segment. As a result, the PWR SST precisely fits *in situ* SST with global SD ≈ 0.25 K and, therefore, it may be viewed as an estimate of SSTdepth. However, the accuracy of reproducing the DC in SSTdepth is limited by the fact that the observed brightness temperatures are sensitive to SSTskin, which is, in general, biased with respect to SSTdepth.

3. IMPROVING SSTSKIN ESTIMATES

The newly developed **Piecewise Regression skin (PWRskin) SST** algorithm reduces variability of biases and sensitivity, typical for GR SST, brings the mean sensitivity closer to its optimal value of 1 and reduces variations in sensitivity. This is achieved by using the segmentation of the SST domain the same way as it is used in the current PWR SST. However, in contrast with the PWR SST, the PWRskin coefficients are trained by fitting *in situ* SST within each segment under the constraint that mean sensitivity is equal to 1.

Table 1. Bias and standard deviation of AHI GR SST and PWRskin SST with respect to in situ SST, sensitivities to SSTskin, and standard deviations of sensitivities averaged over matchups with V>6m/s within the validation MDS,.

Algorithm	Bias	SD	Mean sensitivity	SD of sensitivity
GR SST	0.125 K	0.44 K	0.94	0.10
PWRskin SST	-0.08 K	0.40 K	1.00	0.06

In order to minimize the effect of variable bias between SSTskin and SSTdepth, the PWRskin SST coefficients are trained against matchups with drifters and moored buoys, selected from the iQuam system (Xu and Ignatov, 2009) under the condition that wind speed over sea surface *V*> 6 m/s, according to the Global Forecast system (GFS). Training dataset of matchups (MDS) for AHI included 318662 matchups collected from January to December 2016. The validation MDS includes 131943 matchups (80700 matchups with *V*>6 m/s) collected from January to April 2017.

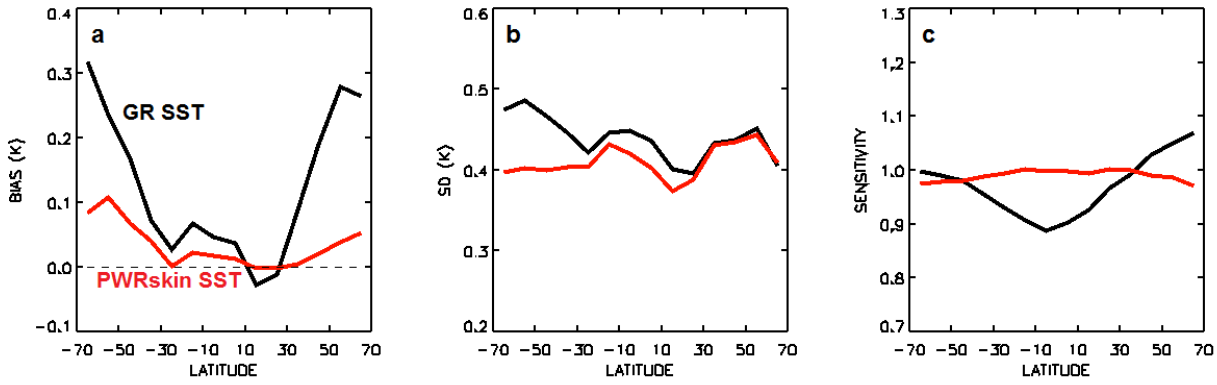

Figure 1. (a) Bias and (b) SD with respect to in situ SST; (c) mean sensitivity as functions of latitude, averaged over matchups with high winds within the validation MDS. (Black) GR SST and (red) PWRskin SST. Validation MDS, matchups with V>6 m/s.

Table 1 shows the statistics for AHI GR SST and PWRskin SST with respect to *in situ* SST averaged over the matchups with *V*>6 m/s within the validation MDS. PWRskin SST reduces global SD with respect to *in situ*

SST, which suggests more uniform regional biases. It also optimizes mean sensitivity and reduces its variations.

Fig. 1 shows biases and SDs of GR SST and PWRskin SST with respect to *in situ* SST and mean sensitivities as functions of latitude. The biases and sensitivity of GR SST are more non-uniform than for PWRskin SST and increase from low to high latitudes. The SDs for GR SST are in general larger than for PWRskin SST, suggesting larger variability of biases within the corresponding latitudinal bands. Fig. 2 shows the dependencies of biases in GR SST, PWRskin SST and *in situ* SST with respect to CMC on local solar time (LST) averaged over all matchups, with low and high winds, within the validation MDS. More uniform biases and sensitivity in PWR SST reduce the magnitude of diurnal signal from 0.45 K to 0.28 K. Note also that maxima and minima of diurnal signals in both GR and PWRskin SSTs occur earlier than in *in situ* SST, as expected for SSTskin estimates.

4. IMPROVING SSTDEPTH ESTIMATES

The Piecewise Regression SSTdepth (PWRdepth SST) algorithm is a modification of the current PWR SST aimed at improved reproduction of DC in SSTdepth. The PWRdepth SST algorithm accounts for two additional variables driving biases between SSTskin and SSTdepth. The first variable, *V*, is obtained from GFS data and added to Eq. (1) as a new regressor. More complicated dependency of SSTskin/SSTdepth bias from the second variable - LST - is introduced by modification of the offsets in the PWRdepth equations by averaging over matchups for every LST hour. During L2 processing, the hourly offsets are interpolated to real LST for a given pixel. The AHI PWRdepth SST was trained and validated against the MDS described in Section 3, using matchups for all wind speeds.

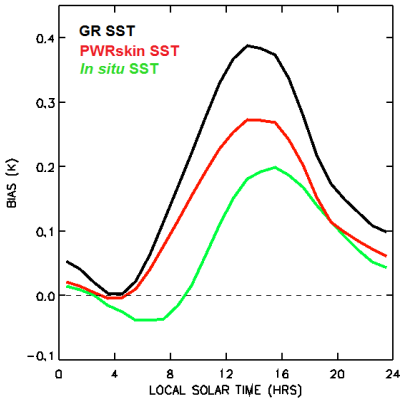

Figure 2. Biases in GR, PWRskin and in situ SSTs as functions of LST. Validation MDS, all-wind matchups.

Table 2 shows the global statistics of PWR and PWRdepth SSTs with respect to *in situ* SST and CMC, and the statistics of *in situ* SST with respect to CMC within the validation MDS. Accounting for wind speed and LST reduces SD of PWRdepth SST - *in situ* SST but increases SD with respect to CMC, bringing the latter closer to SD of *in situ* SST - CMC. Fig.3 shows the biases of PWR SST, PWRdepth SST and *in situ* SST with respect to CMC as functions of LST within the validation MDS. Accounting for wind speed and LST increases the DC magnitude in PWRdepth SST from 0.18 K to 0.21 K, bringing it closer to the DC magnitude in *in situ* SST (0.24 K). The magnitude of deviations from *in situ* SST substantially reduces from 0.15 K for PWR SST to 0.04 K for PWRdepth SST. The times of DC maximum and minimum shift from 3:30 and 13:30 for PWR SST to 5:30 and 15:30 for PWRdepth SST, getting much closer to the corresponding times for *in situ* SST (6:30 and 15:30, respectively).

Table 2. Global statistics of PWR and PWRdepth SSTs against in situ SST and CMC over the validation MDS

SST	SST – in situ SST		SST-CMC	
	Bias	SD	Bias	SD
In situ	-	-	0.07 K	0.27 K
PWR SST	0.02 K	0.26 K	0.08 K	0.17 K
PWRdepth SST	0.02 K	0.25 K	0.08 K	0.20 K

5. EXAMPLE OF RETRIEVAL OF DIURNAL CYCLES FROM AHI DATA

The PWRskin and PWRdepth SST algorithms were implemented and tested within the experimental ACSPO version using GR SST as a benchmark. Fig. 4 shows the time series of biases and SDs with respect to CMC for three SSTs, produced from AHI data for the period from 1 to 5 January 2016. Reduced variability in biases and sensitivity to true SSTskin results in reduced DC magnitudes and SDs of PWR SSTskin, compared with GR SST. The DC magnitudes and SDs of PWRdepth SST are even smaller than in PWRskin SST. The maxima and (especially) the minima of DC in PWRdepth SST are delayed with respect to the minima and maxima in GR and PWRskin SSTs, consistently with expected difference between SSTskin and SSTdepth.

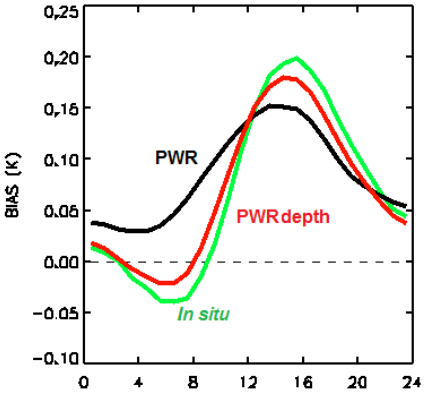

Figure 3. Biases in PWR, PWRdepth and in situ SSTs as functions of LST. Validation MDS, matchups for all wind speeds.

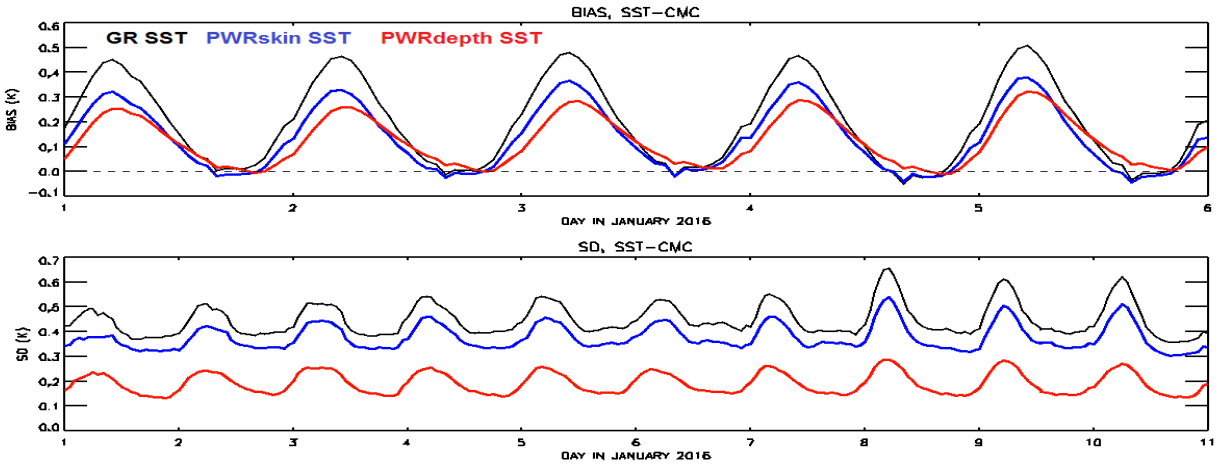

Figure 4. Time series of bias and SD of GR, PWRskin and PWRdepth SSTs with respect to CMC. AHI, 1-10 January 2016.

6. SUMMARY AND FUTURE WORK

Two new SST algorithms, aimed at improved monitoring the diurnal signals in SSTskin and SSTdepth from GOES-16 ABI and Himawari-8 AHI, have been developed and tested within the experimental version of the ACSPO. The newly developed PWRdepth SST algorithm improves the precision of SSTdepth retrieval, compared with the current PWR SST, and makes the shape of diurnal cycle more consistent with DC in *in situ* SST (this includes the magnitudes and the times of maximum and minimum).The PWRskin SST reduces variability of biases and sensitivities compared with the current GR SST and, therefore, it is expected to better reproduce the diurnal cycle in SSTskin.

The future work will be focused at extensive testing and further enhancement of the PWRskin and PWRdepth SST products, including validation in the SST Quality Monitor (SQUAM, Dash et al. (2010), available at https://www.star.nesdis.noaa.gov/sod/sst/squam/index.html). Due to the lack of reliable ground truth for SSTskin data, validation of the PWRskin SST and finding the alternative of the information on SSTskin, will be important and challenging parts of this activity. After the testing period, these algorithms may be implemented in one of the future versions of ACSPO.

7. REFERENCES

Dash, P.; Ignatov, A.; Yuri, K.; Sapper, J. (2010), The SST quality monitor (SQUAM), J. Atmos. Ocean. Technol., 27, 1899–1917, DOI: http://dx.doi.org/10.1175/2010JTECHO756.1

Kramar, M., Ignatov, A., Petrenko, B., Kihai, Y., and Dash, P. (2016), Near real time SST retrievals from Himawari-8 AHI at NOAA using ACSPO system, Proc. of SPIE, 9827, 98270L, doi: 10.1117/12.2229771

Merchant, C.J., Harris, A.R., Roquet H., and Le Borgne, P. (2009), Retrieval characteristics of non-linear sea surface temperature from the Advanced Very High Resolution Radiometer, Geophys. Res. Lett., 36, L17604, doi: 10.1029/2009GL039843.

Petrenko, B., Ignatov, A., Kramar, M., and Kihai, Y. (2016a), Exploring new bands in multichannel regression SST algorithms for the next generation infrared sensors at NOAA. Proc. of SPIE, 9827, 98270N, doi: 10.1117/12.2229578

Petrenko, B., Ignatov, A., Kihai, Y., and Dash, P. (2016b), Sensor-Specific Error Statistics for SST in the Advanced Clear-Sky Processor for Oceans, J. Atmos. Oceanic Technol., 33, 345-359, doi:10.1175/JTECH-D-15-0166.1.

Xu, F., and Ignatov, A. (2014), In situ SST Quality Monitor (iQuam). J. Atmos. Oceanic Tech., 31, 164-180, doi:10.1175/JTECH-D-13-00121.1.

RADIATIVE TRANSFER MODEL BASED BIAS CORRECTIONS IN INSAT-3D/3DR IMAGER OBSERVATIONS TO IMPROVE SEA SURFACE TEMPERATURE RETRIEVAL

Rishi Kumar Gangwar[(1)], Buddhi Prakash Jangid[(2)] and Pradeep Kumar Thapliyal[(3)]

(1) Space Applications Centre (ISRO), Jodhpur-Tekra, Ahmedabad, Gujarat, India
Email: rgbly1986@sac.isro.gov.in
(2) Space Applications Centre (ISRO), Jodhpur-Tekra, Ahmedabad, Gujarat, India
Email: buddhi@sac.isro.gov.in
(3) Space Applications Centre (ISRO), Jodhpur-Tekra, Ahmedabad, Gujarat, India
Email: pkthapliyal@sac.isro.gov.in

ABSTRACT

India has recently launched an advanced meteorological geostationary satellite INSAT-3DR in September 2016, which is similar to the INSAT-3D that was launched in July 2013. The Imager channels in these satellites are providing accurate Sea Surface Temperature (SST) observations using split thermal infrared window and mid infrared channel over Indian Ocean region. These products are operationally generated and hosted at MOSDAC web-portal (www.mosdac.gov.in) for scientific users. Recently, to improve the SST quality a Radiative Transfer (RT) model dependent bias correction procedure as a function of satellite zenith angle was applied to the INSAT-3D/3DR Thermal IR channels before using in the retrieval algorithm. This was done using collocated INSAT-3D/3DR and RT model simulated observations using ECMWF analysis. The retrieved SST products from bias corrected observations have been validated with in-situ as well MODIS SST products. The comparison analysis shows significant improvement in the accuracy of SST product as compared to the previous version of the operational product. When compared with in-situ, the bias in the retrieved SST was reduced from -0.69 to -0.20K and the standard deviation of the difference reduces to 0.6K from 1.4K. Comparison with MODIS derived SST product shows ~50% improvement in the SST accuracy. Recently, this bias correction procedure has been implemented at MOSDAC for operational use.

1. INTRODUCTION

India launched the advanced meteorological satellite, INSAT-3DR, on 26th September 2016 in the geostationary orbit located at 74˚E. The inheritance of this satellite has come from INSAT-3D satellite. These satellites have two meteorological payloads onboard - a 6 channel Imager and 19 channel Sounder providing useful applications for cyclone and monsoon monitoring, cloud motion vectors winds, rainfall estimation, floods/intense precipitation monitoring, snow cover detection, mesoscale studies etc. Details of Imager channels are given in Table-1.

Band no./name	Wavelength(µm)	Resolution Km)	S/N or NEDT (K)
1 (VIS)	0.52 – 0.72	1	150:1
2 (SWIR)	1.55 – 1.70	1	150:1
3 (MIR)	3.80 – 4.00	4	0.27
4 (WV)	6.50 – 7.00	8	0.18
5 (TIR1)	10.3 – 11.2	4	0.10
6 (TIR2)	11.5 – 12.5	4	0.25

Table-1: INSAT-3D/3DR Imager channel characteristics

The SST is derived from the thermal split-window channels#5-6 during daytime and using additional channel#3 during nighttime, over cloud free regions. The most important part of the SST retrieval from IR observations is the atmospheric correction. Over tropics the atmospheric correction is dominated by the high spatio-temporal variability on the atmospheric water vapor. This correction can be determined through suitable characterization of tropical atmospheres in radiative transfer model to simulate the brightness temperatures of INSAT-3DR channels and then generating the regression coefficients for SST retrieval.

2. THEORETICAL BACKGROUND

Radiance from Earth's terrestrial emission peaks at around 10 µm, which falls well within the atmospheric window (10-12 µm), where gaseous absorption is minimum in the atmosphere. Therefore, in order to measure earth's surface skin temperature, most space-borne sensors are designed within this window. Still this band is not completely transparent and the atmospheric water vapour is the major gas that absorbs the IR radiation reaching at the top of the atmosphere. Therefore, retrieval of the SST from TIR window channels require atmospheric corrections arising due to the absorption by the variable water vapor. This correction is more in tropics during summers due to higher amount of atmospheric moisture (Barton 1983, Anding and Kauth 1970, Gohil et al 1994, Mathur & Agarwal 1991, 2002, Shenoy 1999). A radiative transfer simulation study has shown that with proper characterization of tropical conditions in the atmosphere, a suitable algorithm can be developed for accurate SST retrieval (<0.7K) using TIR and MIR window channels, provided the sensor noise is of the order of 0.1K.

INSAT-3D/3DR make use of the following generalized expression of the non-linear SST (NLSST) estimator:

$$SST = a_0 + a_1T_1 + a_2(T_1 - T_2) + a_3(T_1 - T_2).(T_1 - T_2) + a_4(sec\theta - 1).(T_1 - T_2) \quad (1)$$

where, T_1 and T_2 are the brightness temperatures of TIR-1 and TIR-2, $a_{0\text{-}4}$ are the regression coefficients computed using simulated dataset.

2.1. Radiative transfer model

We have simulated the brightness temperatures corresponding to INSAT-3D Imager channels using PFAAST RT model. The atmospheric profiles and required surface variables have been taken from ECMWF diverse profile dataset. The simulations have been performed for the cloud free regions within 0E–130E and 60S–60N corresponding to INSAT-3D for satellite zenith angle ranging from nadir to 60°.

2.2. Bias correction in satellite observations

While comparing with simulated brightness temperatures using ECMWF analysis, the satellite observations have shown a zenith angle dependent bias (Fig.1). We made an attempt to model this bias as a quadratic function of the difference between observed and simulated brightness temperature with the satellite zenith angle (θ). Fig.2 shows the difference in the simulated and actual brightness temperatures after RT model bias correction. The table-2 shows the bias, RMSD and standard deviation of the difference (STD) between observed and simulated brightness temperatures before and after correction. This table clearly shows that after removing the zenith angle dependency in brightness temperatures the bias and RMSD reduces in all the channels. Presently, due to relatively larger uncertainties in the MIR brightness temperatures, it is not being used for night-time SST retrieval.

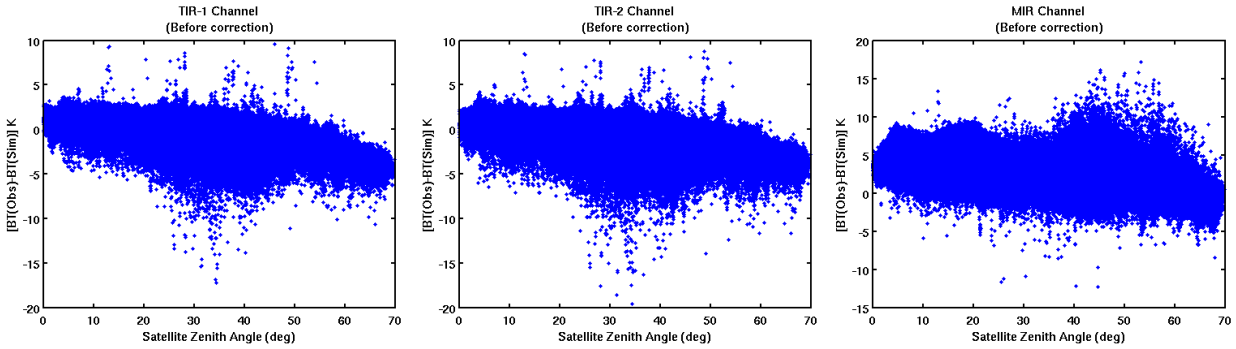

Figure 1: TIR1, TIR2 and MIR channels before bias correction

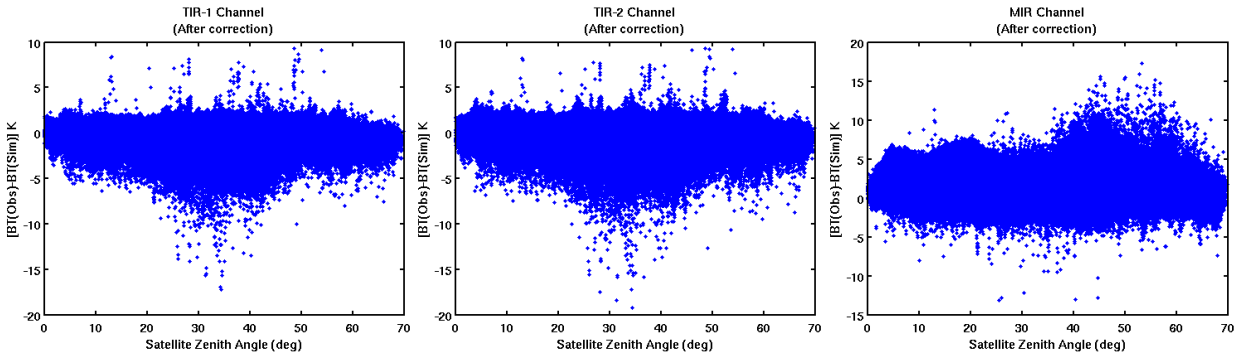

Figure 2: TIR1, TIR2 and MIR channels after bias correction

Channel		Bias (K)	RMSD (K)	STD (K)
TIR-1	Before	-0.15	1.26	1.25
	After	-0.13	0.88	0.87
TIR-2	Before	-0.52	1.30	1.19
	After	-0.09	0.96	0.96
MIR	Before	1.46	2.30	1.76
	After	0.36	1.61	1.57

Table 2: Comparison statistics after zenith angle dependent bias correction

3. RESULTS AND DISCUSSION

To assess the merit of the proposed improved algorithm we have compared the retrieved SST products using present as well as operational algorithm with the in-situ as well as MODIS SST during 17-25 December, 2016. The collocation criteria have been taken as 4 km in space and 15 minutes in time. To compare the INSAT-3D retrieved SST with the MODIS SST, we have considered day-time (0000-1230 GMT) and night-time (1300-2330 GMT) acquisitions, separately.

Fig.3 shows the scatter plot of the INSAT-3D retrieved SST with the in-situ SST for both operational and modified algorithms. This figure shows that the extent of the scatter and the bias have reduced in the modified algorithm significantly. Similarly, density scatter plots in the figures 4 & 5 show that the errors in SST products retrieved using modified algorithm show a significant improvement over the operational algorithm when compared with the MODIS SST products for both day as well as night time.

The modified algorithm has been made operational for both INSAT-3D and INSAT-3DR.

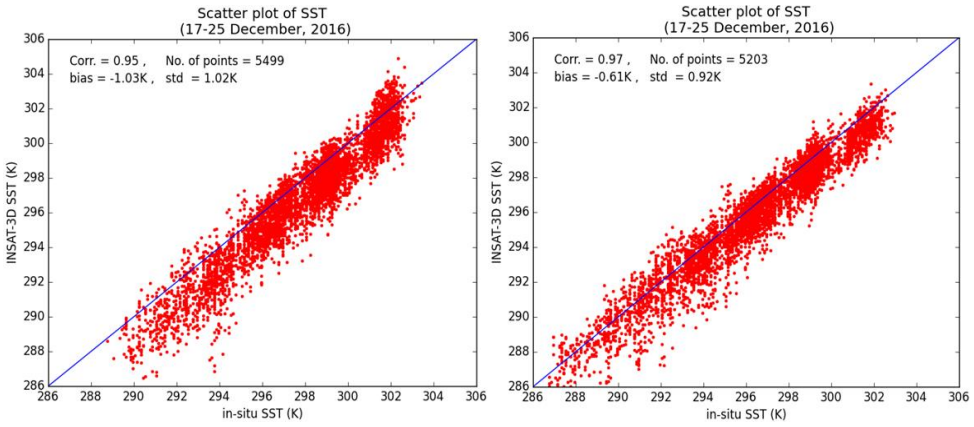

(a) (b)

Figure 3: Comaprison of INSAT-3D derived SST with in-situ (a) Operational Algotithm (b) Modified Algorithm

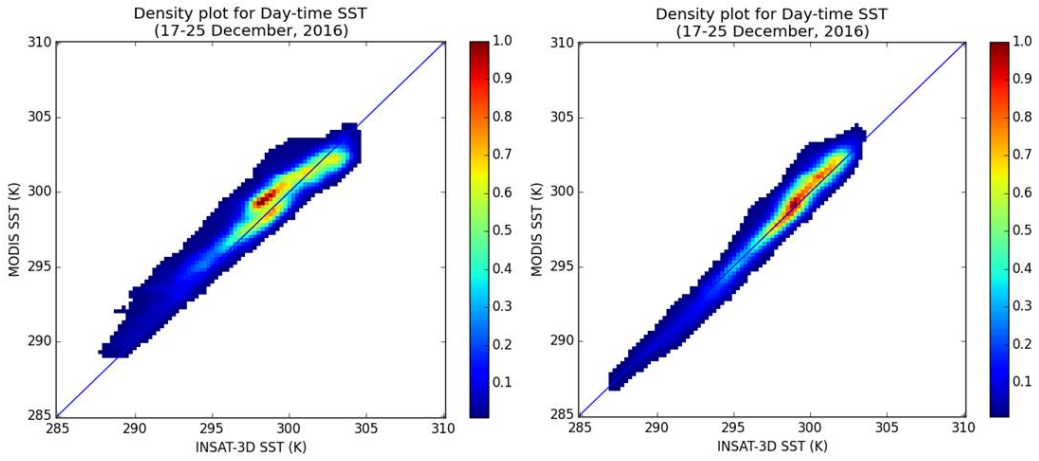

(a) (b)

Figure 4: Comaprison of Day-time INSAT-3D derived SST with MODIS (a) Operational Algotithm (b) Modified Algorithm

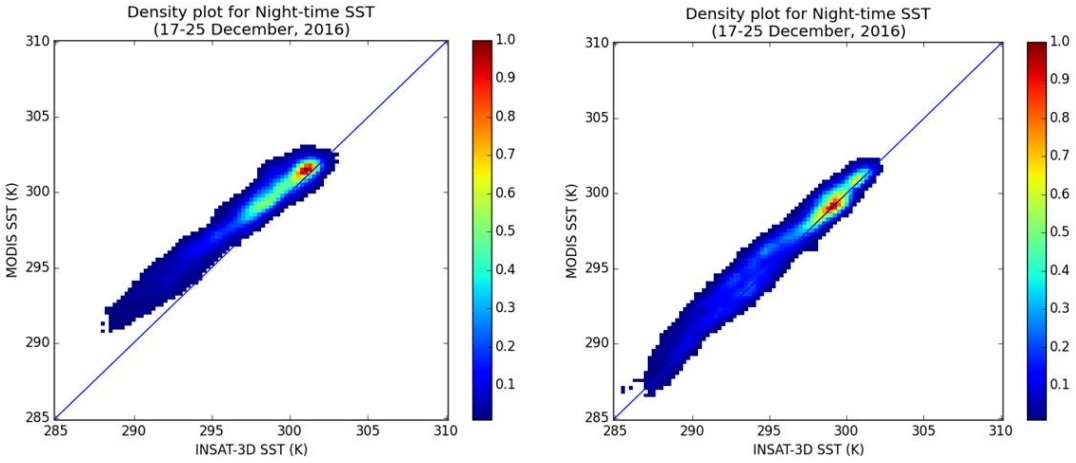

(a) (b)

Figure 5: Comaprison of Night-time INSAT-3D derived SST with MODIS (a) Operational Algotithm (b) Modified Algorithm

Algorithm	Statistical variable	Day-time	Night-time
Operational	Bias (K)	-0.40	-1.11
	RMSD (K)	1.10	1.47
	STD (K)	1.02	0.97
Modified	Bias (K)	-0.23	-0.50
	RMSD (K)	0.81	0.96
	STD (K)	0.78	0.82

Table-3: Validation statistics for INSAT-3D SST using modified and operational algorithms

4. CONCLUSIONS

In this study we have analyzed the observations from INSAT-3D/3DR Imager which shows a satellite zenith angle dependent bias with respect to simulated observations. We further tried to model this bias as a polynomial function of zenith angle. Through this function we have removed the bias from the observed brightness temperatures before the SST retrieval. To assess the quality of the modified algorithm including bias correction we have compared the retrieved SST with concurrent in-situ as well as MODIS SST products. From the comparison analysis we have observed that the modified algorithm shows a significant improvement over operational algorithm for both INSAT-3D & 3DR observations.

5. REFERENCES:

1. Anding D. and R. Kauth, Estimation of sea surface temperature from space, *Remote Sensing of Environment*, 1, 217-220, 1970.

2. Barton I. J., Dual channel satellite measurements of sea surface temperature, *Quarterly journal of Royal Meteorological Society*, 109,365-378, 1983.

3. Barton, I. J., A. J. Prata, and D. T. Llewellyn-Jones, The Along Track Scanning Radiometer-an Analysis of coincident ship and satellite measurements, *Adv. Space Res.*, 13(5), 69, 1993.

4. Deschamps, P. Y. and T. Phulpin, Atmospheric corrections of infrared measurements of sea surface temperature using channels at 3.7 µm, 11 µm and 12 µm. *Boundary Layer Meteor.*, 18, 131-143, 1980.

5. Gohil B. S., A. K. Mathur and P. C. Pandey, An algorithm for sea surface temperature estimation from ERS-1 ATSR using moisture dependent coefficients: a simulation study, *International Journal of Remote Sensing*, Vol. 15, No.5, 1161-1167, 1994.

6. Llewellyn-Jones, D.T., P.J. Minnett, R.W. Saunders and A.M. Závody, Satellite multi-channel infrared measurements of sea surface temperature of the N.E. Atlantic Ocean using AVHRR/2. *Quart. J. R. Met. Soc.,* 110, 613-631, 1984.

7. Mathur A.K. and V.K. Agarwal, A quantitative study on the effect of water vapour on estimation of sea surface temperature using satellite IR observations, *Oceanography of the Indian Ocean, B. N. Desai, Ed., Oxford & IBH publishing Co. Pvt. Ltd.*, 673-680, 1991.

8. Mathur A. K., V. K. Agarwal and T. C. Panda, Validation of ERS-1/ATSR derived SST in Indian waters, *International Journal of Remote Sensing*, Vol. 23, No. 24, 5155-5163 pp, 2002.

9. Minnett P. J., Satellite Infrared Scanning Radiometers-AVHRR and ATSR/M, Microwave Remote Sensing for Oceanographic and Marine Weather-Forecast Models, *edited by R. A. Vaughan, Kluwer Academic Publishers, Dordrecht,* 1998.

10. Mutlow C. T., A. M. Zavody, I. J. Barton, and D. T. Llewellyn-Jones, Sea surface temperature measurements by the along-track scanning radiometer on the ERS-1 satellite, Early results, *J. Geophys. Res.*, 99, 22575-22588, 1994.

11. Prabhakar C., G. Dalu and V. G. Kunde, Estimation of Sea surface temperature from remote sensing in 11-13 µm window region, *Journal of Geophysical research*, 79, 5039-5044, 1974.

12. Shenoy S. C., On the suitability of global algorithms for the retrieval of SST from the north Indian Ocean using NOAA/AVHRR data, *International Journal of Remote Sensing*, 20, 1, 11-29, 1999.

FELYX IN ACTION FOR SENTINEL-3 CAL/VAL AND CLIMATE DATA RECORD ASSESSMENT

Jean-François Piollé[(1)], Jamie Shutler[(2)], Igor Tomazic[(3)], Sylvain Herlédan[(4)], Craig Donlon[(5)], Philippe Goryl[(6)]

(1) Institut Français de Recherche pour l'Exploitation de la Mer (Ifremer), France, Email: jfpiolle@ifremer.fr
(2) University of Exeter, UK, Email: J.D.Shutler@exeter.ac.uk
(3) EUMETSAT, Germany, Email: igor.tomazic@eumetsat.int
(4) OceanDataLab, France, Email:sylvain.herledan@oceandatalab.com
(5) European Space Agency (ESA/ESTEC), Italy, Email: craig.donlon@esa.int
(6) European Space Agency (ESA/ESRIN), Italy, Email: philippe.goryl@esa.int

1. INTRODUCTION

felyx is a EO data analytics tool funded by ESA and implemented by a consortium led by Ifremer. It aims at bringing to the user community a generic open source solution for the analysis and intercomparison of EO datasets, for application such as :

- sensor calibration & validation
- products or algorithm intercomparison
- analysis of long time series of multiple parameters (climate change, trends, …)

The basic concept of *felyx*, based on miniprods and metrics, has been presented at previous GHRSST meetings and its implementation has since been completed to the point where it can be used for real end-user applications. This presentation will illustrate the usage of felyx in two contexts:

- how *felyx* is used as a critical resource in Sentinel-3 cal/val by supporting the generation of match-up databases between Sentinel-3 instruments and in situ data sources (high resolution drifters, moored buoys and Argo floats from Coriolis service, and in situ radiometer data from various cruises). This will be illustrated with Sentinel-3 data but we will also emphasize that this can be run in the same way for any other GHRSST source.
- how *felyx* can also be used for instance as a common GHRSST tool to assess in a uniform and consistent way if a dataset fits the requirements to be labeled as a climate data record. In this context, felyx is provided on a virtual machine with all the in situ sources and diagnostics required to run this assessment on a user dataset.

2. *FELYX* FOR SENTINEL-3

felyx has been used extensively in support to the cal/val of Sentinel-3 mission, mostly for SLSTR but also OLCI instruments, to generate match-up databases.

Sentinel-3 provides a wide range of products for each instrument (from L1 to L2), in different timeliness (near real time, none time critical) with also frequent updates and reprocessings being performed as improvements and fixes are implemented. These multiple versions and changes require quick but careful performance evaluation and intercomparison for which match-up databases are a key asset. Having a single configurable framework like felyx generating different match-up database versions in a consistent way from the same set of in situ measurements greatly helps to support this tedious task.

The set of in situ data used for SLSTR MDBs include:

- real time drifter, Argo and moored buoy data provided by Copernicus marine in situ service (CMEMS/In situ, operated by Ifremer/Coriolis). About 40000 in situ measurements are collected daily.
- high quality shipborne radiometer data provided by the International Shipborne Radiometer Network. These data were only available in delayed mode and therefore used for reprocessed MDBs only.

The colocation criteria used for the match-up extraction were 2 hours (12 hours for Argo) and 5 km maximum distance. Each extracted match-up includes:

- all variables from SLSTR L1 and L2 products (more than 600 variables!) in a 21x21 pixel box centered on the matching pixel
- cross-overs with other sensors such as Metop/AVHRR, MSG/Seviri or SLSTR/OLCI when matched in the same 2 hours time window : this capability to generate multi-sensor match-ups is one of the powerful features of felyx.
- Additional fields such as experimental SST calculations post-processed over the extracted match-ups and allowing to quickly process and assess algorithm improvements
- full history within +/-6 hours of the in situ measurements, providing therefore also the variability of SST over each match-up location
- complete traceability to the source files used for the match-up extraction (file, indices,…) allowing investigation of outliers in a semi-automated way through the combination with jupyter notebooks (http://jupyter.org).

The match-ups were assembled into daily files and made available to the Sentinel-3 validation teams every day.

Further improvements are planned such as adding visible SLSTR channels in the match-ups, adjusting SST to in situ measurement depth or adding match-ups with sea ice temperature. The collection of in situ data will also be extended to high resolution drifters and more shipborne radiometers.

The SLSTR MDBs were used by different groups at Eumetsat, within S3VT and MPC

Sentinel-3 for SLSTR, and by OSI SAF experts. They were a major asset for various activities such as:

- L1 cloud screening validation (RAL)
- L2 SST coefficient estimation (Univ. of Reading)
- L2 Quality level stratification and uncertainties estimation (Univ. Of Leicester)
- SST validation : OSI SAF (Meteo-France / DMI / MetNo), NOAA, Eumetsat
- Metis intercomparison framework (Eumetsat)

3. *FELYX* IMPROVEMENTS

The Sentinel-3 cal/val was a tremendous opportunity to put *felyx* in action, collect feedback and implement or plan improvements, such as:

- improved integration with open source analytics tools such as *jupyter* (http://jupyter.org), big data analytics in the *Elasticsearch* ecosystem (*kibana, grafana, x-pack*)
- improved integration in processing environments for deployment (*ansible*), scheduling (*airflow*) or supervision (*supervisor*)

Significant improvements will also be released in Fall 2017 : deployment procedures (with *ansible*), improved error monitoring and reporting, documentation and additional resources for match-up database generation.

Felyx is meant to be a community tool and we encourage its usage or shared development by interested parties. Don't hesitate to contact us (jfpiolle@ifremer.fr)!

4. REFERENCES

Contact : Jean-François Piollé (jfpiolle@ifremer.fr)

Web site: http://hrdds.ifremer.fr

Documentation: http://felyx.readthedocs.io

Packages: https://felyx.cersat.fr/download/source/1.0.0/

Source code: https://git.cersat.fr/groups/felyx

Virtual machines for testing (virtualbox):

- Bare configuration: ftp://ftp.ifremer.fr/ifremer/cersat/projects/felyx/download/vm/2016-09-19_felyx-1.0.0.ova
- Pre-configured for OLCI & SLSTR datasets: ftp://ftp.ifremer.fr/ifremer/cersat/projects/felyx/download/vm/felyx_olci.ova

PLENARY SESSION IV: SURFACE FLUXES

SESSION IV REPORT

Chair: Chelle Gentemann[(1)] - Rapporteur: Salvatore Marullo[(2)]

1 ZHANG, HAIFENG AND BEGGS, HELEN: EVALUATION OF SEA SURFACE TEMPERATURE DIURNAL VARIATION MODELS AGAINST MTSAT-1R DATA IN THE TROPICAL WARM POOL

1. Inclusion of Diurnal Variability (DV) in coupled numerical models
2. Test in the SST tropical warm pool (TWP)

In the TWP an inter-comparison among different DV models using a variety of NWP has been done. TWP has been selected because it presents higher SST values in a relatively more cloud free region.

- The comparison between models and data has been done using the GHRSST TWP DV dataset.
- 4 DV models (ZB05, ZB+T, CG03, UMGC2) have been used: 1 empirical, 2 physical plus a coupled ocean-atmosphere mode. All model produce a sub-skin SST

1. Good agreement for CG03 and ZB+T
2. Positive bias in ZB05

For UMGC2: the larger positive bias, delay in the peak (1-2 hours later than in the MTSAT-1R data)

The comparison shows that the models are able to reproduce the spatial distribution DV but fail in reproducing larger Diurnal Warming events (underestimation), while moderate DV are overestimated.

Considering the wind models overestimate DV at low wind regime while, in general, the contrary happens for high wind regimes.

In conclusion all model are able to produce a Diurnal Cycle but overestimation of underestimation happen depending from the wind regime

2 WONG, ELIZABETH AND MINNETT, PETER: THE RESPONSE OF THE OCEAN THERMAL SKIN LAYER WITH AIR-SEA SURFACE HEAT FLUXES

A detailed physical discussion has been given on how the heat is absorbed in the sea. In fact longwave is absorbed within the thermal skin. What is the physical mechanism to propagate the heat below? Molecular transfer play the most important (probably the only) role.

This is very important for climate change studies because it means that the longwave component of the heat radiative transfer only contribute to heating the first millimetre of water. Shortwave incoming radiation is the component that most contribute to transfer heat to the upper ocean.

Test of this hypothesis have been done using large dataset of M-AERI measurements trying to better understand the physics of the heat transfer in the first millilitre of the ocean. a spectral analysis of the M-AERI data has been applied, this allowed to investigate the effect of the wind variation the temperature profile within this first millimetre.

They concluded that the heat below the thermal skin layer is provided by solar heating.

3 LIU-XIE: SEA SURFACE TEMPERATURE INFLUENCE ON OCEAN CARBON CYCLE

A statistical model to estimate the partial pressure of carbon dioxide at sea surface (pCO2) from space-based observations of sea surface temperature, chlorophyll, and salinity has been presented. The train of the model is based on a selection of in situ data while for the validation an independent data set has been used.

The pCO2 estimate from space is based either on relation between pCO2 and SST or a relation between pCO2, SST and chlorophyll a (Chl_a). It results that SST is the dominant factor in pCO2 changes, particularly in the subtropical oceans, and chlorophyll becomes important at extra-tropical latitudes and coastal regions, where biological productivity is strong.

Time series of pCO2 maps show a clear annual signal and, in addition, a relation is observed also with Nino index and TIW are visible in the pCO2 maps.

Its concluded that produce maps of pCO2 from space is feasible as demonstrated by the results od the validation even if the seasonal signal have a reduced amplitude and trend are not exactly reproduced.

Future developments will include the use of the salinity obtained from SMOS and SOCAT space missions.

COMPARISON OF SST DIURNAL VARIATION MODELS OVER THE TROPICAL WARM POOL

Haifeng Zhang[(1)], Helen Beggs[(2)], Xiao Hua Wang[(3)], José Rodríguez[(4)], Livia Thorpe[(5)], Michael Brunke[(6)], Leon Majewski[(7)], Andrew E. Kiss[(8)], and Chelle Gentemann[(9)]

(1) The Sino-Australian Research Centre for Coastal Management, UNSW Canberra @ ADFA, ACT, Australia. Email: haifeng.zhang@student.adfa.edu.au
(2) Bureau of Meteorology, Melbourne, Australia. Email: Helen.Beggs@bom.gov.au
(3) The Sino-Australian Research Centre for Coastal Management, UNSW Canberra @ ADFA, ACT, Australia. Email: X.Wang@adfa.edu.au
(4) Met Office, Exeter, UK. Email: jose.rodriguez@metoffice.gov.uk
(5) Met Office, Exeter, UK. Email: Livia.Thorpe@metoffice.gov.uk
(6) Department of Hydrology and Atmospheric Sciences, The University of Arizona, Tucson, Arizona, USA. Email: brunke@atmo.arizona.edu
(7) Bureau of Meteorology, Melbourne, Australia. Email: Leon.Majewski@bom.gov.au
(8) The Sino-Australian Research Centre for Coastal Management, UNSW Canberra @ ADFA, ACT, Australia. Email: A.Kiss@adfa.edu.au
(9) Earth and Space Research, Seattle, Washington, USA. Email: cgentemann@gmail.com

ABSTRACT

Four sea surface temperature (SST) diurnal variation (DV) models have been compared against Multi-functional Transport Satellite – 1R (MTSAT-1R) SST measurements over the Tropical Warm Pool region (TWP, defined in this study as 90°E-170°E, 25°S-15°N) for four months from January to April 2010. The four models include one empirical model (*Gentemann et al.,* [2003]: hereafter CG03), two physical models (*Zeng and Beljaars,* [2005] and *Takaya et al.,* [2010]: hereafter ZB05 and ZB+T), and one air-sea coupled model (the Met Office Unified Model Global Coupled configuration 2, hereafter UMGC2) with ZB05 warm layer scheme implemented.

DATA SETS

The reference SST dataset used in this study is the four months (January – April 2010) Australian Bureau of Meteorology (Bureau) reprocessed version 3 (v3) MTSAT-1R SSTskin data with 4 km resolution [*Beggs et al.,* 2013]. This data set is a contribution to the "TWP+ data set", a comprehensive dataset used to quantify DV events and test DV models as part of the Group for High Resolution SST (GHRSST) Tropical Warm Pool Diurnal Variability (TWP+) Project. The v3 MTSAT-1R data have been comprehensively validated for DV studies in *Zhang et al.* [2016].

MODELS

CG03 Model

An empirical DV model was formulated in *Gentemann et al.* [2003] using non-linear least-squares regression of passive microwave SST and surface wind speed data, from the Tropical Rainfall Measuring Mission (TRMM) Microwave Imager (TMI), and top-of-atmosphere modelled insolation data. In this study, we used a regression formula developed by Chelle Gentemann in 2008, that uses the method described in *Gentemann et al.* [2003], but which is derived using hourly, ~5 km resolution, SSTskin data from the Meteosat Second Generation (MSG) Spinning Enhanced Visible and Infrared Imager (SEVIRI). For details, please see *Gentemann et al.* [2003].

ZB05 Model

Zeng and Beljaars [2005] proposed a prognostic skin SST DV scheme. In the ZB05 model, with prior knowledge of the wind speed, surface fluxes, and foundation SST (SSTfnd) data, SSTskin can be calculated in two steps: the cool skin effect scheme and the warm layer profile scheme.

ZB+T Model

Takaya et al. [2010] proposed two refinements to the warm layer scheme in the ZB05 model, including the modification of a Monin-Obukhov similarity function for stable conditions and the introduction of the mixing enhancement by the Langmuir circulation.

UMGC2 Model

The UMGC2 model was released in March 2014. It is the latest configuration of the Met Office Unified Model [*Williams et al.,* 2015]. For this study, a DV scheme that consists of a warm layer and a cool skin scheme has been added to the coupled model. The warm layer scheme is the same as in ZB05, and the cool skin scheme is based on *Artale et al.* [2002].

The meteorological inputs (e.g., wind speeds, solar short-wave insolation (SSI), heat flux, etc.) of the CG03, ZB05, and ZB+T models are obtained from the Bureau's ACCESS-R (Australian Community Climate and Earth System Simulator-Regional) model [*Puri et al.,* 2013]. The Bureau's operational daily, 1/12° resolution, Regional Australian Multi-Sensor SST Analysis (RAMSSA; *Beggs et al.,* 2011) data have been used as SSTfnd inputs for the CG03, ZB05, and ZB+T models. In UMGC2, the SSTfnd is generated dynamically by the ocean submodel.

It should also be noted that the DV of SSTsubskin, rather than of SSTskin, is analysed in this study mainly due to the retrieval nature of the MTSAT-1R and SEVIRI SSTskin data [see *Zhang et al.,* 2017].

RESULTS

Before introducing the results, several concepts should be illustrated first: (1) SSTfnd: calculated as the average value of the values from 0:30 to 5:30 LST. (2) dSST: hourly SST minus the SSTfnd at one grid point. (3) dSSTmax: the maximum dSST within one solar day.

The distributions of dSSTmax values in MTSAT-1R and in each model are shown in Figure 1. Compared to MTSAT-1R, CG03 best captures the shape but estimates few dSSTmax > 3 K. ZB05 and UMGC2 estimate too many dSSTmax values > 2 K and > 3 K. Significantly more dSSTmax values < 0.3 K are found in ZB+T.

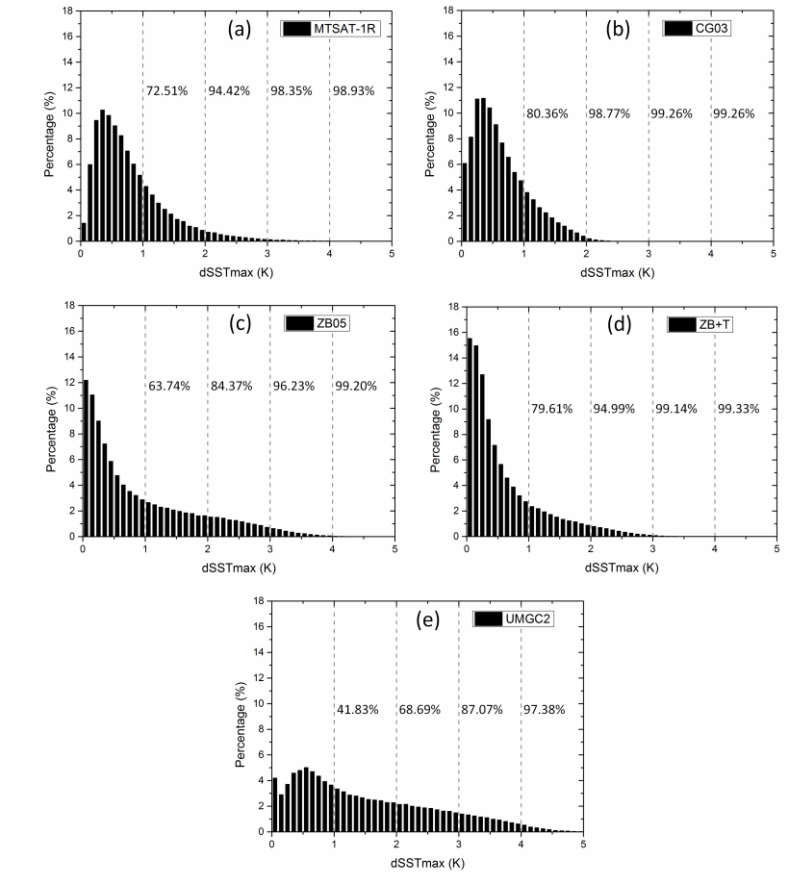

Figure 1. Distribution of dSSTmax values from: (a) MTSAT-1R; (b) CG03; (c) ZB05; (d) ZB+T; and (e) UMGC2 on 0.1 K intervals. The percentages are the accumulated proportions of dSSTmax < 1 K, < 2 K, < 3 K, and < 4 K (the dashed reference lines).

The SST DV cycles under different MTSAT-1R observational dSSTmax conditions are shown in Figure 2. Best agreement between MTSAT-1R and CG03, ZB05, and ZB+T are found when MTSAT-1R dSSTmax are between 1-2 K. All models underestimate the DV amplitude when MTSAT-1R dSSTmax are > 3 K.

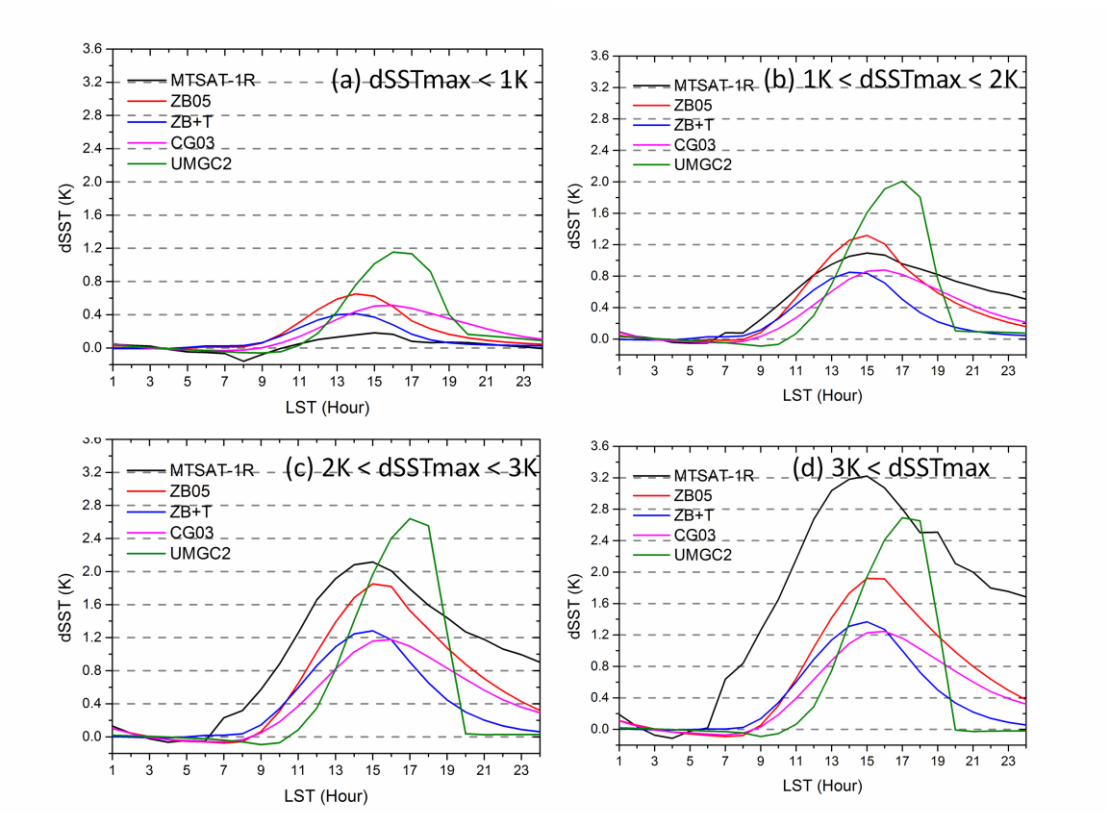

Figure 2. Average DV cycles from MTSAT-1R and four models for different MTSAT-1R dSSTmax conditions: (a) dSSTmax < 1 K; (b) 1 K < dSSTmax < 2 K; (c) 2 K < dSSTmax < 3 K; (d) dSSTmax > 3 K.

The SST DV cycles under different wind speed conditions are shown in Figure 3. For low winds, all models tend to overestimate the observed dSSTmax values. Noticeable overestimation is found only in UMGC2 for high winds.

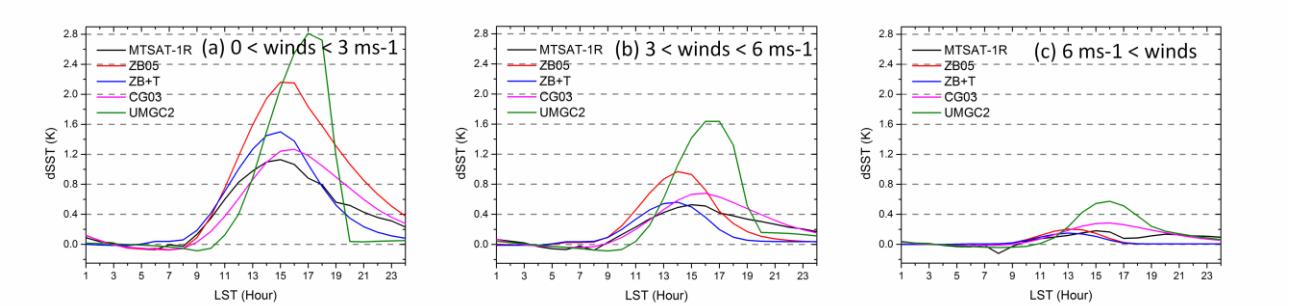

Figure 3. Average DV cycles from MTSAT-1R and all four models for different wind speed conditions: (a) wind speed < 3 ms-1; (b) 3 ms-1 < wind speed < 6 ms-1; (c) wind speed > 6 ms-1. Note that the 24 hr forecast ACCESS-R 10 m wind speeds are given as an average at the end of each hour.

Spatial distributions of temporally averaged dSSTmax values over the whole study period for MTSAT-1R and all models are plotted along with the collocated mean wind speeds (Figure 4). It shows that CG03 and ZB+T reflect the distribution quite well, both spatially and amplitude-wise. ZB05 has good spatial agreement with MTSAT-1R but with larger amplitudes for most DV events. Strong DV overestimation over a much larger region is seen in UMGC2.

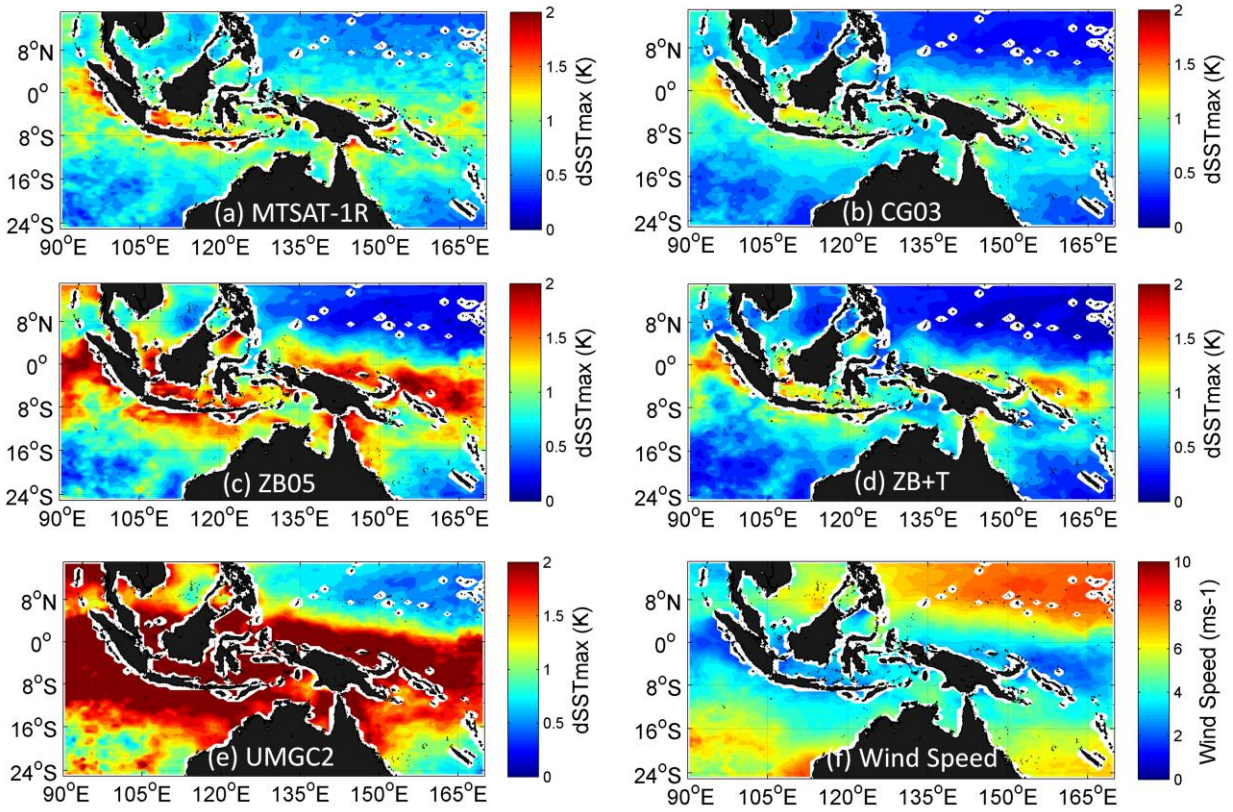

Figure 4. Spatial distribution of temporally averaged dSSTmax values from the (a) MTSAT-1R; (b) CG03; (c) ZB05; (d) ZB+T; and (e) UMGC2 models. Panel (f) shows the average of the collocated wind speed.

CONCLUSION

Assuming the v3 MTSAT-1R SSTs capture the full diurnal cycle, then the results indicate that all models are able to capture the general DV patterns but with differing accuracies and features. In general, all models are able to resolve the DV patterns under most conditions. However, statistically, they all underestimate very large DV events (with dSSTmax > 2-3 K). Specifically, CG03 agrees well with MTSAT-1R data for small to moderate DV events (dSSTmax < 2 K) but predicts few dSSTmax values > 3 K. ZB05 tends to overestimate small to moderate DV events, but can potentially predict large DV cases more accurately. As an updated version of ZB05, the skill of ZB+T is improved, showing better estimation in most DV ranges and in terms of the spatial distribution and amplitude. UMGC2 has a clear tendency to highly overestimate DV events. 1-2 hr lags in warming start and peak times in UMGC2 are also found. Work is underway to estimate the sensitivity of the v3 MTSAT-1R SST data set to capture the diurnal cycle, by comparing with collocated drifting buoy SST observations over the TWP+ domain and 4 month period.

REFERENCES (selected)

Artale et al., 2002, *J. Geophys. Res.,* 107(C8), doi:10.1029/2000JC000452.

Beggs et al., 2011, *Aust. Meteorol. Oceanogr. J.*, 61(1), 1-22.

Beggs et al., 2013, *Proceedings of the GHRSST XIV Science Team Meeting,* 104-121.

Gentemann et al., 2003, *Geophys. Res. Lett.,* 30(3), doi:10.1029/2002GL016291.

Puri et al., 2013, *Aust. Meteorol. Oceanogr. J.,* 63, 265-284.

Takaya et al., 2010, J*. Geophys. Res.,* 115(C6), doi:10.1029/2009JC005985.

Williams et al., 2015, *Geosci. Model Dev.,* 8(5), 1509-1524, doi:10.5194/gmd-8-1509-2015.

Zeng and Beljaars, 2005, *Geophys. Res. Lett.,* 32(14), doi:10.1029/2005GL023030.

Zhang et al., 2016, *Remote Sens. Environ.,* 183, 1-12, doi:10.1016/j.rse.2016.05.002.

Zhang et al., 2017, *J. Geophys. Res.,* in prep.

THE RESPONSE OF THE OCEAN THERMAL SKIN LAYER WITH AIR-SEA SURFACE HEAT FLUXES

Elizabeth W. Wong[(1)], Peter J. Minnett[(2)]

(1) University of Miami, 4600 Rickenbacker Causeway, Miami, FL 33149, Email: ewong@rsmas.miami.edu
(2) University of Miami, 4600 Rickenbacker Causeway, Miami, FL 33149, Email: pminnett@rsmas.miami.edu

ABSTRACT

There is much evidence that the ocean is heating due to an increase in concentrations of greenhouse gases (GHG) in the atmosphere from human activities. GHGs absorb infrared (IR) radiation and re-emit the radiation back to the ocean's surface where it is absorbed. However, the incoming longwave radiation, LW_{in}, is absorbed within the top micrometers of the ocean's surface, where the thermal skin layer (TSL) exists and does not directly heat the upper few meters of the ocean. We are therefore motivated to investigate the physical mechanism between the absorption of IR radiation, and its effect on heat transfer at the air-sea boundary. In this presentation, we hypothesize an indirect mechanism of the heating of the ocean and test this by investigating the variations in LW_{in} due to cloud forcing with retrieved average TSL vertical profiles from a shipboard IR spectrometer from two research cruises. The results show the absorbed IR in the TSL adjusts the curvature of the TSL such that a lower gradient occurs at the boundary between the TSL and the mixed layer. This hinders the heat from the mixed layer to be conducted into the TSL and subsequently released back into the atmosphere. Heat in the upper few meters of the ocean, which is due to the absorption of solar radiation during the day, is thus retained, causing an increase in upper ocean heat content.

SEA SURFACE TEMPERATURE INFLUENCE ON OCEAN CARBON CYCLE

W. Timothy Liu[(1)] and Xiaosu Xie[(2)]

Jet Propulsion Laboratory, California Institute of Technology, Pasadena, CA 91109, USA.
Emails: (1) w.t.liu@jpl.nasa.gov, (2) xiaosu.xie@jpl.nasa.gov

ABSTRACT

We have developed and validated a statistical model to estimate the partial pressure of carbon dioxide at sea surface (pCO2) from space-based observations of sea surface temperature (SST), chlorophyll, and salinity. We have produced and made accessible 9 years (2002–2010) of the pCO2 at 0.5 degree and daily resolutions over the global oceans. The outputs are found to be sensitive to variability from intra-seasonal to inter-annual and from equatorial to high-latitude oceans. They agree with 9-year time series at two tropical stations in annual phase and magnitude. Our data set is shown to pick up the spring blooms at high latitudes. The inter-annual anomalies of our data set follow the known response to El Nino episodes. The westward propagations of our outputs follow closely the tropical instability waves at intraseasonal scales.

1. INTRODUCTION

The alarmingly rapid increase of global atmospheric carbon dioxide (CO2) content has been well documented and is ascribed as the main factor in global warming. The net influx of CO2 to the ocean causes change in the carbonate system, referred as ocean acidification. Significant acidification will be deleterious to many marine ecosystems. The net CO2 flux between the ocean and the atmosphere has been parameterized in terms of a transfer (piston) velocity and (ΔpCO2), which is the difference between the partial pressure of CO2 in sea (pCO2s) and that in air near the surface (pCO2a). This study is focused on the estimation of pCO2s. pCO2s has been measured largely on ships. The conventional methods are not sufficient to characterize spatial and temporal variability.

Attempts have been made to establish regional and seasonal relations between pCO2s and variables that are more readily measured. In almost all studies, the relationships between pCO2s and other parameters are developed with co-incident measurements on cruises, mostly covering a limited region and a particular season. The correlation coefficients between pCO2s and oceanic parameters change from positive to negative over various regions. A single universal linear or polynomial regression, as derived in these studies, would not work over the global ocean across all seasons. Multiple relations covering different regions and seasons would have strong boundary discontinuity problems. Support vector regression (SVR) with location and time (season) as input parameters, will address such problems, and a universal model has been established for continuous and global coverage.

2. STATISTICAL MODEL

A statistical model has been developed to retrieve pCO2s from space-based observations using a state-of-the-art statistical method – SVR. More than a quarter million in situ measurements coincident with satellite data were compiled; 40,000 were randomly selected and set aside for validation and then another 40,000 were selected to train the model. For the 40,000 data pairs used in validation, the mean difference between model predictions and measurements is –0.17 µatm and the root-mean-square (RMS) difference is 16.37 µatm; the latter is 6% of the data range of approximately 270 µatm.

3. ANNUAL CYCLE

In the subtropical oceans, the annual variations of the model outputs are compared with in situ measurement of Hawaii Ocean Time-series (HOT) at Station ALOHA (22°45'N, 158°00'W) and the Bermuda Atlantic Time-series Study (BATS) near Bermuda (64°W, 32°N) in Fig 1. For BATS, the mean and standard deviation of the difference between the 2 time series are -6.9 µatm and 15.3 µatm respectively. The standard deviation is 16% of the annual range of 93.5 µatm for measurements. For HOT, mean and standard deviation of the difference are 6.0 µatm and 8.2 µatm. The standard deviation is 22% of the annual range. The annual range of model outputs is 71.4 and 34.4 µatm at BATS and HOT respectively. It is obvious from the figures and the annual ranges that the model outputs have smaller range than observations, although they track the annual variation well. The measurements increase at rates of 2.0 and 1.7 µatm per year for BATS and HOT respectively, but no significant increasing trend is found in the model outputs.

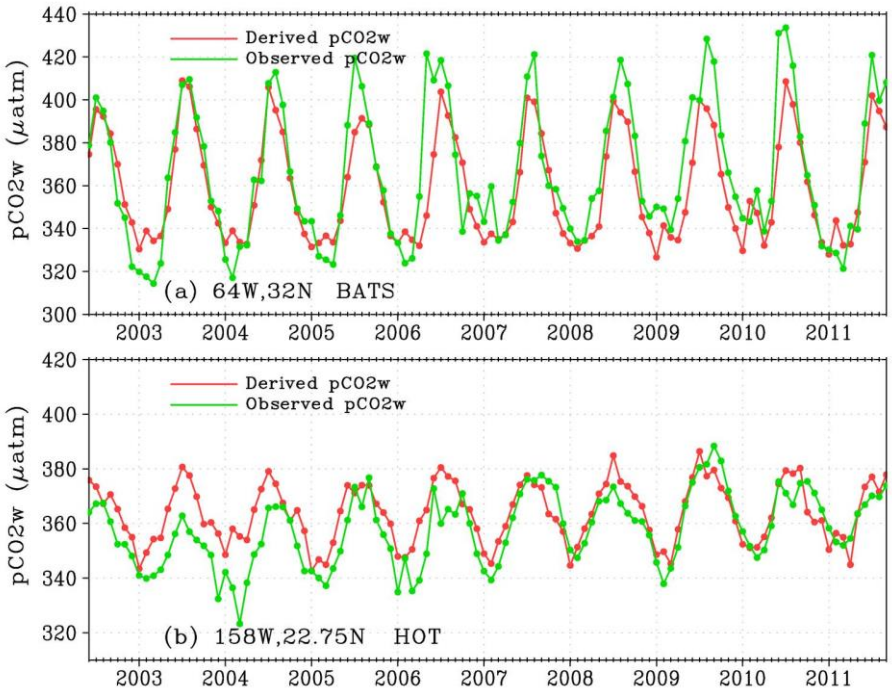

Fig. 1 Comparing 9 years of monthly pCO2s measured at Station (a) BATS, and (b) ALOHA with model outputs.

4. SPRING BLOOM

Ocean biological productivity becomes an important factor for pCO2s at extra-tropical latitudes. The conventional hypothesis is that ocean vertical mixing brings nutrient to the surface during winter. Increasing sunlight during spring allows strong increase in photosynthesis that depletes surface CO2. We examine several arbitrarily chosen 5-10° latitude-longitude boxes in the North Atlantic Ocean to find cruise measurements of pCO2s. Fig. 2 shows a example in a region (45N-50N, 45°W-55°W) in 2007, where a reasonable number of measurements covering the spring bloom are found. The time series at daily resolution show a major and a minor drop in model pCO2s during spring and fall, corresponding to rises in Chl-a, in consistent with ship data.

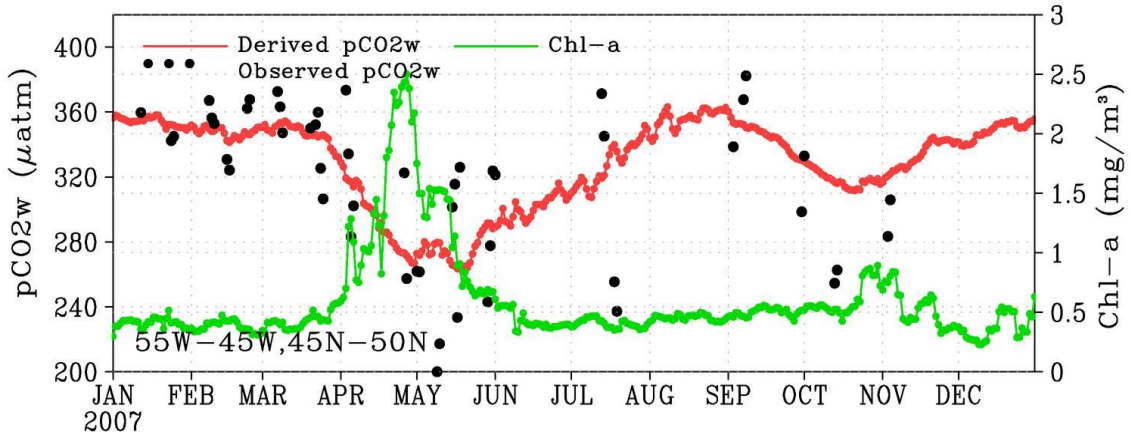

Fig. 2 Time series of pCO2s from model output and Chl-a at daily resolution for 2007 for an area in North Atlantic. Measurements from ships are superimposed.

5. INTERANNUAL ANOMALIES OF EL NINO

As we approach the equator from the subtropics, vertical advection and upwelling become increasingly important, bring cold and CO2-rich water to the surface. A negative correlation between pCO2s and SST has been found. The conventional El Nino indices are represented by inter-annual SST anomalies (with the climatological annual cycle removed) at two locations centered on the equator in the Pacific. They are Nino3, between 150°W and 90°W and Nino4 between 160°E and 150°W. The inter-annual anomalies of pCO2s from our model, with annual cycle derived from the 9-year of data removed, show opposite phases with the two El Nino indices in Fig.3. Positive anomalies (El Nino) correspond to negative pCO2s anomalies

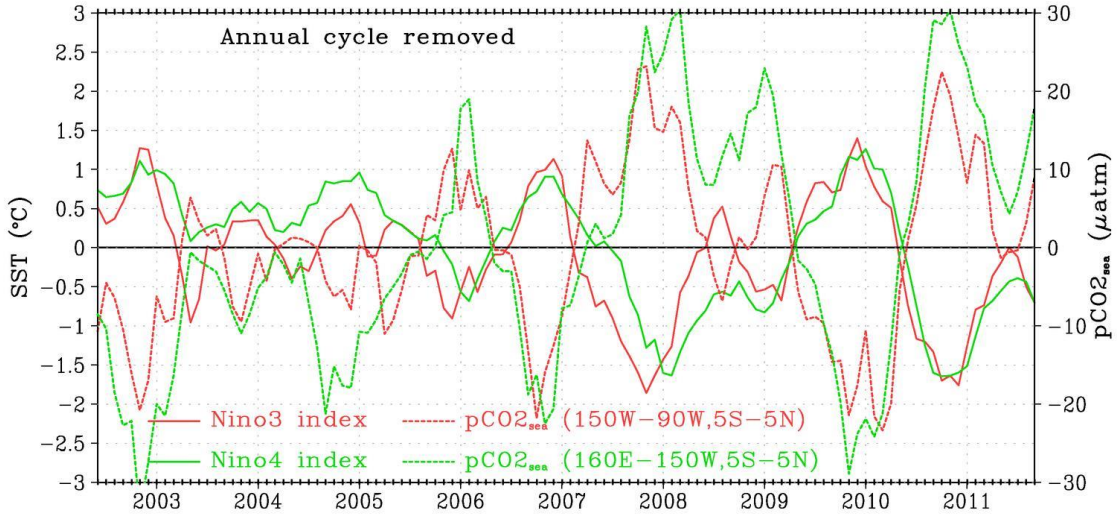

Fig. 3 Inter-annual anomalies of pCO2s from model outputs and El Nino indices at Nino3 and Nino4 locations.

(2002-2003, 2004-2005). This is in agreement with conventional knowledge, showing that our product picks up inter-annual anomalies.

6. HIGH FREQUENCY VARIATION OF THE TROPICAL INSTABILITY WAVES

In additional to the inter-annual episodes like El Nino, a dominant feature in the Equatorial oceans is the propagation of intra-seasonal tropical instability waves (TIW). TIW varies in exact location and phase velocity. Such waves were best observed by radiometers on geostationary satellites as meanders of the temperature front between the cold upwelling water of the Pacific equatorial cold tongue and the warm water to the north. In general, the waves propagate westward, with period of approximately 30 days, wavelength of 1100 km, and phase speed of 0.5 m/s. The waves are stronger from June to November and during La Nina episodes. The pCO2s from the model clearly show the manifestation of TIW: the data in 2007 are shown as an example in Fig. 4. High SST corresponds to low pCO2s. At 2ºN, both signals propagate westward approximately at same speed and period, which vary with latitude. Both signals are stronger in fall/winter than spring/summer.

7. DISCUSSION

The study has demonstrated the feasibility of continuous coverage of pCO2s over the global oceans from a few days to a few years using satellite data through a single statistical model. SST is the dominant factor in pCO2s changes, particularly in the subtropical oceans. The continuous availability of microwave radiometer with 7 GHz channel is uncertain after the Global Change Observation Mission for sufficient accuracy in the cold water of high latitude oceans.

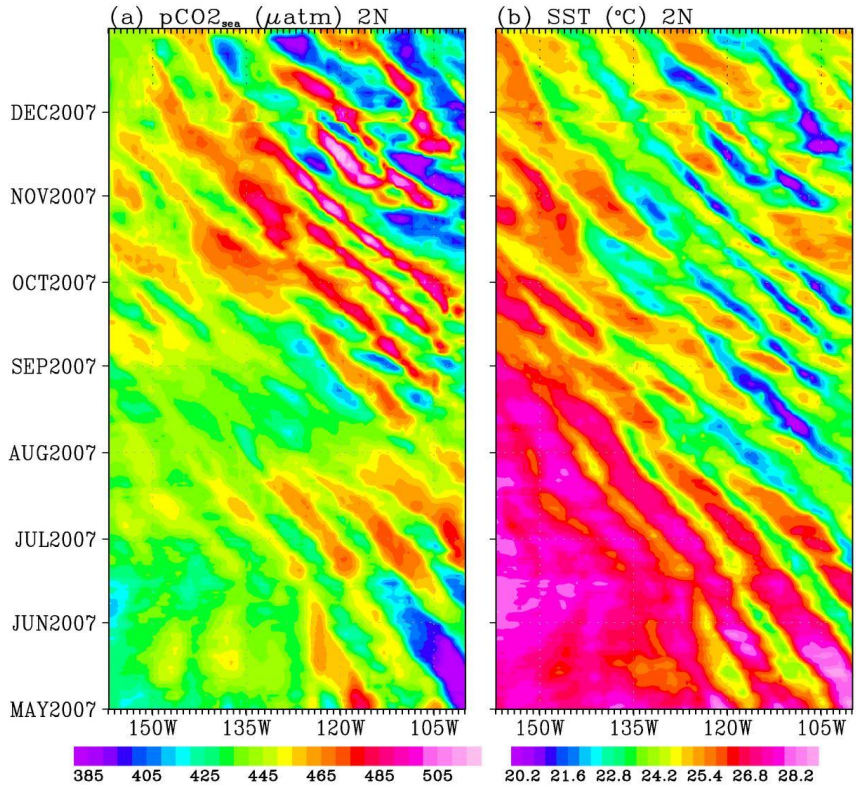

Fig. 4 Temporal and longitude variation at 2°N in the Pacific for (a) pCO2s from model output and (b) SST.

PLENARY SESSION V: SAMPLING

SESSION V REPORT

Chair: Peter Cornillon [(1)] - Rapporteur: Prasanjit Dash [(2)]

(1) University of Rhode Island, USA Email: pcornillon@me.com
(2) EUMETSAT, Germany and CSU CIRA, USA Email: prasanjit.dash@eumetsat.int

ABSTRACT

The session featured three speakers representing three organizations, and an open floor discussion.

1. SUMMARY OF SPEAKERS AND ORGANIZATIONS

1. Evaluation of the precision in L2 VIIRS and AVHRR SST fields (20min) – Fan Wu
2. ACSPO L3U SST products (20min) – Sasha Ignatov
3. Feature resolution in OSTIA L4 analyses (20min) – Chongyuan Mao
4. Open floor discussion (30min)

2. SUMMARY OF PRESENTATIONS

The highlights for each talk and floor discussion are given below.

2.1 Evaluation of the precision in L2 VIIRS and AVHRR SST fields – Fan Wu

This presentation was made on behalf of Ocean University of China and University of Rhode Island. The presentation highlighted the importance of assessing "spatial precision" of SST fields and argued that most attention is given to temporal accuracy and reports bias and standard deviation in comparison to collocated *in situ* measurements. The presentation demonstrated an approach to evaluate the spatial fidelity of satellite-derived SST fields, applied to VIIRS and AVHRR SST retrievals. The talk suggested instrument noise levels to be ~0.25 K for AVHRR and 0.05 K for VIIRS. It showed VIIRS to be an excellent sensor, from which night along-scan spectra provide excellent estimates of the spectral slope from 0.75 km to 50 km.

2.2 ACSPO L3U SST products – *Sasha Ignatov*

This presentation showcased overview of JPSS/Metop and L3U (level 3 un-collated; remapped level 2 data at 0.02º resolution; 10min granules) product from the VIIRS sensor generated by the NOAA heritage Advanced Clear-Sky Processor for Ocean (ACSPO) processor. It showed product improvement since last GHRSST XVII meeting and demonstrated that L3U-L2P and L3U-L4 CMC biases are reduced and spatial patterns better preserved. The presentation also provided some details of the averaging method that initially was based on the ABoM L3 binner but is subsequently modified using an *inverse distance bi-lateral weighted averaging* approach. Performance of newly added masking flags was also shown and tentative data release time was mentioned. Sasha emphasized that many users want L3 products as L2 could be too heavy to handle. The presentation generated an extensive discussion (and some disagreement) on binning approaches.

2.3 Feature resolution in OSTIA L4 analyses – Chongyuan Mao

The presentation was made on behalf of UK MetOffice that has been generating L4 OSTIA reanalysis product for several years. The talk reiterated the difference between grid and feature resolution and showed results

of spectral analysis on a new version of OSTIA. This new version intends to replace the currently operational OI-based approach with a 3D-VAR assimilation scheme. Data from dynamic areas including Gulf Stream, Kuroshio Current and Agulhas Current was used for demonstration of improved feature resolution in the newer product. The feature resolution of this newer version was compared to with those from CMC and RTG. Also, preliminary result of the impact of ingesting SLSTR L2P SST product was shown.

3. SUMMARY OF FLOOR DISCUSSION (DISCUSSION/SUGGESTIONS/ACTION)

3.1 Evaluation of the precision in L2 VIIRS and AVHRR SST fields

- **Q: Helen Beggs: sorry missed the part, which NOAA satellite**

  A: NOAA 15; background: observed cross-track anomalous results in AVHRR
- Jon Mittaz (comment): NOAA15 has significant CAL issues. If you can redo, I suggest using Metop.
- Sasha Ignatov (comment): Also, use FRAC
- Peter Cornillon (comment): We wanted to establish the method; and in next steps, all AVHRRs.
- **Q:** Helen Beggs: tested it on HRPT?
  A: not yet
- **Q:** Helen Beggs: Would you like to?
  A: (Peter Cornillon): Yes. These are L2 SSTs but not in GHRSST data format
- Andy Harris (comment): attempted to give the cause of observed cross-track anomalous observations; along-track: jumps, cross: smearing.
- Peter Cornillon (comment): We want to first know the small stuff. What is intriguing here is the VIIRS.

Action: Fan Wu/Peter Cornillon: When possible, try on Metop and let the community know.

3.2 ACSPO L3U SST products

- **Q: Helen Beggs: I'm keen to use reprocessed data; does that use this new method?**

  A: Not yet, we will do soon.
- Helen Beggs (comment): We will reprocess IMOS as well
- Sasha Ignatov (further answer/comment): Everything is based on priority. If you put a user request, we will make our best efforts.
- **Q:** Jorge Vazquez: Between the choice of Nearest Neighbor (NN) and Bilinear (BL) method, is it possible that BL destroys the frontal features?
  A: We have looked at 100s of images and have not seen any such example yet.
- **Q:** Feng Lu: Will the spatial resolution of all L3s from all satellite sensors be the same?
  A: Yes. It (0.02º) will be difficult for ABI/AHI. It will be likely 0.05º, we can't make it 0.02º.

At this point there was extensive Q/A, back and forth between C. Merchant and S. Ignatov regarding the implications of QL in data-sparse regions. Essentially, Chris wanted to know how the method copes when there are only a few pixels with coincidentally high QL, how is it assigned in the L3 grid.

- **Q:** Chris Merchant: When creating L3 grid from L2P, it can introduce additional data (coverage?). In sparse areas with higher QF, how is it assigned/handled?
  A: We don't introduce artificial features but some gap filling in continuous areas.

  (The QF/QL question and the answer about 'non-introduction of artificial feature was repeated)
- Chris Merchant (further comment): You successfully did not answer my question for the 3rd time and it was agreed to take the discussion offline (non-conclusive).
- **Q:** Andy Harris: What do you do about SSES while binning and how it copes in sparse areas?
  A: similar approach; separate discussion. But we don't see any major artifacts.
- **Q:** Andy Harris: Same for QL?
  A: majority is chosen (*i.e.*, the predominant QL).
- Helen Beggs (comment): BoM is doing this for years, i.e., Chris Griffin. Chris Griffin did not write any paper but has a long manual. He describes in great length how to composite SSES/QL.
- Sasha Ignatov (comment): Chris Griffin spoke about "L3 to L3U/L3C"; I spoke about "L2 to L3".
- Helen Beggs (comment): I will provide the manual.

Action: Sasha Ignatov/Chris Merchant: Touch base on the inconclusive discussion.

Action: Helen Beggs: Provide the Manual by Chris Griffin that attempts to explain this challenge.

3.3 Feature resolution in OSTIA L4 analyses

- Xu Li (comment): Mentioned about the cold bias in RTG and spoke about "something" they will try. Q/Comment: Rosa Santoleri: It doesn't surprise me there is no difference in mean and standard deviation for the two approaches. What is the advantage of *NEMOVAR over OI?

  (*NEMOVAR is 3D-Var data assimilation method for use with the NEMO ocean model)

  A: I can only say superficial "Scientifically Robust".
- **Q:** Rosa Santoleri: When available?
  A: Soon. We are debating between 50km and 40km for correlation length scale.
- **Q:** Andy Harris: There are different correlation length scales. You spoke about climatology. Where does the **flow-dependent component come from

  A: previous day

  (**if the length scales used for daily analysis is too long, oceanographic features will be smoothed out. So, a flow-dependent component to determining an effective length-scale is used in NEMOVAR)
- **Q:** Jorge Vazquez: Will it be worth doing PSD (power spectral density) for other areas and times? Is it realistic?

  A: Yes, we will.
- **Q:** Chris Merchant: You said PSD is necessary for assessing feature resolution? Can you make some comparison of analysis against other real observations? Do you agree that it is useful?

A: Yes, we agree. We will be doing it in the future

- **Q:** Peter Cornillon: In areas such as Gulf Stream, Agulhas, the spectra can change dramatically, time to time. Did you do some temporal stability analysis to check this?
  A: We will.
- **Q:** Helen Beggs: The correlation length scale is background or observational?
  A: Background
- **Q:** Helen Beggs: Why 40km? It is too long. Is it to make smoother NWP-suitable data?
  A: Yes, for NWP purposes; also, due to the presence of noise.
- **Q:** Helen Beggs: Is it documented?
  A: Yes, we are writing a CCI paper.

Action: Chongyuan Mao: PSD for other areas and times; temporal stability of spectra in highly dynamic area.

EVALUATION OF THE PRECISION IN LEVEL 2 VIIRS AND AVHRR SEA SURFACE TEMPERATURE FIELDS

Fan Wu[(1)(2)], Peter Cornillon[(2)], Lei Guan[(1)] , Brahim Boussidi[(2)]

(1) Ocean University of China, Qingdao, Shandong, China, Email: wufan620@126.com
(2) University of Rhode Island, Narragansett, RI, USA, Email: pcornillon@me.com

1. INTRODUCTION

A great deal of attention has been focused on the temporal accuracy of satellite-derived sea surface temperature (SST) fields with little attention being given to their spatial precision. Specifically, the primary measure of the quality of SST fields has been the bias and variance of selected values minus co-located (in space and time) in-situ values. Contributing values, determined by the location of the in-situ values and the necessity that the satellite-derived values be cloud free, are generally widely separated in space and time hence provide little information related to the pixel-to-pixel uncertainty in the retrievals. But the main contribution to the uncertainty in satellite-derived SST retrievals relates to atmospheric contamination and because the spatial scales of atmospheric features are, in general, large compared with the pixel separation of modern infrared sensors, the pixel-to-pixel uncertainty is often smaller than the accuracy determined from in-situ match-ups. This makes selection of satellite-derived datasets for the study of submesoscale processes, for which the spatial structure of the upper ocean is significant, problematic.

An approach developed to evaluate the spatial fidelity of satellite-derived SST fields is presented here. Applying this approach to AVHRR and VIIRS level-2 SST products, we find that VIIRS night along-scan spectra provide excellent estimates of the spectral slope from 0.75 km to 50 km. The analysis also shows more energy at day than at night. AVHRR spectra, by contrast, have elevated energy at the submesoscale due to higher noise levels, the increase in noise overwhelming the diurnal signal. Preliminary evaluation suggests instrument noise levels (standard deviations) to be approximately 0.25 K for AVHRR and 0.05 K for VIIRS, with variance in VIIRS retrievals depending on the along-scan versus along-track directions.

2. EXTENDED ABSTRACT

The primary measure of the quality of sea surface temperature (SST) fields obtained from satellite-borne infrared sensors has been the bias and variance of matchups with co-located in-situ values. Because such matchups tend to be widely separated, these bias and variance estimates are not necessarily a good measure of small scale (several pixels) gradients in these fields because one of the primary contributors to the uncertainty in satellite retrievals is atmospheric contamination, which tends to have large spatial scales compared with the pixel separation of infrared sensors. Hence, there is not a good measure to use in selecting SST fields appropriate for the study of submesoscale processes and, in particular, of processes associated with near-surface fronts, both of which have recently seen a rapid increase in interest. In this study, two methods are examined to address this problem, one based on spectra of the SST data and the other on their variograms.

To evaluate the methods, instrument noise was estimated in Level-2 VIIRS and AVHRR SST fields of the Sargasso Sea. The two methods provided very nearly identical results for AVHRR: along-scan values of approximately 0.18 K for both day and night and along-track values of 0.21 K also for day and night. By contrast, the instrument noise estimated for VIIRS varied by method, scan geometry and day-night. Specifically, daytime, along-scan (along-track), spectral estimates were found to be approximately 0.05 K (0.08 K) and the corresponding nighttime values of 0.02 K (0.03 K). Daytime estimates based on the variogram were found to be 0.08 K (0.10 K) with the

corresponding nighttime values of 0.04 K (0.06 K). Taken together: AVHRR instrument noise is significantly larger than VIIRS instrument noise, along-track noise is larger than along-scan noise and daytime levels are higher than nighttime levels. Given the similarity of results for AVHRR, and the less stringent preprocessing requirements, the variogram is the preferred method for sensors with significant instrument noise. For the higher quality instruments the variogram will provide an upper limit on the estimate but, for a more accurate estimate, either the spectral approach should be used or the variogram method should be modified to address the apparent overestimate in the noise.

Finally, simulations of the impact of noise on the determination of SST gradients show that on average the gradient magnitude for typical ocean gradients will be accurately estimated with VIIRS but substantially overestimated with AVHRR.

3. FIGURES AND TABLES

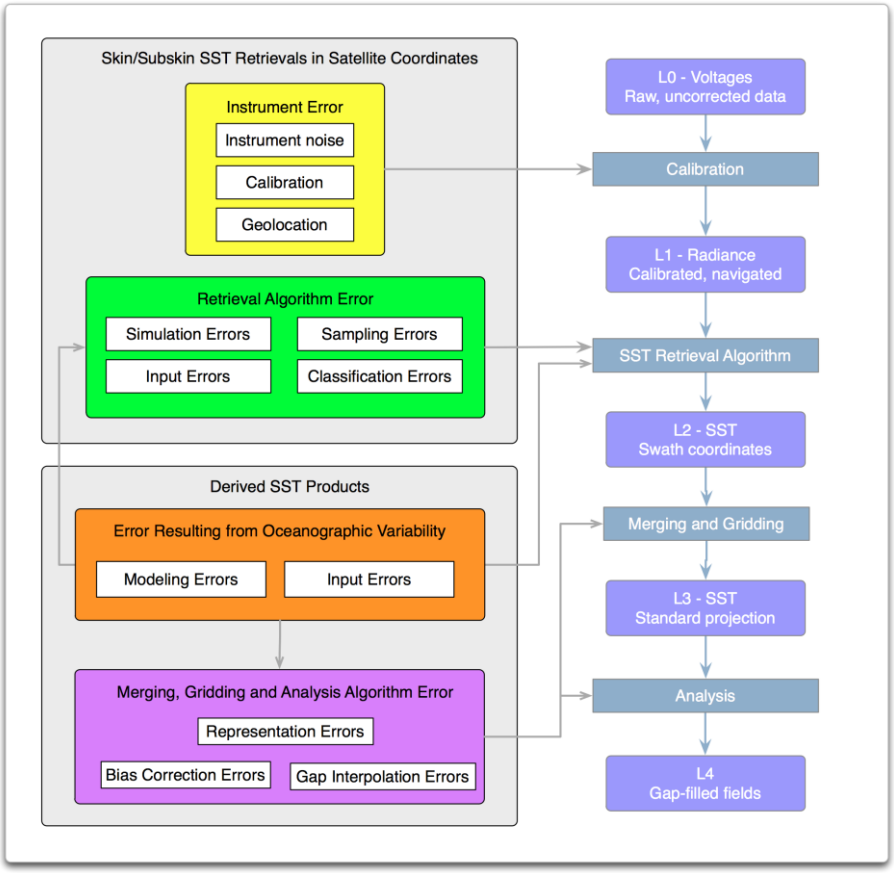

Figure 5. The error budget developed by the NASA-NOAA SST Science Team for satellite-derived SST fields.

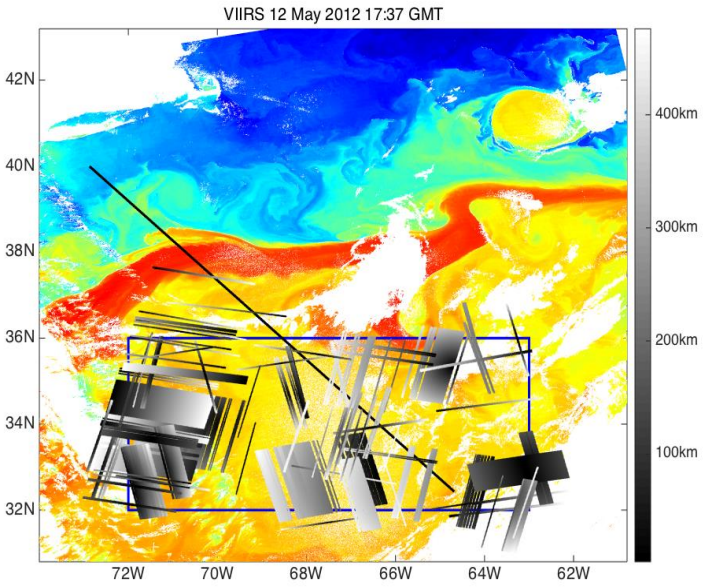

Figure 6. VIIRS SST image from 12 May 2012. The long black line (73.5W, 40N to 64.8W, 32.6N) indicates the nominal Oleander track. Blue frame denotes the region of the Sargasso Sea considered in this study. Shades of gray denote the location of sections extracted from VIIRS SST fields – discussed. The gray scale indicates distance from nadir (discussed in detail in subsequent sections). Sections with a constant gray level are along-track sections; those with a gradient in gray are along-scan. Along-track (along-scan) sections with a negative slope and along-scan (along-track) sections with a positive slope are daytime (nighttime) sections. The SST field is simply provided as a background reference field and corresponds to only one of the images used.

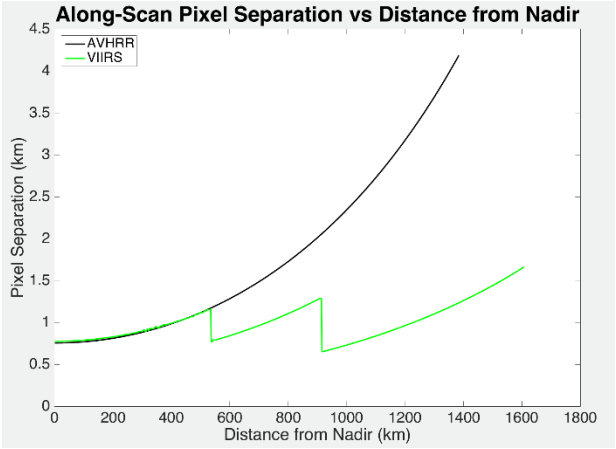

Figure 7. Spacing in the along-scan direction for AVHRR and VIIRS pixels in L2 fields as a function of distance from nadir.

Table 3. Number of sections meeting the given selection criteria discussed in this section.

	Day		Night	
	Along-Scan	**Along-Track**	**Along-Scan**	**Along-Track**
VIIRS	126	517	561	615
AVHRR	266	256	104	193
Oleander		42		

Table 4. Grouping of along-scan sections based on mean pixel spacing of the temperature section. The values indicated correspond to the lower limit on the range – the value to which temperatures sections in this range are interpolated – the upper limit on the range.

	Group 1 (m)	**Group 2** (m)	**Group 3** (m)
VIIRS	770-805-820	860-885-910	940-995-980
AVHRR	760-765-810	820-865-920	940--947980

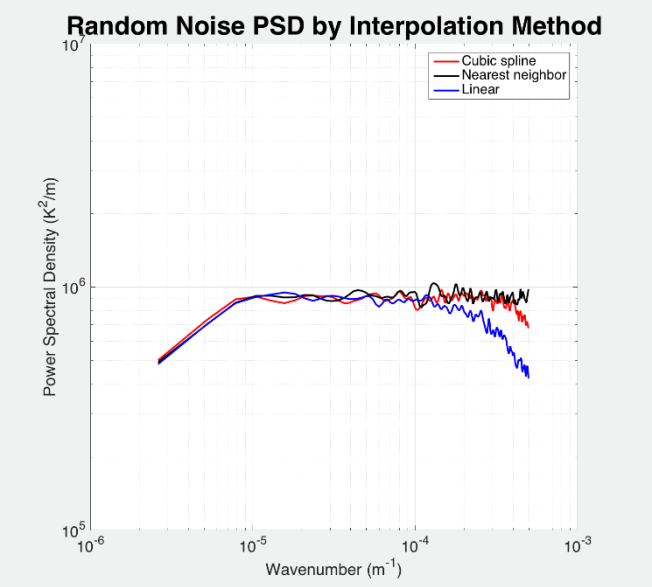

Figure 8. Spectral response of the interpolation methods applied to white noise.

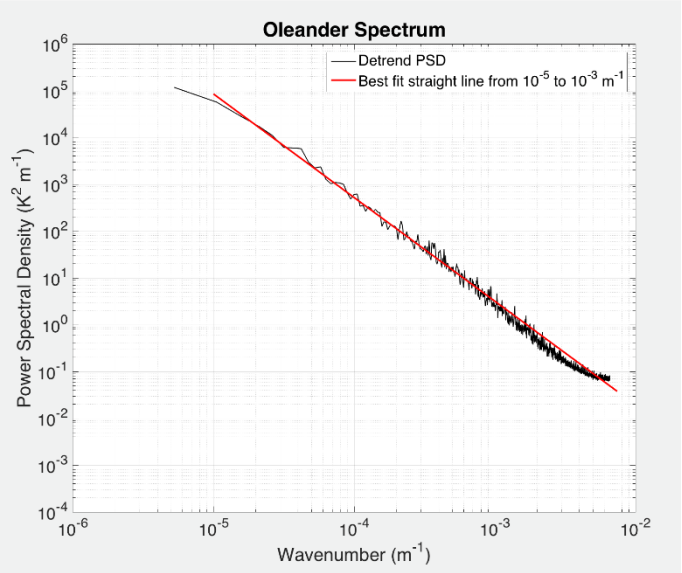

Figure 9. Power spectral density from Oleander TEX for all Oleander summer sections (June-August) of 2008 through 2013 with maximum sample separation less than 150 m. Temperature sections detrended prior to determining and ensemble averaging the spectra. Straight red line: least squares best fit straight line (slope = -2.12) of log_{10}(PSD) to log_{10}(wavenumber) between 10^{-5} and 10^{-3}.

Table 5. Estimated instrument noise in satellite-derived SST fields. Numbers in parentheses are the number of subgroups from which the means are determined. The indicated uncertainty of the means is the square root of the variance of the contributing subgroups over the number of subgroups.

	Method	Day (K)		Night (K)	
		Along- Scan	**Along-Track**	**Along- Scan**	**Along-Track**
AVHRR	**Spectra**	0.172±0.001 (5)	0.209±0.001 (7)	0.173±0.003 (2)	0.209±0.008 (4)
	Variogram	0.185±0.004 (5)	0.219±0.006 (7)	0.183±0.001 (2)	0.219±0.006 (4)
	Upper Limit	0.189	0.218	0.194	0.208
VIIRS	**Spectra**	0.046±0.001 (4)	0.076±0.002 (10)	0.021±0.001 (24)	0.032±0.002 (14)
	Variogram	0.081±0.013 (4)	0.097±0.006 (10)	0.042±0.004 (24)	0.056±0.004 (13)
	Upper Limit	0.078	0.101	0.050	0.057

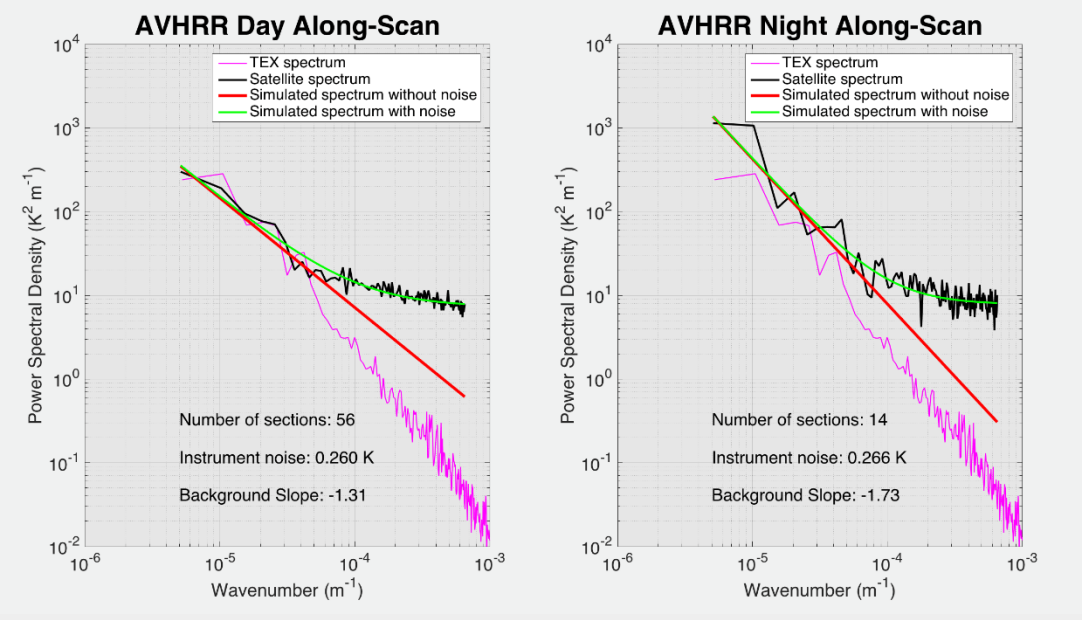

Figure 10. Mean AVHRR spectra for contiguous along-scan sections (black). Best-fit linear spectra with noise to the mean VIIRS spectra (green). Best-fit linear portion of the best-fit linear spectra with noise (red). Mean TEX spectrum shifted vertically to allow for comparison (magenta).

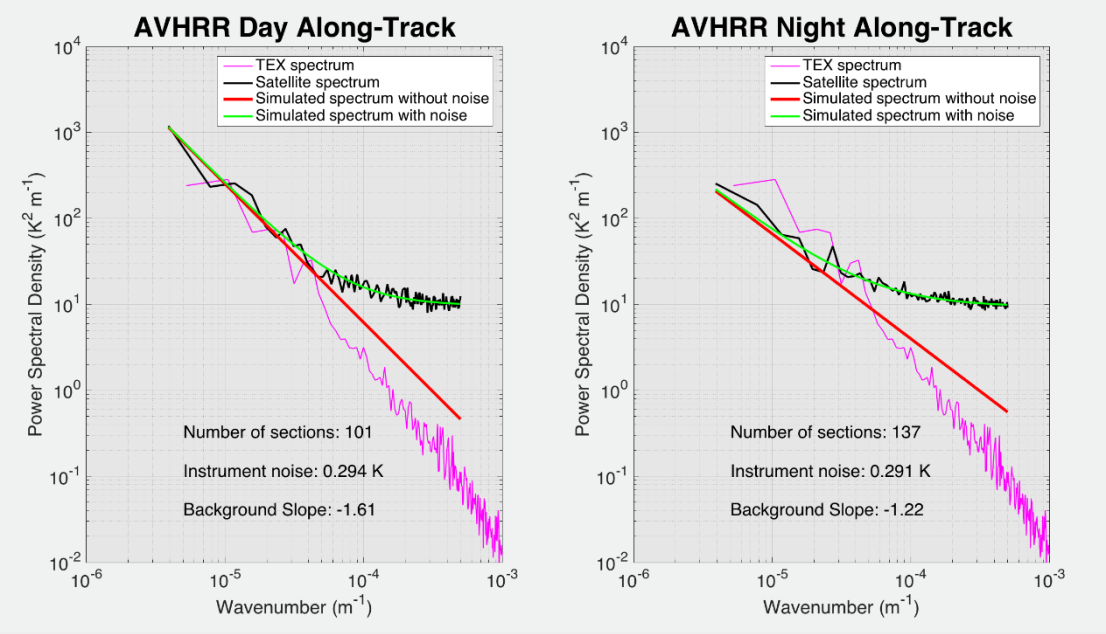

Figure 11. Mean AVHRR spectra similar to Figure 6 except for along-track sections. Daytime spectrum for 21:08 GMT on 10 June 2012. Nighttime spectrum for 09:34 GMT on 23 June 2012.

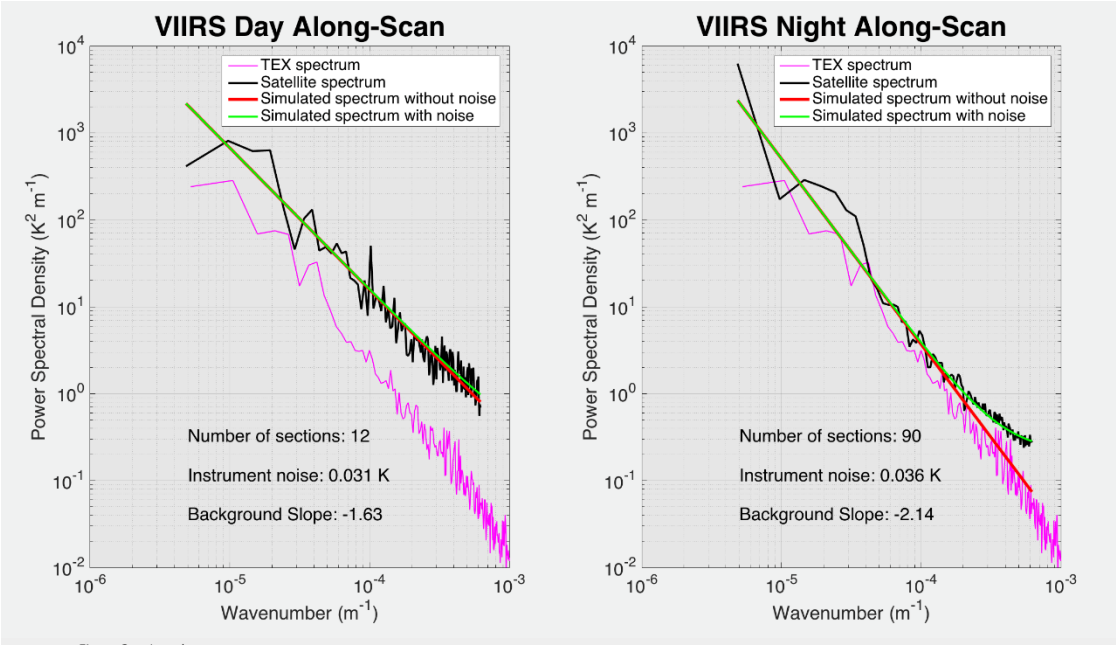

Figure 12. Mean VIIRS spectra similar to the AVHRR spectra in Figure 6.

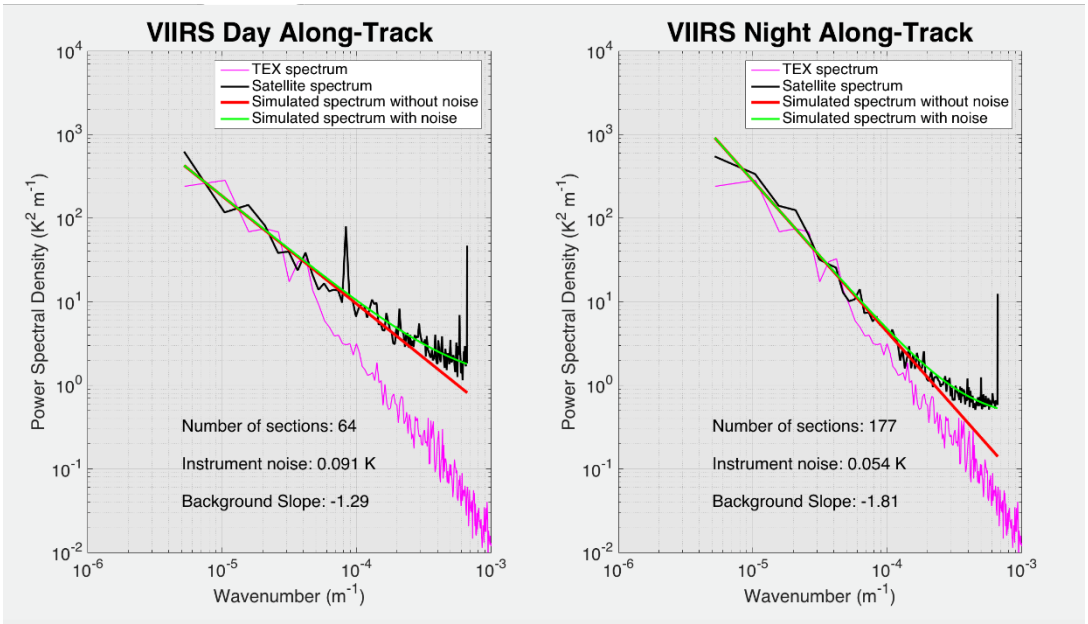

Figure 13. Mean VIIRS spectra similar to the AVHRR spectra in Figure 7. Daytime spectrum for 17:56 GMT on 11 June 2012. Nighttime spectrum for 06:21 GMT on 1 June 2012.

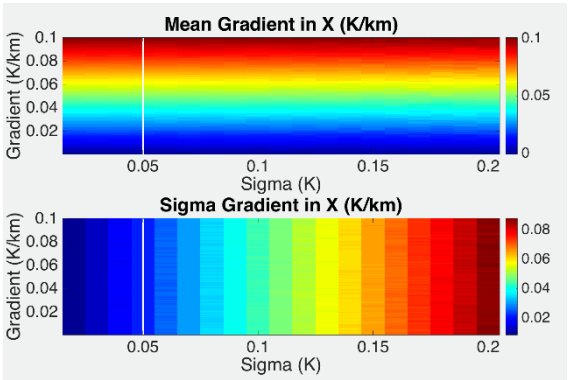

Figure 14. Simulated impact of Gaussian white noise of magnitude sigma imposed on a field with an x-gradient indicated on the vertical axis. The vertical white line is an imposed noise level typical of VIIRS values

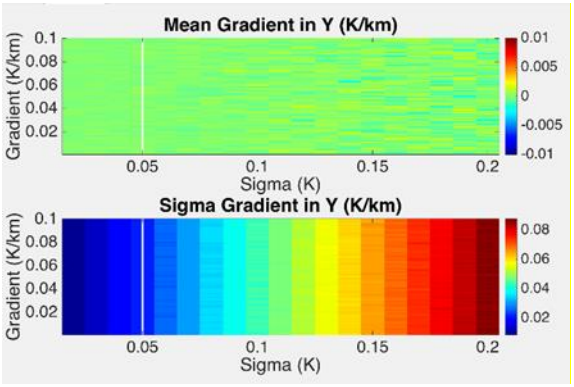

***Figure 15**. As in Figure 14 except for the y-component of the gradient.*

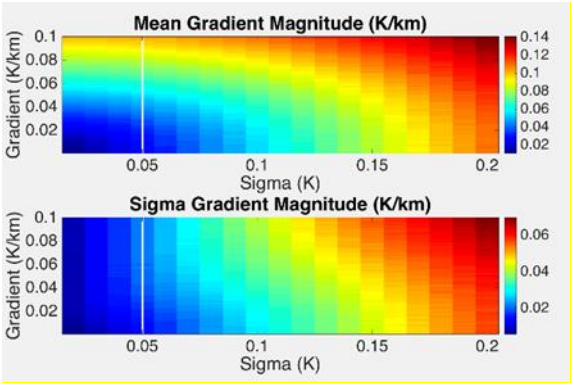

***Figure 16**. As for Figure 14 except for the gradient magnitude.*

4. RESULTS

THE LOCAL PRECISION OF SATELLITE-DERIVED SST RETRIEVALS. THE NOISE RESULTING FROM PROCESSES IN THE YELLOW AND

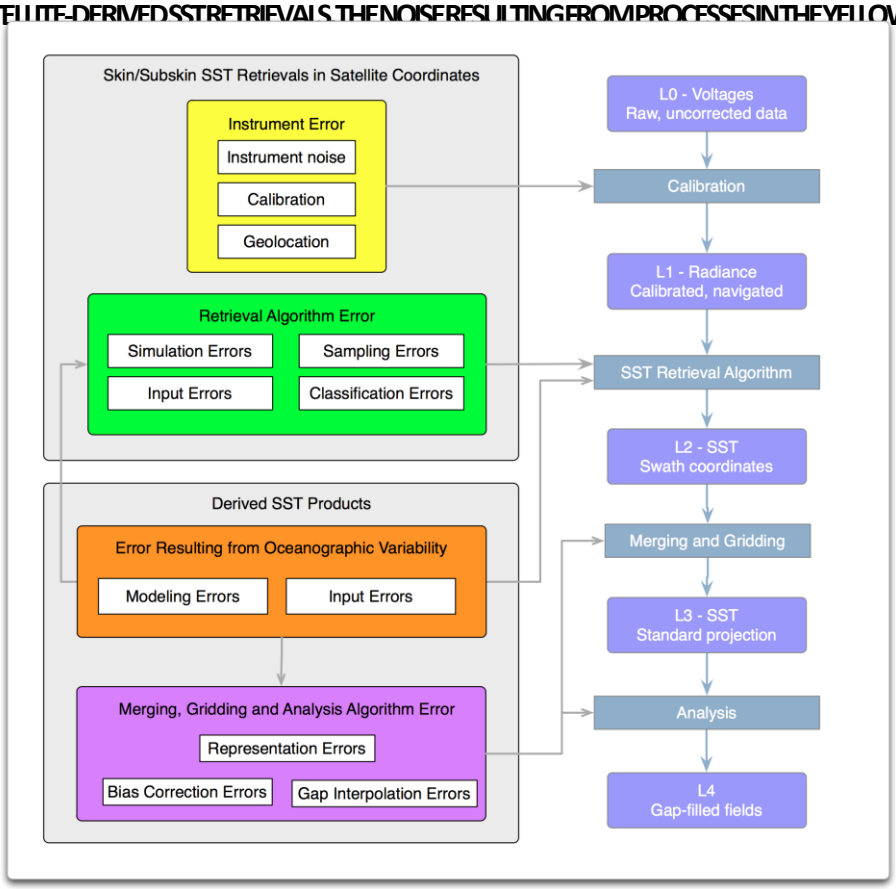

GREEN BOXES OF

Figure 5, which we refer to as instrument noise here, is shown in Table 5 for each of the along-scan/along-track, day/night combinations. The first row for each sensor (labeled *Spectra*) corresponds to the estimates obtained from the spectral method. Only subgroups consisting of five or more temperature sections and

with a spectral slope steeper than -1 were used. The instrument noise for subgroups with shallower spectral slopes tended to dominate the geophysical signal increasing the uncertainty in the fit of Eq. 5. The noise estimates provided in the table are the means of the estimates associated with each subgroup. The uncertainty is the square root of the variance of these means over the number of contributing subgroups. Variogram estimates follow in the next row (labeled *Variogram*) for each sensor, the mean of the estimates from the same subgroups used in the spectral approach and the uncertainty is calculated as for the spectral approach. The quoted uncertainty is the square root of the variance of all nuggets over the total number of sections. The final row of the table (labeled *Upper Limit*) for each sensor is an 'upper limit' on the instrument noise assuming that the pixel-to-pixel noise is white. This was obtained by noting that the variance of the difference of adjacent SST values, $\sigma^2(\Delta x_{\min})$, is the sum of the variances of the noise of each of the two values, $2\sigma_i^2$, plus the contribution due to the geophysical variance between the two values, $\sigma_{geo}^2(\Delta x_{\min})$:

$$\sigma^2(\Delta x_{\min}) = 2\sigma_i^2 + \sigma_{geo}^2(\Delta x_{\min}) \implies \sigma_i \leq \frac{\sigma(\Delta x_{\min})}{\sqrt{2}} \quad (11)$$

If the noise is not white, for example, the actual level of noise may, in fact, be larger than the 'upper limit'.

4.1. AVHRR

Day-versus-night, along-scan instrument noise levels obtained for the AVHRR data are not statistically distinguishable. Nor are the along-track levels. The levels for the variogram estimates based on the same subgroups as the spectral estimates (2nd row) are also statistically similar[1]. Furthermore, although somewhat larger the variogram estimates are quite close to the spectral estimates and all of the estimates are close to the 'upper' limit for the given sensor/day-night/scan-track combination suggesting that the instrument noise is white. It is possible that the pixel noise is correlated at small scales but, again, the mechanism for this is not obvious.

The along-scan AVHRR spectra are shown in Figure 10 for a daytime subgroup and a nighttime subgroup. Also shown in the figure are the best-fit linear spectra with noise, obtained as discussed. Figure 11 shows the corresponding along-track AVHRR spectra. In all four cases, noise is seen to impact the spectrum for wavelengths (wavenumbers) up (down) to approximately 25 km (0.04 km-1). Also apparent from these plots is that the approximately linear portion of the AVHRR spectrum corresponds to a small fraction (~10%) of the 129 spectral values. This means that relatively small changes in the low wavenumber end of these spectra will have a more significant impact on the estimated background slope than for spectra less impacted by noise. However, the spectral method for determining instrument noise is relatively insensitive to this; significant changes in slope and intercept result in virtually identical values of instrument noise. For example, for the spectrum shown in the left panel of Figure 7, a slope, offset combination of (-1.7570, -6.2730) yields the same level of instrument noise. This is because the instrument noise is one to two orders of magnitude larger that the assumed geophysical signal, the straight line portion of the spectrum, over a significant fraction of the spectrum (remember the fits are in regular, not log-log space) so changes in the slope do not result in a significant difference in the squared sum of the differences between the model and the observed spectrum. For spectra that level off substantially at large wavenumbers, the noise is effectively determined by the power spectral density level at these wavenumbers. This is readily seen in Figure 7 and 8; the high wavenumber end of the simulated spectra with noise are at a similar level for the along-scan sections and at a slightly higher level for the along-track sections. Care must be taken however when the level of instrument noise is similar, or smaller, in magnitude to the geophysical signal at these wavenumbers, as will become clear in the analysis of the VIIRS spectra.

AVHRR along-track instrument noise is approximately 20% larger than along-scan instrument noise. This is presumably due to the line-by-line calibration undertaken in the development of the L1b data product used as input to the L2 retrieval algorithm.

[1] In the remainder of the discussion we focus on the first of the two variogram estimates to facilitate comparison of the methods.

4.2. VIIRS

Mean VIIRS spectra similar to those shown for AVHRR in 6 and 7 are shown in 8 and Figure 13, respectively. The spectra in these figures differ in several key ways from those associated with AVHRR. First, the level of instrument noise is, in all cases, *substantially* lower than that for AVHRR. Second, spectral peaks, especially in the daytime spectra, are evident at 1.5, 2.2, and 2.9 km as well as a broad peak at 12 km in the along-track spectra (Figure 13). As previously noted, there are 16 detectors for each of the VIIRS moderate resolution bands used for SST retrievals, hence, one scan of the instrument consists of 16 scan lines. The gain of these detectors may differ slightly and this difference is not regular; i.e., it changes along-scan and between scans. This is what gives rise to the observed peaks; the peaks at 1.5, 2.2, and 2.9 km correspond to a separation of one, two and three pixels and the peak at 12 km corresponds to the 16 pixel repeat scans of the instrument (750 m × 16 detectors = 12 km). Reassuringly, the along-scan spectra do not show these peaks. Also note that the noise from the different detectors contributes to a general elevation of the large wavenumber end of the spectrum – the simulated spectra with noise in Figure 13 tend to separate from the associated straight line spectrum at wavelengths smaller than approximately 8 km for along-track sections compared with approximately 5 km for along-scan sections. The point of separation is, of course, a function of the magnitude of the geophysical signal. In regions with a significantly larger geophysical signal, in the vicinity of the Gulf Stream for example, instrument noise will likely have no effect on the spectrum, with the possible exception of a few of the peaks.

The third significant difference between AVHRR and VIIRS spectra relates to the daytime spectra compared with the nighttime spectra. Specifically, there is a statistically significant difference between daytime and nighttime VIIRS spectra, with the daytime spectra being more energetic at wavelengths smaller than approximately 100 km. This is likely due to diurnal warming, which occurs frequently in the Sargasso Sea in summer months [6, 10]. Also note that the slope of nighttime spectra for both along-scan and along-track sections is closer to that of the TEX spectrum than the daytime spectra. Surprisingly, the level of instrument noise is also larger at daytime than at nighttime as is evident both from the figures and from 3. This may result from the sensitivity of the banding to the energy in the SST field. Banding is difficult to correct for because it is not the entire scan line that has higher values than its neighbors, but rather, what appear to be randomly located segments of a given scan line. Furthermore, the magnitude of the difference in these regions appears to be related to the magnitude of the retrieved temperature.

Finally, the level of instrument noise estimated with the spectral approach is substantially smaller than (as much as one half) that estimated based on the variogram. This may result from an overestimate of the nugget in the variogram approach due to energy aliased into the signal for wavelengths larger than the Nyquist frequency as described. The spectral approach to determine instrument noise attempts to compensate for this. Specifically, the aliased energy results in a leveling off of the spectrum at large wavenumbers, a leveling off that is similar to that associated with instrument noise. This is compensated for by simulating temperature sections at 10 times the sampling frequency of the satellite data, averaging over the satellite spatial scale, decimating by 10 and then adding noise. This will result in a lower level of noise than one would get by assuming no geophysical energy at larger wavenumbers. The variogram approach does not compensate for this.

4.3. Comparison of the AVHRR L2 instrument noise estimates Tandeo et al's results

Tandeo et al. estimated the nugget in the L3 Meteosat AVHRR data set produced by the O&SI SAF Project Team [1, 14]. This product was assembled by remapping the full resolution nighttime AVHRR fields onto a regular 0.05° × 0.05° global grid and averaging the results into 12 h fields. They found $\sigma_o \approx 0.14$ K for the study area. This is larger than would be expected if instrument noise of the full resolution Meteosat AVHRR

data is similar to that found for NOAA-15 AVHRR (on the order of 0.20 K) and if this noise is uncorrelated from pixel-to-pixel, the assumption made in the analyses presented herein. Specifically, we would expect the noise for the L3 product to be approximately 0.05 K since order 25 pixels are averaged for each 0.05° × 0.05° SST estimate. It is possible that the level of instrument noise (elements in the yellow block of Fig. 1) associated with the AVHRR on Meteosat is higher than that of NOAA-15. More likely however is that the difference results from the addition of specification errors associated with cloud flagging (the most significant element in the green block). Specifically, (Tandeo et al. 2014) processed all of the data for one year, 2008; i.e., they did not constrain their analysis to relatively cloud free fields as we did. Cloud-contaminated L2 pixels were, of course, excluded from the production of the L3 fields and (Tandeo et al. 2014) also excluded pixels flagged as cloud-contaminated. However, the likelihood of misclassification, cloud-contaminated pixels not being flagged as such, increases as the fraction of cloud cover increases. Furthermore, classification errors tend to be small-scale errors, a small number of pixels here, a small number of pixels there, as opposed to large regions, which are misclassified. This means that such errors will likely contribute to noise at small spatial scales. A histogram of Tandeo et al. (2014) nuggets (not shown) shows a broad distribution ranging from σ_o in the 0.05 K range to order 0.3 K with a peak around 0.14 K. If the nugget resulted primarily from instrument errors (those in the yellow block), one would expect a relatively narrow peak; the instrument noise is unlikely to vary substantially for the region. Thus the broad σ_o range suggests that it is a combination of *classification errors* and *instrument noise*. Because our analysis required long sections of cloud-free pixels the data were likely much more clear, on average, than those of Tandeo et al. (2014). Also contributing to the difference between our estimate of local noise and that of Tandeo et al. (2014) is that noise may be added through the combination of L2 fields to obtain the L3 product. Using nighttime only data, as Tandeo et al. (2014) have done, will minimize, but not completely remove, this. Finally, we found that the model, which best fits the SST field in the Sargasso Sea, varies from an exponential form to a Gaussian form, hence our use of the standard model. Tandeo et al. (2014) used the exponential form. This will likely result in an overestimate of the instrument noise in regions in which a mixed form is more appropriate [1].

4.4. Impact of noise on Sobel Gradient

Of interest is how levels of noise, typical of the values found thus far, impact gradients and fronts. In order to address this, we simulated 10,000 3 × 3 pixel squares for a given gradient in x, added Gaussian white noise to each of the elements, applied the 3 × 3 Sobel gradient operator in x and y to these squares and then determined the mean gradient and the standard deviation of the gradient. This was done for gradients ranging from 0.001 K to 0.01 K, values typical in the ocean, and for levels of instrument noise ranging from 0.001 K to 0.02 K. Figure 10 and 11 show the means and standard deviations of the x- and y-components of the gradient, respectively. The mean x- and y-components are unaffected by the noise; the mean x-component is the same as the initial value and the mean y-component is very nearly zero. The standard deviation of the components is very nearly independent of the imposed noise. For a noise level typical of VIIRS, 0.05 K, the white lines in the figures, the uncertainty of each of the components is approximately 0.022 K and for a level typical of AVHRR, 0.2 K, the uncertainty in the components is 0.09 K. In general, the uncertainty in the given component is approximately one half of the level of imposed noise.

The impact on the gradient magnitude （Figure 12） is more dramatic. The mean of the estimated gradient is no longer equal to the magnitude of the imposed gradient. For example, for a relatively robust gradient of 0.05 K/km, the mean of the estimated gradient ranges from 0.05 to in excess of 0.1 K/km as the imposed noise ranges from 0 to 0.2 K/km. Note that contours of the estimated gradient tend to become level for imposed noise levels less than approximately 0.07 K. This means that VIIRS estimates of the mean gradient

magnitude will be centered on the actual value of the gradient, but that it will be substantially overestimated in AVHRR fields. The uncertainty of the estimated gradient magnitude increases with the imposed noise, nearly doubling from the value associated with a zero imposed gradient to an imposed gradient of 0.1 K/km. These observations do not mean that a front with a gradient of this magnitude (0.05 K/km) is undetectable in a field with an AVHRR noise level but detection will be problematic. Simulations using front detection algorithms need to be undertaken to evaluate this.

5. CONCLUSIONS

The accuracy with which the local gradient of any digital field can be determined is a function of the local precision of the underlying data, where the local precision is defined as the square root of the variance of individual pixel values following removal of real trends in the data and removal of noise that is correlated over scales that are large compared with the scale used to calculate the gradient. In the case of fields obtained from satellite-borne sensors this noise is attributed to characteristics of the sensor, 'instrument noise', and to the retrieval process, 'retrieval noise'. Two approaches, a spectral-based approach and a variogram-based approach, were used to estimate the instrument portion of this noise in L2 AVHRR and VIIRS SST fields. In order to reduce the non-instrument portion of the local noise in the analysis, only cloud free sections were used, the assumption being that the dominant contribution to the non-instrument local noise is due to the misclassification of clouds. Because instrument noise was thought to differ between the along-scan and along-track directions and because the geophysical variance was thought to differ between day and night, the analysis was performed separately for the four along-scan/along-track and day/night combinations.

Both methods yielded similar results for AVHRR, with daytime and nighttime along-scan values of ~0.18 K and along-track values of 0.21 K. VIIRS instrument noise, on the other hand, was found to differ by method, scan geometry and day-vs-night – ranging from 0.021 K for the nighttime, along-scan spectral estimate to 0.097 K for the daytime, along-track variogram estimate. Day and night along-scan estimates based on the spectral approach are close to one half those based on the variogram. For both methods, the nighttime estimates are also roughly one half the corresponding daytime estimates. Finally, the along-track estimates are roughly twice as large as the along-scan estimates for the spectral approach but only about one quarter as large when based on the variogram. In all cases, the estimates were smaller than the 'upper' limit.

In summary: VIIRS instrument noise is substantially smaller than AVHRR instrument noise, with levels as low as 0.02 K in the along-scan direction at nighttime. In fact, VIIRS instrument noise under these conditions is near the level of the geophysical signal in the dynamically quietest regions in the ocean.

6. REFERENCES

1. Tandeo, P.; Autret, E.; Chapron, B.; Fablet, R.; Garello, R. SST spatial anisotropic covariances from METOP-AVHRR data. J. Remote Sens. Environ. 2014, 141, 144–148.
2. Schloesser, F.; Cornillon, P.C.; Donohue, K.; Boussidi, B.; Iskin, E. Evaluation of Thermosalinograph and VIIRS Data for the Characterization of Near-Surface Temperature Fields. J. Atmos Ocean Tech. 2016, 33, 1843–1858.
3. Seaman, C.; Hillger, D.; Kopp, T.; Williams, R.; Miller, S.; Lindsey, D. Visible Infrared Imaging Radiometer Suite (VIIRS) imagery environmental data record (EDR) user's guide. Version 1.1, NOAA Tech. Rep. 2014, 35 pp.
4. Schueler, C.F.; Clement, J.E.; Ardanuy, P.E.; Welsch, C.; DeLuccia, F.; Swenson, H. NPOESS VIIRS sensor design overview. International Symposium on Optical Science and Technology, International Society for Optics and Photonics. 2002, 11–23.

5. Kilpatrick, K.A.; Podestá, G.P.; Evans, R. Overview of the NOAA/NASA advanced very high resolution radiometer Pathfinder algorithm for sea surface temperature and associated matchup database, J. Geophys. Res. 2001, 106, no. C, pp. 9179–9198.
6. Stramma, L.; Cornillon, P.C.; Weller, R.A.; Price, J.F.; Briscoe, M.G. Large Diurnal Sea Surface Temperature Variability: Satellite and In Situ Measurements. J. Phys. Oceanogr. 1986, 16, 827–837.
7. Wang, D.P.; Flagg, C.N.; Donohue, K.; Rossby, H.T. Wavenumber spectrum in the Gulf Stream from shipboard ADCP observations and comparison with altimetry meaurements. J. Phys. Oceanogr. 2010, 40, 840 – 844.
8. Cayula, J.F.P.; Cornillon, P.C. Edge detection algorithm for SST images. J. Atmos. Ocean. Tech. 1992, 9, 67–80.
9. Bouali, M.; Ignatov, A. Adaptive Reduction of Striping for Improved Sea Surface Temperature Imagery from Suomi National Polar-Orbiting Partnership(S-NPP) Visible Infrared Imaging Radiometer Suite (VIIRS). J. Atmos. Ocean. Tech. 2014, 31, 150–163.
10. Cornillon, P.C.; Stramma, L. The distribution of diurnal sea surface warming events in the western Sargasso Sea. J. Geophys. Res. 1985, 90, 11811–11815.
11. Barnes, S.L. A technique for maximizing details in numerical weather map analysis. J. Appl. Meteor. 1964, 3, 396–409.
12. Wackernagel, H. Multivariate geostatistics: an introduction with applications. Springer Science & Business Media: New York, NY, USA, 2013.
13. Cressie, N.A.C. Statistics for spatial data (revised ed.). John Wiley and Sons; Inc. New York, USA, 1993.
14. O&SI SAF Project Team. Low earth orbiter sea surface temperature product user manual. Technical report (available at http://www.osi-saf.org) , 2013.

ACSPO L3U SST PRODUCTS

Yanni Ding[1], Irina Gladkova[2], Alexander Ignatov[3], Fazlul Shahriar[4], Boris Petrenko[5], Yury Kihai[6]

STAR, NOAA NCWCP / CIRA, CSU, USA, Email: yanni.ding@noaa.gov
City College of New York, USA, Email: irina.gladkova@gmail.com
STAR, NOAA NCWCP, USA, Email: alex.ignatov@noaa.gov
City College of New York, USA, Email: fshahriar@gmail.com
STAR, NOAA NCWCP, USA, Email: boris.petrenko@noaa.gov
STAR, NOAA NCWCP, Email: yury.kihai@noaa.gov

ABSTRACT

NOAA has started operationally generating the Advanced Clear-Sky Processor for Ocean (ACSPO) L3U (level 3 un-collated; remapped level 2 data at 0.02º resolution) product from the VIIRS onboard S-NPP in May 2016. Both L2P and L3U are reported as 10-min granule, with L3U data being significantly smaller (< 1GB/day compared to ~27 GB in L2P). The initial implementation presented at GRSST-17 has been updated, based on the extensive evaluation of the L3U product. As a result, the biases between L3U and L2P, and L3U and L4 CMC as seen in the initial implementation, have been significantly reduced, and spatial patterns are now better preserved. The full set of masking flags (cloud and ice masks, etc.) are added, consistently with ACSPO L2P GDS2 files.

The L2P-to-L3U (swath-to-equiangular) projection code employs the bi-lateral weighted averaging approach. The SST value at each grid cell is computed based on spatial proximity to the cell as well as the proximity of the SST value to median SST of the spatially-close L2 swath values. This approach is known to better reduce noise while preserving the edges, thus minimizing distortions to the high-resolution SST structure in swath L2P data.

The updated VIIRS L3U SST product has been tested experimentally at STAR since Dec. 2016, and will be implemented in NOAA operations by GRSST-18. We are also working to generate consistent L3U products for other platforms, with 0.02º resolution for high-resolution sensors, AVHRR FRAC and MODIS, and 0.08º resolution for AVHRR GAC, using the same algorithm but adjusting the weighting parameters depending upon sensor.

This presentation discusses the L3U v2 algorithm, the biases between L3U and L2P, and L3U and L4 CMC for VIIRS and other platforms. The data coverage, preservation of spatial patterns, and the performance of newly added masking flags are also presented.

FEATURE RESOLUTION IN OSTIA L4 ANALYSES

Chongyuan Mao[(1)], Emma Fiedler[(1)] and Simon Good[(1)]

(1) Met Office, Fitzroy Road, Exeter, Devon EX1 3PB, United Kingdom,
Email: chongyuan.mao@metoffice.gov.uk

ABSTRACT

A new version of the OSTIA L4 processing system that uses a NEMOVAR data assimilation scheme (NEMOVAR OSTIA) has been developed at the Met Office, with the aim to replace the current OSTIA system that uses an OI-type (optimal interpolation) data assimilation scheme (OI OSTIA). Spectral analysis is used to assess the feature resolution in the two versions of OSTIA L4 analyses. We focused on three regions of interest with strong horizontal sea surface temperature (SST) gradients: Gulf Stream (GS) and Agulhas Current Retroflection (ACR). Preliminary results show that the NEMOVAR OSTIA analysis has sharper features than in the current OI OSTIA analysis. The power spectra from the two OSTIA L4 analyses are also compared to results from other L4 products, such as CMC 0.1 degree and Real Time Global (SST) data.

In addition to the adaptation of new data assimilation scheme in OSTIA system, the use of new observation data in OSTIA system is also assessed. Here the impact of ingesting SLSTR L2P SST product is tested in a trial near real time NEMOVAR OSTIA system. If the data quality permits, the global and regional statistics of the pre-operational run against independent Argo floats will be compared to those from the current operational NEMOVAR OSTIA system.

1. INTRODUCTION

The Operational Sea Surface Temperature (SST) and Ice Analysis (OSTIA) has been developed at the Met Office to produce L4 analyses of SST and sea ice using observations from satellite and in situ platforms. A new version of the OSTIA L4 processing system that uses a NEMOVAR data assimilation scheme (NEMOVAR OSTIA) has been developed at the Met Office, with the aim to replace the current OSTIA system that uses an OI-type (optimal interpolation) data assimilation scheme (OI OSTIA). NEMOVAR has been developed with international collaboration for use in the NEMO ocean model. This scheme has been used in the Forecasting Ocean Assimilation Model (FOAM) successfully at the Met Office. A NEMOVAR dual length scale correlation operator has been implemented for NEMOVAR in OSTIA, which combines the short length scale and long length scale based on the ratio of short and long background error variances to calculated the effective length scale. However, the pre-defined background error variances vary spatially and seasonally but not on shorter timescales. Genuine SST features therefore may be smoothed out when the derived effective length scale is too long.

A flow-dependent component determining the length scale ratio has been developed under the ESA SST CCI project to resolve this issue. First, the total horizontal gradient of the background SST field is used to identify highly variable regions (Figure 1). For regions where the SST gradients are between 20 and 50 mK/km, the flow-dependence method linearly reduces the ratio of the two length scales, and sets the effective length scale to the shortest length scale for regions where the SST gradient is above 50 mK/km.

2. METHODS

2.1. Experiment set up

The feature resolution of three OSTIA configurations are compared: 1) OI OSTIA, 2) NEMOVAR OSTIA and 3) NEMOVAR OSTIA + Flow-dependent component (NEMOVAR + FD OSTIA). The long and short length scales are set to 300 km and 40 km for both NEMOVAR OSTIA runs. All three runs were conducted over the period of June 2016 – March 2017. The analysis focuses on periods of July – September 2016 and January – March 2017, with June 2016 as the spin-up. In this presentation, results from hemispherical winter in the Gulf Stream (GS, 39° - 45° N, 50° - 65° W, March 2017) and the Agulhas Current Retroflection (ACR, 25° - 45° S, 10° - 50° E, September 2016) are shown.

2.2. SPECTRAL ANALYSIS

Spatial power spectral analysis is used to assess the results: 1) power spectra are calculated for each latitude (latitudes with land grid points are excluded); 2) these spectra are then averaged over the latitudes to get regional daily power spectra; 3) daily spectra are then averaged over each month to get monthly power spectra. Results for NEMOVAR OSTIA runs are calculated on the ORCA12 grids. The monthly power spectra are then compared against power law gradients that explain the theoretical decay of power spectra (Le Traon et al., 2008):

- K^{-5} power law demonstrates the quasi-geostrophic (QG) turbulence at wavelength over 100 km
- $K^{-11/3}$ power law demonstrates the surface quasi-geostrophic (SQG) theory

In addition to the comparison of the three OSTIA runs described above, power spectral analysis is also applied to other L4 analyses and the results are compared to the main experiment:

- NEMOVAR OSTIA + FD run with shortest length scale set to 15 km
- CMC 0.1° produced by the Canadian Meteorological Centre
- Real Time Global (RTG) SST data from NCEP, produced on 0.5° grid
- AVHRR_OI analysis
- Multi-scale Ultra-high Resolution (MUR) SST data from JPL, produced on 1 km resolution
- Ocean only model run with no observation assimilation on ORCA12 grid (data used here are from the last year of a climatology run, 1971 – 1995)

Spatial power spectral analysis is applied to these analyses in the same manner as described above, results shown here are also from hemispheric winter in GS and ACR regions.

3. RESULTS

3.1. Comparison of three OSTIA runs

Figure 2 shows the monthly power spectra averaged over the GS region in March 2017. The power spectra of all three OSTIA runs follow the $K^{-11/3}$ power law at wavelengths between ~75 and 150 km, suggesting SQG turbulence in this region. Below 75 km, the power spectrum of NEMOVAR OSTIA falls faster than the other two runs. NEMOVAR + FD OSTIA has higher power at wavelengths below 40 km than OI OSTIA. The

dominating power law for turbulence on shorter scales is still under debate, especially for those below the Rossby radius, which is ~20 km for this region (Chelton et al., 1998).

The power spectral results for the ACR region in September 2016 (not shown) are similar to those in Figure 2. For all power spectral results, a flat line suggests noise in the data instead of real signal.

3.2. Comparison of OSTIA and other l4 analyses

The power spectra of all participating analyses in the ACR region in September 2016 are shown in Figure 3. The power spectra of all analyses except RTG have comparable slope at wavelengths above 100 km and the slope is slightly flatter than the $K^{-11/3}$ power law. NEMOVAR + FD OSTIA with short length scale set to 15 km increases the power spectrum of the analysis for wavelengths between 20 km and 100 km compared to the other three OSTIA runs. The power spectra of the ocean only model run and MUR data follow the $K^{-11/3}$ to the wavelength permitted by its grid size, ~20 km for model run and ~5km for MUR. However, it is debatable if the power spectrum for MUR indicates real signal or calculated noise, especially for shorter wavelengths where SQG theory does not apply.

The message delivered in the power spectral results (not shown) for the GS region in March 2017 is very similar to those in Figure 3. Figure 4a shows the averaged SST horizontal gradient field of NEMOVAR + FD OSTIA (short length scale = 15 km) and Figure 4b shows the same field for MUR in ACR in September 2016. It is clear that MUR demonstrates many very fine scale structures, but could also include spurious noise compared to the SST horizontal field for NEMOVAR + FD OSTIA. Further evidence is required to confirm the statement.

3.3. Validation of NEMOVAR OSTIA

Table 1 shows the validation of the three main OSTIA runs (for NEMOVAR OSTIA used here, the short length scale is set to 40 km) using independent near-surface Argo temperature floats. Results shown here are calculated for the global ocean over the period of Jul – Sep 2016 and Jan – Mar 2017. Compared to OI OSTIA, NEMOVAR OSTIA shows modest but consistent improvements using Argo as the validation reference. The flow-dependent component does not change the statistics against Argo observations.

Table 2 shows the validation of the three main OSTIA runs in the context of Numeric Weather Prediction (NWP) system, which uses OSTIA SST as its boundary condition. Results shown here are for Jul – Sep 2016. The NWP tests have been found to be sensitive to time period investigated. Fore the tested period, NEMOVAR OSTIA demonstrates improvements compared to the OI OSTIA system and the flow-dependent component improves NWP performance further, especially for longer range forecasts.

4. FIGURES AND TABLES

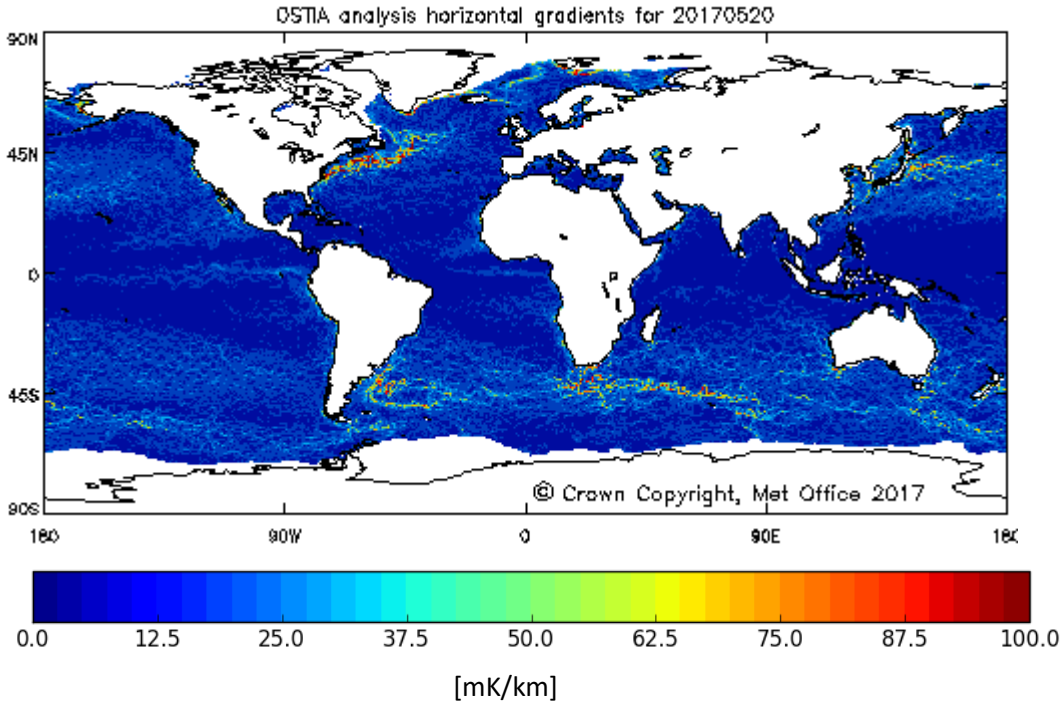

Figure 1: Example of the SST horizontal gradient field that used to determine highly variable regions.

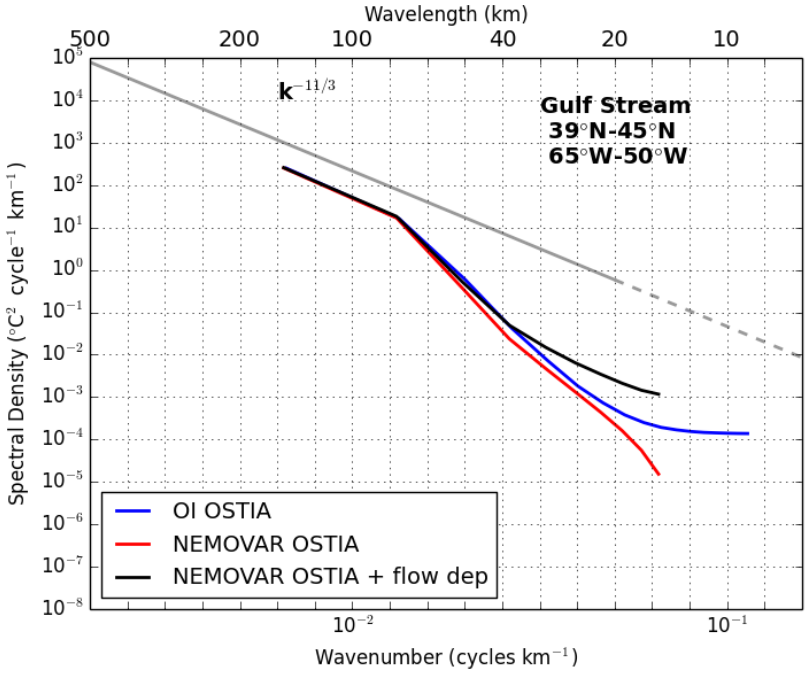

Figure 2: Power spectra of three OSTIA runs (OI OSTIA in blue line, NEMOVAR OSTIA in red line and NEMOVAR + FD OSTIA in black line) in the Gulf Stream in March 2017.The gray line demonstrate the $K^{-11/3}$ theoretical power law with power law below local Rossby radius in dashed line.

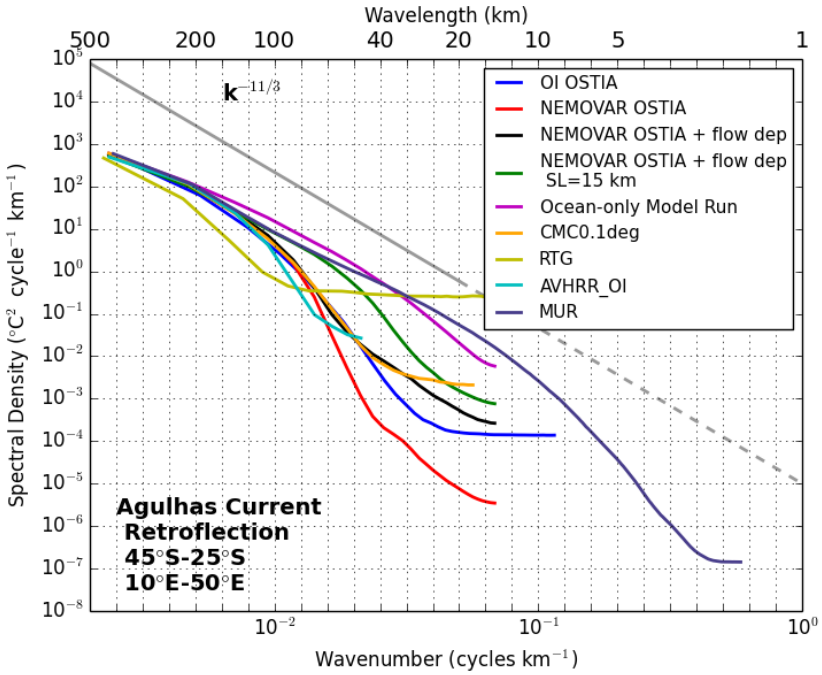

Figure 3: Power spectra of all participating L4 analyses in the Agulhas Current Retroflection region in September 2016.The gray line demonstrate the $K^{-11/3}$ theoretical power law with power law below local Rossby radius in dashed line.

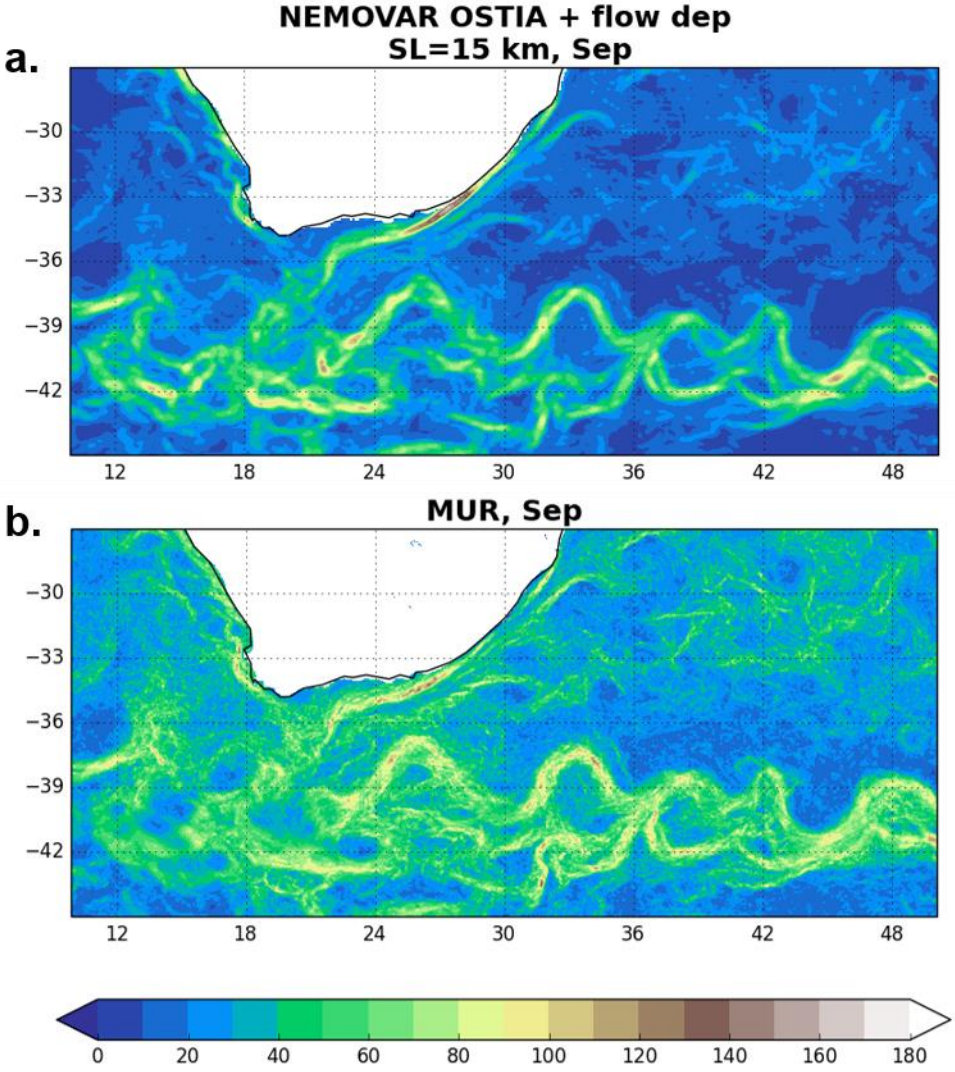

Figure 3a: SST horizontal gradient for NEMOVAR + FD OSTIA with short length scale set to 15 km; 4b: SST horizontal gradient for MUR, both fields are in the Agulhas Current Retroflection region in September 2016.

Analysis	Mean Difference, Argo – OSTIA (K)		Standard Deviation, Argo – OSTIA (K)		Number of Observations	
	Jul – Sep	Jan – Mar	Jul – Sep	Jan – Mar	Jul – Sep	Jan – Mar
OI	0.06	0.05	0.43	0.41	28832	30644
NEMOVAR	0.05	0.06	0.42	0.40		
NEMOVAR + FD	0.05	0.06	0.42	0.40		

Table 1: Validation of NEMOVAR OSTIA using global Argo statistics. All statistics are calculated for Argo minus analysis matchup at the location of Argo floats

NWP Index	Compared to observations (NEMOVAR + FD OSTIA minus OI OSTIA)	Compared to analyses (NEMOVAR + FD OSTIA minus OI OSTIA)	Compared to observations (NEMOVAR OSTIA minus OI OSTIA)	Compared to analyses (NEMOVAR OSTIA minus OI OSTIA)
Global NWP Index change (RMS % change)	0.29 (0.29%)	0.40 (0.31%)	0.13 (0.13%)	0.25 (0.20%)

Table 2: Validation of NEMOVAR OSTIA using global Numeric Weather Prediction (NWP) Index.

5. CONCLUSION

- The NEMOVAR assimilation scheme with additional flow-dependent adjustment of background error covariance length scales captures the most power at shorter wavelengths compared to NEMOVAR OSTIA and OI OSTIA, without the introduction of spurious noise
- The latest NEMOVAR + FD OSTIA system with short length scale set to 15 km improves the power spectrum of the analysis, especially for wavelengths below 100 km
- The spectral analysis suggests that the dominating signal in the Gulf Stream and Agulhas Current Retroflection regions follow the $K^{-11/3}$ power law at wavelengths over 100 km, demonstrating surface quasi-geostrophic turbulence instead of the quasi-geostrophic turbulence (K^{-5} power law)
- Further study required to understand the power spectra at shorter wavelengths
- Improvement of the Quality Level (QL) in SLSTR L2P SST data significantly improved the statistics of observation-minus-background field in NEMOVAR OSTIA (not shown), especially for RMS. Further improvement to daytime SST observation should improve the performance of SLSTR data in OSTIA system.

6. REFERENCES

Chelton, D. B., R. A. Deszoeke, M. G. Schlax, K. El Naggar and N. Siwertz, 1998: Geographical Variability of the First Baroclinic Rossby Radius of Deformation, *J. Phys. Oceanogr.,* **28**, 433 – 460.

Le Traon, P. Y., P. Klein, B. L. Hua and G. Dibarboure, 2008: Do Altimeter Wavenumber Spectra Agree with the Interior or Surface Quasigeostrophic Theory? *J. Phys. Oceanogr.,* **38**, 1137 – 1142.

PLENARY SESSION VI: CLIMATE

SESSION VI REPORT

Chair: Jon Mittaz[1] – Rapporteur: Owen Embury[2]

(1) University of Reading, UK, Email: j.mittaz@reading.ac.uk
(2) University of Reading, UK, Email: o.embury@reading.ac.uk

1. ABSTRACTS

The climate plenary session covered the various reprocessing efforts to create long term satellite Climate Data Records (CDRs). Reports were given by the Pathfinder, MODIS, SST-CCI, and OSI-SAF reprocessing teams, and Salvatore Marullo gave a presentation research using the 35-year Mediterranean SST product from CMEMS.

A major concern in the audience was the future of the Pathfinder AVHRR project, which is now in hibernation mode due to lack of ongoing funding. If audience members felt strongly about the discontinuation of the Pathfinder project then they could contact Huai-Min Zhang (huai-min.zhang@noaa.gov).

2. PATHFINDER AVHRR - KEN CASEY

The Pathfinder AVHRR project is now in hibernation mode with all remaining funds being used to ensure all the processes and systems are fully documented. This will allow the project to continue in the future if further funds are acquired. The currently released v5.3 data, covering 1981 – 2014, will remain available. However, the more recent data has not been archived and cannot be released.

The science team expressed concern about the lack of ongoing funding for Pathfinder AVHRR as it is a widely used dataset and also input to many of the L4 analysis systems.

3. MODIS AND VIIRS SSTS - PETER MINNETT

Peter presented the current work on the MODIS/VIIRS SST Climate Data Record. Both sensors use a variant of NLSST with additional terms for the scan mirror effects. However, there are currently two different cloud mask algorithms in use: binary decision tree for MODIS, and alternating decision tree for VIIRS data. This results in different spatial coverages from the two types of sensors (ACD performs better especially in high-latitudes and near SST fronts), therefore the next MODIS reprocessing will switch to the ACD method used by VIIRS.

Prototype algorithms are currently being tested before being transferred to the reprocessing centre, a full reprocessing has been requested and is expected to occur later this year.

Users have noticed regional biases – for instance extensive warm biases around Australia for all four sensors (N19, VIIRS, and both MODIS). This will require further investigation, but NLSST is known to have issues with anomalous atmospheric conditions (e.g. very dry etc.)

4. SST CCI PHASE 2 - CHRIS MERCHANT

The ESA SST-CCI project is producing a SST Climate Data Record based on AVHRR and ATSR observations. It aims to minimise the use of in situ observations by using physically based retrievals rather than regression

to in situ. Work since the phase 1 dataset was released include adapting the Bayesian cloud detection to AVHRR instruments, further work on inter-satellite harmonisation, and extensive work on AVHRR calibration.

Questions included how independence was achieved using a physically based retrieval (which will include prior information such as NWP). Optimal estimation allows both maximum-likelihood (best fit to observations) and maximum a posteriori (best fit to observation and prior information) forms. The SST-CCI retrieval uses an inflated prior SST uncertainty to give a ML-type retrieval with respect to SST and MAP with respect to atmospheric state. A further check on SST sensitivity rejects any pixels where estimated sensitivity to SST drops below 90%.

The target requirements for accuracy etc. were taken from the GCOS requirements for SST.

The Phase II data have not yet been compared with Pathfinder.

Phase II data will include L2, L3, and L4 and will be publicly released in 2018 after internal assessment has been complete.

A check will be made wrt other quality metrics such as the Koner et al. metric for cloud detection though it is expected to be close to the Bayesian approach.

5. OSI SAF REPROCESSING OF MSG/SEVIRI - STÉPHANE SAUX PICART

OSI SAF is reprocessing the MSG/SEVIRI archive to generate a 2004-2012 hourly L3 product at 0.05 degree resolution. This includes adjustments for the 3.9 micron channel drift and uses the method of Le Borgne et al. (2011) to reduce regional biases.

The diurnal cycle of 0.3 K appears low; however, the data do not include a constraint on SST sensitivity so the cycle may be underestimated.

There are biases seen at very high satellite zenith angles. This may be due to NWP data in the area, surface emissivity model, or the high view angle.

6. SST CCI PASSIVE MICROWAVE RETRIEVALS - JACOB HØYER

DMI is investigating passive microwave SST retrievals as part of the ESA SST-CCI project. This builds on earlier sea-ice retrievals in the ESA CCI Sea Ice, and SST from ATSR and AVHRR in the ESA CCI SST projects. Two algorithms are under investigation: a regression algorithm (similar to work done at RSS) and optimal estimation (similar to other CCI work). Currently the regression algorithm performs better in terms of validation against in situ drifters, but the OE algorithm provides useful information on quality. Ship and non-drifter data is not yet included in the analysis.

7. LONG TERM CHANGES IN ATLANTIC AND MEDITERRANEAN SST - SALVATORE MARULLO

Salvatore Marullo presented findings from the CMEMS regional Mediterranean and north-western Atlantic SST product. The 35 years of satellite data were consistent with historical datasets HadISST and ERSSTv4 in the period of overlap. The Mediterranean showed a warming trend of 0.03 C/year and is still warming, but the area of the Atlantic Ocean included in the analyses paused around 2001.

PATHFINDER VERSION 5.3 AVHRR LEVEL-2 PROCESSED GLOBAL SEA SURFACE TEMPERATURE

Sheekela Baker-Yeboah[1,2], Korak Saha[1,2], Kenneth S. Casey [2], Dexin Zhang[2,3], Katherine. A. Kilpatrick[4], Susan Walsh[4], R. Evans[4], and Thomas Ryan[2]

(1) University of Maryland CICS, College Park, MD 20740, USA, Email: sbyeboah@umd.edu, karak.saha@noaa.gov;
(2) NOAA/NESDIS/National Centers for Environmental Information (NCEI), 1315 East West Highway, Silver Spring, MD 20910, USA, Email: Kenneth.Casey@noaa.gov;
(3) Science and Technology Corporation, 21 Enterprise Parkway, Suite 150, Hampton, VA 23666-6413, Email: Dexin.Zhang@noaa.gov;
(4) University of Miami Rosenstiel School for Marine and Atmospheric Science, 4600 Rickenbacker Causeway, Miami Florida 33143, Email: kkilpatrick@rsmas.miami.edu;
(5) North Carolina State University Cooperative Institude for Climate and Satellites and Asheville, NC 28801 and NOAA/NESDIS/NCEI.

ABSTRACT

Long-term, climate data records of global sea surface temperature (SST) are important for ocean and climate variability studies. Pathfinder global SST product from the Advanced Very High Resolution Radiometers (AVHRR) aboard NOAA polar-orbiting satellites, going back to 1981, remain the longest high resolution SST climate data record available, and are used for a variety of applications. The Pathfinder SST algorithm is based on the non-linear SST algorithm, applied consistently over the full time period of August 1981 - December 2014, to produce a validated multi-decade record of IR SST from a suite of eight AVHRR sensors with similar overpass times. Algorithm coefficients for this SST product were generated using regression analyses with co-located in situ and satellite measurements and the product is produced using the modernized NASA SeaWiFS Data Analysis System (SeaDAS6.4). The entire Pathfinder time series has recently been reprocessed by NOAA (V5.3), and for the first time GHRSST formatted L2P files are now available publicly, in addition to the standard L3 global 4km products historically produced. Validation results of the PFSST 5.3 Level-2 processed (L2P) data will be presented. This work continues the long historical aspect of Pathfinder SST products.

LONG-TERM GLOBAL TIME SERIS OF MODIS AND VIIRS SSTS

Peter J. Minnett[(1)], Katherine Kilpatrick, Guillermo Podestá, Elizabeth Williams, Yang Liu, Susan Walsh and Miguel-Angel Izaguirre

(1) Dept. Ocean Sciences, Rosenstiel School of Marine and Atmospheric Science, University of Miami, Miami, FL, USA, Email: pminnett@rsmas.miami.edu

ABSTRACT

The generation of long-time series of consistent and accurate variables is an important step towards studying the response of the climate to changing forcing. The objective of climate fingerprinting does not necessarily require the stringent accuracies required of an SST Climate Data Record, as a long time series of consistent SSTs can provide useful information on changes in the regional and temporal structure of temperature anomalies. The SSTs derived from measurements on the two MODISs on Terra and Aqua and from VIIRS on S-NPP are retrieved using the same algorithms for cloud screening and atmospheric correction, modified for the particular characteristics of each sensor, thus ensuring a consistent time series. The presentation will provide an update on the algorithms used to retrieve the MODIS and VIIRS SSTs, and the errors and uncertainties in the derived fields.

OSI SAF SEA SURFACE TEMPERATURE REPROCESSING OF MSG/SEVIRI ARCHIVE.

S. Saux Picart[(1)], G. Legendre[(1)], A. Marsouin[(1)], S. Péré[(1)], H. Roquet[(1)]

[(1)] Météo-France, Lannion, France, Email: stephane.sauxpicart@meteo.fr

1. INTRODUCTION

The Ocean and Sea-Ice Satellite Application Facility (OSI-SAF) of the European Organisation for the Exploitation of Meteorological Satellites (EUMETSAT) is planning to deliver a reprocessing of Sea Surface Temperature (SST) from Spinning Enhanced Visible and Infrared Imager/Meteosat Second Generation (SEVIRI/MSG) archive (2004-2012) by the end of 2017. This reprocessing is drawing from experiences of the OSI SAF team in near real time processing of MSG/SEVIRI data.

The retrieval method consists in a non-linear split-window algorithm including the algorithm correction scheme developed by Le Borgne et al. (2011). The bias correction relies on simulations of infrared brightness temperatures performed using Numerical Weather Prediction model atmospheric profiles of water vapour and temperature, and RTTOV radiative transfer model.

The cloud mask used is the Climate SAF reprocessing of the MSG/SEVIRI archive. It is consistent over the period in consideration.

Atmospheric Saharan dusts have a strong impact on the retrieved SST, they are taken into consideration through the computation of the Saharan Dust Index (Merchant et al., 2006) which is then used to determine an empirical correction applied to SST.

The MSG/SEVIRI SST reprocessing dataset consists in hourly level 3 composite of sub-skin temperature projected onto a regular 0.05° grid over the region delimited by 60N,60S and 60W,60E.

2. METHODOLOGIES

A classic split-window algorithm is used to compute the so-called classical SST. The formulation of the algorithm is given below:

$$SST = aT_{10.8} + (bS_\vartheta + cT_{clim})(T_{10.8} - T_{12.0}) + d + eS_\vartheta$$

where $T_{10.8}$ and $T_{12.0}$ are the brightness temperature at 10.8 and 12.0µm, S_ϑ is the secant of the satellite zenith angle and T_{clim} is the climatological temperature. The coefficient *a* to *e* are determined by regression using simulations of Brightness Temperature (BT) on a set of atmospheric profiles extracted from ECMWF model. BTs are reprocessed and near real-time data from EUMETSAT central facility. Climatology is derived from OSTIA daily reanalysis.

All non-cloudy pixels are processed. Non-cloudy conditions are detected using the Climate Monitoring SAF reprocessed cloud mask.

The formulation of Saharan Dust Index from Merchant et al. (2006) is used to apply an SST correction when possible. Some modifications to the original method were developed in particular to compute SDI during daytime.

In addition, the bias correction scheme developed by Le Borgne et al. (2011) is used. BT simulations are performed for each pixel of each slot using RTTOV model. Its inputs include ERA interim atmospheric profiles of temperature, water vapour, pressure and ozone, the OSTIA reanalysis of SST and the instrument filter functions. After adjustment (taking into account errors arising from RTTOV or its inputs), the simulated

BTs are then used to compute a so-called simulated sea surface temperature (as opposed to the observed SST computed using observed BTs). The difference between the simulated SST and the OSTIA reanalysis is considered to be a correction term that is added to the observed SST.

Along the process of computing SST, SDI and the bias correction several consideration are made to quantify the relative quality of the retrieved SST. The list of tests is presented in Table Tableau. Each of these tests results in an indicator value between 0 and 100. Indicator values are combined to produce a quality level for each pixel.

Test	Description/purpose
SST value	Compares SST to SST climatology.
SST spatial variability	Compares the local value of the SST gradient to a climatology of maximum gradient.
SST temporal variability	Detects quickly changing SST.
Aerosol dust	Penalises pixels with high SDI.
Distance to cloud	Penalises pixels in the vicinity of clouds.
Sea ice	Detects pixels containing sea ice.
Satellite zenith angle	Penalises pixels with high satellite zenith angle.

Table 1: List of tests performed during SST retrieval.

3. RESULTS

The ERA-clim dataset (Atkinson et al., 2014) is used to evaluate the reprocessing. More specifically only the drifting buoy measurements of the dataset are used. Collocated satellite SST is extracted together with a set of variables such as satellite zenith angle, simulated SST, and so on. The resulting dataset contains over 900000 match-ups during 2004-2007 (MSG1).

The following criteria are used to compute the statistics:

- Quality level between 3 and 5
- Time difference between satellite acquisition and in situ measurement less or equal to 15 minutes
- Absolute difference between in situ measurement and SST climatology less or equal to 5K

		Uncorrected				Corrected			
	Num	bias	STD	median	RSD	bias	STD	median	RSD
Night	432100	-0.07	0.51	-0.03	0.43	-0.06	0.44	-0.03	0.35
Day	470168	-0.05	0.48	-0.01	0.41	0.01	0.42	0.04	0.34

Table 2: Global statistics SST_{sat}-$SST_{in\ situ}$ for MSG1

Table Tableau Table gives the global statistics computed from the matchup dataset for MSG1 in terms of bias, standard deviation, median and Robust Standard Deviation $(RSD = \left(75^{th}percentile(SST_{sat} - SST_{insitu}) - 25^{th}percentile(SST_{sat} - SST_{insitu})\right)/1.348)$.

Figure shows the time evolution of the monthly statistics for MSG1. Results are very stable over time, display a very small bias and a standard deviation of about 0.4 for both day and night.

Figure shows the geographic distribution of the bias for 2006. No noticeable regional bias can be observed. A weak negative bias may be observed North of the equator and a weak positive bias may be observed at high satellite zenith angle in the Northwest of the domain and in the South of the African continent.

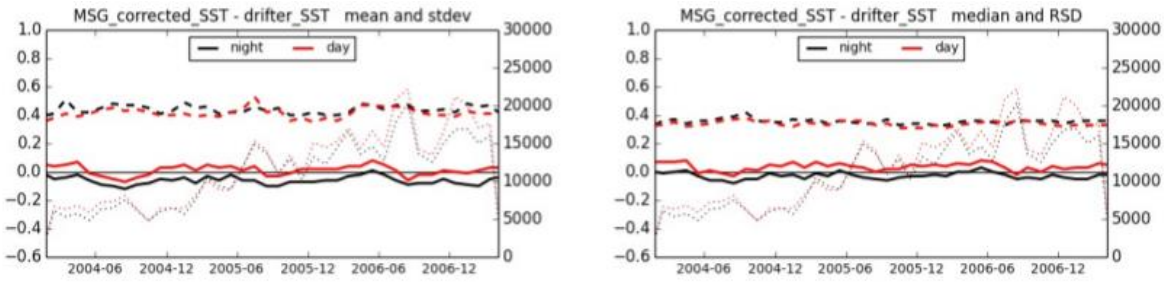

Figure 1: Monthly statistics for MSG1. Mean and standard deviation on the left, Median and robust standard deviation on the right

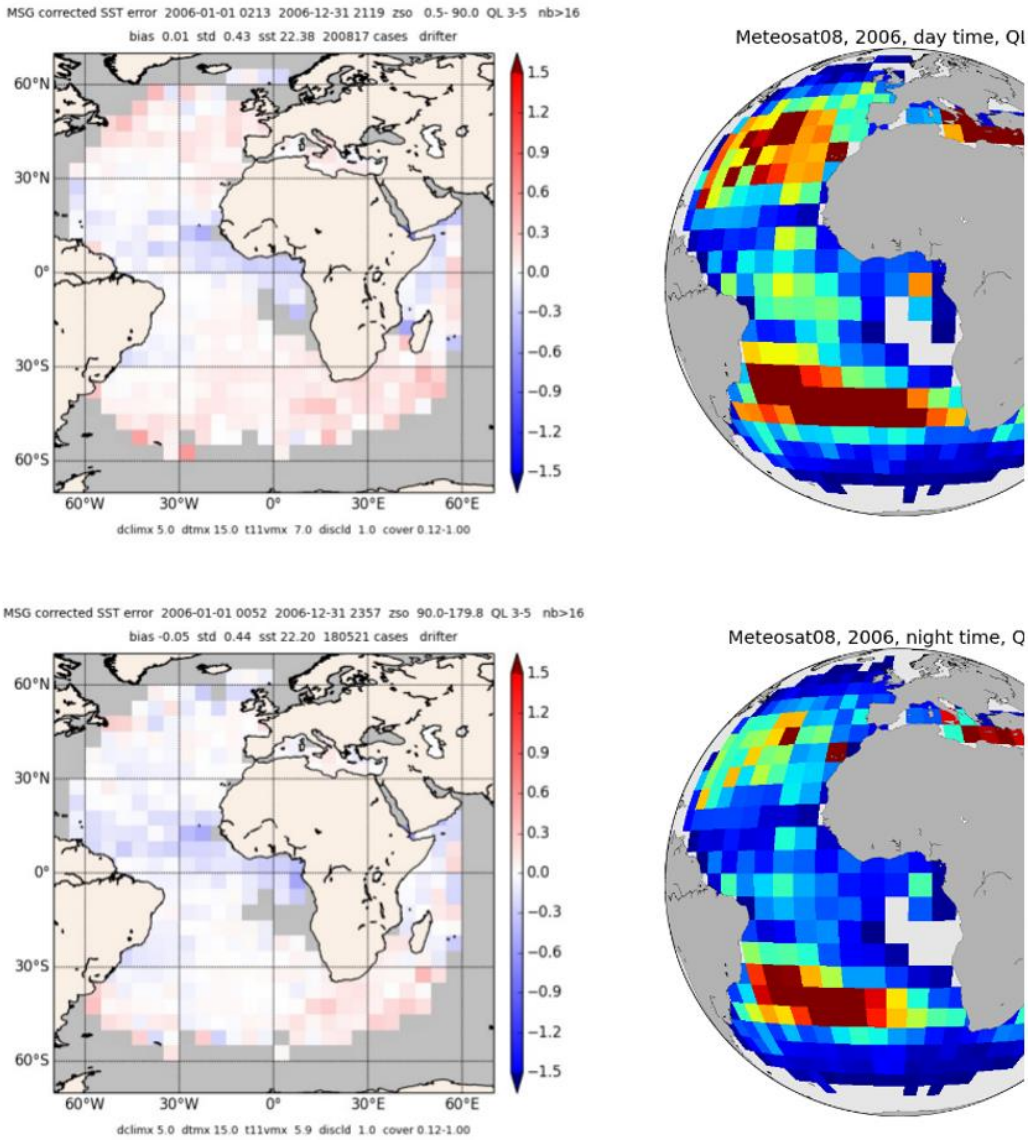

Figure 17: Binned statistics in 5x5° boxes for one year of data (2006). Bias on the left; Number of matchups on the right.

4. CONLUSION

So far the reprocessing has been validated for the first period only (MSG1, 01/2004-04/2007). It has shown good results compared to drifting buoy measurements. The reprocessing of MSG2 is now completed and is undergoing validation. A Climate Data Record-type validation as recommended by GHRSST Climate Data Record Validation Technical Advisory Group (CDR-TAG) for the Climate Data Assessment Framework (CDAF) will be performed. The official delivery of the reprocessed dataset is planned for the end of 2017.

GENERATING AN SST CLIMATE DATA RECORD FROM PASSIVE MICROWAVE OBSERVATONS

Jacob L. Høyer[(1)], Jörg Steinwagner[(1)], Leif Toudal Pedersen[(1)]

Danish Meteorological Institute, Denmark, Email: jlh@dmi.dk

ABSTRACT

Climate data records of SST have been developed for many years using the Infra-red sensors from. All the infrared observations are, however limited, by cloud cover and the errors typically arise from the same parameters, such as: atmospheric humidity, aerosols and so on. Microwave observations of SST are not limited by clouds offer a truly independent observational record.

This presentation will give an overview on the activities within the ESA Climate Change Initiative (CCI) project on SST on generating a climate data record from passive microwave observations. The activities include the creation of several multi-sensor match-up dataset (MMS) consisting of the AMSR-E and AMSR-2 matched against in situ observations and against AVHRR. The MMS is used for algorithm development, to test the performance of an optimal estimation algorithm. A thorough assessment of the algorithm performance has been carried out against in situ observations, where the performance of the OE state retrievals has been examined according to wind speed dependency, scan angle, atmospheric state, etc. The selected algorithm will be used to generate a climate data record from AMSR-E and AMSR2 and to assess the performance of the data set, against independent in situ observations.

LONG-TERM CHANGES IN THE NORTHWESTERN ATLANTIC AND MEDITERRANEAN SST FROM 1982 TO 2016: A CONTRIBUTION OF THE OPERATIONAL OCEANOGRAPHY TO THE DETERMINATION OF THE PRESENT DAY CLIMATE

A. Pisano[1], S. Marullo[1,3], V. Artale[1,3], B. Buongiorno Nardelli[1,2], and R. Santoleri[1]

(1) Institute of Atmospheric Sciences and Climate (ISAC) of the Italian National Research Council (CNR), Roma, Italy, Email: andrea.pisano@artov.isac.cnr.it, rosalia.santoleri@artov.isac.cnr.it
(2) Institute for the Coastal Marine Environemnt (IAMC) of the Italian National Research Council (CNR), Napoli, Italy, Email: bruno.buongiornonardelli@cnr.it
(3) Agenzia Nazionale per le Nuove Tecnologie, l'Eenergia e lo Sviluppo Economico Sostenibile, ENEA, Centro Ricerche Frascati , Frascati, Italy, Email: salvatore.marullo@enea.it, vincenzo.artale@enea.it

ABSTRACT

Estimating long-term SST changes is crucial to evaluate global warming impact at regional scales. Here, we analyze the Mediterranean (MED) and the Northwestern Atlantic Box (NWA) SST changes over the last 35 years (1982 - 2016) by combining reprocessed (REP) and near-real-time (NRT) data. The Italian National Research Council (CNR) has recently produced daily (nighttime), 4 km resolution REP MED level 4 datasets (REP L4), also covering the adjacent Atlantic region, based on the latest Pathfinder v5.2 AVHRR dataset (1982-2012). These data represent the longest satellite MED SST L4 time series and are freely distributed through the European Copernicus Marine Environment Monitoring Service (CMEMS). However, as Pathfinder has not yet released an update of its product, the REP data end in 2012. To fill in the gap between 2013 and 2016, we investigated the possibility to extend the time series by using the Mediterranean near real time (NRT), multi-sensor L4 SST data at Ultra-High spatial Resolution (UHR) produced by CNR, which are distributed through CMEMS and now mirrored at GHRSST. Since this product is available since 2008, the consistency with the REP has been assessed. Combining the REP L4 data (1982-2012) and a bias-corrected version of the NRT L4 data (2013-2016), we built the SST time series and provided updated estimates of the MED and NWA SST trends. The analysis shows that The Atlantic Box and The Mediterranean Sea have similar trend behavior until 2008. Afterward the Mediterranean Sea SST continued to increase while the Atlantic persisted in its warming pause.

PLENARY SESSION VII: BREAKOUTS

REPORT OF DAS TAG SESSION AT GHRSST-XVIII

Jean-François Piollé[(1)], Ed Armstrong[(2)]

(1) Ifremer, France, Email: jfpiolle@ifremer.fr,
(2) JPL/PO.DAAC, USA, Email: Edward.M.Armstrong@jpl.nasa.gov

1 INTRODUCTION

This is the summary report of the DAS TAG session of GHRSST-XVIII in Qingdao, hold on Tuesday 6th June 2017.

The DAS TAG session focused this year on two main topics :

- revision and update of GDS to fix pending issues and ambiguities
- revision of GHRSST system implementation and proposition of a new R/GTS

2 REVISION AND UPDATE OF GDS

Some ambiguities or missing information in the GDSv2r5 were reported that were discussed during the session together with some proposals made by the DAS TAG, regarding in particular two aspects :

- missing or improper content for some global NetCDF attributes
- missing or ambiguous format specifications for geostationary products

2.1 GDS global attributes (discussion led by Ed Armstrong)

The GDS follows the CF convention, complemented with the additional global netCDF attributes defined by ACDD convention. The additional attributes are part of some producing agencies requirements (https://podaac.jpl.nasa.gov/PO.DAAC_DataManagementPractices#Metadata Conventions) and also helps to bring more consistency with other non GHRSST datasets. Non compliances or missing attributes wrt conventions have been reported, and new versions of the used conventions have been released, that require an update of GDS. **The proposed new baseline for this conventions is CF-1.6 and ACDD-1.3.**

The proposed update of the GDS is defined in such a way that no change in existing products is required. New release of existing products or new products should however comply to the latest GDS attribute requirements:

The proposed new attributes **should not be mandatory** (to preserve forward compatibility of existing products), and therefore are just **recommended**.

The new attributes **should not break anything in current GDS**, so that files in revised format can be read without changing anything to current software code (backward compatibility), meaning:

- No change in definition or content of existing attributes
- No removal of existing attributes
- Only exception may be some obsolete and redundant attributes (but should be assessed carefully)
- « **add** » rather than « **delete** » or « **replace** »

The following new list of attributes is proposed to replace the existing tables in the GDSv2r5. New attributes are highlighted in blue. Note also that the content or format of some existing attributes is revised (usually to provide more details) such as:

- *Conventions* (misspelled in GDS)
- time attributes (*time_coverage_start, time_coverage_end,...*) : use the **extended** ISO time format rather than the basic format (ex: "2007-04-05T14:30:00Z")

Attribute Name	**Type**	**Definitions**	**Example Implementation**	**Source**
title	string	A short phrase or sentence describing the dataset. In many discovery systems, the title will be displayed in the results list from a search, and therefore should be human readable and reasonable to display in a list of such names. This attribute is recommended by the NetCDF Users Guide (NUG) and the CF conventions.	title = "VIIRS L2P Sea Surface Skin Temperature" ;	ACDD 1.1, ACDD 1.3, CF 1.6
summary	string	A paragraph describing the dataset, analogous to an abstract for a paper.	summary = "Sea surface temperature (SST) retrievals produced at the NASA OBPG for the Visible Infrared Imaging Radiometer Suite (VIIRS) sensor on the Suomi National Polar-Orbiting Parnership (Suomi NPP) platform. These have been reformatted to GHRSST GDS version 2 Level 2P specifications by the JPL PO.DAAC." ;	ACDD 1.1, ACDD 1.3
keywords	string	A comma-separated list of key words and/or phrases. Keywords may be common words or phrases, terms from a controlled vocabulary (GCMD is often used), or URIs for terms from a controlled vocabulary (see also "keywords_vocabulary" attribute).	keywords = "Oceans, Ocean Temperature, Sea Surface Temperature , Sea Surface Skin Temperature" ;	ACDD 1.1, ACDD 1.3
keywords_vocabulary	string	If you are using a controlled vocabulary for the words/phrases in your "keywords" attribute, this is the unique name or identifier of the vocabulary from which keywords are taken. If more than one keyword vocabulary is used, each may be presented with a prefix (e.g., "CF:NetCDF COARDS Climate and Forecast Standard Names") and a following comma, so that keywords may optionally be prefixed with the controlled vocabulary key.	keywords_vocabulary = "NASA Global Change Master Directory (GCMD) Science Keywords" ;	ACDD 1.1, ACDD 1.3
Conventions	string	A comma-separated list of the conventions that are followed by the dataset. For files that follow this version of ACDD, include the string 'ACDD-1.3'. (This attribute is defined in NUG 1.7.)	Conventions = "CF-1.6, ACDD-1.3, ISO 8601";	ACDD 1.3, CF 1.6
id	string	An identifier for the data set, provided by and unique within its naming authority. The combination of the "naming authority" and the "id" should be globally unique, but the id can be globally unique by itself also. IDs can be URLs, URNs, DOIs, meaningful text strings, a local key, or any other unique string of characters. The id should not include white space characters.	id = "VIIRS_NPP-JPL-L2P-v2016.0" ;	ACDD 1.1, ACDD 1.3

Attribute Name	Type	Definitions	Example Implementation	Source
uuid	string	A uuid (Universal Unique Identifier) is a 128-bit number used to uniquely identify some object or entity on the Internet. Depending on the specific mechanisms used, a uuid is either guaranteed to be different or is, at least, extremely likely to be different from any other uuid generated until 3400 A.D.	uuid = "b6ac7651-7b02-44b0-942b-c5dc3c903eba" ;	PO.DAAC
naming_authority	string	The organization that provides the initial id (see above) for the dataset. The naming authority should be uniquely specified by this attribute. We recommend using reverse-DNS naming for the naming authority; URIs are also acceptable. Example: 'edu.ucar.unidata'.	naming_authority = "org.ghrsst" ;	ACDD 1.1, ACDD 1.3
cdm_data_type	string	The data type, as derived from Unidata's Common Data Model Scientific Data types and understood by THREDDS. (This is a THREDDS "dataType", and is different from the CF NetCDF attribute 'featureType', which indicates a Discrete Sampling Geometry file in CF.)	cdm_data_type = "swath" ;	ACDD 1.1, ACDD 1.3
history	string	Provides an audit trail for modifications to the original data. This attribute is also in the NetCDF Users Guide: 'This is a character array with a line for each invocation of a program that has modified the dataset. Well-behaved generic netCDF applications should append a line containing: date, time of day, user name, program name and command arguments.' To include a more complete description you can append a reference to an ISO Lineage entity; see NOAA EDM ISO Lineage guidance.	history = "VIIRS L2P created at JPL PO.DAAC by combining OBPG SNPP_SST and SNPP_SST3, and outputing to the GHRSST GDS2 netCDF file format" ;	ACDD 1.1, ACDD 1.3, CF 1.6
source	string	The method of production of the original data. If it was model-generated, source should name the model and its version. If it is observational, source should characterize it. This attribute is defined in the CF Conventions. Examples: 'temperature from CTD #1234'; 'world model v.0.1'.	source = "VIIRS sea surface temperature observations for the OBPG" ;	ACDD 1.3, CF 1.6
platform	string	Name of the platform(s) that supported the sensor data used to create this data set or product. Platforms can be of any type, including satellite, ship, station, aircraft or other. Indicate controlled vocabulary used in platform_vocabulary.	platform = "Suomi-NPP" ;	ACDD 1.3
platform_vocabulary	string	Controlled vocabulary for the names used in the "platform" attribute.	platform_vocabulary = "GCMD platform keywords";	ACDD 1.3
instrument	string	Name of the contributing instrument(s) or sensor(s) used to create this data set or product. Indicate controlled vocabulary used in instrument_vocabulary.	sensor = "VIIRS" ;	ACDD 1.3
instrument_vocabulary	string	Controlled vocabulary for the names used in the "instrument" attribute.	instrument_vocabulary = "GCMD instrument keywords";	ACDD 1.3
processing_level	string	A textual description of the processing (or quality control) level of the data.	processing_level = "L2P" ;	ACDD 1.1, ACDD 1.3

Attribute Name	Type	Definitions	Example Implementation	Source
comment	string	Miscellaneous information about the data, not captured elsewhere. This attribute is defined in the CF Conventions.	comment = "L2P Core without DT analysis or other ancillary fields; Night, Start Node:Descending, End Node:Descending; WARNING Some applications are unable to properly handle signed byte values. If values are encountered > 127, please subtract 256 from this reported value; Quicklook" ;	ACDD 1.1, ACDD 1.3
standard_name_vocabulary	string	The name and version of the controlled vocabulary from which variable standard names are taken. (Values for any standard_name attribute must come from the CF Standard Names vocabulary for the data file or product to comply with CF.) Example: 'CF Standard Name Table v27'.	standard_name_vocabulary = "NetCDF Climate and Forecast (CF) Metadata Convention" ;	ACDD 1.1, ACDD 1.3
acknowledgement	string	A place to acknowledge various types of support for the project that produced this data.	acknowledgment = "The VIIRS L2P sea surface temperature data are sponsored by NASA. Data may be freely distributed" ;	ACDD 1.1, ACDD 1.3
license	string	Provide the URL to a standard or specific license, enter "Freely Distributed" or "None", or describe any restrictions to data access and distribution in free text.	license = "GHRSST and PO.DAAC protocol allow data use as free and open." ;	ACDD 1.1, ACDD 1.3
metadata_link	string	A URL that gives the location of more complete metadata. A persistent URL is recommended for this attribute.	metadata_link = "http://podaac.jpl.nasa.gov/ws/metadata/dataset/?format=iso&shortName=VIIRS-JPL-L2P-v2016.0" ;	ACDD 1.3
product_version	string	Version identifier of the data file or product as assigned by the data creator. For example, a new algorithm or methodology could result in a new product_version.	product_version = "2016.0" ;	ACDD 1.3
references	string	Published or web-based references that describe the data or methods used to produce it. Recommend URIs (such as a URL or DOI) for papers or other references. This attribute is defined in the CF conventions.	references = "GHRSST Data Processing Specification v2r5" ;	ACDD 1.3, CF 1.6
creator_name	string	The name of the person (or other creator type specified by the creator_type attribute) principally responsible for creating this data.	creator_name = "JPL PO.DAAC" ;	ACDD 1.1, ACDD 1.3
creator_email	string	The email address of the person (or other creator type specified by the creator_type attribute) principally responsible for creating this data.	creator_email = "ghrsst@jpl.nasa.gov" ;	ACDD 1.1, ACDD 1.3
creator_url	string	The URL of the of the person (or other creator type specified by the creator_type attribute) principally responsible for creating this data.	creator_url = "http://podaac.jpl.nasa.gov" ;	ACDD 1.1, ACDD 1.3
creator_type	string	Specifies type of creator with one of the following: 'person', 'group', 'institution', or 'position'. If this	creator_type = "Institution":	ACDD 1.3

Attribute Name	Type	Definitions	Example Implementation	Source
		attribute is not specified, the creator is assumed to be a person.		
creator_institution	string	The institution of the creator; should uniquely identify the creator's institution. This attribute's value should be specified even if it matches the value of publisher_institution, or if creator_type is institution.	creator_institution = = "JPL PO.DAAC/GHRSST";	ACDD 1.3
institution	string	The name of the institution principally responsible for originating this data. This attribute is recommended by the CF convention.	institution = "NASA Jet Propulsion Laboratory (JPL) Physical Oceanography Distributed Active Archive Center (PO.DAAC)/NASA Goddard Space Flight Center (GSFC), Ocean Biology Processing Group (OBPG)/University of Miami Rosential School of Marine and Atmospheric Science (RSMAS)" ;	ACDD 1.1, ACDD 1.3, CF 1.6
project	string	The name of the project(s) principally responsible for originating this data. Multiple projects can be separated by commas, as described under Attribute Content Guidelines. Examples: 'PATMOS-X', 'Extended Continental Shelf Project'.	project = "Group for High Resolution Sea Surface Temperature" ;	ACDD 1.1 ACDD 1.3
program	string	The overarching program(s) of which the dataset is a part. A program consists of a set (or portfolio) of related and possibly interdependent projects that meet an overarching objective. Examples: 'GHRSST', 'NOAA CDR', 'NASA EOS', 'JPSS', 'GOES-R'.	program= " NASA Earth Sciecne Data Information and System (ESDIS)"	ACDD 1.3
contributor_name	string	The name of any individuals, projects, or institutions that contributed to the creation of this data. May be presented as free text, or in a structured format compatible with conversion to ncML (e.g., insensitive to changes in whitespace, including end-of-line characters).	contributor_name = "PO.DAAC/OBPS/REMAS";	ACDD 1.3
contributor_role	string	The role of any individuals, projects, or institutions that contributed to the creation of this data. May be presented as free text, or in a structured format compatible with conversion to ncML (e.g., insensitive to changes in whitespace, including end-of-line characters). Multiple roles should be presented in the same order and number as the names in contributor_names.	contributor_role = "PO.DAAC convert the VIIRSS_NPP SST to GDS2 format, OBPS processed the L2P SST, and REMAS provided the algorithm model ";	ACDD 1.3
publisher_name	string	The name of the person (or other entity specified by the publisher_type attribute) responsible for publishing the data file or product to users, with its current metadata and format.	publisher_name = "The GHRSST Project Office" ;	ACDD 1.1 ACDD 1.3
publisher_email	string	The email address of the person (or other entity specified by the publisher_type attribute) responsible for publishing the data file or product to users, with its current metadata and format.	publisher_email = "ghrsst-po@nceo.ac.uk" ;	ACDD 1.1 ACDD 1.3
publisher_url	string	The URL of the person (or other entity specified by the publisher_type attribute) responsible for publishing the data file or product to users, with its current metadata and format.	publisher_url = "http://www.ghrsst.org" ;	ACDD 1.1 ACDD 1.3

Attribute Name	Type	Definitions	Example Implementation	Source
publisher_type	string	Specifies type of publisher with one of the following: 'person', 'group', 'institution', or 'position'. If this attribute is not specified, the publisher is assumed to be a person.	publisher_type = "instituion";	ACDD 1.3
publisher_institution	string	The institution that presented the data file or equivalent product to users; should uniquely identify the institution. If publisher_type is institution, this should have the same value as publisher_name.	publisher_institution = "PO.DAAC";	ACDD 1.3
geospatial_bounds	float	Describes the data's 2D or 3D geospatial extent in OGC's Well-Known Text (WKT) Geometry format (reference the OGC Simple Feature Access (SFA) specification). The meaning and order of values for each point's coordinates depends on the coordinate reference system (CRS). The ACDD default is 2D geometry in the EPSG:4326 coordinate reference system. The default may be overridden with geospatial_bounds_crs and geospatial_bounds_vertical_crs (see those attributes). EPSG:4326 coordinate values are latitude (decimal degrees_north) and longitude (decimal degrees_east), in that order. Longitude values in the default case are limited to the (-180, 180) range. Example: "POLYGON ((40.26 -111.29, 41.26 -111.29, 41.26 -110.29, 40.26 -110.29, 40.26 -111.29))".	geospatial_bounds = "(-143.09, -63.1404, -88.893, -36.7432)";	ACDD 1.1 ACDD 1.3
geospatial_bounds_crs	string	The coordinate reference system (CRS) of the point coordinates in the geospatial_bounds attribute. This CRS may be 2-dimensional or 3-dimensional, but together with geospatial_bounds_vertical_crs, if that attribute is supplied, must match the dimensionality, order, and meaning of point coordinate values in the geospatial_bounds attribute. If geospatial_bounds_vertical_crs is also present then this attribute must only specify a 2D CRS. EPSG CRSs are strongly recommended. If this attribute is not specified, the CRS is assumed to be EPSG:4326. Examples: "EPSG:4979" (the 3D WGS84 CRS), "EPSG:4047".	geospatial_bounds_crs = "WGS84";	ACDD 1.3
geospatial_bounds_vertical_crs	string	The vertical coordinate reference system (CRS) for the Z axis of the point coordinates in the geospatial_bounds attribute. This attribute cannot be used if the CRS in geospatial_bounds_crs is 3-dimensional; to use this attribute, geospatial_bounds_crs must exist and specify a 2D CRS. EPSG CRSs are strongly recommended. There is no default for this attribute when not specified. Examples: "EPSG:5829" (instantaneous height above sea level), "EPSG:5831" (instantaneous depth below sea level), or "EPSG:5703" (NAVD88 height).	geospatial_bounds_vertical_crs = "EPSG:5831";	ACDD 1.3
geospatial_lat_min	float	Describes a simple lower latitude limit; may be part of a 2- or 3-dimensional bounding region. Geospatial_lat_min specifies the southernmost latitude covered by the dataset.	geospatial_lat_min = -63.1404f ;	ACDD 1.1, ACDD 1.3
geospatial_lat_max	float	Describes a simple upper latitude limit; may be part of a 2- or 3-dimensional bounding region. Geospatial_lat_max specifies the northernmost latitude covered by the dataset.	geospatial_lat_max = -36.7432f ;	ACDD 1.1, ACDD 1.3

Attribute Name	Type	Definitions	Example Implementation	Source
geospatial_lat_units	string	Units for the latitude axis described in "geospatial_lat_min" and "geospatial_lat_max" attributes. These are presumed to be "degree_north"; other options from udunits may be specified instead.	geospatial_lat_units = "degrees_north" ;	ACDD 1.1, ACDD 1.3
geospatial_lat_resolution	float	Information about the targeted spacing of points in latitude. Recommend describing resolution as a number value followed by the units. Examples: '100 meters', '0.1 degree'. For level 1 and 2 swath data this is an approximation of the pixel resolution.	geospatial_lat_resolution = 0.0075f ;	ACDD 1.1, ACDD 1.3
geospatial_lon_min	float	Describes a simple longitude limit; may be part of a 2- or 3-dimensional bounding region. geospatial_lon_min specifies the westernmost longitude covered by the dataset. See also geospatial_lon_max.	geospatial_lon_min = -143.09f ;	ACDD 1.1, ACDD 1.3
geospatial_lon_max	float	Describes a simple longitude limit; may be part of a 2- or 3-dimensional bounding region. geospatial_lon_max specifies the easternmost longitude covered by the dataset. Cases where geospatial_lon_min is greater than geospatial_lon_max indicate the bounding box extends from geospatial_lon_max, through the longitude range discontinuity meridian (either the antimeridian for -180:180 values, or Prime Meridian for 0:360 values), to geospatial_lon_min; for example, geospatial_lon_min=170 and geospatial_lon_max=-175 incorporates 15 degrees of longitude (ranges 170 to 180 and -180 to -175).	geospatial_lon_max = -88.893f ;	ACDD 1.1, ACDD 1.3
geospatial_lon_units	string	Units for the longitude axis described in "geospatial_lon_min" and "geospatial_lon_max" attributes. These are presumed to be "degree_east"; other options from udunits may be specified instead.	geospatial_lon_units = "degrees_east" ;	ACDD 1.1, ACDD 1.3
geospatial_lon_resolution	float	Information about the targeted spacing of points in longitude. Recommend describing resolution as a number value followed by units. Examples: '100 meters', '0.1 degree'. For level 1 and 2 swath data this is an approximation of the pixel resolution.	geospatial_lon_resolution = 0.0075f ;	ACDD 1.1, ACDD 1.3
geospatial_vertical_min	float	Describes the numerically smaller vertical limit; may be part of a 2- or 3-dimensional bounding region. See geospatial_vertical_positive and geospatial_vertical_units.	geospatial_vertical_min = 0.00f;	ACDD 1.1, ACDD 1.3
geospatial_vertical_max	float	Describes the numerically larger vertical limit; may be part of a 2- or 3-dimensional bounding region. See geospatial_vertical_positive and geospatial_vertical_units.	geospatial_vertical_max = 1000.00f;	ACDD 1.1, ACDD 1.3
geospatial_vertical_resolution	float	Information about the targeted vertical spacing of points. Example: '25 meters'	geospatial_vertical_resolution = 25.0f;	ACDD 1.1, ACDD 1.3

Attribute Name	Type	Definitions	Example Implementation	Source
geospatial_vertical_units	string	Units for the vertical axis described in "geospatial_vertical_min" and "geospatial_vertical_max" attributes. The default is EPSG:4979 (height above the ellipsoid, in meters); other vertical coordinate reference systems may be specified. Note that the common oceanographic practice of using pressure for a vertical coordinate, while not strictly a depth, can be specified using the unit bar. Examples: 'EPSG:5829' (instantaneous height above sea level), 'EPSG:5831' (instantaneous depth below sea level).	geospatial_vertical_units = 'meters';	ACDD 1.1, ACDD 1.3
geospatial_vertical_positive	string	One of 'up' or 'down'. If up, vertical values are interpreted as 'altitude', with negative values corresponding to below the reference datum (e.g., under water). If down, vertical values are interpreted as 'depth', positive values correspond to below the reference datum. Note that if geospatial_vertical_positive is down ('depth' orientation), the geospatial_vertical_min attribute specifies the data's vertical location furthest from the earth's center, and the geospatial_vertical_max attribute specifies the location closest to the earth's center.	geospatial_vertical_positive = 'down';	ACDD 1.1, ACDD 1.3
time_coverage_start	string	Describes the time of the first data point in the data set. Use the ISO 8601:2004 date format, preferably the extended format as recommended in the Attributes Content Guidance section.	time_coverage_start = "2016-09-01T08:12:01" ;	ACDD 1.1, ACDD 1.3
time_coverage_end	string	Describes the time of the last data point in the data set. Use ISO 8601:2004 date format, preferably the extended format as recommended in the Attributes Content Guidance section.	time_coverage_end = "2016-09-01T08:17:59" ;	ACDD 1.1, ACDD 1.3
time_coverage_duration	string	Describes the duration of the data set. Use ISO 8601:2004 duration format, preferably the extended format as recommended in the Attributes Content Guidance section.	time_coverage_duration = "P4Y6M15DT20H30M40S";	ACDD 1.1, ACDD 1.3
time_coverage_resolution	string	Describes the targeted time period between each value in the data set. Use ISO 8601:2004 duration format, preferably the extended format as recommended in the Attributes Content Guidance section.	time_coverage_resolution = "00:05:58";	ACDD 1.1, ACDD 1.3
date_created	string	The date on which this version of the data was created. (Modification of values implies a new version, hence this would be assigned the date of the most recent values modification.) Metadata changes are not considered when assigning the date_created. The ISO 8601:2004 extended date format is recommended, as described in the Attribute Content Guidance section.	date_created = "2016-10-14T21:00:25" ;	ACDD 1.1, ACDD 1.3
date_modified	string	The date on which the data was last modified. Note that this applies just to the data, not the metadata. The ISO 8601:2004 extended date format is recommended, as described in the Attributes Content Guidance section.	date_modified = "2016-10-14T21:00:25" ;	ACDD 1.1, ACDD 1.3

Attribute Name	Type	Definitions	Example Implementation	Source
date_issued	string	The date on which this data (including all modifications) was formally issued (i.e., made available to a wider audience). Note that these apply just to the data, not the metadata. The ISO 8601:2004 extended date format is recommended, as described in the Attributes Content Guidance section.	date_issued = "2016-10-14T21:00:25" ;	ACDD 1.1, ACDD 1.3
date_metadata_modified	string	The date on which the metadata was last modified. The ISO 8601:2004 extended date format is recommended, as described in the Attributes Content Guidance section.	date_metadata_modified = "2016-10-14T21:00:25" ;	ACDD 1.3

Table 1: Global CF-1.6 and ACDD-1.3 attributes (new in GDS are highlighted in blue)

Attribute Name	Type	Definitions	Example Implementation	Source
start_time	string	Representative date and time of the start the granule in the ISO 8601 compliant format of "yyyymmddThhmmssZ". The exact meaning of this attribute depends the type of granule: • L2P: last measurement in granule • L3U: stop time of granule • L3C and L3S: representative stop time of last measurement in collation • L4: representative stop time of the analysis (start_time and stop_time together represent the valid period of the L4 granule)	start_time = "2016-09-01T08:12:01" ;	GDS2
stop_time	string	Representative date and time of the end of the granule in the ISO 8601 compliant format of "yyyymmddThhmmssZ". The exact meaning of this attribute depends the type of granule: • L2P: last measurement in granule • L3U: stop time of granule • L3C and L3S: representative stop time of last measurement in collation • L4: representative stop time of the analysis (start_time and stop_time together represent the valid period of the L4 granule)	stop_time = "2016-09-01T08:17:59" ;	GDS2
northernmost_latitude	float	Decimal degrees north, range -90 to +90. This is equivalent to ACDD geospatial_lat_max.	see example of geospatial_lat_max	GDS2
southernmost_latitude	float	Decimal degrees north, range -90 to +90. This is equivalent to ACDD geospatial_lat_min.	see example of geospatial_lat_min	GDS2
westernmost_longitude	float	Decimal degrees east, range -180 to +180. This is equivalent to ACDD geospatial_lon_min	see example of geospatial_lon_min	GDS2
easternmost_longitude	float	Decimal degrees east, range -180 to +180. This is equivalent to ACDD geospatial_lon_max	see example of geospatial_lat_max	GDS2

Attribute Name	Type	Definitions	Example Implementation	Source
uuid	string	A Universally Unique Identifier (UUID). Numerous, simple tools can be used to create a UUID, which is inserted as the value of this attribute. See http://en.wikipedia.org/wiki/Universally_Unique_Identifier for more information and tools.		GDS2
gds_version_id	string	GDS version used to create this data file. For example, “2.0”.		GDS2
netcdf_version_id	string	Version of netCDF libraries used to create this file. For example, “4.1.1”		GDS2
file_quality_level	integer	A code value: 0 = unknown quality 1 = extremely suspect (frequent problems, e.g. with known satellite problems) 2 = suspect (occasional problems, e.g. after launch) 3 = excellent (no known problems)		GDS2
sensor	string	Duplication of ACDD instrument attribute. Sensor(s) used to create this data file. Select GDS from the entries found in the Satellite Sensor column of Table 7-5 and provide as a comma separated list if there is more than one.		GDS2

Table 2: carry-over attributes from GDSv2

Attribute Name	Type	Definitions	Example Implementation	Source	Variable Type
long_name	string	A long descriptive name for the variable (not necessarily from a controlled vocabulary). This attribute is recommended by the NetCDF Users Guide, the COARDS convention, and the CF convention.	long_name = "sea surface temperature" ;	ACDD 1.1, ACDD 1.3, CF 1.6	measurement/auxillary/quality variables
standard_name	string	A long descriptive name for the variable taken from a controlled vocabulary of variable names. We recommend using the CF convention and the variable names from the CF standard name table (http://cfconventions.org/Data/cf-standard-names/36/build/cf-standard-name-table.html). This attribute is recommended by the CF convention.	standard_name = "sea_surface_skin_temperature" ;	ACDD 1.1, ACDD 1.3, CF 1.6	measurement/auxillary/quality variables
units	string	The units of the variable's data values. This attribute value should be a valid udunits string. The "units" attribute is recommended by the NetCDF Users Guide, the COARDS convention, and the CF convention (http://www.unidata.ucar.edu/software/udunits/udunits-1/udunits.txt).	units = "kelvin" ;	ACDD 1.1, ACDD 1.3, CF 1.6	measurement/auxillary/quality variables

Attribute Name	Type	Definitions	Example Implementation	Source	Variable Type
coverage_content_type	string	An ISO 19115-1 code to indicate the source of the data --MD_CoverageContentTypeCode (https://geo-ide.noaa.gov/wiki/index.php?title=ISO_19115_and_19115-2_CodeList_Dictionaries#CI_PresentationFormCode). For example, image, thematicClassification, physicalMeasurement, auxiliaryInformation, qualityInformation, referenceInformation, modelResult, or coordinate.	coverage_content_type = "physicalMeasurement" ;	ACDD 1.1, ACDD 1.3	measurement/auxillary/quality variables
valid_range	float	Comma seperated minimum and maximum values of the physical quantity defining the valid measuremnt range.	valid_range = 0.0f, 500.0f;	CF 1.6	measurement/auxillary/quality variables
coordinates	string	This attribute contains a space seperated list of all the coordinates corresponding to the variable.The list should contain all the arxiliary coordinate variables and optionally the coordinate variables.	coordinates = "lat lon";	CF 1.6	measurement/auxillary/quality variables
scale_factor	float	Slope of scaling relationship applied to transform measuement data to appropriate geophysical quantity representations. Should not be used if the scale_factor is '1' and add_offset is '0'	scale_factor = 0.005f ;	CF 1.6	measurement/auxillary/quality variables
add_offset	float	Intercept of scaling relationship applied to transform measuement data to appropriate geophysical quantity representations. Should not be used if the scale_factor is '1' and add_offset is '0'	add_offset = 273.15f ;	CF 1.6	measurement/auxillary/quality variables
_FillValue	float	Assigned value in the data file desiganting a null or missing observation	_FillValue = -32767s ;	CF 1.6	measurement/auxillary/quality variables
grid_mapping	string	Describes the horizontal coordinate system used by the data. The grid_mapping attribute should point to a variable which would contain the parameters corresponding to the coordinate system. There are typically several parameters associated with each coordinate system. CF defines a separate attributes for each of the parameters. Some examples are "semi_major_axis", "inverse_flattening", "false_easting"	grid_mapping = "TBD"	CF 1.6	measurement/auxillary/quality variables
comment	string	Optional attribute field allowing provision of further free-form information about the variable	comment = "sea surface temperature from 11 and 12 um (thermal IR) channels" ;	CF 1.6	measurement/auxillary/quality variables

Attribute Name	Type	Definitions	Example Implementation	Source	Variable Type
flag_masks	unsigned byte	A number of independent Boolean conditions using bit field notation by setting unique bits in each flag_masks value. The flag_masks attribute is the same type as the variable to which it is attached, and contains a list of values matching unique bit fields. (CF document 3.5 Flags;http://cfconventions.org/Data/cf-conventions/cf-conventions-1.6/build/cf-conventions.pdf)	flag_masks = 1b, 2b, 4b, 8b, 16b;	CF 1.6	quality variable
flag_meanings	string	Define the physical meaning of each flag_masks bit field with a single text string. CF allows a single variable to contain both flag_values and flag_masks. The interpretation of the flags in such cases is slightly tricky. In such cases flag_masks is used to "group" a set of flag_values into a nested conditional. Please see the example 3.5 in the CF document on how to interpret flag_meanings in such cases. NCEI recommends that boolean and enumerated flags be kept in separate variables.	flag_meanings = "microwave land ice lake river" ;	CF 1.6	quality variable
flag_values	unsigned byte	Its values identify the flagged conditions by performing a bitwise AND of the variable value and each flag masks value. For example, if the variable value is of type unsigned byte and equal to 5 and the flag_masks are 1b, 2b, 4b, 8b, 16b, 32b. The binary encoding of 5 is 00000101 and the binary encoding of the flags are 00000001, 00000010, 00000100, 00001000, 00010000, 00100000. Now bitwide AND of the value with the masks returns 00000001, 00000000, 00000100, 00000000, 00000000, 00000000 respectively or 1b,0,4b,0,0,0,0,0 in decimal. So the masks corresponding to 1b and 4b are "true", rest are "false".	flag_values = 1b, 5b ;	CF 1.6	quality variable

Table 3: variable attributes (in red, definition that need to be improved before updating the GDS)

Attribute Name	Type	Definitions	Example Implementation	Source	Variable Type
long_name	string	custom/long descriptive name of variable	long_name = "latitude or longitude";	ACDD 1.1, ACDD 1.3, CF 1.6	geo-reference variables
standard_name	string	standard variable name used to describe the georefencing variable (eg. latitude, longitude, height)	standard_name = "latitude or longitude";	ACDD 1.1, ACDD 1.3, CF 1.6	geo-reference variables

Attribute Name	Type	Definitions	Example Implementation	Source	Variable Type
units	string	standard unit name for the standard georeferencing variable (eg. "degrees_north", "degrees_east", "m"	units = "degrees_north or degree_east";	ACDD 1.1, ACDD 1.3, CF 1.6	geo-reference variables
axis	string	Corresponding variable axis for plotting (eg. X, Y, Z)	axis = "X or Y";	CF 1.6	geo-reference variables
_FillValue	float	Assigned value in the data file desiganting a null or missing observation. NASA best practices specifies that for satellite datasets there should not be a _FillVlalue for these geolocation variables.	_FillValue = -9999.0f ;	CF 1.6	geo-reference variables
valid_min	float	The minimum values of georeferancing variables (eg. latitude, longitude, height)	valid_min = -90.f (for lat); valid_min = -180.f (for lon);	CF 1.6	geo-reference variables
valid_max	float	The maximum values of georeferancing variables (eg. latitude, longitude, height)	valid_max = 90.f (for lat); valid_max = 180.f (for lon);	CF 1.6	geo-reference variables
comment	float	Optional attribute field allowing provision of further free-form information about the variable	comment = "geographical coordinates, WGS84 projection" ;	CF 1.6	geo-reference variables

Table 4: geo-reference attributes (attributes of spatial variables)

Attribute Name	Type	Definitions	Example Implementation	Source	Variable Type
long_name	string	custom/long descriptive name of variable	long_name = "time of measurement" ;	ACDD 1.1, ACDD 1.3, CF 1.6	time variables
standard_name	string	standard variable name used to describe the temporal variable (ie. time)	standard_name = “time”;	ACDD 1.1, ACDD 1.3, CF 1.6	time variables
units	string	standard unit descriptor (eg. days, hours, seconds etc) cited against a standard reference date ("since".. date/time in ISO 8601 format)	units = "seconds since 1981-01-01 00:00:00" ;	ACDD 1.1, ACDD 1.3, CF 1.6	time variables
axis	string	Corresponding variable axis for plotting (eg. T)	axis = "T";	CF 1.6	time variables
_FillValue	float	Assigned value in the data file desiganting a null or missing observation. NASA best practices specifies that for satellite datasets there should not be a _FillVlalue for time variables.	_FillValue = -9999.0f;	CF 1.6	time variables
comment	float	Optional attribute field allowing provision of further free-form information about the variable	comment = "time of first sensor observation" ;	CF 1.6	time variables

Table 5: time attributes

2.2 Product level discussion

Ambiguities on what product level should be used were reported from the GDS and as a matter of fact, different producers are using different product level naming for similar products, in particular for geostationary satellite products. There are also reported ambiguities related to the downgrading of product resolution or whether some gap filling is applied.

A few of these ambiguous cases were discussed but no decision was made. A general approach for discussion and update of the GDS was however proposed : **all possible transformation applied to data by a producer should be specified in a table, deriving for all these transformations a proper product level in an incremental manner. This table should be proposed and discussed by the science team.**

It is not (and will not be) required to change their existing product names. This disambiguition effort will likely make some existing product naming in conflict with the new rules (as different producer's similar datasets are already in conflict with each other) but changes will only be required for future products.

The following subsections detail some of the cases that were discussed.

2.2.1 Swath products with downgraded resolution

This includes for instance VIIRS product at downgraded 1500m resolution but still in swath projection. Resampling or regridding usually qualifies the product as L3 but there is then a possible confusion with fixed grid L3 products (all L3U / L3C products and L3S so far).

Suggestion : to keep L2 for any LEO dataset in swath projection, as swath products are more associated with « L2 » concept from user perspective

2.2.2 L2 with gap filling

Interpolation or any method used for filling cloud covered pixels could semantically be called L4 but this brings a risk of confusion with fixed grid L4 analysed products like OSTIA, CMC, etc... which what users expect.

Suggestion : to keep L2 for any LEO dataset in swath projection, whether gap filling is applied or not.

2.2.3 Geostationary products : L2 or L3 ?

The GDSv2r5 is ambiguous on whether geostationary products with L2P type of content (one snapshot with all variables from L2P) are actually L2 or L3.

As a reminder:

Un-collated (L3U): L2 data granules remapped to a space grid without combining any observations from overlapping orbits

Collated (L3C): observations combined from a single instrument into a space-time grid

The definition of L3U matches single geostationary snapshot (full temporal resolution, one snapshot image regridded from disk projection) of geostationary except possibly for « L2 » mention (when processing is done from L1). However some producer are using the “L2P” product level for such products...

The definition of L3C matches composite geostationary products (ex : hourly with some merging, downgraded temporal resolution) with a possible confusion with some L3C products (merging of L2 LEO orbits)

Suggestion : geostationary products, being gridded product on a fixed grid, are from user perspective more associated with « L3 » concept. Use L3U and L3C product type for geostationary products depending if they are single or composite images.

This suggestion was much debated and no consensus could be reached. The incremental approach to define the different product levels (and associated data transformation) that was proposed in the discussion will help to move forward and try to reach a consensus. The GDS will need to be cleaned and clarified with respect to the changes we will decide.

3 REVISION OF GHRSST R/GTS

The main discussion topic of the session was the new proposed organization for GHRSST system (R/GTS), based on initial directions discussed at GHRSST-XVII in Washington.

The following diagram describes the existing “classic” GHRSST organization:

- All “official” data flow from RDAC (producers) to GDAC to LTSRF
- Data is accessible at all levels
- RDACs are free to do whatever they like, as long as they submit GDS-compliant data to GDAC
- the metadata “grows as it flows” from one level to the next
- LTSRF publishes collection metadata

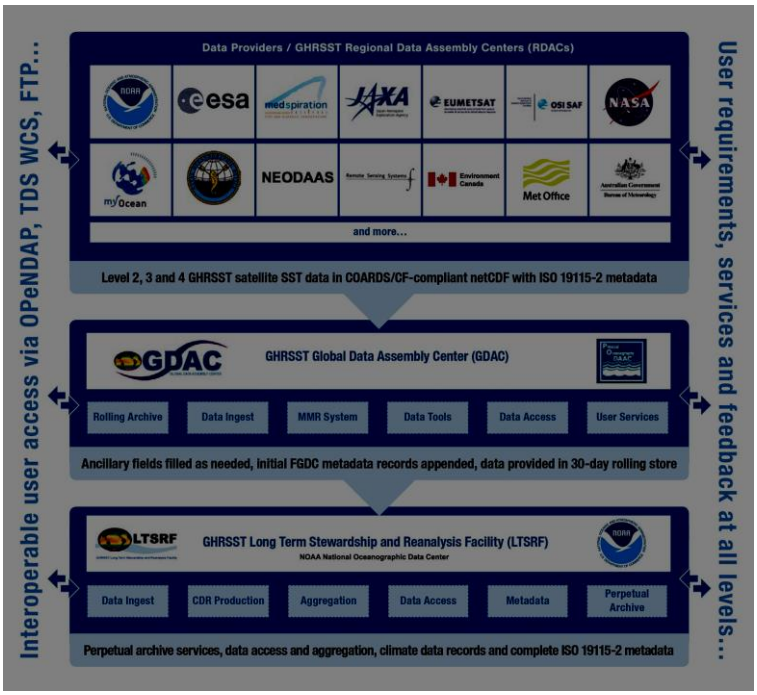

This model was considered highly successful, and nothing is “broken”, though a few inconsistencies and shortcomings were identified:

- the current GDACs or LTSRF don't or can't archive all GHRSST products or won't in the future, due to the growing number of products and infrastructure and cost limitations. As a consequence, they tend to select or focus on datasets of interest for their own usage or of national responsibility
- this highly centralized model involves complex data exchange procedures or monitoring requiring frequent interactions with data providers
- some agencies may wish to be sole access point and archive for their products (data policy, user registration,...)
- it is difficult for central repository help desks (GDACs or LTSRF) to support users on products they are not responsible for
- there is a conceptual weakness as central system elements are critical while being also dependent on funding of the agencies performing this central services
- the « physical » central repository of products concept may be somewhat obsolete or not bringing much advantages – single access point for users is the main benefit and can be « logical »

The DAS TAG therefore defined an evolution of the current R/GTS towards a more **distributed system** where different "GHRSST DACs" or data producers themselves (GDPs) ensure data dissemination and archiving functions. This is often the case already since many data producers have their own distribution capability but requires common interfaces to link all these systems to each other and still deliver a central vision of GHRSST products catalogue and access, through a **central portal for data discovery and inventory search**.

The new proposed organization is as follow:

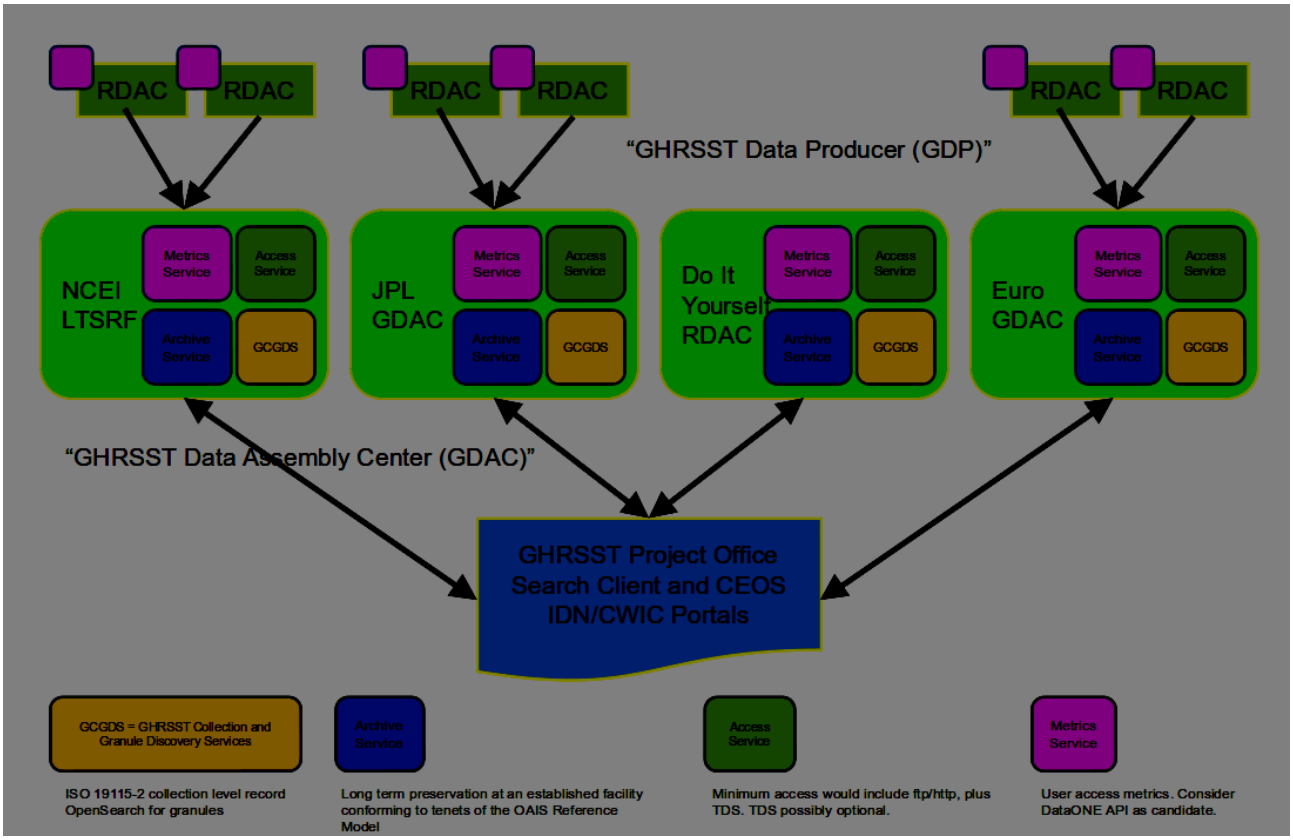

In this new organization, there is no more a central GDAC or long-term archive. There can be several of them, serving different data from one or more producers (the RDACs are now **GHRSST Data Producers – GDP**). GDACs therefore does not hold any "global" scope, they are now **GHRSST Data Assembly Centers**, providing a set of services and interfaces in a consistent way for each of them. A producer (GDP) can be its own GDAC, offering access only to its own products, if it implements the required GDAC services and interfaces.

The central access point to all GDAC datasets is implemented at GHRSST project office and this is where users are redirected: it federates all GDACs and it is the place where all GHRSST data, no matter where they reside, can be discovered. When access is initiated, this central catalogue provides the granule data access links to the data files at the appropriate repository in the data hosting GDAC.

The different categories of services and interfaces to be implemented by GHRSST system elements include:

- **data access services** : interfaces for the dissemination of the data to users, that must be implemented by each GDAC (or GDP acting as its own GDAC)
- **GHRSST Collection and Granule Discovery Services ("GCGDS")** : interfaces for the catalogue and inventory of the distributed different datasets, implemented by each GDAC and federated by GHRSST project office. This offers a central overall view of all GHRSST data wherever they reside.
- **metric services** : provide metrics on system availability, data production, usage and distribution
- **archiving services** : provides long term preservation of the produced data

For each of these services, protocols and interfaces are defined that must be implemented by the dissemination centers (GDACs). **The compliance to these requirements by each agency is critical as the interoperability between these agencies will break if they are not strictly followed.** These requirements, still to be approved, are defined so that it requires minimum investment by each agencies that need to expose these services, takes full advantage of existing software while complying to already existing general requirements in ocean/weather community.

The following implementation is proposed for these services. The requirements for each of these services is not yet fully mature and will have to be investigated and defined further by the DAS TAG team.

3.1 Data access services

Mandatory data access services to be provided by GDACs (or GDP acting as its own GDAC) are:

- **http** access to data folder (or **https**)

Strongly recommended services are:

- ftp (or sftp) as used today by most GHRSST DACs. Ftp tends to be discarded by more and more agencies and therefore is no more mandatory.
- DAP : several implementations of DAP can be used here by GDACs such as OpenDAP, Thredds or Hyrax

Recommended services are:

- **WMS** and **WCS** protocols : this only concerns L3 and L4 (fixed grid) products

3.2 Collection and Granule Discovery Services

The proposed dataset discovery (catalogue) protocol is **CSW**.

The proposed protocol for granule search and discovery (inventory) is **Opensearch**.

These protocols **must be implemented by each dissemination center** (GDAC, GDP acting as its own GDAC). There will be a central GHRSST Project office portal, connecting to each of these services and aggregating the results from each of them upon a user search request to this central portal.

There are already many implementations of these protocols and many agencies are using them already, as they are required in various national or international projects to offer consistent discovery of all available data. However the interoperability of the different implementations is not guaranteed, in particular with opensearch as the vocabulary requirements are quite loose and not every agency is using the same which prevent from implementing the new GHRSST federated query system without additional implementation requirements.

Four implementation scenarios were presented by the DAS TAG team, in particular to try to cope with the above issue. They were presented and discussed during the DAS TAG session, and narrowed down to the two following ones.

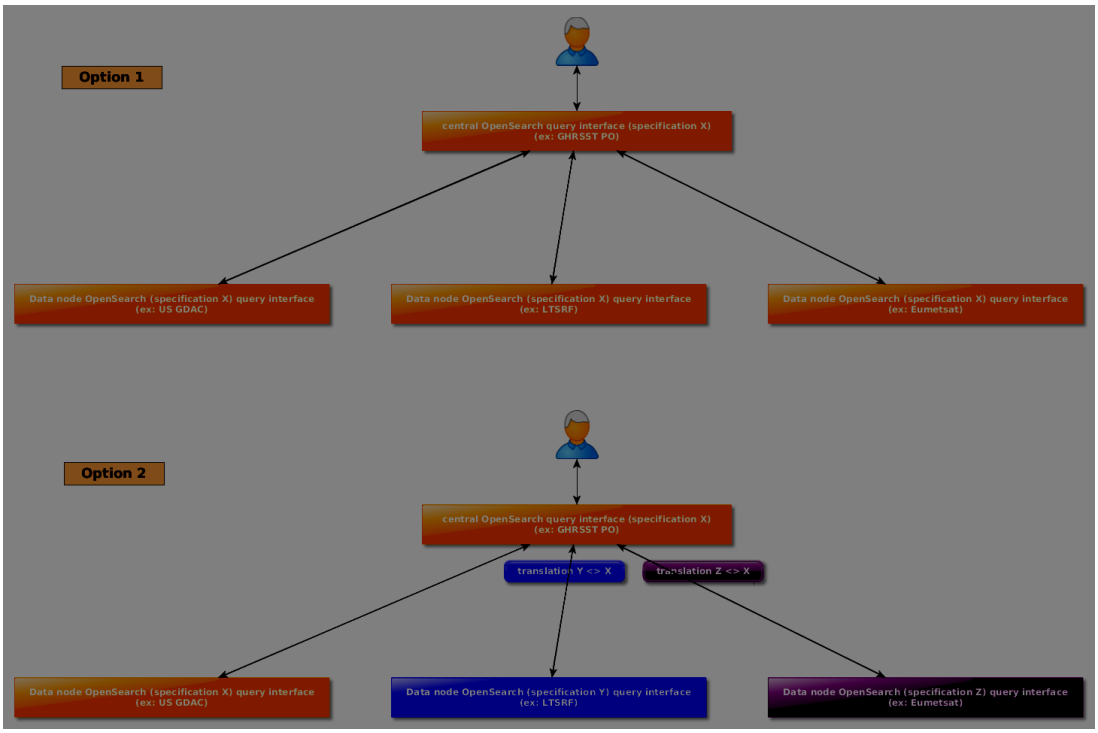

In both scenarios, a user request sent to the central portal (at GHRSST project office) is forwarded to each GDAC interconnected with the portal, the result from the different subrequests assembled and returned to the user.

In **scenario 1**, we assume that all entities (central portal and GDACs) implement the CSW and Opensearch services in exactly the same way, using the same request and response format and vocabulary. This is the most simple implementation (everybody using the same interfaces) but it does not take advantage of existing services already in place that may implement these interfaces in a slightly different way (using for instance a different vocabulary).

In scenario 2, the GHRSST PO portal would first translate the subrequest to the exact format and vocabulary expected by the GDAC interface it is sent to, and then translate its response back to a common single format and vocabulary allowing the assembling of the different responses from the different GDACs before returning this assembled response to the user. This solution takes advantage of already existing services at some GDACs but makes the implementation of the GHRSST PO portal much more complicate and difficult to maintain.

The preferred scenario is the scenario 1 from technical perspective. No strong feeling against it were expressed against this but it will be further assessed by the DAS TAG in terms of feasability. In particular it requires a common software that can be easily deployed and used by each GDAC, in any country. One possible solution is the open source implementation of opensearch suggested by JPL suggested by Thomas Huang:

> EDGE: Extensible Data Gateway Environment, implementation of OpenSearch and support on-the-fly metadata translation to ISO-19115, GCMD, DIFF, standards, https://github.com/dataplumber/edge

It was also suggested by Peter Cornillon to offer to users a single virtual directory tree giving a central access to all GHRSST granule files in a seamless manner, as if they were all stored on the same physical server (as currently available when going to PODAAC or LTSRF). This can probably be dynamically built on top of opensearch protocol.

3.3 Archiving services

The archiving service addresses the long-term preservation of the produced datasets (involving data back-up on tape library etc...). A proper archiving of each released GHRSST dataset shall be performed and a GHRSST data producer (GDP) has to commit to the archiving of its datasets. If a GDP does not have this capacity, it should be done in relation with an attached GDAC.

They are no recommendations from GHRSST in terms of software or interfaces, but it is proposed that each GDAC or GDP implements its archiving services and provides to GHRSST Project Office a written response to a short document template about how they meet **Open Archival Information System (OAIS)** Reference Model responsibilities (Ingest, Archival Storage, Access, etc.).

https://public.ccsds.org/pubs/650x0m2.pdf

3.4 Metric services

The GHRSST project office (GPO) needs to establish a verification capability to ensure all components provide reliable services, as well as collecting data usage information.

User metrics services would be very simple at first, focused on data volumes, files, and numbers of users. GPO would aggregate these numbers. However it is also an objective to estimate these metrics in a consistent manner in every GDACs, as such a simple thing as “unique users” can be estimated in numerous ways giving inconsistent numbers.

The availability and reliability of GHRSST system and its components (GDACs and GDPs). The corresponding metrics for this need also to be further defined to ensure consistency across all GDACs/GDPs. Some tools have been suggested (like https://statuschecker.fgdc.gov) that allow to independently monitor some data access services but they don't cover the full range of services recommended for GHRSST data access.

Of all the services defined for the new GHRSST R/GTS, the metric services are the less mature and will require further definition and requirements from the DAS TAG team.

PLENARY SESSION VIII: IN SITU

SESSION VIII REPORT

Chair: Alexander Ignatov [(1)]; Rapporteur: Werenfried Wimmer [(2)]

(1)NOAA STAR, Email: Alex.Ignatov@noaa.gov
(2)University of Southampton, Email: W.Wimmer@soton.ac.uk

ABSTRACT

The session featured three oral presentations and an open floor discussion.

SUMMARY OF SPEAKERS AND ORGANIZATIONS

1. Shipboard measurements of skin SST in the NW Pacific (20min) – Lei Guan, Ocean U. of China
2. IMOS ship SST for satellite SST validation (20min) – Helen Beggs, BoM, Australia
3. The improvement of ICOADS3.0 and its application to DOISST (20min) – Chunying Liu, NOAA, USA
4. Open floor discussion (30min)

1. SUMMARY OF PRESENTATIONS

The highlights for each talk and floor discussion are given below.

1.1. SHIPBOARD MEASUREMENTS OF SKIN SST IN NW PACIFIC – LEI GUAN, OCEAN U OF CHINA

Lei Guan started off with introducing ISAR measurements. First ISAR arrived in Qingdao in 2007 and data collection started shortly hereafter. Location of ISAR on the ship, with data logging system and ancillary measurements was described. CEOS inter-comparison was performed at NPL in 2009. BB-ASSISTIILR was bought in 2008, and since 2009, 61 cruises performed. Calibration on ship is conducted before and after each cruise. After the cruise, typical bias is <0.05K and SD~0.03K. Mirror contamination is controlled. OUC instrument still testing. FRM4STS was performed at NPL in 2016. New research vessel will be ready in 2018. The ISAR data have been employed to validate several satellite SST products. Based on N=493 matchups (with 0.01deg/1hr window), SNPP VIIRS SST bias <0.14K with SD~0.35K. With more stringent QC (based on N=122 matchups), mean bias <0.09K and SD~0.21K. Validation of HY-1B SST (based on IR data) against buoy SST with the same match-up criteria, shows bias 0.72K and SD~1.82K (based on N=1,097 matchups). These statistics are less favorable than validation for MODIS NLSST. Data of HY-2 (MW) are noisier and show larger biases compared to WindSat SST. In terms of data sharing: matchups can be probably shared, but not original in situ data.

Q (Craig Donlon): congratulations on an impressive data set! On data sharing, we have to find ways to move forward. ESA is issuing a contract to WW, TN, JH for radiometer network. Maybe in the next few years we can get data sharing underway? Should take an action. Maybe GHRSST can help start the process. We also should look at passive MW, long mission to 2025. GHRSST can help w/knowledge/expertise to improve data processing

A: EUMETSAT might be used as collaboration mechanism.

Q (Helen Beggs): It is impressive to have 12 years of ISAR data! Should we consider with CSIRO and Minglun Yang an OUC ISAR comparison on the RV Investigator?

A: Shipping might be an issue – no way to send as luggage. Good idea, but logistics might be tricky. We need a smaller ISAR. CD FRM4STS has shipborne comparison project, probably more important than laboratory comparisons.

Q (Helen Beggs): Satellite vs. shipborne comparisons: which one is closer to truth?

A: Should be shipborne measurements.

Q (Craig Donlon): Interesting question. On some satellite/buoy comparison, the satellite SST is better. But it is space average to point comparison. A key problem that is not easy to answer.

A: Agree.

1.2. IMOS SHIP SST FOR SATELLITE SST VALIDATION – HELEN BEGGS (BOM, AUSTRALIA)

Helen started off with posing a question: Why do we need IMOS ships? Looking at the iQuam map of observations, drifters tend to concentrate in some regions but not others. There are very few buoys in the Tropical Warm Pool. Ship engine intake data are usually noisy and not accurate, but onboard RV and IMOS ships, data are well calibrated and at least as good as buoys. Argo also have good accuracy, but their coverage is only 1% of drifting buoys. She then described the IMOS portal for ship SST (http://imos.org.au/sstsensors.html) which currently reports past and present SST observations from 9 SBE38 and 12 SBE48 ship-mounted sensors. Four of these ships are RVs so also report air-sea flux measurements. Ship SST documented in JOO paper (Beggs et al, 2012). Automated QC method is employed. Showed iQuam v2 plot of IMOS SST distribution. IMOS ship are currently also ingested in ICOADS and available via GTS. Showed validation of AVHRR HRPT data at BoM. Time series begin from 1994 against drifting buoy data (not many in situ observations before that). IMOS ship SST validation available from 2008-on. Showed comparison of validation against drifting buoys vs. ship SST for NOAA-15/16/18/19. The validation results compare favorably, suggesting that accuracy/precision of IMOS ship data is at least comparable to that of drifting buoys, and fills an important void in drifters' coverage. Then Helen went on to describe the ISAR onboard RV Investigator. The Real time RV data are on the IMOS portal, including ISAR data. The RV Investigator ISAR participated in FRM4STS inter comparison in 2016 at NPL. Reprocessed data using Werenfrid Wimmer's ISAR uncertainty codev2.7.0 available on www.marlin.csiro.au. Ingested into Felyx MDB. . Results from IN2017_V01 Jan 2017 Antarctic cruise show some diurnal variability events. Future cruise links are available online at CSIRO's MNF web site (http://mnf.csiro.au/Voyages/Investigator-schedules/Plans-and-summaries.aspx). Ship SST at BOM are currently coordinated by HB, but will be handed over to operations on 1 July 2017. From late 2017 ISAR SSTskin will be used for Cal/Val of Himawari-8 SST. All ISAR data will be reprocessed to L2R, when the new code is available. (Update from HB 27 Mar 2018: Nicole Morgan (CSIRO) reprocessed all ISAR data from 26 October 2014 to December 2017 to "GHRSST" L2R NetCDF format using Werenfrid Wimmer's v3.1 Uncertainty Code. Data available at http://www.marlin.csiro.au/geonetwork/srv/eng/search#!bdf91f86-2968-4711-873e-2761383bb207)

Q (??): Good to see the IMOS ship SST is better than ships of opportunity (SOOP). What is the problem with conventional SOOP SST observation?

A: Nick Rayner and Liz Kent, among others, have discussed this before. Bucket SST may be of poor quality/accuracy because of human operator errors. Thermistors may be in unsuitable locations, and therefore need great care to get good data. SBE48, for example, need insulation around them to get good data. As a result, SOOP SST observations may need bias correction and have large random errors.

Q (Craig Donlon): Many papers show issues with SOOP SST. Need to understand lots of issues. For engine intakes, waterline might change by loading. VOSCLIM tries to include this information. In the past, port met officers might have checked instrumentation calibration, but not anymore. Maintenance is very expensive. John Kennedy wrote a review paper on all those issues. Sensor drift can introduce all sorts of issues.

A: Agree.

Q (??): Modern ships should not have some of the historic issues. Some problems are cheap to solve?

A: Funding is low for such activities which makes it hard to get good quality ship SST.

1.3. THE IMPROVEMENT OF ICOADS 3.0 AND ITS APPLICATION TO DAILY OISST – CHUNYING LIU, NOAA/NCEI, USA

Chunying started with ICOADS Release 3.0 overview. Many different input data streams are collated into the International Climate Ocean-Atmosphere Data Set (ICOADS), which forms the observational in situ foundation for the ocean-atmosphere interface and has very large user community. Data available from NCAR and NCEI. Information at http://icoads.noaa.gov. Historical data from the 1662-2014 are merged into ICOADS R3.0. Increased data from 1800 to 1835 and during the WW1. Data format documented online. More information on the Release 3.0 is available in the paper led by Eric Freeman in the Int. J. Clim. (June 2016). She went on to characterize the daily OISST product (documented in paper led by Dick Reynolds, J. Clim., 2007) which blends together satellite AVHRR data with in situ data (buoys and ships) SST and ice data from Sep 1981 – present. AVHRR + AMSR version of the data is also available from 2002 -2011, which additionally includes AMSR-E data in addition to satellite AVHRR. Historical (reprocessed) OISST uses in situ data from ICOADS and real time data from GTS. Currently, ICOADS R2.5 is used, and OISST will be reprocessed soon with ICOADS R3.0, using increased number of in situ observations. From 2000-2016, number of ship and buoy reports in R3.0 is larger by 20% and 10%, respectively, compared with R2.5. Trend in in situ SSTs is slightly reduced from R2.5 to R3.0, but still warming. R2.5 to 3.0 differences are mainly in high gradient regions, Gulf Stream, Kuroshio, and up-welling regions.

Q (Helen Beggs): Good talk. When was R3.0 released? What version of OISST it will go into?

A: R3.0 was released in June 2016. I am not sure when OISST will use R3.0.

Q (Helen Beggs): What ICOADS release is used in iQuam?

A (Sasha Ignatov): Still R2.5, R3.0 is in the works.

Q (Helen Beggs): BoM climate monitoring services also currently use R2.50. Do you ingest data in TRACKOB format?

A: We do not process TRACKOB reports for ICOADS. We use SHIP (FM13).

Q (Sasha Ignatov): What's the difference between the TRACKOB and SHIP formats?

A (Helen Beggs): There are two ASCII formats for ship SST: SHIP (FM13 low frequency, 0.1 degree lat/lon resolution format) and TRACKOB (FM62 high-frequency and 0.01 degree lat/lon resolution format).

Q (Ken Casey): Are ICOADS R3.0 data available in NetCDF, in addition to IMMA?

A: Yes they are. ICOADS files in NetCDF format are available at NCAR in DS548.0: https://rda.ucar.edu/datasets/ds548.0/#access Monthly Summaries NetCDF files access: https://rda.ucar.edu/datasets/ds548.1/#access. Users will need to register on the NCAR site (once) but data is free to download.

SUMMARY OF FLOOR DISCUSSION (DISCUSSION/SUGGESTIONS/ACTION)

- Sasha Ignatov (Lei Guan): Are your validation statistics for VIIRS, HY, FY stratified by day and night?
- Lei Guan: Not yet, but working on it.
- Sasha Ignatov: Should we include radiometer data in iQuam? Do users want that? Currently there are 8 in situ data sources in iQuam. If needed and wanted, we can add.
- Helen Beggs: The issue might be that it is not real time. Is that a problem for iQuam?
- Sasha Ignatov: Is not a problem to include non-real time data. We do process in NRT, but assimilate several delayed mode data (ARGO, ICOADS) so it's not an issue.
- Lei Guan: How often are data updated in iQuam? What release of ICOADS?
- Sasha Ignatov: Twice daily. ICOADS R2.50; R3.0 is being explored. Are IMOS ships in ICOADS?
- Helen Beggs: They are all on the GTS so those that are reported in SHIP (FM13) format should be in ICOADS. However, the IMOS ship SST data streams only reported in TRACKOB (FM62) format will not be in ICOADS.
- Sasha Ignatov: Yes then they should but I am unsure if they are

SHIPBOARD MEASUREMENTS OF SEA SURFACE SKIN TEMPERATURE IN THE NORTHWEST PACIFIC

Lei Guan, Kailin Zhang, Minglun Yang, and Liqin Qu

Department of Marine Technology, College of Information Science and Engineering,
Ocean University of China, 238 Songling Road, Qingdao, 266100, China
Email: leiguan@ouc.edu.cn

1. INTRODUCTION

Sea Surface temperature (SST) is an essential indicator for climate change. High accuracy and stability of the satellite SST products are required for long-term climate data records of global SST [Ohring et al., 2005]. It is important to routinely collect in situ sea surface skin temperature measurements for the evaluation and improvement of satellite SST products. The infrared SST autonomous radiometer (ISAR) is designed as a self-calibrating instrument capable of measuring *in situ* sea surface skin temperature to an accuracy of 0.1 K and operating autonomously without service up to 3 months [Donlon et. al., 2008]. An ISAR made by the University of Southampton, has been deployed on the research vessel Dong Fang Hong II of Ocean University of China (OUC) since 2009. The skin SST measurements have been carried out during 57 cruises, mainly in the northwest Pacific. The first infrared radiometer for measurements of SST (OUCFIRST) made by OUC has a similar self-calibrating system as ISAR. The OUCFIRST has been deployed on the research vessel for testing in several cruises since 2015. Both infrared radiometers participated in the comparison of IR brightness temperature measurements in support of satellite validation at NPL, UK in 2016. The shipboard measurements of skin SST and evaluation of the satellite SST products are presented and discussed.

2. *IN SITU* MEASUREMENTS OF THE SKIN SST

The ISAR was calibrated at National Physical Laboratory, UK, in June 2009, through the Committee on Earth Observation Satellites (CEOS) comparison of Infrared radiometry in support of satellite calibration and validation for measuring SST for studies of climate change [Theocharous et al., 2010] before deploying for the first campaign. The results demonstrate the designed accuracy of the instrument. It has been deployed on the compass deck of R/V Dong Fang Hong II of Ocean University of China, about 13 m above the sea surface since 2009 (See figure 1). A precipitation sensor made by Adolf Thies GmbH & Co. KG, is used to control the shutter of the ISAR [Donlon et. al., 2008]. Two video cameras are deployed, one used to monitor the sea state and the other used to monitor the shutter of the radiometer. Besides the original data logging system of the instrument, a backup data logging system was developed. The backup data are automatically recorded in the flash disks. Figure 2 shows the data logging system in the lab. The ISAR operated in the China Sea for the first cruise in September 2009 and has been deployed on R/V Dong Fang Hong II to collect skin SST measurements for 57 cruises, mainly in the northwest Pacific. Figure 3 is the skin SST measurements by ISAR in a campaign conducted in the Northwest Pacific. The OUCFIRST was made by OUC with similar self-calibration system as ISAR and has been deployed on the same research vessel for testing in several cruises since 2015. A portable blackbody system made by LR TECH Inc. has been used to calibrate the shipboard radiometers before and after each cruise. Both infrared radiometers and the blackbody system participated in the comparison of IR brightness temperature measurements in support of satellite validation at National Physical Laboratory (NPL), UK in 2016. The radiometers also participated in the water surface temperature comparison of radiation thermometers at Wraysbury reservoir in 2016. The results of

the comparisons demonstrate that the shipboard radiometers and the blackbody system meet the requirements of the satellite SST validations.

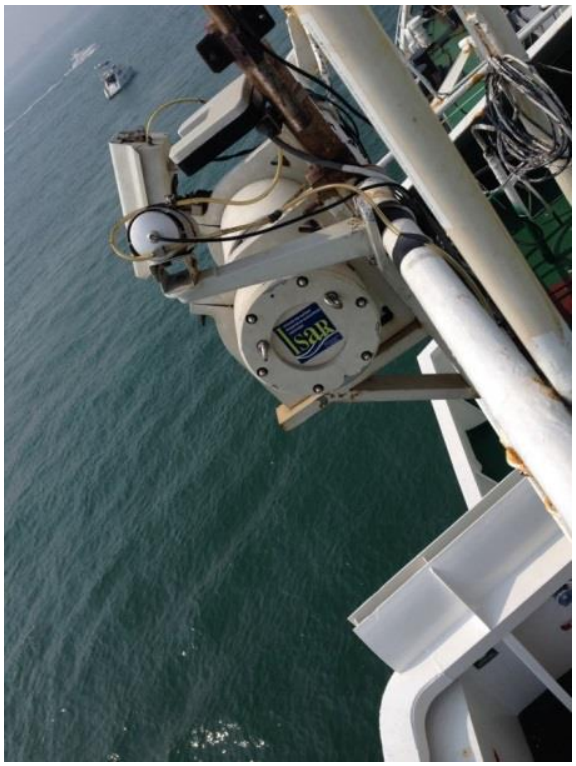

Figure 1. ISAR deployed on R/V Dong Fang Hong II

Figure 2. Data logging system in the lab

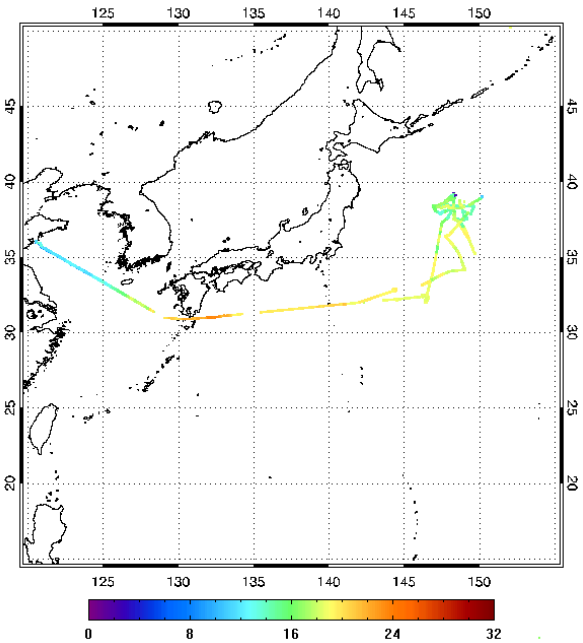

Figure 3. ISAR measurements of skin SST in the northwest Pacific

3. COMPARISON OF THE VIIRS SST PRODUCTS WITH *IN SITU* SKIN SST MEASUREMENTS

The collected ISAR SST measurements are used to evaluate the SST products from the Visible Infrared Imaging Radiometer Suite (VIIRS) onboard the Suomi National Polar-orbiting Partnership (NPP). The NOAA Joint Polar Satellite System (JPSS) Interface Data Processing Segment (IDPS) VIIRS SST products were archived from 2012 to 2017 on NOAA Comprehensive Large Array-data Stewardship System (CLASS) [Petrenko et. al., 2014]. The matchups between JPSS IDPS VIIRS SST products and ISAR skin SST data were generated with the temporal window of 1 hour and spatial window of 0.01º. Preliminary results using the three cruises in the China Seas wwere obtained. The location of the matchups is shown in figure 4. The number of matchups is 475 including the high quality and degraded VIIRS SST data. The bias is 0.14 K and the standard deviation is 0.35 K. For high quality flagged VIIRS SST, the number of matchups is 122. The bias is 0.09 K and the standard deviation is 0.21 K. The evaluation of the higher quality, replacement products, NOAA ACSPO VIIRS SST products is ongoing.

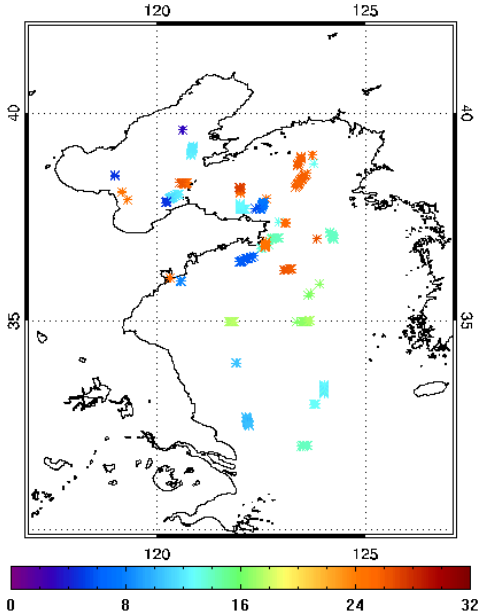

Figure 4. Locations of SST matchups

4. SUMMARY

The ISAR and OUCFIRST have been deployed on R/V Dong Fang Hong II, continually collecting the *in situ* measurements of skin SST in the northwest Pacific. The data are used to evaluate satellite products. Multi-sensor matchups will be generated in the future.

5. REFERENCES

Donlon, C., I. S. Robinson, M. Reynolds, W. Wimmer, G. Fisher, R. Edwards, T. J. Nightingale, An Infrared Sea Surface Temperature Autonomous Radiometer (ISAR) for Deployment aboard Volunteer Observing Ships (VOS). J. Atmos. Oceanic Technol., 25, 93-113, 2008.

Ohring, G., B. Wielicki, R. Spencer, B. Emery, and R. Datla, Satellite Instrument Calibration for Measuring Global Climate Change: Report of a Workshop. Bulletin of the American Meteorological Society, 86, 1303-1313, 2005.

Petrenko, B., A. Ignatov, Y. Kihai, J. Stroup, P. Dash, Evaluation and Selection of SST Regression Algorithms for JPSS VIIRS. J. Geophys. Res., 119, 4580-4599, 2014.

Theocharous, E. E. Usad, N. P. Fox,: CEOS comparison of IR brightness temperature measurements in support of satellite validation. Part I: Laboratory and Ocean surface temperature comparison of radiation thermometers. *NPL Report OP 3*, July 2010.

IMOS SHIP SST FOR SATELLITE SST VALIDATION

Helen Beggs[(1)], Nicole Morgan[(2)] and Janice Sisson[(3)]

(1) Bureau of Meteorology, Melbourne, Australia, Email: helen.beggs@bom.gov.au
(2) CSIRO Oceans and Atmospheres, Hobart, Australia, Email: Nicole.Morgan@csiro.au
(3) Bureau of Meteorology, Melbourne, Australia, Email: janice.sisson@bom.gov.au

ABSTRACT

We report on the Australian Integrated Marine Observing System (IMOS) ship SST data sets – nine years of in situ subsurface "SSTdepth" and two years of ship-based remotely sensed "SSTskin" quality-assured observations from ships of opportunity - and their application for satellite SST validation.

1. SHIP SSTDEPTH

Since 2008, IMOS (http://www.imos.org.au) has enabled accurate, quality controlled (QC'd), in situ SST observations at several meters depth ("SSTdepth") below the surface to be supplied in near real-time from 21 Ships of Opportunity and research vessels in the Australian region. Nine vessels used SeaBird SBE 3 or SBE 38 temperature sensors, located in the water intake, and 12 used SBE 48 sensors positioned against the inside of the ship hull (http://www.seabird.com/). The data are valuable for satellite SST validation as they provide QC'd, in situ observations in coastal regions not sampled by either drifting buoys, moorings or Argo floats, and many of the vessels also provide QC'd meteorological observations, including wind speed. For more information see Beggs et al. (2012), http://imos.org.au/sstsensors.html and http://imos.org.au/airseaflux.html. Information on vessels, sensors and data streams is at http://imos.org.au/facilities/shipsofopportunity/sstsensors/sst-deployments/.

(a) (b)

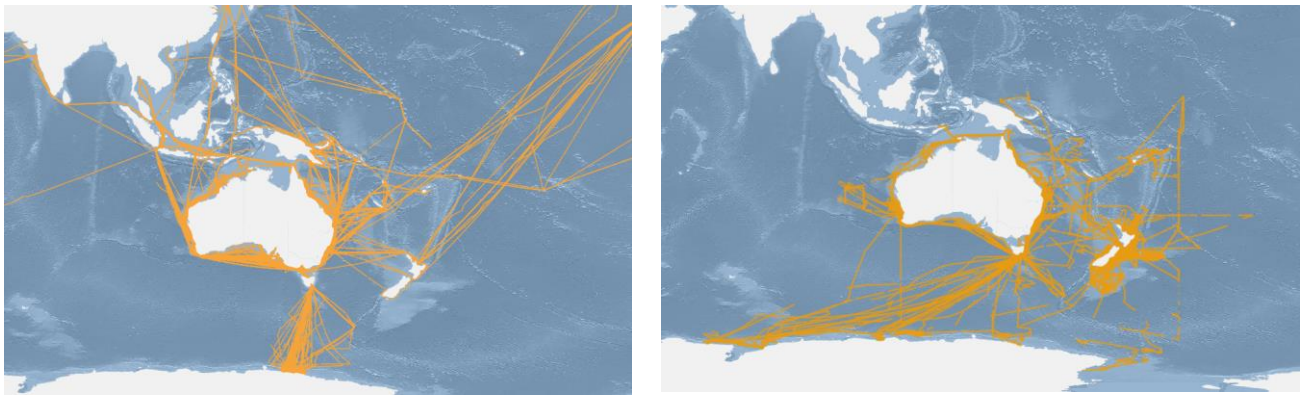

Figure 1: Tracks of the (a) ships of opportunity that contributed SSTdepth data, and (b) research vessels that contributed meteorological, air-sea flux and SSTdepth data to the IMOS Project from January 2008 to June 2017 (accessed from https://portal.aodn.org.au on 29 June 2017).

1.1. Quality Control

The Bureau of Meteorology employs an automated QC method based on the Shipboard Automated Meteorological and Oceanographic System (SAMOS: http://samos.coaps.fsu.edu/html/) for all IMOS ship meteorological and SST measurements. The QC tests in order of application are:

1. Known instrument malfunction (QC flag 'M')
2. Verify existence of time, latitude and longitude for every record (QC flag 'F')
3. Flag data not within physically possible bounds (QC flag 'B')
4. Flag non-sequential and/or duplicate times (QC flag 'C', 'H' or 'T')
5. Flag positions where vessel over land (QC flag 'L')
6. Flag unrealistic vessel speeds (QC flag 'F')
7. Low platform speed test (SST only): Flag data where ship speed is below 2.5 m/s (QC flag 'Q') (Note: does not apply to research vessels VLHJ, VLMJ, VNAA or ZMFR)
8. Climatology test: flag SST observation more than 3°C above/below Bureau's most recent daily foundation SST analysis (either RAMSSA or GAMSSA, Beggs et al., 2011). Different climatology tests are applied to other meteorological variables. (QC flag 'G')
9. Statistical test (1 minute data only): flag step, discontinuity or spike in data (QC flag 'U', 'V', 'X' or 'Y')

Once a flag is changed, it will not be altered further by any subsequent test. The IMOS QC system sets one QC flag for each variable for each time step. All data are retained in the final IMOS netCDF files but until 7th July 2017 only SST data that were flagged as having passed all QC tests (QC flag 'Z') were uploaded to the Global Telecommunications System (GTS) in "Trackob" (FM 62) format (see Section 1.3). After that date, SST data that had failed the climatology test (QC flag 'G') were also uploaded to the GTS, to permit near-coastal SSTs to be included.

1.2. Use in Satellite SST Validation

Comparisons with SST observations from satellites indicate that the IMOS ship SST data streams from the calibrated SBE 48 and SBE 38 sensors provide SSTdepth observations with comparable differences to those available from drifting buoys (Beggs et al., 2012), also demonstrated in Figure 2. The IMOS ship SSTdepth data are used in real-time by the Bureau of Meteorology as an independent data source for validating the IMOS Advanced Very High Radiometer (AVHRR) SSTs from NOAA polar-orbiting environmental satellites (http://imos.org.au/sstdata_validation.html).

(a)

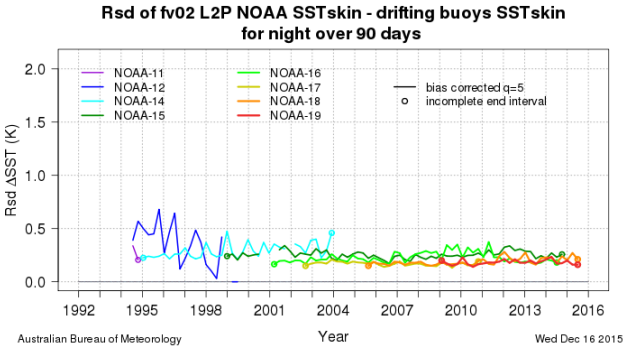

(b)

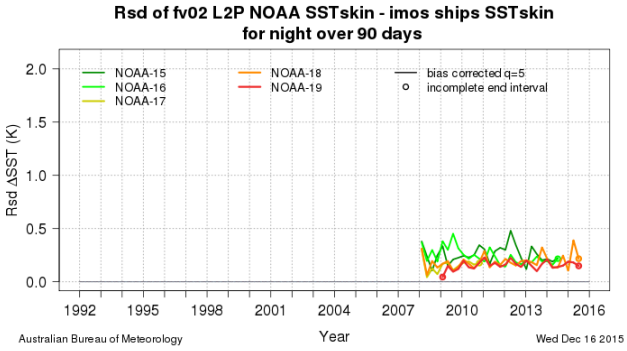

Figure 2: Example plots of robust standard deviation of night-time IMOS "fv02" High Resolution Picture Transmission (HRPT) AVHRR level 2 pre-processed (L2P) SSTskin (from NOAA-11 to NOAA-19) minus (a) drifting buoy SST and (b) IMOS ship SST. The L2P SSTs have been filtered on quality_level 5 and bias-corrected by subtracting sses_bias (see http://imos.org.au/facilities/srs/sstproducts/sstdata0/). The drifting buoy and IMOS ship SSTdepth values have been adjusted to SSTskin by subtracting 0.17°C. Figure accessed from http://opendap.bom.gov.au:8080/thredds/fileServer/abom_imos_ghrsst_archive/v02.0fv02/Validation/web/index.html on 29 June 2017.

1.3. Data Access

The IMOS ship SSTdepth data are available in near real-time from:

(i) GTS in ASCII format as hourly "SHIP" (FM 13) or 1-minute "Trackob" (FM 62) messages;

(ii) NOAA's iQUAM v2 portal (http://www.star.nesdis.noaa.gov/sod/sst/iquam/v2/data.html) in "L2i" netCDF format (platform type = 7); and

(iii) IMOS THREDDS server (http://thredds.aodn.org.au/thredds/catalog/IMOS/SOOP/SOOP-SST/catalog.html and http://thredds.aodn.org.au/thredds/catalog/IMOS/SOOP/SOOP-ASF/catalog.html) in daily IMOS netCDF format files (containing navigation, meteorological and SST data, along with QC flags for each variable).

2. SHIP SSTSKIN

Although the SSTdepth measurements from ships can be used for validation of remotely sensed SST measurements, this application is limited by the thermal stratification of the top few metres of the ocean, particularly in regions of high solar insolation and low winds. In October 2014, an Infra-red Autonomous Radiometer model 5D (ISAR: Donlon et al., 2008; http://www.isar.org.uk/), manufactured by National Oceanography Centre Southampton, was installed on Australia's Marine National Facility, RV Investigator (Figure 3). The ISAR is a self-calibrating instrument measuring in situ ocean temperatures at the same depth as infrared radiometers on satellites ("SSTskin"), using wavelengths of 9.6 to 11.5 µm, accurate to around 0.1°C RMSE (Donlon et al., 2008).

(a) (b)

Figure 3: Photos of the ISAR instrument as installed on RV Investigator, showing (a) view from port-side bridge deck during installation, and (b) view from above at sea.

In order to measure SSTskin accurately from a ship, radiometric measurements of both the sea surface radiance (L_{sea}) and downwelling atmospheric radiance (L_{sky}) must be obtained and the value of seawater emissivity should be known accurately. The ISAR installation configuration used on RV Investigator is shown in Figure 4. The SST Radiometer is mounted on the port bridge wing, approximately 19.593 m above the summer load line. The emissivity is set as constant in the RV Investigator ISAR processing system, as 0.99164, based on a nadir viewing angle, ϑ, of 25° (Werenfrid Wimmer, *pers. com.*, *25 March 2016*, after Niclos et al., 2009). Before and after each cruise, the radiometer is calibrated with reference to a CASOTS II National Oceanographic Centre Southampton manufactured black body, while immersed in a water bath controlled with a reference HART platinum resistance thermometer (http://www.isar.org.uk/calibration).

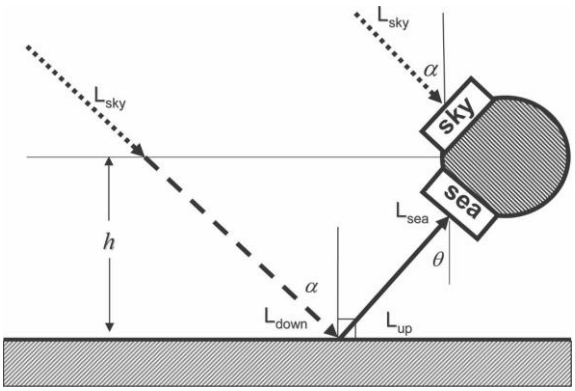

Figure 4: Geometrical set up of the ISAR on RV Investigator (Figure taken from Donlon et al., 2008). In this case the nadir viewing angle, ϑ, is 25° and the height, h, above the ocean surface is typically ~19.6 m.

2.1. Quality Control

The results of the June/July 2016 National Physical Laboratory (NPL) laboratory inter-comparison of the RV Investigator ISAR SST radiometer with a reference blackbody and 34 other ship-borne SST radiometers

(from 12 agencies) were published in Barker-Snook et al. (2016). This report showed that the RV Investigator ("CSIRO") ISAR instrument compared very favourably with other similar radiometers within the SST measuring range (0°C to 45°C), being 0.04 to 0.15°C colder than the NPL reference blackbody. The results of a 5-day June/July 2016 side-by-side inter-comparison of 10 SST radiometers measuring surface temperatures of the Wraysbury Reservoir, UK, were published in Barker-Snook et al. (2017). This report showed that the RV Investigator ("CSIRO") ISAR measured surface water temperatures that were on average 0.189°C colder than the mean water temperatures of the 10 radiometers over the same 5-day period.

Following ISAR calibration after each RV Investigator cruise, the ISAR SSTskin data has been reprocessed using uncertainty code (v2.7.0) supplied by Dr Werenfrid Wimmer (Wimmer and Robinson, 2016). See Section 2.2 for data access. An example of the reprocessed ISAR SSTskin data is shown in Figure 5, along with the total expanded uncertainty for the ISAR radiometric skin SST ("TS2") value, being a combination of random (type A), systematic (type B), instrument and measurement uncertainty (Wimmer and Robinson, 2016). The ISAR expanded uncertainty is an estimate of the SST that differs from its true value by less than the stated uncertainty in 95% of cases, and can be considered as twice the standard deviation. Figure 5 illustrates the close agreement between the reprocessed ISAR SSTskin values (green line) and the SBE 38 SSTdepth values on the vessel, except during periods of diurnal warming of the surface ocean that are associated with low wind speeds (< 6 ms^{-1}) and at least moderate shortwave solar radiation (> 200 Wm^{-2}).

Both real-time and reprocessed ISAR data also undergo the QC procedure described in Section 1.1. Users wishing to study diurnal warming or cold upwelling events, where SSTskin may be more than 3°C above or below the corresponding foundation SST analysis, are advised to ignore the ISAR SST "value_exceeds_threshold" flag (TEMP_2_quality_control = 'G') in the IMOS format files.

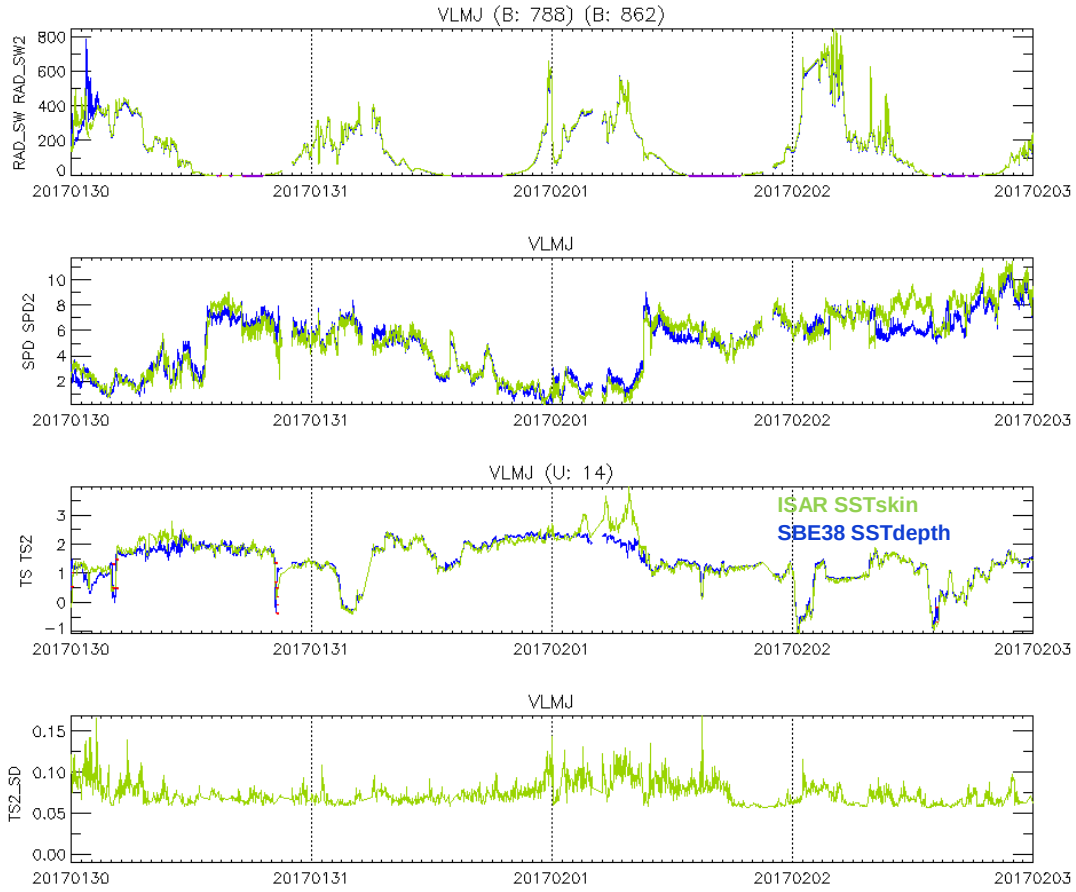

Figure 5: Example time series (from top) of short-wave solar radiation (Wm^{-2}), wind speed (ms^{-1}), SBE 38 SSTdepth (blue) (°C), reprocessed ISAR SSTskin (green) (°C) and ISAR expanded uncertainty (2 x standard deviation) for Antarctic Cruise IN2017_V01 during 30th January to 3rd February 2017.

2.2. Data Access

Real-time ISAR data has been available from the IMOS THREDDS server (http://thredds.aodn.org.au/thredds/catalog/IMOS/SOOP/SOOP-ASF/VLMJ_Investigator/meteorological_sst_observations/catalog.html) since 26 March 2016. As the ISAR calibration may vary throughout a deployment due to contamination of the ISAR optical system, the real-time data are less useful for satellite SST validation than the reprocessed data described in section 2.1. Figure 6 shows the locations of the real-time ISAR SST data for the period 24th March 2016 to 16 June 2017.

The reprocessed ISAR data (back to October 2014) are available in ASCII format from RV Investigator's ocean data archive (http://www.marlin.csiro.au/geonetwork/srv/eng/search#fast=index&from=1&to=10&any_OR_geokeyword=ISAR&hitsperpage=10). The reprocessed ISAR data are also available in IMOS netCDF files (containing navigation, meteorological and SST data, along with QC flags for each variable) for the period 31 August 2016 to 5 May 2017 from http://thredds.aodn.org.au/thredds/catalog/IMOS/SOOP/SOOP-ASF/VLMJ_Investigator/meteorological_sst_observations/2016/ISAR-QC/catalog.html and http://thredds.aodn.org.au/thredds/catalog/IMOS/SOOP/SOOP-ASF/VLMJ_Investigator/meteorological_sst_observations/2017/ISAR-QC/catalog.html. Additional data

files back to March 2015 will be posted to these THREDDS directories in future. An example of some of the variables available from the reprocessed IMOS ISAR data set, useful for satellite SST validation, is shown in Figure 5. Other variables not shown are air temperature, humidity, air pressure, precipitation, sea surface salinity, long-wave radiation, photosynthetically active radiation, ship speed, latitude, longitude and heading.

Following release of updated ISAR processing code, we intend to reprocess the RV Investigator ISAR data to netCDF "L2r" format to contribute to the Shipborne Radiometer Network (http://www.shipborne-radiometer.org/).

On 14 March 2017 Ifremer and EUMETSAT ingested the reprocessed RV Investigator ISAR SSTskin data for the period 12 July to 15 November 2016 into the Sentinel-3 SLSTR SST Matchup Dataset v4.1 (http://www.ifremer.fr/cerweb/sentinel-3/mdb-slstr).

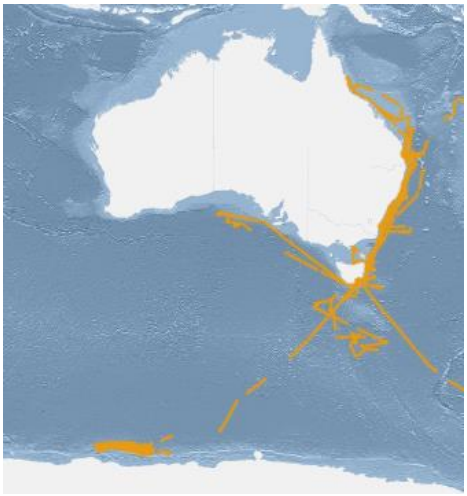

Figure 6: Tracks of the RV Investigator (call sign: VLMJ) cruises that provided real-time ISAR SSTskin, SBE 38 SSTdepth and other meteorological data to the IMOS THREDDS server for the period 24th March 2016 to 5th May 2017 (accessed from https://portal.aodn.org.au on 30th June 2017).

3. PLANS FOR 2017/2018

- From 1st July 2017, Joel Cabrie (Marine Operations Manager, BoM) will take over leading the IMOS Ship SST Sensors Sub-facility from Helen Beggs.
- As at 30th June 2017, nine vessels provide near real-time, QC'd, SSTdepth data to the IMOS project – PV Spirit of Tasmania II, MV Stadacona, PV SeaFlyte, RTM Wakmatha, RSV Aurora Australis, RV Investigator, RV Tangaroa, RV Cape Ferguson and RV Solander. Additional ships are planned to be instrumented with SBE 48 sensors over the coming year.
- Future RV Investigator cruises will provide ISAR SSTskin data, provided the ISAR is operating on the voyage. Cruise plans (including voyage tracks) can be found at http://mnf.csiro.au/Voyages/Investigator-schedules/Plans-and-summaries.aspx .
- Minglun Yang (OUC PhD student) will participate in RV Investigator cruise IN2017_T01 from Hobart to Brisbane in April 2018, to estimate how the different sky view zenith or azimuth

direction, surface roughness, time difference between sea and sky view measurements, or ship movement affect the accuracy of ISAR retrieved SSTskin.

- The IMOS ISAR data sets will be used to validate the BoM Himawari-8 SST data.
- All RV Investigator ISAR data (October 2014 to present) will be reprocessed to "L2r" netCDF format for upload to the Shipborne Radiometry Network database (http://www.shipborne-radiometer.org).

4. ACKNOWLEDGEMENTS

The authors would like to thank Dr Werenfrid Wimmer (University of Southampton) for advice regarding the RV Investigator ISAR and for providing his ISAR processing software. We are very grateful to Martin Buggeln (Lothlorien Electronics), John Horvath (BoM) and Alan Thomas (ex-BoM) for the design and installation of the IMOS hull temperature sensor system.

5. REFERENCES

Barker-Snook, I., E. Theocharous and N. P. Fox, 2016: 2016 comparison of IR brightness temperature measurements in support of satellite validation. Part 2: Laboratory comparison of radiation thermometers, NPL Report ENV 14, National Physics Laboratory, London, UK. 134 pp.

Barker-Snook, I., E. Theocharous and N. P. Fox (2017) 2016 comparison of IR brightness temperature measurements in support of satellite validation. Part 3: Water surface temperature comparison of radiation thermometers, NPL Report ENV 15, National Physics Laboratory, London, UK. 45 pp.

Beggs H., A. Zhong, G. Warren, O. Alves, G. Brassington and T. Pugh (2011) RAMSSA – An Operational, High-Resolution, Multi-Sensor Sea Surface Temperature Analysis over the Australian Region, *Australian Meteorological and Oceanographic Journal*, 61, 1-22. http://www.bom.gov.au/jshess/papers.php?year=2011

Beggs H., R. Verein, G. Paltoglou, H. Kippo and M. Underwood, 2012: Enhancing ship of opportunity sea surface temperature observations in the Australian region. *Journal of Operational Oceanography* (ISSN: 1755-8778), 5, 59-73. http://imos.org.au/fileadmin/user_upload/shared/SOOP/SST_2016/beggs_etal2012.pdf

Donlon, C., I. Robinson, M. Reynolds, W. Wimmer, G. Fisher, R. Edwards, and T. Nightingale, 2008: An infrared sea surface temperature autonomous radiometer (isar) for deployment aboard volunteer observing ships (vos). J. Atmos. Oceanic Technol., 25, 93–113.

Niclos, R. I., Caselles, V., Valor, E. and Sanchez, C. C. J. M., 2009: A simple equation for determining sea surface emissivity in the 3-15 m region. *International Journal of Remote Sensing*, **30**, Number 6, 1603–1619.

Wimmer, W., and I. Robinson, 2016: The ISAR instrument uncertainty model. J. Atmos. Oceanic Technol. doi:10.1175/JTECH-D-16-0096.1. http://journals.ametsoc.org/doi/abs/10.1175/JTECH-D-16-0096.1

THE IMPROVEMENT OF ICOADS3.0 AND ITS APPLICATION TO DOISST

Chunying Liu[1], William Angel[2], Eric Freeman[1], Boyin Huang[2], Huai-min Zhang[2]

ERT, Inc. 14401 Sweitzer Lane Suite 300 Laurel, MD 20707 USA chunying.liu@noaa.gov
NOAA National Centers for Environmental Information (NCEI), Asheville, NC 28801 USA

ABSTRACT

The International Comprehensive Ocean-Atmosphere Data Set (ICOADS) Release 3.0 is the newest release with a significant increase in the number of marine reports and area of ocean coverage especially in the recent years.

The 1/4° NOAA Daily Optimally Interpolated SST (DOISST), which covers the period from 1981 to present, is based on in situ, satellite, and ice data. In the current version of DOISST the in situ data is ICOADS Release 2.5.

The DOISST depends critically on the amount of marine observations and their spatial distribution. This study exhibits the improvement of ICOADS3.0 over ICOADS2.5 and explores its potential contribution to the improvement of DOISST, such as increasing coverage and decreasing uncertainty.

The metadata information in ICOADS3.0 allows us to separate the in situ marine observations by different observing systems, including the broad-scale global array of temperature/salinity profiling floats, known as Argos and the tropical in situ mooring arrays (TAO). This enables us to assess the impact of different types of in situ observations such as Argos and TAO to DOISST in the global and tropical Pacific oceans. Preliminary study shows that the combined impact of buoy and Argo observations on the global average SST is relatively large. The Southern Hemisphere SST is more affected by individual Argo or buoy observations. The impact of observations from the Tropical Atmosphere/Ocean array (TAO) on DOISST is small, because the observations from ships, drifting buoys, and Argo floats have overwhelmed the TAO observations.

PLENARY CLOSING SESSION

MEDSPIRATION : FROM DEMONSTRATION TO OPERATION, HISTORY AND LEGACY

Jean-François Piollé[(1)], Emmanuelle Autret[(2)], Olivier Arino[(3)], Craig Donlon[(4)], Ian Robinson, Pierre Leborgne, Jean Tournadre, Dave Poulter, Bruno Buonjurno-Nardelli, Steinar Eastwood, Gérard Legendre, Jacques Stum, Gilles Larnicol, Cédric Prevost, Romain De Joux, et al.

(1) Ifremer, Plouzané, France, Email: jfpiolle@ifremer.fr
(2) Ifremer, Plouzané, France, Email: eautret@ifremer.fr
(3) ESA/ESRIN, Frascati, Italy, Email: olivier.arino@esa.int
(4) ESA/ESTEC, Noordwijk, Netherlands, Email: craig.donlon@esa.int

1. HISTORY

1.1. Project initial ambitions and objectives

Medspiration was ESA/Data User Element funded call launched in 2004 with multiple goals.

Medspiration initiative took place in the early stages of GHRSST-PP (Global High Resolution Sea Surface Temperature Pilot Project), itself spawned by GODAE, whose main objective was to build a network of providers for high quality sea surface temperature products in a homogeneous way, following consistent practices and specifications. Medspiration was meant to implement the European component to this framework which at this stage was still a conceptual view.

A secondary objective was also to enhance the uptake of Envisat AATSR data by the user community. Due to complex format and content, the usage of AATSR was not yet up to his reputation as a high quality reference sensor.

The third objective was to take advantage of the growing number of sea surface temperature measuring instruments with increasing operationality and timeliness, to define and implement new multi-sensor products with higher temporal and spatial resolution.

1.2. 2004-2006 : implementation and demonstration

The Medspiration project was kicked off in 2004 with a multi-partner team including:

- the University of Southampton (Ian Robinson), as project leader, with the support of Vega
- Meteo-France and Ifremer implementing the main infrastructure and production system
- CLS providing the initial software for multi-sensor merging
- associated parters such as CNR and MetNo as representative of user community assessing the system and its products

The team conceived from requirement baseline to implementation in 7 months an automated real-time system producing and delivering to the user community :

- L2P (swath) global products for a wide range of European and US sensors: AATSR, AVHRR on NOAA series, GOES and MSG series

- a L4 multi-sensor product over the Mediterranean sea
- match-up databases for each sensor ingested in the system, using the in situ data from GTS through Coriolis system

Main achievements:

- first implemented and operated node of GHRSST system, with the first initial set of L2P products produced and available within a less than 12 hours latency
- complete development of a real-time production platform in about 6-months at Ifremer, still used today
- extension of Coriolis scope to ocean surface measurements from ships, drifters and moored buoys
- first multi-sensor high resolution (2km) merged product readily produced and available in less than 24 hours every day, initially over Mediterranean Sea with the later addition of North-Western shelves

1.3. 2007- 2012 : Extension and transition to operational services

The effort in the following years was focused on two aspects:

1) transitioning the well acknowledged Medspiration products to more sustained and operational services
2) implementing specific products for well identified research projects with no operational context or framework that could justify to be implemented in aforementioned operational contexts

The first Medspiration phase having successfully demonstrated the benefit of a coordinated system such as GHRSST, with a growing number of users and the progressive integration of its products and services into operational systems (e.g.: OSTIA analysis at UK MetOffice), it was necessary to sustain these services into more long-term and operational contexts. In the case of Medspiration it was achieved in three ways:

- production of single sensor L2 products (GHRSST L2P) by Eumetsat funded Ocean & Sea-Ice Satellite Application Facility (OSI SAF), with the same initial partners as in Medspiration: Meteo-France/CMS for the production and Ifremer for the dissemination and accessible
- production of multi-sensor L4 products in the context of operational oceanography projects (Mersea, then MyOcean, MyOcean-2 and now CMEMS). The Medspiration North Western Shelves product generated at Ifremer was directly moved to these new contexts whereas the Medspiration product was now covered by CNR using a similar methodology. More importantly new high resolution products (L3 and L4) were implemented in order to cover new areas and needs (Baltic, Black sea, Arctic, Global) and the merging methodologies were improved, in particular thanks to the availability of Medspiration L2P for AATSR now widely acknowledge as a reference sensor that could be used for cross sensor calibration.
- Support by ESA in the context of a Medspiration extension of AATSR NRT production (the follow-on – SLSTR – would by natively produced by the ground segment) until the end of its life time

Last, new regional high resolution products were occasionally produced for identified projects limited in time, for which there was no possible operational framework or no justification for. This included for instance:

- high resolution multi-sensor daily analysis over Coco islands and Galapagos, for a ESA supported project on hammerhead shark monitoring
- high resolution multi-sensor daily analysis over Greenland

In that perspective, Medspiration therefore also continued to complement operational services by ensuring a link toward more research oriented applications and usages with experimental or short-lived products for specific application requirements.

Main achievements:

- successful transition to European operational frameworks
- follow-on of Medspiration built team as a core group in operational projects keeping on with continuous and shared improvements of products and methodologies
- AATSR established as reference sensor for multi-sensor calibration, thanks to NRT availability of Medspiration L2P
- support to identified end-user projects

1.4. 2012-2016 : Reaching new user communities

The last incarnation of Medspiration project, "Medspiration Evolution", was completely disconnected from any operational activities (now taken over by dedicated European operational services) but instead dedicated to reaching to new user communities and developing new applications, collecting feedback and identifying shortcomings of existing products and services.

Main activities included:

- reaching out Mediterranean user communities through regional projects like PIM (Small and Medium islands of Mediterranean Sea) or scientific networking
- investigating climatological aspects from long Medspiration time series (Mediterranean Sea warming, Nicolas Reul)
- delivering new high resolution products for specific activities : South Africa (Agulha current area, cooperation with Cape Town University + GlobCurrent project), North-East Brazil (for SMOS), Great Barrier Reef (coral bleaching)
- investigating new multi-sensor methodologies for improved gradient and front restitution in cloud-free L4 products
- investigating the possibility to generate long climatological time series and the required effort, data and methodologies
- developing tools for outreach easier visualization

Main achievements:

- significant amount of connections with new user and applications allowing to draw lessons on existing SST products and way forward

1.5. Heritage

Medspiration project left a major heritage as many of services, products and tools set up for the project are still existing or directly inherited from this initial demonstration:

- The real-time processing platform set-up at Ifremer/Cersat, based on different subsystems for job scheduling, data and execution flow monitoring, and specifically implemented for Medspiration project is still the backbone of Cersat platform today and it has been the core element to a long string of projects thanks to its generic and multi purpose design : GlobWave, GlobCurrent, GHRSST, OSI SAF, Mersea, MyOcean and Copernicus CMEMS or upcoming CFOSAT/IWWOC mission center. Medspiration has been a turning point in Ifremer/Cersat history, by switching fro manual operations to an automated real-time system.
- Medspiration brought together a team of experts and engineers from different organizations that are still collaborating with each other as of today. The products and services moved to OSI SAF or CMEMS frameworks still rely on the on the same logic and methodologies as developed in Medspiration, with subsequent improvements developed and shared among the same team. It is fair to say that it structured a European group for operational sea surface temperature.
- The delivery of Medspiration products and follow-on has been sustained until today through new and more operational framework, ensuring continuity now and in the future
- tools developed for Medspiration such as the HR-DDS (High Resolution Diagnostic Dataset) and the MDB (Match-up database) were the direct matrix from which systems like felyx (hrdds.ifremer.fr) are now inherited and support the cal/val of existing missions such as Sentinel-3. They have been designed and implemented by the same teams brought together in Medspiration, based on this experience.

2. SELECTION OF USER CASES AND APPLICATIONS

This section presents the user feedback collection. This collection has been focused on the L4 and L3 products generated by the ODYSSEA system. User feedback was collected through various ways:

- direct discussion with end users in meetings and projects
- email exchanges with a few users
- survey of publications

This user feedback collection showed that Medspiration products are used in various topics such as studies related to marine ecology, ocean dynamics and ocean and atmosphere interactions.

The products have been used in many publications in various journals such as *Journal of Physical Oceanography, Deep Sea Research Part II, Remote sensing of Environment, Continental Shelf Research, Journal of Atmospheric and Oceanic Technology, Quarterly Journal of the Royal Meteorological Society, Geophysical Research Letters, Ocean Modelling, Global change biology, Journal Of Biogeography, Biogeosciences, International Journal of Climatology.*

They have been used in several PhD or MSc thesis as well.

It is worth to note that even though most of the products have been available since 2006, most of the research activities were published within 2012-2017.

The list of publications collected up to now is given in the last part of the section. The following paragraphs aim to highlight some studies using the Medspiration data.

2.1. Medspiration products and studies related to marine ecology

This is one of the main applications using the Medspiration data, with publications, exchanges with end-users by emails or during a research stay. In this domain, the global or the regional products are used for a better understanding, modeling or characterization of migrations, habitats and recruitments of various species. These studies focuses either on particular events, for instance during an upwelling events, or in the frame of the global change.

For example, *Trindade et al, 2015* focus on the cross-shore transport of barnacle larvae on the southwestern Iberian coast in a daily varying upwelling regime. They combine numerical simulations and observations (Figure 1 extracted from the paper shows different upwelling conditions from Medspiration products) to better understand the physical mechanisms that may promote larval onshore transport. Figure 2 shows a picture of the barnacle larvae.

Another example is the study from *Lambert et al., 2016, PartI and Part II*, investigating how ocean seasonality drives habitat preferences of highly mobile top predators in the north-western Mediterranean Sea. The L4 SSTs (in terms of mean, variance and gradient) are used as environmental predictors in Generalized Additive Models (GAM) for habitats modelling for four groups of cetaceans such as striped dolphins (Figure 3) or fin whales and three groups of seabirds such as storm petrels (Figure 4) and Cory's Shearwaters.

Other works dealing with habitats modelling using SSTs from Medspiration are presented in *Racine, 2015, Vieira, 2010 and Virgili et al., 2014*.

Woillez at al, 2016 also used Medspiration SSTs in a study proposing a HMM-based model to geolocate pelagic fish from high-resolution individual temperature and depth histories.

Habitats modelling or migrations are also studied in a global change context. For example, *Thomas et al., 2016*, investigated how global change relates to the invasion of European coasts by non-native marine invertebrate, the Pacific oyster *Crassostrea gigas. MacKenzie et al, 2014* shows that a cascade of warming impacts brings bluefin tuna to Greenland waters. *Auber et al, 2017* investigated the decline of cold-water fish species in the Bay of Somme in response to ocean warming.

This topic also included 3 two-month research stays in the Laboratoire d'Océanographie Physique et Spatiale, Ifremer, in 2016. Two undergraduate students from the University of Fuerzas Armadas, Sangolqui, Ecuator, worked on the SST and chlorophyll spatio-temporal variability in the Galapagos Marine Protected Area. A PhD student from the University of Vigo visited us during 2 months. The goal of her thesis is to study the temporal and spatial distribution of several cetacean species in the Azores Archipelago sighed from opportunistic whale watching platforms and to link their distribution with environmental variables (SST, Chl, …). In this on-going work, SSTs from Medspiration has been used in terms of mean, variance, gradient and distance to fronts, as predictors in Generalized Additive Models.

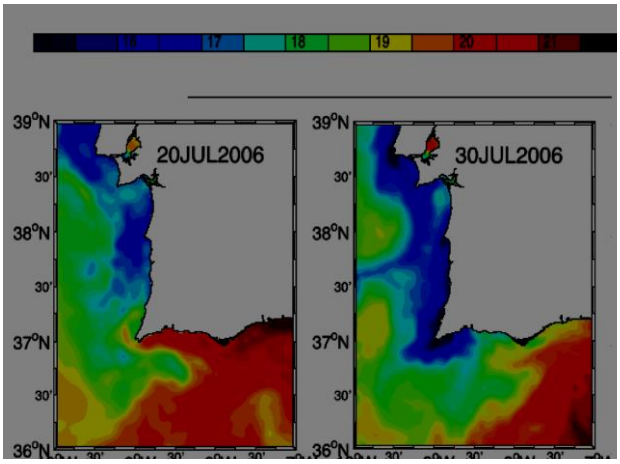

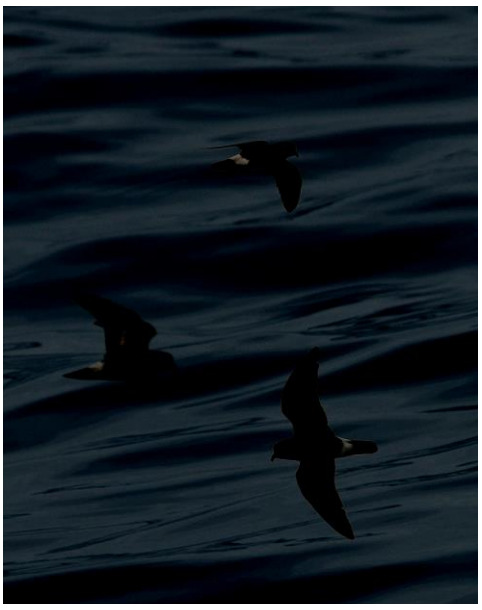

2.2. Medspiration products and studies related to ocean dynamics

Medspiration products are used in several studies related to ocean dynamics or ocean and atmosphere interactions. For example, a study related to submesoscale cyclones in the Aghulas Current (AC) is presented in Krug et al., 2017. In this study, Medspiration SSTs have been used to during the deployment of several gliders. Moreover, their analysis of the AC frontal variability using ODYSSEA SST observations has confirmed the increase in the meandering of the AC front south of 34°S as noted in a previous work. Figure 5 shows some plots extracted from the publication. This figure presents the positions of the AC front estimated from ODYSSEA.

Medspiration SSTs are also used in *Guihou et al., 2013* presenting a case study of the mesoscale dynamics in the North-Western Mediterranean Sea combining data and model (Figure 6). Another example is the study presented in *Caniaux et al., 2017*. The authors propose an inverse method to derive fluxes from the

closure of oceanic heat and water budgets. The method is applied to the north-western Mediterranean Sea. In *Nardelli et al., 2012*, a novel approach for high resolution mapping of 3-D mesoscale dynamics from observations is proposed. The method uses the ODYSSEA SSTs as input. The authors also used the Medspiration products in Nardelli et al, 2013, Nardelli et al., 2012b and in Droghei et al., 2016. Other publications are listed in the next paragraph.

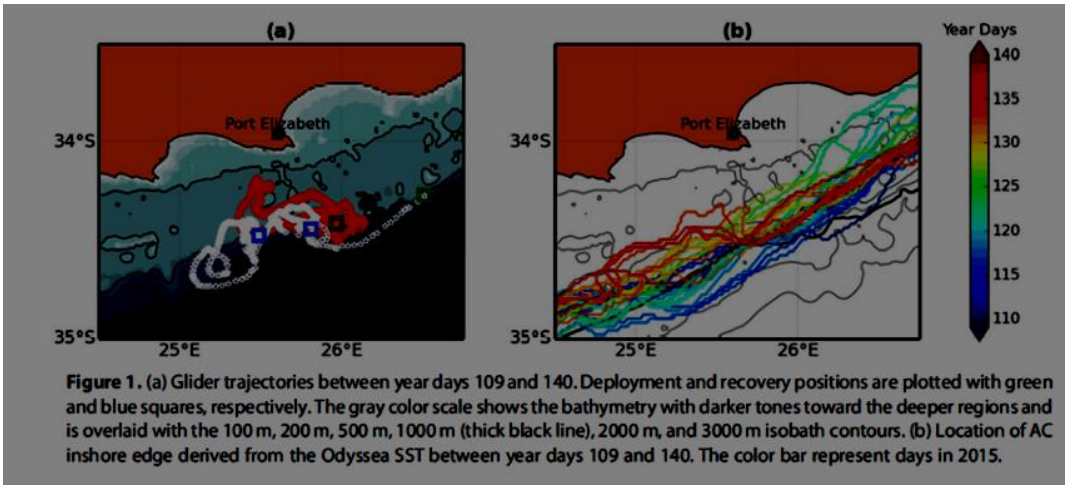

Figure 5: Figure extracted from Krug et al., 2017.

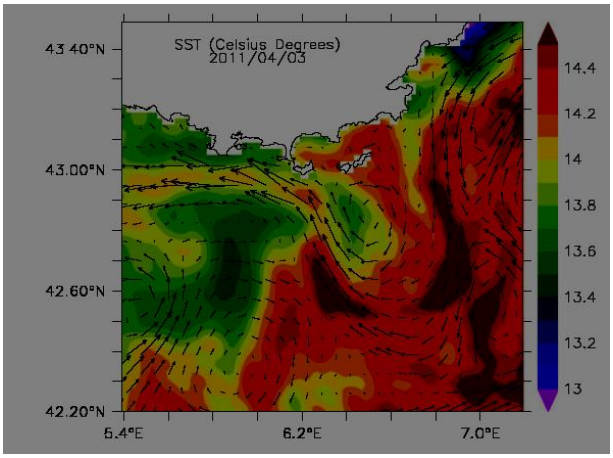

Figure 6: Figure extracted from Guihou et al., 2013: "SST in degree Celsius (L4 product Medspiration project). GLAZUR64-simulated surface velocities for the corresponding dar are superimposed".

3. LESSONS LEARNT

3.1. Product usage

Medspiration registered about 250 users, and tracked down more than 50 publications using Medspiration products or refering to Medspiration as a system implementation model.

However:

- it proved difficult to track down the data usage and citation as they are rarely explicitly cited unlike publications. DOIs may help to improve citation and should be minted for each product. Having

publications associated with each dataset creation would also improve very likely the data traceability, which we did not do in Medspiration.

- The benefit in terms of publication come several years after demonstration phase and reaching out user community takes time, usually beyond 2 year demonstration phase : in our case, it is in particular related to the fact that Medspiration delivered real-time products and it took years to build a significant time series : **the vast majority of users request long time series,** wether it is to investigate a particular situation some day in the past or for temporal analysis.
- Reaching out new user communities (unfamiliar with satellite data for instance) require pro-active support (mini project, use case, ...) which was only implemented at a later stage in Medspiration

The level 2 products (L2P) are still an issue for a lot of users because of their complexity of use:

- most user prefer periodic level 4 cloud-free products
- this can be an issue in terms of usage as users see these level 4 products as the same as level 2 but just easier to use whereas they are strong shortcomings in terms of definition (average instead of direct observation), resolution (the grid resolution is not the true resolution because of the interpolation methods used), gap filling issues (interpolation, use of climatology to fill in cloud covered areas)
- for any product, users request both long time series, updated frequently though very few users request any real-time

Lastly, particular effort must be paid to data display through web tools for simple visualization or more advance data assessment, either as a work tool (some user mostly need to look at images, not necessarily at the numerical values) or to build confidence.

3.2. Structuring communities

Medspiration kicked off GHRSST system, by implementing the European component of this system.

We believe such projects greatly help in structuring the data producer and expert community by bringing the experts together, committed to a real practical achievement, and building up team cooperation that will last beyond the project frame. This is what happened in Medspiration where the team set up for the project has kept the same core along the subsequent operational frameworks, still working together and improving the methodologies and tools set up during the early Medspiration era.

3.3. Innovation

While the operational frameworks that took over Medspiration helped avoiding the team to disband and sustaining the effort, they tend to favor consistency and continuity over innovative approaches.

Demonstration projects are needed and absolutely complementary to operational projects by nursing improvement and innovation, that can be later transferred to more operational frameworks if they prove successful.

These demonstration “companion” frameworks are fundamental to complement operation frameworks.

4. LIST OF PUBLICATIONS USING THE L4 OR L3 ODYSSEA/MEDSPIRATION PRODUCTS

Allou, A., Forget, P., & Devenon, J. L. (2010). Submesoscale vortex structures at the entrance of the Gulf of Lions in the Northwestern Mediterranean Sea. *Continental Shelf Research*, *30*(7), 724-732.

Alvera-Azcárate, A., Sirjacobs, D., Barth, A., & Beckers, J. M. (2012). Outlier detection in satellite data using spatial coherence. *Remote Sensing of Environment, 119*, 84-91.

Auber, A., Gohin, F., Goascoz, N., & Schlaich, I. (2017). Decline of cold-water fish species in the Bay of Somme (English Channel, France) in response to ocean warming. *Estuarine, Coastal and Shelf Science*.

Assassi, C. (2015). *Interannual variability and analysis of geostrophic turbulence in the Bay of Biscay from simulations* (PhD thesis, Université de Bretagne Occidentale (UBO)).

Autret, E. (2014). Analyse de champs de température de surface de la mer à partir d'observations satellite multi-sources, Thèse de Doctorat.

Beggs, H., Zhong, A., Warren, G., Alves, O., Brassington, G., & Pugh, T. (2011). RAMSSA—An operational, high-resolution, Regional Australian Multi-Sensor Sea surface temperature Analysis over the Australian region. *Australian Meteorological and Oceanographic Journal*, 61(1), 1.

Berger, H., Dumas, F., Petton, S., & Lazure, P. (2014). Evaluation of the hydrology and dynamics of the operational Mars3d configuration of the bay of Biscay. *Mercator Ocean Newsletter*, *49*.

Bouffard, J., Roblou, L., Birol, F., Pascual, A., Fenoglio-Marc, L., Cancet, M., ... & Menard, Y. (2011). Introduction and assessment of improved coastal altimetry strategies: Case study over the northwestern Mediterranean Sea. In *Coastal altimetry* (pp. 297-330). Springer Berlin Heidelberg.

Boussidi, B., Fablet, R., Autret, E., & Chapron, B. (2013). Accroissement stochastique de la résolution spatiale des traceurs géophysiques de l'océan: application aux observations satellitaires de la température de surface de l'océan. *Revue française de photogrammétrie et de télédétection*, (202), 66-78.

Buarque, S. R., Crosnier, L., Landes, V., Soulat, F., & Drévillon, M. L4 sea surface temperature applications at mercator ocean.

Cardellach, E., & Oliveras, S. (2016). Assessment of a potential reflection flag product, IEEE Spain.

Caniaux, G., Prieur, L., Giordani, H., & Redelsperger, J. L. (2017). An inverse method to derive surface fluxes from the closure of oceanic heat and water budgets: Application to the north western Mediterranean Sea. *Journal of Geophysical Research: Oceans*.

Cavagna, A. J., Dehairs, F., Bouillon, S., Woule-Ebongué, V., Planchon, F., Delille, B., & Bouloubassi, I. (2013). Water column distribution and carbon isotopic signal of cholesterol, brassicasterol and particulate organic carbon in the Atlantic sector of the Southern Ocean. *Biogeosciences*, *10*, 2787-2801.

Dash, P., Ignatov, A., Martin, M., Donlon, C., Brasnett, B., Reynolds, R. W., ... & Grumbine, R. (2012). Group for High Resolution Sea Surface Temperature (GHRSST) analysis fields inter-comparisons—Part 2: Near real time web-based level 4 SST Quality Monitor (L4-SQUAM). *Deep Sea Research Part II: Topical Studies in Oceanography*, *77*, 31-43.

Desportes, C., Drévillon, M., Régnier, C., Greiner, E., Benkiran, M., Verbrugge, N., ... & Lellouche, J. M. (2011). QuO Va Dis? Quarterly Ocean Validation Display# 3.

Droghei, R., Nardelli, B. B., & Santoleri, R. (2016). Combining In Situ and Satellite Observations to Retrieve Salinity and Density at the Ocean Surface. *Journal of Atmospheric and Oceanic Technology*, *33*(6), 1211-1223.

Fablet, R., & Rousseau, F. (2016). Joint Interpolation of Multisensor Sea Surface Temperature Fields Using Nonlocal and Statistical Priors. *IEEE Journal of Selected Topics in Applied Earth Observations and Remote Sensing*, *9*(6), 2665-2675.

Guihou, K., Marmain, J., Ourmières, Y., Molcard, A., Zakardjian, B., & Forget, P. (2013). A case study of the mesoscale dynamics in the North-Western Mediterranean Sea: a combined data–model approach. *Ocean Dynamics*, *63*(7), 793-808.

Hood, R. R., Bange, H. W., Beal, L., Beckley, L. E., Burkill, P., Cowie, G. L., ... & Honda, M. the second international indian ocean expedition (IIOE-2).

Johannessen, J. A., Chapron, B., Collard, F., & Backeberg, B. (2014). Use of SAR data to monitor the Greater Agulhas Current. In *Remote Sensing of the African Seas* (pp. 251-262). Springer Netherlands.

Koseki, S., Koh, T. Y., & Teo, C. K. (2013). Effects of the cold tongue in the South China Sea on the monsoon, diurnal cycle and rainfall in the Maritime Continent. *Quarterly Journal of the Royal Meteorological Society*, *139*(675), 1566-1582.

Krug, M., Swart, S., & Gula, J. (2017). Submesoscale cyclones in the Agulhas Current. *Geophysical Research Letters*.

Lambert, C., Laran, S., David, L., *et al.* How does ocean seasonality drive habitat preferences of highly mobile top predators? Part I: The north-western Mediterranean Sea. *Deep Sea Research Part II: Topical Studies in Oceanography*, 2016.

Lambert, C., Pettex, E., Dorémus, G., Laran, S., Stéphan, E., Van Canneyt, O., & Ridoux, V. (2016). How does ocean seasonality drive habitat preferences of highly mobile top predators? Part II: The eastern North-Atlantic. *Deep Sea Research Part II: Topical Studies in Oceanography*.

Lampert, L. (2015). Etude sur la température de surface de la mer des eaux guyanaises dans le contexte DCE.

Lekouara, M. (2013). *Exploring frontogenesis processes in new satellite sea surface temperature data sets* (Doctoral dissertation, University of Southampton).

L'Hévéder, B., Speich, S., Ragueneau, O., Gohin, F., & Bryère, P. (2016). Observed and projected sea surface temperature seasonal changes in the Western English Channel from satellite data and CMIP5 multi-model ensemble. *International Journal of Climatology*.

MacKenzie, B. R., Payne, M. R., Boje, J., Høyer, J. L., & Siegstad, H. (2014). A cascade of warming impacts brings bluefin tuna to Greenland waters. *Global change biology*, *20*(8), 2484-2491.

Mather, P. M., & Koch, M. (2011). *Computer processing of remotely-sensed images: an introduction*. John Wiley & Sons.

Martin, M., Dash, P., Ignatov, A., Banzon, V., Beggs, H., Brasnett, B., ... & Grumbine, R. (2012). Group for High Resolution Sea Surface temperature (GHRSST) analysis fields inter-comparisons. Part 1: A GHRSST multi-product ensemble (GMPE). *Deep Sea Research Part II: Topical Studies in Oceanography*, *77*, 21-30.

Maturi, E., Harris, A., & Sapper, J. A New Ultra High Resolution Sea Surface Temperature Analyses.

Morris, T. C. (2015). Fish parasites as bio-indicators of heavy metals in two South African embayments (Doctoral dissertation, University of Cape Town).

Nardelli, B. B., Guinehut, S., Pascual, A., Drillet, Y., Ruiz, S., & Mulet, S. (2012). Towards high resolution mapping of 3-D mesoscale dynamics from observations. *Ocean Science*, *8*(5), 885.

Nardelli, B. B. (2012). A novel approach for the high-resolution interpolation of in situ sea surface salinity. *Journal of Atmospheric and Oceanic Technology*, *29*(6), 867-879.

Nardelli, B. B. (2013). Vortex waves and vertical motion in a mesoscale cyclonic eddy. *Journal of Geophysical Research: Oceans*, *118*(10), 5609-5624.

Pinto, L., Campuzano, F., Fernandes, R., Fernandes, L., & Neves, R. (2012). An operational model for the Portuguese coast. *Book of abstracts of the 2IH Jornadas (This volume)*.

Racine, Mélanie. *Développement de modèles d'habitats pour les tortues caouannes (Caretta caretta) de Méditerranée occidentale*. 2015. *Agrocampus Ouest, Rennes*

Reed, C. C. (2015). A review of parasite studies of commercially important marine fishes in sub-Saharan Africa. *Parasitology*, *142*(01), 109-124.

Reul, N., Chapron, B., Lee, T., Donlon, C., Boutin, J., & Alory, G. (2014). Sea surface salinity structure of the meandering Gulf Stream revealed by SMOS sensor. *Geophysical Research Letters*, *41*(9), 3141-3148.

Saha, K., Ignatov, A., Liang, X. M., & Dash, P. (2012). Selecting a first-guess sea surface temperature field as input to forward radiative transfer models. *Journal of Geophysical Research: Oceans*, *117*(C12).

Senatore, A., Mendicino, G., Knoche, H. R., & Kunstmann, H. (2014). Sensitivity of modeled precipitation to sea surface temperature in regions with complex topography and coastlines: a case study for the Mediterranean. *Journal of Hydrometeorology*, *15*(6), 2370-2396.

Shrira, V. I., & Forget, P. (2015). On the nature of near-inertial oscillations in the uppermost part of the ocean and a possible route toward HF radar probing of stratification. *Journal of Physical Oceanography*, *45*(10), 2660-2678.

Small, R. J., Campbell, T., Teixeira, J., Carniel, S., Smith, T. A., Dykes, J., ... & Allard, R. (2011). Air–sea interaction in the Ligurian Sea: Assessment of a coupled ocean–atmosphere model using in situ data from LASIE07. *Monthly Weather Review*, *139*(6), 1785-1808.

Sotillo, M. G., Amo-Baladrón, A., Padorno, E., Garcia-Ladona, E., Orfila, A., Rodríguez-Rubio, P., ... & Fanjul, E. A. (2016). How is the surface Atlantic water inflow through the Gibraltar Strait forecasted? A lagrangian validation of operational oceanographic services in the Alboran Sea and the Western Mediterranean. *Deep Sea Research Part II: Topical Studies in Oceanography*, *133*, 100-117.

Thakur, K., Revie, C., Vanderstichel, R., & Patanasatienkul, T. (2016). Suitability of remotely-sensed sea surface temperature for aquaculture research: Comparison with in situ records from salmon farms in British Columbia (BC), Canada. In *Frontiers in Veterinary Science Conference: AquaEpi I-2016*.

Thomas, Y., Pouvreau, S., Alunno-Bruscia, M., Barillé, L., Gohin, F., Bryere, P., & Gernez, P. (2015). Global change and climate-driven invasion of the Pacific oyster (Crassostrea gigas) along European coasts: a bioenergetics modelling approach. *Journal Of Biogeography*.

Trancoso, A. R. R. (2012). *Operational modelling as a tool in wind power forecasts and meteorological warnings* (Doctoral dissertation, Instituto Superior Técnico).

Trindade, A., Peliz, A., Dias, J., Lamas, L., Oliveira, P. B., & Cruz, T. (2016). Cross-shore transport in a daily varying upwelling regime: A case study of barnacle larvae on the southwestern Iberian coast. *Continental Shelf Research*, *127*, 12-27.

Troupin, C., Alvera-Azcárate, A., Barth, A., & Beckers, J. M. (2010, September). EOF analysis of Sea Surface Temperature in the Canary Island-Madeira region. In *Geophysical Research Abstracts* (Vol. 13).

Troupin, C., Mason, E., Beckers, J. M., & Sangrà, P. (2012). Generation of the Cape Ghir upwelling filament: A numerical study. *Ocean Modelling*, *41*, 1-15.

Vieira, N., Carvalho, I., Costa, J. L., Almeida, P. R., Quintella, B., Cabral, H., & Brito, C. (2010). Comparison of habitat use of common dolphin (delphinus delphis) and bottlenose dolphin (tursiops truncatus) in portugal mainland. *Faculdade de Ciências*, 12.

Virgili, A. (2014). Predicting variations in coastal seabird habitats to assess marine protected areas. *Ingénieur des sciences agronomiques, agroalimentaires, horticoles et du paysage. Agrocampus Ouest, Rennes, 44p*.

Woillez, M., Fablet, R., Ngo, T. T., Lalire, M., Lazure, P., & De Pontual, H. (2016). A HMM-based model to geolocate pelagic fish from high-resolution individual temperature and depth histories: European sea bass as a case study. *Ecological Modelling*, *321*, 10-22.

ESA ACTIVITIES RELEVANT TO GHRSST

Craig Donlon

ESA/ESTEC, The Netherlands

ABSTRACT

Sentinel-3A was launched on 4th February 2016 from Plesetsk Cosmodrome. It is an operational mission in high-inclination, low earth orbit for the provision of observational data to marine and land monitoring services. The operational character of the mission implies a high level of availability of the data products and fast delivery time, which have been important design drivers for the mission. Full performance will be achieved with a constellation of two identical satellites, separated by 180 degrees in the same orbital plane. The overall service duration is planned to be 20 years and is expected to be fulfilled by a series of several satellites. Three more Sentinel-3 satellites are in development with Sentinel-3B planned for launch in 2017. Procurement of the C and D satellites is ongoing. The mission carries the Sea and Land Surface Temperature Radiometer instrument (SLSTR) providing continuity of dual-view along-track scanning data streams established by the (A)ATSR series on board ESA's ERS and ENVISAT satellites.

A series of new technology development and Pre-PhaseA studies for a new high resolution (~100m resolution) satellite Thermal Infrared Radiometer are in progress.

ESA is also spearheading the development of Fiducial Reference Measurements (FRM) for SST.

SECTION 3: POSTERS

POSTERS LIST

Posters are published on the GHRSST website and can be found in the 'Event Resources' of the G-XVIII meeting page (https://www.ghrsst.org/agenda/ghrsst-xviii/).

Posters 1-to 22 can be found in the 'Monday 5th June' section, under 'Interactive presentations part 1'

Posters 23 to 43 can be found in the 'Tuesday 6th June' section, under 'Interactive presentations part 2'.

Number	Presenter	Title
1	Armstrong, Edward	Recent updates to PO.DAAC tools and services for oceanographic data
2	Chen, Yuanyuan	Determination of sea surface temperature from Chinese Gaofen-5 satellite
3	Dash, Prasanjit	Routine analyses of Sentinel-3A SLSTR SST employing Monitoring & Evaluation of Thematic Information From Space (METIS)
4	Ding, Yanni	Regional validation and potential enhancements to NOAA polar ACSPO SST products
5	Donlon, Craig	ESA activities relevant to GHRSST
6	Embury, Owen	Interim climate data records: From Climate Change Initiative to the Copernicus Climate Change Service
7	Gentemann, Chelle	Microwave SST Single Sensor Error Statistics
8	He, Kai	SST Quality Monitor Release 2 (Squam2)
9	Hernaman, Vanessa	Trial of including new L4 SST analyses in GHRSST Multi-Product Ensemble
10	Huang, Boyin	Extended Reconstructed Sea Surface Temperature Version 5 (ERSST v5): Upgrades, validations, and intercomparisons
11	Huang, Thomas	A webservice platform for big ocean data science
12	Kim, Jae-Gwan	The COMS measurements of sea surface temperature at KMA

Number	Presenter	Title
13	Kurihara, Yukio	Cross calibration for SST
14	Maturi, Eileen	Physical retrieval and high-resolution blended SST products at NOAA NESDIS
15	Nightingale, Tom	The SISTeR processor
16	O'Carroll, Anne	Operations of Sentinel-3A SLSTR SST and EUMETSAT activities
17	Park, Kyung-Ae	Comparisons of sea surface temperature algorithms for GEO-KOMPSAT-2A geostationary satellite data
18	Piollé, Jean-François	CMEMS OSI TAC progress report
19	Saux Picart, Stéphane	EUMETSAT OSI SAF sea surface temperature activities and products
20	Tomazic, Igor	Overview of Sentinel-3 SLSTR L1 and marine L2 products
21	Vazquez, Jorge	CEOS Ocean Variables Enabling Research and Applications for GEO (Coverage)
22	Zhou, Xinjia	Recent improvements to the NOAA iQuam 2.10 system
23	Banyouko Ndah, Anthony	Centennial-scale surface temperature variability in the South China Sea: A perfect reflection of global ocean-climatic variability cycles?
24	Banzon, Viva/ Huang, Boyin	Why is summer DOISST warm in the Arctic and how to fix it
25	Bulgin, Claire/ Merchant, Chris	Bayesian cloud detection for AVHRR SST retrieval
26	Embury, Owen	Stratospheric aerosol and impacts on infrared SST retrievals
27	Govekar, Pallavi/ Beggs, Helen	Use of ACSPO VIIRS L3U SST in the Australian Bureau of Meteorology
28	He, Kai	Monitoring AVHRR/2 in the NOAA Sensor Stability for SST (3S) Version 2

Number	Presenter	Title
29	Hihara, Tsutomu	Constructing an ocean data assimilation product using satellite sea surface temperature
30	Liu, Mingkun	Inter-calibration of brightess temperature from HY-2 scanning microwave radiometer over ocean
31	Liu, Yang	Long-term impact of sampling bias in NASA MODIS and AVHRR Pathfinder Level 3 SSTs
32	Luo, Bingkun	The impact of Saharan outflow on satellite retrieved infrared sea surface temperature
33	Park, Kyung-Ae	Short-term variations of sea surface currents estimated from geostationary satellite sea surface temperature images
35	Saux Picart, Stéphane	A machine learning approach for MSG/SEVIRI SST bias estimation
36	Surcel Colan, Dorina	The sensibility of CMC analysis to the characteristics of different observation data sets
37	Szczodrak, Goshka/ Minnett, Peter	Retrieval of MODIS SST with optimal estimation
38	Tomazic, Igor	Ongoing comparison between Sentinel-3A SLSTR and IASI aboard Metop-A and –B
39	Vazquez, Jorge	Evaluation of the Multi-Scale High Resolution (MUR) analysis of lake surface temperature
40	Wei, Ji-An	Assessment of Landsat 8 TIRS sea surface temperature retrieval algorithms
41	Xi, Xin/ Ignatov, Alexander	Developing an atmospheric correction of tropospheric dust in the infrared SST retrieval for the NOAA ACSPO system
42	Xu, Bin	CMA Ocean Data Merging System (COMS)
43	Yang, Minglun	Effect of emissivity on shipboard sea surface skin temperature measurements
44	Zhu, Xiaofang/ Harris, Andrew	A near-global physical retrieval based geostationary sea surface temperature reanalysis

POSTER ABSTRACTS

RECENT UPDATES TO PO.DAAC TOOLS AND SERVICES FOR OCEANOGRAPHIC DATA

Edward M. Armstrong[(1)], Thomas Huang[(1)], Chaowei Yang[(2)], Vardis Tsontos[(1)], Mike Gangl[(1)], Flynn Platt[(1)], Aaron Plave[(1)], Richard Kim[(1)], Yongyao Jiang[(2)], Yun Li [(2)]

(1) NASA Jet Propulsion Laboratory, California Institute of Technology, 4800 Oak Grove Dr., Pasadena, CA 91109, USA, Email: Edward.m.armstrong@jpl.nasa.gov
(2) George Mason University, 4400 University Drive, Fairfax, VA 22030, USA

ABSTRACT

This presentation will summarize recent improvements and the evolution of tools and services at The Jet Propulsion Lab (JPL) Physical Oceanography Distributed Active Archive Center (PO.DAAC) in support of the GHRSST mission. These include enhancements to the Level 2 subsetting capability, known as HiTIDE, the visualization tool SOTO, and improved web services. With HiTIDE, GHRSST Level 2 datasets can be easily spatially and temporally subsetted by specific variables. The SOTO tool now supports complete time series visualization, overlays and animations of select PO.DAAC datasets. Associated web services that in part provide the "glue" for these tools have been improved for discovery, access and subsetting of individual granules.

In addition to these core set of PO.DAAC services there is a suite of emerging technologies developed at the NASA Jet Propulsion in collaboration with various partners to address concerns of even higher volume, variety, velocity, veracity of data in the near future. The Virtual Quality Screening Service (VQSS), described at a previous meeting, is now operationally deployed and represents a web service paradigm to apply quality screening information (quality, uncertainty, and ancillary variables) to GHRSST granules and extract out subsetted SST values. Mining and Utilizing Dataset Relevancy from Oceanographic Dataset (MUDROD), in partnership with George Mason University, is a NASA funded project to improve search relevance and dataset ranking using machine learning techniques based on a) characterizing user behavior from the mining and modeling of web access logs, b) metadata for oceanographic data, and c) ontologies from SWEET, GCMD, and PO.DAAC. This project in part targeted SST datasets to improve the ranking of the wide variety of GHRSST products. And finally, the Oceanographic In-situ Interoperability Project (OIIP) project is a very recent activity to improve the accessibility of in situ data to the satellite community, addressing issues of satellite-insitu data interoperability and visualization with a focus also on emerging datasets from the marine electronic tagging community.

DETERMINATION OF SEA SURFACE TEMPERATURE FROM CHINESE GAOFEN-5 SATELLITE

Yuanyuan Chen[1,2], Zhao-Liang Li[1,2,*]

1. Key Laboratory of Agri-informatics, Ministry of Agriculture/Institute of Agricultural Resources and Regional Planning, Chinese Academy of Agricultural Sciences, Beijing 100081, China;
2. ICube (UMR7357), UdS, CNRS, 300 Bld Sébastien Brant, CS10413, Illkirch 67412, France
Email: cy1305153@163.com (Y. Chen); lizhaoliang@caas.cn (Z.-L. Li)[*]

ABSTRACT

Sea surface temperature (SST) is a significant parameter in air–sea interactions. The Chinese Gaofen-5 (GF-5) satellite, which can collect the surface information at a spatial resolution of 40-meter for thermal infrared channels, is planned to be launched in 2017. This study aims to develop the suitable algorithm that permits determining the SST from GF-5 satellite. First, the different algorithms for retrieving SST were evaluated based on the radiative transfer simulation. From the operational application point of view, the quadratic split-window algorithm was then selected and developed to determine SST from Gaofen-5 data. To correct the effect of the sea surface emissivity (SSE) on SST, the SSE values of 0.99055 and 0.98685 for two split-window channels, which were calculated based on the spectrum samples of sea water from the Johns Hopkins University (JHU), were used when top-of-atmosphere brightness temperatures were obtained. Using the simulated data, a RMSE of 0.3 K was obtained for the developed algorithm. Since the GF-5 data is not available at the time of writing this paper, ASTER_L1B data was used to test the developed algorithm and AST_08 product was used for the inter-comparison purpose to assess the retrieved SST.

ROUTINE ANALYSES OF SENTINEL-3A SLSTR SST EMPLOYING MONITORING & EVALUATION OF THEMATIC INFORMATION FROM SPACE (METIS)

Prasanjit Dash [1,2], Anne O'Carroll[1], Igor Tomazic[1], Jean-Francois Piolle [3], Gary Corlett[4]

(1) EUMETSAT, Darmstadt, Germany, Emails: prasanjit.dash anne.carroll igor.tomazic@eumetsat.int
(2) CSU CIRA, Fort Collins, CO 80521, USA, Email: co-author@address.com
(3) Ifremer, B rest, France, 29280, USA, Email: Jean.Francois.Piolle@ifremer.fr
(4) Univ. of Leicester, Leicester, LE1 7RH, UK, Email: gkc1@leicester.ac.uk

ABSTRACT

A discontinuity of dual-view capability had occurred following the loss of communication with the Envisat satellite in April 2012, which carried the Advanced Along Track Scanning Radiometer ((A)ATSR). The Sea and Land Surface Temperature Radiometer (SLSTR) sensor onboard Sentinel-3A reinstates continuity to the EU flagship dual-view (A)ATSR data, with wider swath, newer channels and an accurate sensor characterization. Solid-state instrumentation and viewing philosophy is, however, one part of the challenge. For accurate retrievals, better algorithms are desirable both for cloud identification and information extraction. This is an incremental process and requires a coordinated effort by various partners, which is duly acknowledged here. Experimental global SST products at native resolution of SLSTR IR bands are being generated since 21 June, 2016. In addition, retrievals from AVHRR and IASI onboard Metop-B are also generated by EUMETSAT OSI SAF and made available publicly. To satisfy the need to routinely evaluate these products, the Monitoring and Evaluation of Thematic Information from Space (METIS) system for remotely sensed products has been recently setup. The prototype is currently accessible with password restriction at http://metis.eumetsat.int and will be open when SLSTR SST data are released publicly. The SST component of METIS, called as METIS-SST, monitors, evaluates and validates the three products mentioned above. The objective is to comprehensively evaluate the products for identifying and alerting anomalous conditions due to algorithm malfunction and steps beyond conventional validation approaches. In addition to the gold-standard *in situ* validation, there will be further diagnostics available for monitoring temporal and spatial stability.

REGIONAL VALIDATION AND POTENTIAL ENHANCEMENTS TO NOAA POLAR ACSPO SST PRODUCTS

Yanni Ding [(1)], Alexander Ignatov[(2)], Michael Grossberg[(3)], Irina Gladkova[(4)], Calvin Chu[(5)]

NOAA STAR and CSU CIRA, USA, Email: yanni.ding@noaa.gov
NOAA STAR, Email: alex.ignatov@noaa.gov
City College of New York, USA, Email: michaeldg@gmail.com
NOAA STAR, City College of New York, and GST Inc, USA, Email: irina.gladkova@gmail.com
City College of New York, USA, Email: cchu111590@gmail.com

ABSTRACT

The ACSPO Regional Monitor for SST (ARMS; www.star.nesdis.noaa.gov/sod/sst/arms/) focuses on areas of interest to SST users (e.g., coastal and internal waters, high-latitudes, dynamic or cloudy regions), which are often challenging for SST producers (e.g., dynamic ocean may be masked by cloud mask, SST algorithms subject to large errors in the high-latitudes, etc.) ARMS complements the continuous global validation of the ACSPO products in the SST Quality Monitor (SQUAM).

Since GHRSST-17, ARMS was updated to version 2. SST images now have better resolution, and ACSPO L3U (level 3, un-collated) SST products have been included with the same masking flags as L2P. Several L4 fields (JPL MUR, Met Office OSTIA and NOAA Geo Polar Blended) have been added for comparison with ACSPO SST products and inter-comparison.

The ARMS supports development of high-quality gridded L3C/S (collated/super-collated; L2 data of the same/multiple satellites mapped into a uniform spatial grid and collated). Preliminary analyses in ARMS suggest that the collation of multiple observations requires reconciling some differences, caused by diurnal warming/cooling, variable cloud conditions and view zenith angles, for which ARMS provides plenty of examples.

This presentation discusses the updates of ARMS, and some preliminary results of validating the ACSPO SSTs in the high latitudes and coastal and dynamic regions. We check the data from different passes and satellites for consistency, taking into account various view zenith angles, cloud conditions, and diurnal warming/cooling.

ESA ACTIVITIES RELEVANT TO GHRSST

Craig Donlon

ESA/ESTEC, The Netherlands

ABSTRACT

Sentinel-3A was launched on 4th February 2016 from Plesetsk Cosmodrome. It is an operational mission in high-inclination, low earth orbit for the provision of observational data to marine and land monitoring services. The operational character of the mission implies a high level of availability of the data products and fast delivery time, which have been important design drivers for the mission. Full performance will be achieved with a constellation of two identical satellites, separated by 180 degrees in the same orbital plane. The overall service duration is planned to be 20 years and is expected to be fulfilled by a series of several satellites. Three more Sentinel-3 satellites are in development with Sentinel-3B planned for launch in 2017. Procurement of the C and D satellites is ongoing. The mission carries the Sea and Land Surface Temperature Radiometer instrument (SLSTR) providing continuity of dual-view along-track scanning data streams established by the (A)ATSR series on board ESA's ERS and ENVISAT satellites.

A series of new technology development and Pre-PhaseA studies for a new high resolution (~100m resolution) satellite Thermal Infrared Radiometer are in progress.

ESA is also spearheading the development of Fiducial Reference Measurements (FRM) for SST.

CLIMATE DATA RECORDS: FROM CLIMATE CHANGE INITIATIVE TO THE COPERNICUS CLIMATE CHANGE SERVICE

Owen Embury [(1)], **Chris Merchant**[(2)]

(1) Department of Meteorology, University of Reading, UK, Email: o.embury@reading.ac.uk
(2) Department of Meteorology, University of Reading, UK, Email: c.j.merchant@reading.ac.uk

ABSTRACT

Projects such as the ESA Climate Change Initiative for SST and NODC AVHRR Pathfinder have produced high quality Climate Data Records (CDR) of SST. With these programs the focus is providing a long-term, stable, satellite-based record suitable for use by climate modelers and researchers. By necessity of their length this involves harmonising data across from multiple different satellite data sets. However, these projects are large reprocessing efforts involving decades of satellite data and typically only produce an updated dataset every few years. This leaves a gap between the long-term CDRs and operational SST products produced in near-real time by satellite data providers.

In this presentation we outline our plans to produce Interim Climate Data Records (ICDRs) for the Copernicus Climate Change Service (C3S) and UK NERC Centre for Earth Observation (NCEO). These will take the processes developed in the ESA CCI project and operate them routinely in short-delay mode in order to produce ICDRs complimenting the CDRs in-between the major reprocessing efforts.

MICROWAVE SST SINGLE SENSOR ERROR STATISTICS

Carl A. Mears[1], Chelle Gentemann[2], and Marty Brewer[1]

[1]Remote Sensing Systems, Santa Rosa California USA
[2]Earth & Space Research, Seattle Washington USA, Email: cgentemann@esr.org

ABSTRACT

We have evaluated single sensor error statistics (SSES) for all satellite-borne microwave sensors that provide sea surface temperature (SST) retrievals. The satellites studied are AMSRE, AMSR2, WindSat, TMI, and GMI. The error statistics were determined by comparing with *in situ* ocean temperature measurements. These measurements are collected from the Global Telecommunications System (GTS) and re-distributed with additional metadata in near real-time by the US Global Ocean Data Assimilation Experiment (USGODAE). The dataset we used in this analysis is referred to as "SFCOBS" and contains surface observations from ships, moored and drifting buoys, and Coastal-Marine Automated Network (CMAN) in-situ surface temperatures. For the analysis presented here, we only use data from moored and drifting buoys because the data are of higher quality for these types of instruments. The results are presented as a function of SST and surface windspeed because these two parameters have the largest effect on microwave SST retrieval quality. We found that the statistics from the satellites that include a low frequency 6.9 GHz channel (AMSRE, AMSR2 and WindSat) show good performance over the entire range of SST and wind speed, while the satellites that lack this channel show degraded performance at SSTs below 12C, particularly at moderate to high windspeed. The results are smoothed and extended using a variational analysis to produce look-up tables that we use to rapidly calculate SSES error estimates for the MISST datasets.

SST QUALITY MONITOR RELEASE 2 (SQUAM2)

Kai He[1,2], Xinjia Zhou[1,3], Sasha Ignatov[1], Maxim Kramar[1,2], Prasanjit Dash[3,4]

[1]NOAA STAR, USA; Emails: Kai.He@noaa.gov; Xinjia.Zhou@noaa.gov; Alex.Ignatov@noaa.gov; Maxim.Kramar@noaa.gov; Prasanjit.Dash@noaa.gov
[2]GST, Inc, Greenbelt, MD 20770, USA
[3]CSU CIRA, Fort Collins, CO 80521, USA
[4]EUMETSAT, Darmstadt, Germany

ABSTRACT

The NOAA SST Quality Monitor (SQUAM) has been widely used in the SST community since its release in 2007, to monitor, validate and compare various community L2, L3 and L4 SST products. Over years, SQUAM has expanded, by adding new data products, improving stability and functionality and serving more users. However, with the introduction of new generation polar (VIIRS onboard SNPP launched in 2011 and J1 planned for launch in 2017, to be followed by J2-J4 in out years) and geostationary (ABI onboard GOES-16 launched in 2016, and follow-on GOES-S/T/U satellites, and Himawari-8/9 launched in 2014 and 2016, respectively), SQUAM is facing the need for reorganization and redesign, due to challenging data volumes and required computing and data storage and distribution resources.

The SQUAM Release 2 comprises three top-level sections, Polar L2/L3, Geo L2/L3, and Analysis L4 SSTs. The L2/L3 sections of SQUAM2 mainly focus on the NOAA Advanced Clear-Sky Processor for Ocean (ACSPO) products, which are grouped by sensors and platforms. Number of L4 references has been reduced, and now includes only CMC, OSTIA, and Reynolds OISST. For *in situ* reference, iQuam1 data have been replaced by iQuam2, and ARGO floats have been added. Two options – to enable SSES bias correction and switch to dynamic regression coefficients – have been added. Two ACSPO Reanalyses v1 (RAN1) data are now available for AVHRR GAC and SNPP VIIRS. In addition to daily statistics, higher level aggregations in time (monthly, yearly, full mission) were added. The new GEO section monitors Himawari-8 AHI, and soon to be available GOES-16 ABI ACSPO SSTs. In addition to the analyses in UTC time domain, SQUAM2 adds analyses in the local solar time domain, to analyze the effects of the diurnal cycle. The SQUAM2 also sees major improvements in the processing speed, as well as in the interface and web functionality, such as introducing new features of permalink and session caching.

TRIAL OF INCLUDING NEW L4 SST ANALYSES IN GHRSST MULTI-PRODUCT ENSEMBLE

Vanessa Hernaman [(1)], Simon Good[(1)], and Emma Fiedler[(1)]

*(1) Met Office, Fitzroy Road, E**xe**ter, Devon, EX1 3PB, United Kingdom,*
Email: vanessa.hernaman@metoffice.gov.uk

ABSTRACT

The GHRSST Multi-Product Ensemble (GMPE) system runs daily at the UK Met Office, and is disseminated via the Copernicus Marine Environment Monitoring Service. The GMPE system takes L4 SST analyses from various international centres as inputs, transfers them onto a common 0.25º grid, and produces an ensemble median and standard deviation.

The current GMPE product consists of up to ten L4 SST analyses. Six new L4 analyses have become available (MUR, G1SST, DMI_OI, CMC0.1º, and two OSPO products), and trials were conducted to determine the impact of the new analyses on the ensemble median and its performance compared to Argo observational data.

The results indicated that the addition of all new L4 analyses consistently produced a GMPE median with generally cooler SSTs (relative to the baseline GMPE median produced using only the current analyses) of 0.05-0.30 Kelvin in many broad regions (e.g., west coasts of South America and central Africa; regions of the Arctic), but consistently warmer SSTs (relative to the baseline) of up to 0.40 Kelvin in specific regions (e.g., Gulf Stream; Svalbard region of the Arctic; Indonesia; Japan). When the new analyses were considered individually, the OSPO products generally produced cooler SSTs relative to the GMPE median, with the rest showing a mixture of warmer and cooler regions.

When compared to Argo observations, GMPE median performance was not greatly affected (within 0.02 Kelvin of baseline GMPE median performance), and performance of the new L4 analyses varied regionally, with CMC0.1º the most consistently high performer of the new analyses.

A WEBSERVICE PLATFORM FOR BIG OCEAN DATA SCIENCE

Thomas Huang [(1)], Edward M. Armstrong[(1)], Joseph Jacob[(1)], Nga T. Quach[(1)] , Vardis Tsontos[(1)] , Brian Wilson[(1)] , Shawn Smith[(2)], Mark A. Bourassa[(2)] , Steve J. Worley[(3)], Chaowei Yang[(4)], Yongyao Jiang[(4)], Yun Li[(4)]

NASA Jet Propulsion Laboratory, California Institute of Technology, 4800 Oak Grove Dr., Pasadena, CA 91109, USA, Email: thomas.huang@jpl.nasa.gov
Center for Ocean-Atmospheric Prediction Studies, 2000 Levy Avenue, Building A, Suite 292, Tallahassee, FL 32306-2741, USA, Email: srsmith@fsu.edu
National Center for Atmospheric Research, P.O. Box 3000, Boulder, CO 80307-3000, USA, Email: worley@ucar.edu
George Mason University, 4400 University Drive, Fairfax, VA 22030, USA, Email: cyang3@gmu.edu

ABSTRACT

This presentation will provide an overview of OceanWorks, the webservice platform for big ocean data science at the NASA's Physical Oceanography Distributed Active Archive Center (PO.DAAC), and to discuss the open source solutions that OceanWorks uses to enable fast analysis of Sea Surface Temperature (SST) data. Funded through the NASA's Advance Information System Technology (AIST) Program and developed collaboratively between JPL, FSU, NCAR, and GMU, OceanWorks will be the platform for the next generation of PO.DAAC data solutions. OceanWorks is an orchestration of several previous funded NASA big ocean data solutions using cloud computing technology, which include on-the-fly data analysis (NEXUS) (Figure 1), anomaly detection (OceanXtremes) (Figure 2), matchup (DOMS) (Figure 3), quality-screened subsetting (VQSS), search relevancy (MUDROD), and web-based visualization (Common Mapping Client).

THE COMS MEASURMENTS OF SEA SURFACE TEMPERATURE AT KMA

Jae-Gwan Kim, Chul-Kyu Park, Chu-Yong Chung, and Seon-Kyun Baek

National Meteorological Satellite Center / KMA, Jincheon (Republic of Korea), Email: kimjgwan@korea.kr

ABSTRACT

National Meteorological Satellite Center (NMSC) of Korea Meteorological Administration (KMA) has been operating the first Korean meteorological geostationary satellite, COMS officially since 2011. KMA developed sixteen baseline meteorological products of the COMS observation data including sea surface temperature (SST) and they have been generated via COMS Meteorological Data Processing System (CMDPS). NMSC evaluated the accuracy and performance of SST product and tried to improve it. The COMS SST product retrieved with Multi-Channel SST algorithm. We tried to reduce biases in comparison with in-situ data and other satellite data using modification of regression coefficients in algorithm. In this presentation, we present the COMS SST retrieval and validation result compared with buoy data for numerical weather prediction model.

CROSS CALIBRATION FOR SST

Yukio Kurihara [(1)], Hiroshi Murakami[(1)], Misako Kachi[(1)]

Japan Aerospace Exploration Agency (JAXA), Tsukuba, Ibaraki, Japan
Email: kurihara.yukio@jaxa.jp

ABSTRACT

JAXA provides SST products generated by using AMSR2, Windsat, GMI, MODIS, VIIRS, and Himawari-8 data. Meanwhile, JAMSTEC in collaboration with JAXA is developing an ocean model that assimilates these products. In the assimilation, not only accuracy but also consistency in products is essential for good results. Furthermore, consistency in satellite SSTs is also important for climate monitoring. JAXA's MODIS, VIIRS, and Himawari-8 SSTs are retrieved from IR data by solving an IR radiative transfer equation. Although these SSTs are determined by solving the same equation, there are systematic differences of around 0~0.3 K between them. To improve these inconsistencies, we developed a new cross-calibration method. The new method calibrates L1 data by using SSTs retrieved from another satellite IR data. We performed the method and calibrated Himawari-8 data by using Terra/MODIS SSTs. Then, we retrieved SSTs from the calibrated Himawari-8 data and compared them with those retrieved from Terra/MODIS data. The comparison result shows an improvement in consistency in Himawari-8 and Terra/MODIS SSTs, i.e., the mean difference of 0.27 K (Terra/MODIS minus Himawari-8) has been reduced to -0.05 K by the calibration. Although the cross-calibration method still needs to be improved, it is expected to improve consistencies in satellite SST products including upcoming JAXA's GCOM-C.

PHYSICAL RETRIEVAL AND HIGH-RESOLUTION BLENDED SST PRODUCTS AT NOAA NESDIS

Eileen Maturi [1], Andy Harris [2], Jonathan Mittaz [3]
Xiaofang Zhu [4], Gary Wick [5], Prabhat Koner [6], William Skirving [7]

(1) NOAA/NESDIS/STAR College Park, MD, U.S.A. Eileen.Maturi@noaa.gov
(2) University of Maryland, CICS, College Park, MD, U.S.A. Andy.Harris@noaa.gov
(3) University of Reading, Dept of Meteorology, Reading, UK J.mittaz@reading.ac.uk
(4) Contractor, Global Science Technology, College Park, MD, U.S.A. Xiaofang.Zhu@noaa.gov
(5) NOAA/OAR/ESRL, Boulder, Co., U.S.A. Gary.Wick@noaa.gov
(6) University of Maryland, CICS, College Park, MD, U.S.A. Prabhat.Koner@noaa.gov
(7) NOAA/NESDIS/STAR Townsville, Queensland, Aus William.Skirving@noaa.gov

ABSTRACT

The National Oceanic and Atmospheric Administration's (NOAA) Office of the National Environmental Satellite, Data and Information Service (NESDIS) generates operational geostationary Level-2P (L2P) sea surface temperature (SST) products in GHRSST GDS2.0 format from GOES-E/W and MSG-3, and blended Level 4 SST analyses to satisfy the requirements of the GHRSST users. The three geostationary satellites (longitudes 75°W, 135°W, and 0°, respectively) provide high temporal SST retrievals for most of the tropics and mid-latitudes, with the exception of a region between ~60°E and ~80°E. A process of continual development has produced regular improvements in the SST product accuracy, most recently with the implementation of a physical retrieval algorithm based on a Modified Total Least Squares algorithm (Koner et al. 2015). These operational geostationary SST L2 products are then blended with the polar operational SSTs to produce daily global, high-resolution (1/20°) SST analyses in GHRSST L4 format (day/night, night time only and diurnally corrected). AMSR-2 SSTs are now being included in these analyses to improve the quality in regions of persistent cloud cover, along with an improved diurnal adjustment.

These temperature products are used by NOAA Coral Reef Watch (CRW) to generate products for Bleaching and Alerts for coastal managers; the management of Mammals and fisheries by the National Marine Fisheries offices; and the Oceanic Heat Content (OHC) products for the national weather service for Hurricane and Typhoon intensity for the Atlantic and Pacific Basins. Reprocessed radiance data holdings for geostationary sensors using our latest SST algorithm are furthering climate applications. The resultant L2 products are, in turn, being included in the production of more than a decade of our daily 1/20 degree blended sea surface temperature product (reprocessed 2002 to 2015). The provision of this extended baseline is invaluable for improving the quality of anomaly-based products, such as those produced by NOAA CRW.

Capabilities under development include: 1) generation of surface lake temperatures for inclusion into NWS Forecast Models; 2) the generation of 1-km Regional SST analysis products; 3) using our physical retrieval algorithm to generate SSTs from Meteosat-8 over the Indian ocean and incorporate it into the blended SST analysis; and 4) a thermal stress forecasting product by combining the OHC products with the Hot Spot product to predict the minimum and maximum length of a bleaching event.

THE SISTeR PROCESSOR

Tim Nightingale [(1)], Arrow Lee[(1)], Eleanor Barber[(1)]

(1) STFC Rutherford Appleton Laboratory, Harwell Campus, Didcot, Oxon OX11 0QX, UK,
Email: tim.nightingle@stfc.ac.uk

INTRODUCTION

The SISTeR in-situ radiometer is a validation radiometer and, as such, must generate traceable estimates of SST, including estimates of the associated type A and type B uncertainties. We describe the design of a new SISTeR processor that propagates uncertainty estimates in parallel with the contributing terms to the calibration and SST equations. Rather than calculating level 2 SSTs from level 1 radiances in the traditional way, the SISTeR processor generates a synthetic SST signal count and calibrates this, to avoid double-counting calibration uncertainties. We also describe the partitioning of the SST equation to include an air temperature anomaly as, in the absence of direct measurements, the anomaly generally can be better estimated than the gross air temperature. The processor outputs level 1, 2 and 3 products. The level 2 and 3 products are generated in an "L2R" format that closely follows GHRSST product design principles and is both CF and ACDD compliant.

OPERATIONS OF SENTINEL-3A SLSTR SST AND EUMETSAT ACTIVITIES

Anne O'Carroll [(1)], Igor Tomazic[(1)], Prasanjit Dash[(1)], Jean-Francois Piolle[(2)], Gary Corlett[(3)], Craig Donlon[(4)]

EUMETSAT, Eumetsat-Allee 1, 64295 Darmstadt Germany
Ifremer, Brest, France
University of Leicester, United Kingdom
ESA/ESTEC, Keplerlaan 1, 2201 AZ, Noordwijk, The Netherlands

ABSTRACT

The first Copernicus Sentinel-3 satellite, Sentinel-3A, was successfully launched on 16th February 2016 from Plesetsk, with the mission to provide a consistent, long-term collection of marine (and land) data for operational ocean analysis, forecasting and service provision. The EUMETSAT marine centre has been preparing to deliver operational Sea Surface Temperature (SST) products based on measurements from the Sea and Land Surface Temperature Radiometer (SLSTR) on board Sentinel-3. Information on the Sentinel-3A SLSTR SST product, which has been developed together with ESA and industry partners, will be described.

Details of the operations of Sentinel-3 SLSTR, the scientific characteristics of the SST product, and information on the algorithm will be given. Details on how to find further information will be presented, and opportunities on how to participate in the ESA and EUMETSAT Sentinel-3 Validation Team for marine surface temperature will be described.

The SLSTR SST product is provided according to the GHRSST specification, and will additionally include some experimental fields. The Sentinel-3 Commissioning Phase was successfully completed in July 2016 and the operational SLSTR SST products are expected to be widely released in May 2017.

An overview of the first validation activities of SST from Sentinel-3A SLSTR from on-going Sentinel-3 Cal/Val activities at EUMETSAT will be explained, together with the Ocean and Sea-Ice Satellite Application Facility (OSI SAF), and the ESA Mission Performance Centre. On-going and upcoming Copernicus projects on improved drifting buoys for satellite SST validation and sea-ice cloud screening for SLSTR will be described.

In addition, further information on other EUMETSAT activities and SST products will be given, including SST from Metop-IASI, third-party data services, and an overview of other EUMETSAT missions in the context of the EUMETSAT OSI SAF.

COMPARISONS OF SEA SURFACE TEMPERATURE ALGORITHMS FOR GEO-KOMPSAT-2A GEOSTATIONARY SATELLITE DATA

Kyung-Ae Park[(1)], Hye-Jin Woo[(2)], Alexander Ignatov[(3)], Boris Petrenko[(4)]

(1) Dep. of Earth Science Education, Seoul National University, Seoul, Korea, Email: kapark@snu.ac.kr
(2) Dep. of Science Education, Seoul National University, Seoul, Korea, Email: hyejinwoo@snu.ac.kr
(3) Center for Satellite Applications and Research, NOAA, Maryland, USA, Email: Alex.Ignatov@noaa.gov
(4) Center for Satellite Applications and Research, NOAA, Maryland, USA, Email: boris.petrenko@noaa.gov

ABSTRACT

To develop sea surface temperature (SST) retrieval algorithms for GEO-KOMPSAT-2A **(***Geostationary* **-** Korea Multi-Purpose Satellite-2A), we compare previously known algorithms such as MCSST and NLSST methods, as well as a recently developed hybrid algorithm and a 4-band algorithm that uses 4-channel brightness temperatures. The traditional empirical algorithms (MCSST and NLSST methods) have been widely used in spite of their local bias according to various and time-varying atmospheric conditions. SST coefficients retrieved by these algorithms are fundamentally based on a regression method between satellite-observed brightness temperatures and in-situ SST measurements from drifters or moored buoys. The hybrid algorithm, based on a regression method between the incremental values and a scaling method, is applied to estimate the coefficients of Himawari-8 data as a proxy for GK-2A data. In addition, the performance of the 4-band algorithm, as another regression method, is tested for SST estimation using Himawari-8 data. Root-mean-square (RMS) and bias errors are presented for each algorithm in comparison to drifter temperatures. The comparison with in-situ SST measurements shows that hybrid SSTs have accuracies similar to the 4-band SSTs, with RMS errors are 0.55°C and 0.48°C, respectively. However, the errors of the estimated SSTs reveal, in some cases, a significant difference between hybrid SSTs and 4-band SSTs in terms of atmospheric variables such as moisture, wind speed, and distance from the cloud edge.

CMEMS OSI TAC PROGRESS REPORT

Jean-François Piollé [(1)], Hervé Roquet[(2)], Françoise Orain[(3)],
Bruno Buongiorno-Nardelli[(4)], Jacob Høyer[(5)], Cecilie D Wettre[(6)], Simon Good[(7)] and others

(1) CERSAT, Institut Français de Recherche pour l'Exploitation de la Mer (Ifremer), Brest, Email: jfpiolle@ifremer.fr
(2) CMS, Météo-France, Lannion, France, Email: Herve.Roquet@meteo.fr
(3) CMS, Météo-France, Lannion, France, Email: Francoise.Orain@meteo.fr,
(4) CNR, Napoli, Italy, Email: Bruno.Buongiornonardelli@cnr.it
(5) DMI, Copenhagen, Denmark, Email: jlh@dmi.dk
(6) Met.no, Oslo, Norway, Email: ositac-manager@met.no
(7) UK Met Office, Exeter, United Kingdom, Email: simon.good@metoffice.gov.uk

ABSTRACT

CMEMS (http://marine.copernicus.eu) is the follow-on to MyOcean EU project, implemented through a Delegation Agreement which has been awarded in 2014 by the European Union to Mercator-Ocean which delegates to other partners - through competitive calls - the operation of the different parts of the service which are not operated by Mercator-Ocean itself.

The WITS (Wind, Sea-ice and Temperature at the Sea Surface Service) is one of these delegated services, producing and delivering in particular a wide range of multi-sensor L3 and L4 sea surface temperature products over global and regional areas, in near real time.

A particular effort was dedicated in 2016 to the reprocessing and delivery of consistent long time series of the L4 products over all the aforementioned areas. These time series were generated from NOAA/Pathfinder v5.2 and ESA CCI datasets. This effort was strongly driven by the production of a global report on the state of the ocean by CMEMS.

EUMETSAT OSI SAF SEA SURFACE TEMPERATURE ACTIVITIES AND PRODUCTS

Saux Picart S [(1)], O'Carroll A.[(2)], Eastwood S.[(3)], Hoyer J.[(4)]

(1)Météo-France, Lannion, France, Email: stephane.sauxpicart@meteo.fr
(2)EUMETSAT, Darmstadt, Germany, Email:anne.ocarroll@eumetsat.int
(3)Norwegian Meteorological Institute, Oslo, Norway, Email:steinare@met.no
(4)Danish Meteorological Institue, Copenhagen, Denmark, Email:jlh@dmi.dk

ABSTRACT

The Satellite Application Facilities (SAFs) are part of the EUMETSAT ground segment, they form a distributed network of thematic application facilities conducting research, development, and operational activities.

The Ocean and Sea Ice SAF is a consortium which provides comprehensive information derived from meteorological satellites at the ocean-atmosphere interface. As far as Sea Surface Temperature is concerned, the OSI SAF is currently delivering a suite of regional and global products in near real time mode. OSI SAF is processing low earth orbiters Metop and SNPP, and geostationary satellites METEOSAT and GOES.

Recent development include the production of High Latitude Level 2 product of SST and Ice Surface Temperature, METEOSAT08 Level 3 product over Indian Ocean and the reprocessing of METEOSAT archive from 2004 to 2012.

This presentation gives an overview of the SST-related OSI SAF current activities and products.

OVERVIEW OF SENTINEL-3 SLSTR L1 AND MARINE L2 PRODUCTS

Igor Tomazic [(1)], Anne O'Carroll[(1)], Prasanjit Dash[(1,4)], Francois Montagner[(1)], Vincenzo Santacesaria[(1)], Steffen Dransfeld[(7)], Dave Smith[(2)], Craig Donlon[(3)], Gary Corlett[(5)], Jean-Francois Piollé[(6)]

(1) EUMETSAT, Eumetsat-allee 1, 64295 Darmstadt (Germany), Email: igor.tomazic@eumetsat.int
(2) RAL Space, Rutherford Appleton Laboratory, Harwell Oxford
(3) ESTEC/ESTEC, Keplerlaan 1, 2201 AZ, Noordwijk, The Netherlands
(4) Associated/affiliated with CSU CIRA and NOAA NESDIS STAR, USA
(5) The University of Leicester, University Road, Leicester,LE1 7RH, United Kingdom
(6) IFREMER, 38 Rue du Port Blanc, 35800 Dinard, France
(7) ESA/ESRIN, Via Galileo Galilei, 00044 Frascati, Italy

ABSTRACT

The Sentinel-3 Sea and Land Surface Temperature Radiometer (SLSTR) instrument has nine channels and dual view scanning technique with 500 m resolution in the visible and the shortwave infrared and 1 km in the thermal infrared with the aim to provide highly accurate sea surface temperature (SST) measurements.

The Sentinel-3 SLSTR set of products encompasses two user products, SLSTR L1B (SL_1_RBT___) and SLSTR L2P (SL_2_WST___) and one internal product (SL_2_WCT___) aimed for internal analysis and cal/val activities. The most comprehensive of all Sentinel-3 products is SLSTR L1B (SL_1_RBT____) that contains different spatial resolution grids: 1 km (for MWIR and TIR channels), 500 m (for VIS and SWIR channels) and tie point grid and different views: nadir and oblique (and agnostic related to tie point grid), spanning in total 111 files and almost 900 variables contained in the single product package. On the opposite side is the L2P SST product (SL_2_WST___) conforming to GHRSST (GDS2) specification.

To ensure a proper use of the data, understanding the formats, projections and associated information is a pre-requisite for the users. An overview of these three products will be given, together with Sentinel-3 SAFE (Standard Archive Format for Europe) definition, explanation of manifest files, list of measurement and annotation data files and information about the S3 SAFE filename convention. Different L1 and L2 grids and views will be presented together with the concept of orphans accompanied with the duplicate and cosmetic pixel flags. For SLSTR L2P product, we will give an overview of different sea surface temperature (SST) algorithms implemented inside the L2P product and related annotation data to help users in understanding the provided SST measurements.

Finally, we will give information how to access SLSTR L1 and L2 marine products and we will provide the list of currently available S3 reading tools so the interested users could join the Copernicus/Sentinel-3 SLSTR train.

CEOS OCEAN VARIABLES ENABLING RESEARCH AND APPLICATIONS FOR GEO (COVERAGE)

Jorge Vazquez [(1)], Vardis Tsontos[(1)] Victor Zlotnicki[(1)]

(1) Jet Propulsion Laboratory, Email: Jorge.Vazquez@jpl.nasa.gov

ABSTRACT

The CEOS Ocean Variables Enabling Research and Applications for GEO (COVERAGE) initiative seeks to develop a more seamless approach for delivering remote sensing data, including near real-time data streams, that are better integrated with in-situ and biological observations, in support of oceanographic and decision support applications for societal benefit. COVERAGE aligns with programmatic objectives of CEOS and the missions of GEO-MBON and Blue Planet, which are to advance and exploit synergies among the many observational programs devoted to ocean and coastal waters. COVERAGE is conceived of as 3 year R&D project focusing on implementing technologies, including cloud based solutions, to provide a data rich, web-based platform for integrated ocean data delivery and access: multi-parameter observations, easily discoverable and usable, thematically organized, available in near real-time, collocated to a common grid and including climatologies. These will be complemented by a set of value-added data services available via the COVERAGE portal including an advanced Web-based visualization interface, subsetting/extraction, data collocation/matchup and other relevant on demand processing capabilities. COVERAGE development will be organized around a priority use cases and applications identified by GEO and agency partners. The initial phase will be to develop co-located 25km products from the four Ocean Virtual Constellations, Sea Surface Temperature, Sea Level Anomaly Ocean Color, and Sea Surface Winds. This aims to stimulate work among the 4 Ocean Virtual while developing products based on the Ocean VCs. Such products as anomalies from a time mean, would build on the theme of applications with a relevance to CEOS/GEO mission and vision.

We invite feedback and discussion from the GHRSST community as we develop and implement COVERAGE around the goals and objectives to better serve users of Ocean Remote Sensing data.

RECENT IMPROVEMENTS TO THE NOAA IQUAM2.10 SYSTEM

Xinjia Zhou [1,2], Alexander Ignatov[1], Feng Xu[1,3,4], Kai He[1,3]

(1) NOAA STAR, College Park, MD 20740, USA, Email: Xinjia.Zhou@noaa.gov
(2) Colorado State University CIRA, Fort Collins, CO 80523, USA
(3) GST Inc., College Park, MD 20770, USA
(4) Fudan University, Shanghai, China

ABSTRACT

The quality of in situ sea surface temperatures (SSTs) is critical for calibration and validation of satellite SSTs. NOAA has established *i*Quam (in situ SST Quality Monitor, www.star.nesdis.noaa.gov/sod/sst/iquam) to support a wide range of its SST Cal/Val responsibilities. The *i*Quam performs three major functions: 1) quality controls (QC) in situ SSTs using consensus state-of-the-art QC algorithms, adopted in the oceanic, meteorological and remote sensing communities; 2) monitors QCed SSTs online in near–real time; and 3) serves them with QC flags and indicators appended, to downstream NOAA applications (SQUAM) and to external users.

Based on experience accumulated with version 1 and beta version 2, *i*Quam is being upgraded to version 2.10 which includes several major updates. Following several major data outages in the input NCEP stream in late 2016, another real-time dataset produced by FNMOC and containing drifting and fixed buoy and ship SST reports, has been added in iQuam2 to improve its stability. The number of observation dropped down in Nov 2016 due to WMO's migration from Traditional Alphanumeric Code (TAC) to BUFR. Following users' requests, several auxiliary layers have been added from NOAA AOML in iQuam2, including deployed ID (note that in contrast with WMO ID, which continues to be reported in iQuam2 and which can be reused, the deployed ID is unique for each buoy and not reused; note that it is also called AOML buoy identification number or PKey). Furthermore, buy manufacturer and drogue on/off information is added.

In addition to monthly statistics available in iQuam1, and daily statistics added in *i*Quam2, the iQuam2.10 webpage now additionally displays hourly distribution, to help check for data interruptions and abnormalities. Hourly density of in situ data is particularly important for creating match-ups with high temporal resolution geostationary data collected by GOES-R Advanced Baseline Imager (ABI; collects full disk data every 15min15) and Himawari-8/9 Advanced Himawari Imager (AHI; collects full disk data ever 10min).

CENTENNIAL-SCALE SURFACE TEMPERATURE VARIABILITY IN THE SOUTH CHINA SEA: A PERFECT REFLECTION OF GLOBAL OCEAN-CLIMATIC VARIABILITY CYCLES?

Anthony Banyouko Ndah

Universiti Brunei Darussalam, Jalan Tungku Link, Gadong, BSB, Brunei Darussalam
Email: Email: tonyban83@163.com

ABSTRACT

Met Office Hadley Centre's (HadISST1) Surface temperature data from 1870-2014 has been analysed for the South China Sea (SCS) using regression analysis, cumulative deviations (Buishand Range) test, standard normal heterogeneity test (SNHT) and low pass filtering technique. The aim is to examine patterns of SST variability at and beyond the seasonal scale. Overall, changes in SST in the SCS seem to follow a well-defined seasonal, inter-annual, decadal and longer term multi-decadal patterns. 'ENSO (El Niño & La Niña) signals were found to be the dominant source of inter-annual patterns. Two significantly strong warming episodes at decadal (1932-1942) and multi-decadal (1965-1998) scales have been identified. About 98% of the SST change in the SCS occurred during these two warm periods. Finally, it has been observed that since the 1997/1998 extreme positive SST anomaly, there has been a slight decline in SST in the SCS despite frequent intense Niño warming events in 2002/2003, 2009/2010 and 2015/2016. This study concludes that the SST variability in the SCS is a perfect reflection of global ocean-atmosphere variability which proceeds in a cyclical pattern. Finally, it is recommended that absent a thorough understanding of the forcing mechanisms and drivers of the various oscillatory patterns of SST, accurately predicting regional monsoon and global changes in the ocean-atmosphere system will remain elusive. This entry is intended for poster presentation.

WHY IS SUMMER DOISST WARM IN THE ARCTIC AND HOW TO FIX IT

Viva Banzon [(1)], Tom Smith[(2)], Mike Steele[(3)], Boyin Huang[(1)]

(1) NOAA/NCEI, Asheville, NC28801 Email: viva.banzon@noaa.gov
(2) NOAA/STAR, and CICS/ESSIC U. Maryland, College Park, MD Email: tom.smith@noaa.gov
(3) Michael Steele, Polar Science Center, U. Washington, Seattle, WA Email: mas @apl.washington.edu

ABSTRACT

A recent comparison of several sea surface temperature (SST) analyses in the Arctic by Castro et al. (2016) found that the 1/4 ° daily Optimum Interpolation Sea Surface Temperature (DOISST) performed consistently but had a warm bias relative to UpTempO buoys deployed during the Marginal ice Zone Processes Experiment. To understand the underlying cause for this bias, a re-examination of the DOISST methodology was conducted. The screening of buoy data was found to be too lax, leading to the inclusion of abnormally warm observations into the analysis. Large scale poleward smoothing allowed temperatures at 80 N to greatly influence estimated SSTs near the North Pole. Originally, the smoothing procedure was developed to infill the pole hole in the sea ice data. The pole hole is the area where there were no ice satellite observations due to the position of the orbits, and was a bigger issue early in the satellite ice record. Until recently, in situ observations have been very limited in the Arctic so DOISST computes a pseudo SST from sea ice data using a regression equation. The choice of ice-to-SST conversion method was less important than the poleward infilling in explaining the warm bias.

BAYESIAN CLOUD DETECTION FOR AVHRR SST RETRIEVAL

Claire Bulgin [(1)], Chris Merchant[(2)], Owen Embury[(3)]

(1) Department of Meteorology, University of Reading, UK, Email: c.e.bulgin@reading.ac.uk
(2) Department of Meteorology, University of Reading, UK, Email: c.j.merchant@reading.ac.uk
(3) Department of Meteorology, University of Reading, UK, Email: o.embury@reading.ac.uk

ABSTRACT

The AVHRR instrument record spans four decades providing the longest climate data record of sea surface temperature. The majority of AVHRR data are provided at one of two data resolutions: full resolution at 1.1 km in the nadir, and Global Area Coverage (GAC) nominally at 4km resolution. GAC data are an average over four full resolution pixels, but represent the equivalent of fifteen full resolution pixels in the Earth view (five across track by three along track). Cloud detection is a fundamental pre-processing step for sea surface temperature retrieval from satellite data, and critical to the production of datasets appropriate for use in climate studies. It still presents challenges in classifying features such as cloud edges, fog and pixel or sub-pixel cloud, and providing consistent masking under sunglint conditions and at sea-ice edges. We demonstrate here a Bayesian cloud detection scheme applied to both full resolution and GAC resolution data. Using SST validation statistics as a metric, the Bayesian cloud detection scheme gives better results (smaller spreads of in-sit-satellite difference) than equivalent operational cloud detection schemes (EUMETSAT mask for full resolution AVHRR data and CLAVR-X for GAC data) for most sensors in the AVHRR series: it reduces both the difference between the standard deviation and robust standard deviations of the satellite to in-situ comparisons and the absolute values, indicative of a reduction of cloud contamination in the clear-sky matches, and the corresponding reduction in nominally clear-sky coverage is reasonable (typically ~10%). We see fairly consistent results across the AVHRR data record from NOAA-06 (1979) to METOP-A (present day).

STRATOSPHERIC AEROSOL AND IMPACTS ON INFRARED SST RETRIEVALS

Owen Embury [(1)], Chris Merchant[(2)], Andy Harris [(3)]

(1) Department of Meteorology, University of Reading, UK, Email: o.embury@reading.ac.uk
(2) Department of Meteorology, University of Reading, UK, Email: c.j.merchant@reading.ac.uk
(3) University of Maryland, College Park, MD, U.S.A., Email: andy.harris@noaa.gov

ABSTRACT

Large explosive volcanic eruptions, such as Mount Pinatubo (1991) and El Chichón (1982), can inject megatons of sulphur dioxide into the stratosphere. The gas quickly forms a sulphuric acid aerosol which remains in the stratosphere for a couple of years. In addition to its direct impact on the planets climate, stratospheric aerosol can cause cold biases over 1 K in infrared SST retrievals from space.

We present here a climatology of infrared aerosol index retrieved from the High-resolution Infrared Radiation Sounder (HIRS) which has been carried on board NOAA polar orbiters since 1978. This aerosol index provides the information necessary to adapt the AVHRR SST retrievals for the present of volcanic sulphate aerosol. We show how this approach reduces the significant biases otherwise present in the AVHRR climate data record.

USE OF ACSPO VIIRS L3U SST IN THE AUSTRALIAN BUREAU OF METEOROLOGY

Pallavi Govekar, Chris Griffin, Helen Beggs and Leon Majewski

Australian Bureau of Meteorology, Melbourne, Australia
Emails: pallavi.govekar@bom.gov.au, christopher.griffin@bom.gov.au, helen.beggs@bom.gov.au and leon.majewski@bom.gov.au

ABSTRACT

Sea surface temperature (SST) products within a few kilometres of coasts that can resolve fine-scale features, such as ocean upwelling, are increasingly in demand. In response to user requirements for gap-free, highest spatial resolution, best quality and best accuracy SST data, the Australian Bureau of Meteorology (ABoM) ingests NOAA Advanced Clear-Sky Processor for Ocean (ACSPO) Visible Infrared Imaging Radiometer Suite (VIIRS) 0.02º L3U products into the ABoM Integrated Marine Observing System (IMOS) 0.02º multi-sensor L3S products. The high spatial resolution (0.75 km) and accuracy of VIIRS SST data, in conjunction with existing 1-4 km High Resolution Picture Transmission (HRPT) Advanced Very High Resolution Radiometer (AVHRR) SST data, shows significant improvement in spatial coverage. The improved L3S SST products provide better input for applications such as ReefTemp NextGen Coral Bleaching Nowcasting and IMOS OceanCurrent. It also provides useful insight into the study of SST diurnal variation and ocean upwelling in near-coastal regions. We discuss performance of the new VIIRS+AVHRR L3S products in near-coastal regions and our plan to improve other ABoM SST products by ingesting VIIRS data into those datasets such as RAMSSA and GAMSSA L4 SST analyses.

MONITORING AVHRR/2 IN THE NOAA SENSOR STABILITY FOR SST (3S) VERSION 2

Kai He[1,2], Sasha Ignatov[1]

[1]NOAA STAR, College Park, USA; Emails: Kai.He@noaa.gov; Alex.Ignatov@noaa.gov
[2]GST, Inc, Greenbelt, MD 20770, USA

ABSTRACT

The NOAA Sensor Stability for SST (3S) system was developed to support the AVHRR SST Reanalysis (RAN) project. The 3S version 1 analyzed calibration data (gain, offset, blackbody and space counts, blackbody temperatures) and observational context (Sun and Moon positions, Equator crossing time, etc.) from seven AVHRR/3 sensors onboard five NOAA (N15 - 19) and two Metop (MA and MB) satellites, from November 1998 – present. It was specifically aimed at supporting the AVHRR GAC RAN version 1, which only included data from AVHRR/3s onboard N16, N17, N18, N19 and MA from 29 August 2002 – 31 December 2015. In preparation for the next reanalysis, RAN2 from AVHRR/2 sensors (which will initially go back to 1994 and eventually to 1981), the 3S has been updated to version 2 with two major additions: 1) five AVHRR/2 sensors (onboard N07, N09, N11, N12, and N14) have been added from August 1981 – Oct 2002, thus covering the full AVHRR SST era; and 2) monitoring of the noise equivalent differential temperature (NEDT), a quantity characterizing the instrument radiometric noise, has been added for all AVHRR/2s and AVHRR/3s. As a first step towards the future AVHRR SST RANs at NOAA, the data availability and well-being of the AVHRR/2 sensors is analyzed and displayed in the 3S v2, and NEDTs for all AVHRR instruments are analyzed. This information is critically important for the selection of the appropriate candidate sensors for the inclusion in the AVHRR GAC RAN2, and selection of the appropriate clear-sky masking and SST retrieval algorithms.

CONSTRUCTING AN OCEAN DATA ASSIMILATION PRODUCT USING SATELLITE SEA SURFACE TEMPERATURE

Tsutomu Hihara [(1)], Yasumasa Miyazawa[(2)], Toru Miyama[(3)], Misako Kachi[(4)], Hiroshi Murakami[(5)], Yukio Kurihara[(6)], Noboka Ono[(7)], Hidenori Aiki[(8)]

(1) APL, JAMSTEC, Yokohama, Japan, Email: hiharat@jamstec.go.jp
(2) APL, JAMSTEC, Yokohama, Japan, Email: miyazawa@jamstec.go.jp
(3) APL, JAMSTEC, Yokohama, Japan, Email: tmiyama@jamstec.go.jp
(4) EORC, JAXA, Tsukuba, Japan, Email: kachi.misako@jaxa.jp
(5) EORC, JAXA, Tsukuba, Japan, Email: murakami.hiroshi.eo@jaxa.jp
(6) EORC, JAXA, Tsukuba, Japan, Email: kurihara.yukio@jaxa.jp
(7) EORC, JAXA, Tsukuba, Japan, Email: ono.nodoka@jaxa.jp
(8) ISEE, Nagoya University, Nagoya, Japan, Email: aiki@nagoya-u.jp

ABSTRACT

The Japan Aerospace Exploration Agency (JAXA) operates the several earth observation satellites, and provides satellite sea surface temperature (SST) data. Satellite capability to detect SST fields is advancing in recent years. However, satellite SST data include some missing depending on the type of satellites and sensors, and don't provide information on vertical oceanic conditions. This study aims at constructing a temporally and spatially uniform ocean dataset, using a data assimilation method which combines the satellite SST and the ocean model data.

Our target area is south of Japan where the Kuroshio flows. The data assimilation technique and ocean model used for the present study are the Local Ensemble Transform Kalman Filter (LETKF) and the Stony Brook Parallel Ocean Model (sbPOM), respectively. LETKF is able to represent small scale variations effectively. We assimilate the observation data including two satellite SST products: Himawari-8 and GCOM-W/AMSR2, provided by JAXA.

We show a typical result of the satellite/analysis SST and the associated vertical temperature distributions obtained in November 2016. A cyclone with cool air passed south of Japan from 23 to 24 November. The analysis data reproduce the observed SST drop caused by the weather disturbances, and reasonably estimate the SST states in the cloudy area and nearshore region missed by the satellite observation. Also, subsurface isotherms became sparse, suggesting the mixed layer deepening induced by the cyclone.

In the presentation, we discuss usability of the satellite SST for data assimilation in detail.

INTER-CALIBRATION OF BRIGHTESS TEMPERATURE FROM HY-2 SCANNING MICROWAVE RADIOMETER OVER OCEAN

Mingkun Liu[(1)], Lei Guan [(2)], and Wei Zhao [(3)]

(1) Department of Marine Technology, Ocean University of China, Qingdao, China,
Email: liumingkun_ouc@126.com
(2) Department of Marine Technology, Ocean University of China, Qingdao, China,
Email: leiguan@ouc.edu.cn
(3) National Satellite Ocean Application Service, State Oceanic Administration, Beijing, China,
Email: zhaowei@mail.nsoas.org.cn

ABSTRACT

Haiyang-2 (HY-2) is the first marine dynamic environmental satellite of China, that was launched on 16 August 2011. The scanning microwave radiometer (RM) onboard HY-2 has low frequency channels with the capability of observing sea surface temperature (SST) from space. The evaluation resultes showed the accuracy of SST from HY-2 RM is relatively low. The large difference between ascending and descending comparisons and the fluctuated bias and standard deviation indicate HY-2 RM is not well-calibrated. In this study, the Level 1B (L1B) brightness temperature of HY-2 RM are compared with the Global Precipitation Measurement (GPM) microwave radiometer (GMI) brightness temperature for the period from March 2014 to December 2015. The collocations of HY-2 RM and GPM GMI brightness temperature data are generated with the spatial window of 0.25º and the temporal window of 0.5 hour. The daily comparison results show that the biases and standard deviations of brightness temperature difference from different channels are relatively large. Except for the difference of center frequencies and Earth incidence angle between HY-2 RM and GPM GMI, the fluctuated daily biases indicate some problems exit in the calibration of HY-2 RM, such as the Earth radiation intrusion into cold mirror. The inter-calibration approach combined with radiative transfer simulation will be used to correct the brightness temperature from HY-2 RM.

LONG-TERM IMPACT OF SAMPLING BIAS IN NASA MODIS AND AVHRR-PATHFINDER LEVEL 3 SSTS

Yang Liu [(1)] , Kay Kilpatrick[(1)], Sue Walsh[(1)], and Peter J. Minnett[(1)]

(1) University of Miami, Miami, FL, USA, yliu@rsmas.miami.edu

ABSTRACT

Liu and Minnett (2016) identified sampling issues in the Level 3 NASA MODIS SST products when 4km observations are aggregated into global grids at different time and space scales, among which the sampling errors due to temporal averaging are larger and are not due to the seasonality of SSTs (Liu et al., 2017). Several dynamical and physical mechanisms involving SST-cloud correlations and feedbacks were attributed for the sampling error characteristics, which indicate potential long term effects. Here we examine this climate-scale effect by comparing the monthly time series (2002-2016) of MUR SSTs subsampled to 9km grid (Level4) and the 9km MUR SSTs sampled by MODIS 9km daily Level 3 quality masks (Pseudo-Level3). Also, the time series of 9km monthly MODIS (Level3) night-time SSTs are compared with the Level4 fields for a first-step quality check. Monthly climatology of the three composited fields shows the warm sampling biases at high latitudes are intrinsic and are not reduced at climate scales of at least a decade. The global local SST and the gap fraction trends are calculated using 14-year daily MODIS and MUR fields. The results indicate a biased trend signal for the last decade is likely to be found especially in the high latitudes. AVHRR-Pathfinder Level3 and AMSR Level3 fields are compared to elucidate the infrared sampling effects on decadal trends.

THE IMPACT OF SAHARAN OUTFLOW ON SATELLITE RETRIEVED INFRARED SEA SURFACE TEMPERATURE

Bingkun Luo [(1)], Goshka Szczodrak[(2)], Katherine Kilpatrick[(2)] and Peter Minnett[(2)]

(1) Meteorology and Physical Oceanography Program, Rosenstiel School of Marine and Atmospheric Science, University of Miami, Miami, FL, USA, Email: lbk@rsmas.miami.edu
(2) Department of Ocean Sciences, Rosenstiel School of Marine and Atmospheric Science, University of Miami, Miami, FL, USA

ABSTRACT

Infrared satellite observations of sea surface temperature (SST) have become essential for many applications in meteorology, climatology and oceanography. Users usually demand high accuracy SST data: for climate research and monitoring an absolute temperature uncertainty of 0.1K and stability of better than 0.04K per decade are required. Tropospheric aerosol concentrations increase infrared signal attenuation and prevent the retrieval of accurate satellite SST. We compare satellite-derived skin SST with measurements from the ship-based Marine-Atmospheric Emitted Radiance Interferometer (M-AERI) deployed on ships during the Aerosols and Ocean Science Expeditions (AEROSE) and with quality-controlled drifter temperatures. After match-up with in-situ SST and filtering of cloud contaminated data, the results indicate that SST retrieved from MODIS (Moderate Resolution Imaging Spectroradiometer) aboard the Terra and Aqua satellites have negative (cool) biases compared to shipboard radiometric measurements. There is also a pronounced negative bias in the Saharan outflow area that can introduce SST errors >1 K at AOD>0.5. We use Cloud-Aerosol Lidar and Infrared Pathfinder Satellite Observation (CALIPSO) datasets to study the vertical structure of aerosol effects on SST. From our studies, dust present at lower altitudes has a smaller effect on the SST errors because the higher dust layers have a larger temperature difference compared to the sea surface. What is more, SST difference is also related to the number of aerosol layers. The goal of this study is to understand the characteristics and physical mechanisms of the aerosol layer effect on satellite retrieved infrared SST, as well as to derive an empirical formula that better corrects for aerosol-related effect.

SHORT-TERM VARIATIONS OF SEA SURFACE CURRENTS ESTIMATED FROM GEOSTATIONARY SATELLITE SEA SURFACE TEMPERATURE IMAGES

Hee-Young Kim[(1)], Hee-Ae Kim[(2)], Kyung-Ae Park [(3)]

(1) Dep. of Science Education, Seoul National University, Seoul, Korea, Email: heeyoungkim@snu.ac.kr
(2) Dep. of Science Education, Seoul National University, Seoul, Korea, Email: heeaekim@snu.ac.kr
(3) Dep. of Earth Science Education, Seoul National University, Seoul, Korea, Email: kapark@snu.ac.kr

ABSTRACTS

Surface geostrophic currents have long been estimated with reliable accuracy from sea surface height anomalies observed by satellite radar altimeters. However, altimeter-based oceanic current fields contain inherent errors related to the spatial distance and temporal discrepancy of measurements between altimeter tracks. Surface currents based on sequential sea surface temperature (SST) images of near-polar orbiting satellites also have disadvantages arising from the small number of data samplings due to frequent cloud cover or other atmospheric and oceanic conditions over relatively long time intervals. Such sparse samplings can be overcome, in part, by high-resolution and frequently observed geostationary satellite SST images. This study assesses the accuracy of the surface currents from subsequent Himawari-8 SST images, as a proxy for GEO-KOMPSAT-2A (Geostationary - Korea Multi-Purpose Satellite-2A) SST, by comparing the quality-controlled currents obtained by the Himawari-8 satellite with the estimated currents obtained from surface drifters in the full-disk region of Himawari-8. Analysis results reveal that the estimated current speeds and directions show good agreement with the drifter-based calculated values, with root-mean-square (bias) errors of 0.15 m/s (-0.05 m/s) and 6.1° (1.8°), respectively. The estimated current field illustrates a rotating feature around a mesoscale anticyclonic eddy, as well as the characteristic meandering pattern of the Kuroshio Current. In addition, we present short-term hourly variations of the surface current and their potential causes, and address the importance of the role of high-resolution geostationary satellite SST measurements in understanding short-term surface current variations.

Issue: Version 3
Date: 15/11/2018

A MACHINE LEARNING APPROACH FOR MSG/SEVIRI SST BIAS ESTIMATION

Blandine Gausset[(1)], S. Saux Picart [(1)], Pierre Tandéo[(2)], Emmanuelle Autret[(3)]

[(1)] Météo-France, Lannion, France, Email:stephane.sauxpicart@meteo.fr
[(2)] Télécom-Bretagne, Plouzané, France, Email:pierre.tandeo@telecom-bretagne.eu
[(3)] Ifremer, Plouzané, France, Email:emmanuelle.autret@ifremer.fr

ABSTRACT

It is increasingly important for applications such as data assimilation or climate studies to have some knowledge about the uncertainties associated with the data being used. The GHRSST has for a long time recommended SST data producers to include Single Sensor Error Statistics (SSES) within their SST products. However there is recommendation as to which method may be used to provide SSES. They are usually understood as the mean and standard deviation of the difference between satellite retrieval and a reference.

This work is an attempt at using advanced statistical methods of machine learning to predict the bias between Ocean and Sea Ice (OSI SAF) Meteosat Second Generation (MSG) SST products and ground truth considered to be drifting buoy measurements. OSI SAF MSG current product is elaborated using a multilinear algorithm using 10.8 and 12µm channels to which a correction is applied in the case of high concentration of atmospheric Saharan dusts. An algorithm correction method based on radiative transfer simulation is also used to account for seasonal and regional biases. A complete description of the retrieval methodology can be found in Le Borgne et al. (2011). However, for this study, the two corrections mentioned above have been removed. This was done to simplify interpretation of the results of statistical models for predicting bias in retrieved SST.

Here we present the results obtained using four different statisticals methods : Linear regression, Least Absolute Shrinkage and Selection Operator (LASSO), Random Forest and Generalized Additive Model (GAM).

THE SENSIBILITY OF CMC ANALYSIS TO THE CHARACTERISTICS OF DIFFERENT OBSERVATION DATA SETS

Dorina Surcel Colan [(1)] and Reine Parent[(1)]

(1)Numerical Environmental Prediction Section, National Prediction Development Division, Meteorological Service of Canada, Environment and Climate Change Canada,
Emails: dorina.surcel-colan@canada.ca, Reine.Parent@canada.ca

ABSTRACT

In an effort to improve the accuracy of the SST analysis and to reduce the volume of dataset to be processed at the Canadian Meteorological Centre a series of sensitivity studies were carried out to evaluate the impact of characteristics of different observation data sets on the SST analysis. The influence of increasing the precision of data assimilated in the SST analysis was first evaluated using data coded in two decimals versus data coded in one decimal. The study was performed following WMO's recommendation to replace TAC (Traditional Alphanumeric Codes) format with BURF (Binary Universal Form Representation) format for insitu observations. The second study is related to using VIIRS L3U data set instead of VIIRS L2P data set, the latter is considerable bigger in data size than the former. The third study examines the degradation of the SST analysis if satellite data is missed for a few days. Results from these numerical experiments will be presented at the meeting.

RETRIEVAL OF MODIS SST WITH OPTIMAL ESTIMATION

Malgorzata Szczodrak[1], Peter Minnett [2]

(1) Rosenstiel School of Marine and Atmospheric Science, University of Miami, Miami, FL, USA, Email: goshka@rsmas.miami.edu
(2) Rosenstiel School of Marine and Atmospheric Science, University of Miami, Miami, FL, USA, Email: pminnett@rsmas.miami.edu

ABSTRACT

The Optimal Estimation (OE) approach is applied to the retreival of sea surface temperature (SST) from MODIS radiance measurements in 11 µm channels and 4 µm channels. Prior knowledge is a state vector consisting of European Center for Medium Range Weather Forecast (ECMWF) interim reanalysis fields of sea surface temperature and column water vapor, and prior observations is a set of MODIS channel 31 and 32 radiances (or channel 22 and 23 radiances) calculated using line-by-line radiative transfer model (LBLRTM) of Clough et al., (2005) for all prior state vectors.

The LBLRTM was also used to compute the partial derivatives of the channel radiances with respect to the elements of the state vector (jacobian matrices). To reduce a computational effort a set of base jacobians were calculated representative of the 5 standard atmospheres (Tropical, Mid-Latitude Summer and Winter, and Subarctic Summer and Winter) and in each case for a range of SST and TCWV values. These base jacobians were then used to build jacobian matrices for the individual state vectors by selecting appropriate model atmosphere based on location and interpolating to the SST and TCWV of the *a priori* state.

The results of the MODIS **OE** SST retrieval are compared with in situ buoy measurements and with the SSTs drived using the curent MODIS non-linear SST (**NLSST**) verison 6 retrieval algorithm, and with concurrent AMSR-E SST measurements.

ONGOING COMPARISON BETWEEN SENTINEL-3A SLSTR AND IASI ABOARD METOP-A AND –B

Igor Tomazic[1], Anne O'Carroll[1], Tim Hewison[1], Jörg Ackermann[1], Craig Donlon[2], Jens Nieke[2], Bouwe Andela[2], Dorothee Coppens[1], Dave Smith[3], Jean-Francois Piolle[4]

[1]EUMETSAT, Darmstadt, Germany
[2]ESA/ESTEC, Noordwijk, The Netherlands
[3]RAL Space, Rutherford Appleton Laboratory, Harwell Oxford, UK
[4]IFREMER, 38 Rue du Port Blanc, 35800 Dinard, (France)

ABSTRACT

Aboard the Sentinel-3 satellite is a dual view Sea and Land Surface Temperature Radiometer (SLSTR) implemented to fulfil requirements of delivering accurate reference surface ocean, land and ice temperature and to maintain continuity with ENVISAT (A)ATSR series of instruments (Donlon et al., 2012). The Infrared Atmospheric Sounding Interferometer (IASI-A) onboard Metop-A/B is used within Global Space-based Inter-Calibration System (GSICS) as a reference instrument for inter-comparison and re-calibration of other instruments. Therefore, to examine the accuracy and continuity we performed comparisons of Sentinel-3A SLSTR against Metop-A IASI measurements. Additionally, applying the same approach, we performed comparison against Metop-B IASI and using double difference method to indirectly assess the differences between Metop-A and Metop-B IASI.

The comparison encompasses SLSTR-IASI crossovers, producing collocations (matchups), applying spectral convolution to IASI radiance spectra and finally aggregating SLSTR pixels within each IASI field of view. The matchups were produced using both simultaneous nadir overpasses (SNOs) and quasi-SNOs (QSNOs) to obtain collocations over the full range of Earth-scene radiances. The SNOs were predicted using orbital modelling (for the satellite ground tracks) and QSNOs were indentified using the NAIAD open-source tool (allowing the usage of instrument swath). SNO based collocations were derived by applying GSICS collocation criteria (Hewison et al, 2013) with constraints on both the time difference (5 min) and viewing angle, where QSNOs analysis were derived using relaxed time difference (up to 20 min) and only analysing collocations over the sea to reduce the impact of temporal mismatches. The IASI hyperspectral radiances were convolved with Sentinel-3A SLSTR spectral response functions (SRF) of bands S8 and S9 (10.8 μm and 12 μm) and SLSTR L1 S8 and S9 BT nadir and oblique view measurements were aggregated (averaged) over the corresponding IASI FOV.

The results show very good consistency of radiometric calibration between SLSTR-A and both IASI-A and –B, with very small and almost constant differences (≤0.1 K) over the brightness temperature range 220 – 280 K. For colder scenes (200 – 220 K), the differences increase, with a mean value of 0.4 K, and small (but significant) differences between IASI-A and –B (≤0.1 K). Ongoing work includes assessment of QSNOs over warm scenes, analysis of SLSTR oblique view measurements, further assessment of the observed cold bias and implementing the processing in the quasi-operational context to allow routine monitoring of the SLSTR calibration.

EVALUATION OF THE MULTI-SCALE HIGH RESOLUTION (MUR) ANALYSIS OF LAKE SURFACE TEMPERATURE

Jorge Vazquez [(1)], Erik Crosman[(2)], Toshio Michael Chin[(3)]

(1) Jet Propulsion Laboratory, Email: Jorge.Vazquez@jpl.nasa.gov
(2)University of Utah, Salt Lake City, Utah USA, Email: erik.crosman@utah.edu
(3) Jet Propulsion Laboratory, Email: toshio.m.chin@jpl.nasa.gov

ABSTRACT

Lake surface temperature is a critical parameter for understanding lake ecosystems, climate change, and input into numerical weather prediction models. However, obtaining sufficiently accurate and timely satellite-derived lake temperature measurements remains a challenge. Error sources include insufficient cloud-masking, large data gaps, temporal averaging errors, and image geolocation errors. In this study, we present preliminary results from a validation study of satellite-derived lake surface temperature from the NASA multi-scale high-resolution (MUR) analysis of global SST, which includes inland water bodies. MUR-derived lake temperature from three lakes are analyzed: A large lake (Lake Michigan, USA), a medium-sized lake (Lake Okeechobee, Florida, USA), and a small lake (Lake Oneida, New York, USA). The MUR lake temperature estimates are excellent over Lake Michigan, where data from multiple satellite platforms are blended with buoy data. The advantages of the MUR analysis for lake temperature include 1) Incorporation of high resolution 1-km MODIS data, 2) synthesis of multiple satellite platforms (including AVHRR), and 3) potential reduction of temporal gap errors through the multi-scale analysis technique. However, the stringent quality flags, a lack of a climatological background temperature, ice mask and adaptable interpolation scales have all been identified as potential sources of error in lake temperature estimates using MUR. Over Lake Oneida, these sources of error appear to result in large springtime biases in MUR lake temperature compared to buoy measurements.

ASSESSMENT OF LANDSAT 8 TIRS SEA SURFACE TEMPERATURE RETRIEVAL ALGORITHMS

Ji-An Wei [(1)], Difeng Wang[(2)]

(1) State Key Laboratory of Satellite Ocean Environment Dynamic, Second Institute of Oceanography, State Oceanic Administration, Hangzhou, China, Email: anserwei@163.com
(2) State Key Laboratory of Satellite Ocean Environment Dynamic, Second Institute of Oceanography, State Oceanic Administration, Hangzhou, China, Email: dfwangi@sio.org.cn

ABSTRACT

Short abstracts: Sea surface temperature (SST) is a crucial parameter for understanding and predicting heat exchanges, gas and momentum transfers at different scales that related to local or global climate. High resolution SST estimation with thermal infrared onboard satellites is widely used in coastal regions for environmental monitoring. Landsat 8 Thermal Infrared Sensor (TIRS) provides two thermal channels, which supplies high resolution image and has a great benefit for the SST retrieval. In this paper, we compared SST retrieval approaches between split-window (SW) algorithm and single-channel (SC) algorithm from TIRS. SST errors due to sensitive input factors including water vapor content (WVC) and sea surface emissivity (SSE) were analyzed, and in-situ buoy data were collected for the two methods' validation. Results show that SW is less susceptible to WVC comparing with SC, whereas SW is more sensitive than SC as SSE deviation increase. An order of 0.1 $\boldsymbol{g/cm^2}$ WVC deviation would introduce an average SST errors of 0.012**K** and 0.070**K** in SW and SC, respectively. 0.005 SSE change could yield SSE errors lower than 0.4K for SC, depending on WVC and sensor bright temperature. However, SSE errors of SW owning to SSE relies on WVC, a 0.005 change in the value of SSE would generate SST errors range from 0.5**K** to 0.8**K**, which lies on the SSE variations of one or both two thermal channels. With obtaining precise input factors (WVC and SSE), algorithms validation result indicate that SW possess higher measurement accuracy than SC.

DEVELOPING AN ATMOSPHERIC CORRECTION OF TROPOSPHERIC DUST IN THE INFRARED SST RETRIEVAL FOR THE NOAA ACSPO SYSTEM

Xin Xi[1,2], Alexander Ignatov[1]

[1]NOAA Center for Satellite Applications and Research (STAR), 5830 University Research Court, College Park, MD 20740, USA. Email: xin.xi@noaa.gov

[2]Cooperative Institute for Research in the Atmosphere, Colorado State University, Fort Collins, CO 80523, USA

ABSTRACT

Wind-blown dust aerosol from dryland regions is known to affect sea surface temperature (SST) retrieval at infrared wavelengths. Prior studies sought to derive the dust-induced SST bias as a function of the so-called Saharan dust index (SDI), which is defined based on the deviation of dust-affected brightness temperature differences in various IR bands from aerosol-free conditions. The formulation of SST bias is derived from radiative transfer simulations, often using a limited number of atmospheric profiles and the generic aerosol data from OPAC or Haywood aerosol models, which may not fully capture the region-specific optical characteristics of dust outflow from, for instance, West Africa, Middle East, and northern China. The SDI-based method is being tested for its potential of correcting regional dust-induced SST biases within the NOAA ACSPO SST retrieval system, using the data of polar VIIRS and MODIS sensors flown onboard SNPP and Aqua, and geostationary ABI and AHI sensors flown onboard Himawari and newly launched GOES-16 platforms. The selection of sensors is due to the spectral channels centered at 3.7, 8.6, 11 and 12 microns, which are all needed for the SDI calculation according to the authors of the concept. In contrast to prior studies, we will be employing a globally representative set of SST, atmospheric water vapor, temperature and dust aerosol mixing ratio profiles from the Modern Era Retrospective Analysis for Research and Applications (MERRA version 2) reanalysis. Also, newly published data sets on dust particle size distributions and infrared refractive indices (Di Biagio et al, ACP, 2016) will be used to improve representation of regional dust spectral absorption properties. Initial results towards the algorithm design and validation against quality controlled in-situ SST measurements will be presented.

CMA OCEAN DATA MERGING SYSTEM(COMS)

Bin Xu, Lei Zhang, Chunxiang Shi, Zijiang Zhou

National Meteorological Information Center, China Meteorological Administration, Beijing, China
Email: xubin@cma.gov.cn

ABSTRACT

The CMA Ocean Data merging system (COMS) was designed to merge multi-platform ocean variable observation to provide more accurate ocean variable data sets. As the first step, global multi-platform Sea Surface Temperature (SST) Merging data has been produced. In this system, the bias of FY-3C/VIRR SST retrievals, METOPA/AVHRR SST retrievals, GCOM-W1/AMSR-2 SST retrievals, and ship SST observation data were all corrected based on PDF matching method using buoy SST observation data. After bias correction, those data and buoy SST observation data were calculated to the SST super observation. Then this SST Super observation were merged with ECMWF SST Forecasting data using Space-Time Multiscale Analysis System(STMAS) to create global 0.25° daily SST merging data. After compared with other SST data sets, COMS SST merging data can capture the main type of SST as same as other data sets, and have highly correlation coefficient with OISST, but can provide more information of typhoon. As the next step, the multi-platform Ocean Wind, Sea Ice merging data sets are under processing.

EFFECT OF EMISSIVITY ON SHIPBOARD SEA SURFACE SKIN TEMPERATURE MEASUREMENTS

Minglun Yang [(1)], Lei Guan[(1)] , Kailin Zhang[(1)] , Liqin Qu[(1)]

(1) Department of Marine Technology, Ocean University of China, Qingdao, China, Email: minglunyang@163.com

ABSTRACT

Generation of Climate Data Records (CDRs) sea surface temperature (SST) from current and future satellite radiometers requires validation of satellite-derived sea surface skin temperature (SST_{skin}) using ship-based radiometers with calibration traceable to National Metrology Institute (NMI) standards. Two infrared radiometers are deployed on the research vessel Dong Fang Hong II of Ocean University of China (OUC) for SST_{skin} measurements and continuously operating in the China Seas. The infrared SST autonomous radiometer (ISAR) is a self-calibrating instrument developed by the University of Southampton. The Ocean University of China First Infrared Radiometer for measurements of SST (OUCFIRST) is made by OUC and also has a self-calibrating system for measuring SST_{skin}. The retrieval of SST_{skin} depends on both the self-calibration process and the correction for sky reflection. The accuracy of measured SST_{skin} is strongly influenced by the estimate of sea surface emissivity (SSE). In this study, an emissivity model is applied to calculate SSE which is used in two radiometers SST_{skin} retrieval process. The effect of wind speed dependent emissivity on the retrieved SST_{skin} during the cruises in 2013, 2014 and 2015 is analyzed. The results show that under high wind speed conditions, approximately higher than 10 m/s, the changes on derived SST_{skin} can reach a magnitude of 0.1 K to 0.2 K. Using in situ measurements of SST, sea and sky view radiations and sea surface net radiations, SSE are calculated and compared with the model results.

A NEAR-GLOBAL PHYSICAL RETRIEVAL BASED GEOSTATIONARY SEA SURFACE TEMPERATURE REANALYSIS

Xiaofang Zhu [(1)], Eileen Maturi[(2)], Andrew Harris[(3)],Jonathan Mittaz[(4)], Mark Eakin

(1) Global Science and Technology, College Park, MD, USA, Email:xiaofang.zhu@noaa.gov
(2)NOAA/NESDIS/STAR, College Park, MD, USA Email:Eileen.maturi@noaa.gov
(3) University of Maryland, CICS,College Park, MD, USA. Andy.Harris@noaa.gov
(4) University of Reading, Dept of Meterology, Reading, UK. J.mittaz@reading.ac.uk
(5)NOAA/NESDIS/CoralReefWatch, College Park, MD, USA Email:Mark.Eakin@noaa.gov

ABSTRACT

Sea Surface Temperature reanalysis with near-global coverage have been generated for the year 2002-2015 using NOAA/NESDIS's latest operational geostationary SST retrieval algorithms. The algorithm calculates SST by utilizing a fully physical retrieval scheme based on modified total least squares (MTLS, Koner et al., 2014) and a probabilistic (Bayesian) approach for cloud masking (Merchant et al., 2005). The geostationary satellites being reprocessed include GOES (GOES-8, 9, 10, 11, 12, 13 &15) satellites from NOAA; MTSAT (MTSAT1-R and MTSAT-2) satellites from Japan Meteorological Agency (JMA); and Meteosat (8, 9 and 10) from Eumetsat. The total raw data volume for geostationary sensors that reprocessed is ~200TB in various data formats (HRIT, GVAR, and MCIDAS Area File). Reprocessed geostationary SST provides a near complete coverage of the tropics and mid-latitudes with at least hourly time resolution. When validating with buoy data, the reprocessed SST show marked improvements in both standard and robust statistics when comparing with operational SST generated at the time. For GOES night time SST for instance, the bias is reduced from -0.4K to -0.1K for night time, and the SD is improved from 0.7K to 0.4K~0.5K. Across all geostationary satellite platforms, we see a 20%-30% drop in SD across using the current physical retrieval method. The resulting dataset is a high temporal resolution, low bias and standard deviation, near global coverage SST with more than a decade of time length with the potential to study many phenomena such as ocean diurnal warming and ocean fronts.

SECTION 4: APPENDICES

APPENDIX 1 – LIST OF PARTICIPANTS

Name	Affiliation	Email
Armstrong, Ed	NASA Jet Propulsion Lab, USA	edward.m.armstrong@jpl.nasa.gov
Baker-Yeboah, Sheekela	University of Maryland, USA	sheekela.baker-yeboah@noaa.gov
Banyouko Ndah, Anthony	University Brunei Darusslam, Brunei	tonyban83@163.com
Beggs, Helen	Australian Bureau of Meteorology	h.beggs@bom.gov.au
Bragaglia-Pike, Silvia	GHRSST Project Office, UK	s.bragagliapike@reading.ac.uk
Casey, Kenneth	NOAA NCEI, USA	kenneth.casey@noaa.gov
Cayula, Jean-François		j.cayula@ieee.org
Chen, Chuqun	South China Sea Institute of Oceanology, Chinese Academy of Sciences	cqchen@scsio.ac.cn
Chen, Shuguo	Ocean University of China	chenshuguo@ouc.edu.cn
Chen, Yuanyuan	Chinese Academy of Agricultural Sciences	cy1305153@163.com
Corlett, Gary	GHRSST Project Office, UK	gkc1@le.ac.uk
Cornillon, Peter	University of Rhode Island, USA	pcornillon@me.com
Dash, Prasanjit	EUMETSAT(emp)/CSU CIRA(affl)	prasanjit.dash@eumetsat.int
Ding, Runjie	Ocean University of China	rj_ding@126.com
Ding, Yanni	CIRA/NOAA, USA	Yanni.Ding@noaa.gov
Donlon, Craig	ESA, The Netherlands	craig.donlon@esa.int
Embury, Owen	University of Reading, UK	o.embury@reading.ac.uk
Feng, Qian	NSOAS, China	fengqian@mail.nsoas.org.cn
Ge, Chen	Ocean University of China	
Gentemann, Chelle	Earth & Space Research	cgentemann@gmail.com
Guan, Lei	Ocean University of China	leiguan@ouc.edu.cn
Harris, Andrew	University of Maryland, USA	andy.harris@noaa.gov
He, Kai	US NOAA/GST	kai.he@noaa.gov
He, Ming-Xia	Ocean University of China	mxhe@ouc.edu.cn
Hihara, Tsutomu	Application Laboratory, JAMSTEC, Japan	hiharat@jamstec.go.jp
Høyer, Jacob	Danish Meteorological Institute	jlh@dmi.dk
Hu, Lianbo	Ocean University of China	hulb@ouc.edu.cn

Name	Affiliation	Email
Huang, Boyin	NOAA/NCEI, USA	boyin.huang@gmail.com
Huang, Thomas	JPL, USA	thomas.huang@jpl.nasa.gov
Ignatov, Alexander	NOAA STAR, USA	alex.ignatov@noaa.gov
Kim, Hee-Young	Seoul National University, Korea	heeyoungkim@snu.ac.kr
Kim, Jae-Gwan	Korea Meteorological Administration	kimjgwan@korea.kr
Koner, Prabhat	NOAA/UMD, USA	prabhat.koner@noaa.gov
Kulkarni, Balasaheb	PVG~S College of Science & Technology	balasahebk@yahoo.com
Kurihara, Yukio	JMA, Japan	ykuri.kiyo@gmail.com yukio.kurihara-a@met.kishou.go.jp
Li, Hengyu	ORSI Ocean University of China	lihengyu3003@qq.com
Li, Wen-Hao	JPL NASA, USA	whl52059@gmail.com
Li, Xu	EMC/NCEP/NOAA, USA	xu.li@noaa.gov
Liu, Chunying	NOAA/NECI, USA	chunying.liu@noaa.gov
Liu, Mingkun	Ocean University of China	liumingkun_ouc@126.com
Liu, W. Timothy	Jet Propulsion Laboratory, USA	w.t.liu@jpl.nasa.gov
Liu, Yang	University of Miami, USA	yliu@rsmas.miami.edu
Lu, Feng	CMA/NSMC/OSPP, China	lufeng@cma.gov.cn
Luo, Bingkun	University of Miami, USA	LBK@rsmas.miami.edu
Mao, Chongyuan	Met Office, UK	chongyuan.mao@metoffice.gov.uk
Marullo, Salvatore	ENEA, Italy	salvatore.marullo@enea.it
Maturi, Eileen	NOAA STAR, USA	eileen.maturi@noaa.gov
Merchant, Christopher	University of Reading / National Centre for Earth Observation, UK	c.j.merchant@reading.ac.uk
Minnett, Peter	University of Miami, USA	pminnett@rsmas.miami.edu
Mittaz, Jonathan	University of Reading/NPL, UK	j.mittaz@reading.ac.uk
Nightingale, Tim	STFC Rutherford Appleton Laboratory, UK	tim.nightingale@stfc.ac.uk
O'Carroll, Anne	EUMETSAT, Germany	Anne.Ocarroll@eumetsat.int
Pan, Gang	South China Sea Institute of Oceanology, CAS	gpan@scsio.ac.cn
Park, Kyung-Ae	Seoul National University, Korea	kapark@snu.ac.kr
Petrenko, Boris	NOAA/STAR, GST, Inc., USA	boris.petrenko@noaa.gov
Piollé, Jean-François	Ifremer, France	jfpiolle@ifremer.fr

Name	Affiliation	Email
Qu, Liqin	Ocean University of China	quliqin@ouc.edu.cn
Santoleri, Rosalia	CNR – ISAC, Italy	r.santoleri@isac.cnr.it
Saux Picart, Stéphane	Météo-France	stephane.sauxpicart@meteo.fr
Sun, Ruyao	Ocean University of China	sunry0616@163.com
Surcel Colan, Dorina	CMC - Environment Canada	dorina.surcel-colan@canada.ca
Thapliyal, Pradeep	Indian Space Research Organisation	pkthapliyal@sac.isro.gov.in
Tomazic, Igor	EUMETSAT, Germany	igor.tomazic@eumetsat.int
Vazquez, Jorge	Jet Propulsion Laboratory/Caltech, USA	Jorge.Vazquez@jpl.nasa.gov
Wan, Liying	National Marine Environmental Forecasting Center, China	wanly@nmefc.gov.cn
Wang, Puwei	Ocean University of China	1286399204@qq.com
Wang, Sujuan	CMA/National Satellite Meteorological Center, China	wangsj@cma.gov.cn
Wei, Ji-an	Satellite Environment Center, Ministry of Environmental Protection	anserwei@163.com
Wimmer, Werenfrid	University of Southampton, UK	w.wimmer@soton.ac.uk
Woo, Hye-Jin	Seoul National University, Korea	hyejinwoo@snu.ac.kr
Wu, Fan	Ocean University of China	wufan620@126.com
Xie, Xiaosu	Jet Propulsion Laboratory, USA	xiaosu.xie@jpl.nasa.gov
Xu, Bin	National Meteorological Information Center, CMA, China	xubin@cma.gov.cn
Yang, Hang	Ocean University of China	sduyanghang@163.com
Yang, Minglun	Ocean University of China	minglunyang@163.com
Zhang, Lei	National Meteorological Information Center, CMA, China	zhang_lei@cma.gov.cn
Zhao, Chaofang	Ocean University of China	zhaocf@ouc.edu.cn
Zhou, Xinjia	NOAA/STAR, USA	xinjia.zhou@noaa.gov
Zlotnicki, Victor	NASA/Caltech/JPL, USA	victor.zlotnicki@jpl.nasa.gov

APPENDIX 2 –PARTICIPANTS PHOTO

APPENDIX 3 – SCIENCE TEAM 2017-18

Anne O'Carroll (Chair)	**EUMETSAT, Darmstadt, Germany**
Ed Armstrong	NASA JPL PO.DAAC, USA
Viva Banzon	NOAA/NCDC, USA
Helen Beggs	Bureau of Meteorology, Melbourne, Australia
Kenneth S Casey	NOAA/NESDIS NODC, USA
Sandra Castro	University of Colorado, Boulder, USA
Jean-François Cayula	Vencore, Inc, Stennis Space Center, Mississippi, USA
Mike Chin	NASA JPL, USA
Carol Anne Clayson	WHOI, USA
Peter Cornillon	University of Rhode Island, USA
Prasanjit Dash	NOAA, USA
Craig J Donlon	European Space Agency, The Netherlands
Steinar Eastwood	Met.no, Norway
Owen Embury	University of Reading, UK
Emma Fiedler	Met Office, UK
Chelle Gentemann	Earth and Space Research, USA
Simon Good	Met Office, UK
Lei Guan	Ocean University of China, China
Andrew Harris	NOAA/NESDIS ORA, USA
Simon Hook	NASA JPL, USA
Jacob Høyer	Danish Meteorological Institute, Denmark
Alexander Ignatov	NOAA/NESDIS/STAR, USA
Misako Kachi	Japan Aerospace Exploration Agency (JAXA), Japan
Alexey Kaplan	Columbia University, USA
Ioanna Karagali	Technical University of Denmark, Denmark
Prabhat Koner	ESSIC, University of Maryland, USA
Yukio Kurihara	Japan Aerospace Exploration Agency (JAXA), Japan
Arrow Lee	Rutherford Appleton Laboratory, UK
W Timothy Liu	NASA JPL, USA
Yang Liu	RSMAS, University of Miami, USA
Salvatore Marullo	ENEA, Italy
Eileen Maturi	NOAA/NESDIS/STAR/SOCD/MECB, USA
Christopher Merchant	University of Reading, UK
Peter Minnett	RSMAS, University of Miami, USA
Jonathan Mittaz	University of Reading, UK
Tim Nightingale	Rutherford Appleton Laboratory, UK
Kyung-Ae Park	Seoul National University, Korea
Jean–François Piollé	IFREMER, France
Rosalia Santoleri	ARTOV.ISAC.CNR, Italy
Stéphane Saux Picart	Météo-France, France
Dorina Surcel Colan	CMC - Environment Canada
Igor Tomazic	EUMESTAT, Darmstadt, Germany
Jorge Vazquez	NASA JPL PO.DAAC, USA
Sujuan Wang	National Satellite Meteorological Center, Met Administration, China
Christo Whittle	CISR, South Africa
Gary Wick	NOAA ETL, USA
Keith Willis	Naval Oceanographic Office, USA
Werenfrid Wimmer	University of Southampton, UK

LAST PAGE